CHARACTERISATION OF THE METABOLISM OF AML AND STROMAL CELLS IN CO-CULTURE

Nuria Vilaplana Lopera

A thesis submitted to the University of Birmingham for the degree of

DOCTOR OF PHILOSOPHY

The Institute of Cancer and Genomic Sciences

College of Medical and Dental Sciences

University of Birmingham

July 2020

ABSTRACT

Acute myeloid leukaemia (AML) cells are located in the bone marrow, surrounded by a complex microenvironment, known as the niche. AML cells are known to interact and modulate niche components into their own support by secreting soluble factors and cytokines. For instance, crosstalk between AML and stromal cells was reported to confer chemoresistance to AML cells. Metabolism in haematopoietic stem cells (HSCs) and AML has been broadly investigated, nonetheless, few studies have focused on understanding metabolic alterations related to the interaction between stromal and AML cells. Identifying metabolic vulnerabilities derived from these interactions can yield novel targets for the development of new therapies.

In this thesis, the metabolic changes that AML and stromal cells display in co-culture compared to single cultures have been characterised using nuclear magnetic resonance spectroscopy. An increased release of acetate into the extracellular medium was found both in AML cell lines and primary AML cells co-cultured with stromal cells, compared to cells cultured alone. Moreover, this enhanced acetate secretion did not occur when using healthy donor cells. Interestingly, increased acetate secretion was also found to be contact dependent. Transcriptomic data revealed that co-culturing AML and stromal cells resulted in a complete rewiring of stromal metabolism. Stromal cell reprogramming included increased glycolysis, accumulation of pyruvate, and decarboxylation of pyruvate to acetate mediated by reactive oxygen species. Moreover, acetate secreted by stromal cells was found to be consumed by AML cells to further use it as a carbon source to replenish the tricarboxylic acid cycle.

Overall, a unique interaction between AML and stromal cells, resulting in a reprogrammed stromal metabolism and an acetate-mediated crosstalk, is presented in this study.

ACKNOWLEDGEMENTS

If there is something that I will always remember about this experience is the people that I got to share it with, that is why I am so grateful to have a long list of people to thank for.

First, I would like to thank my supervisors, Prof. Ulrich Günther and Dr. Paloma Garcia, for encouraging me in this adventure, allowing me to grow as a scientist and supporting me in every step. To Ulrich, for being so passionate and optimistic about my research and for always believing in me. And to Paloma, for adopting me into your group and for everything you have taught me since (in and out of science). Thanks for being so patient, attentive and caring, always having time to help everyone. It has been wonderful to work and learn from you.

I am also grateful to have been part of the Marie Curie HaemMetabolome-ITN and I want to thank everyone that made it possible. I also want to thank Greg for performing the RNA sequencing analysis (and for showing me the best places in Birmingham!). I want to give a special thanks to Prof. J.J. Schuringa, Alan Cunningham and Aysegül Erdem for welcoming me into their lab and helping me with primary samples, and for saving some time to take me out in Groningen.

I could have never done this thesis without the help and support of my two teams. From Ulrich's group, I want to thank Raquel, Jennie and Zuhal for all the help in and out of the lab and for always being ready to have coffee, dinner or spend the whole night playing games. It has been amazing to follow your steps. I would also like to thank Michelle for all the help with NMR-related problems. From Paloma's group, I want to thank Dan for all the help and for being my personal English teacher (and party mate), and Ruba for being the kindest and sweetest lab partner, and for helping with the primary samples. I also want to give a big thanks to all the past and present members of the team that I got to share this experience with: Yara, Ciara, Elena,

Doris, Connor, Miriam, Fiona, Mohannad and Giacomo. It has been fantastic to work with you all and I will always remember all the happy memories in the lab. I cannot forget to thank Cristina, even though she is not part of these teams, for being my Spanish support during lunch and coffee breaks.

I would like to thank Sara, Mark, Sue and Karen from the HWB-NMR facility for ensuring that the NMR experiments were always running smoothly and always having time to share their NMR knowledge and help me out. I also want to thank Christian for all the NMR lessons and scientific discussions.

I am also deeply grateful to Gaëlle, my housemate/partner in crime during all these years. I couldn't imagine someone better than you to share the PhD experience. You have been my strongest support, always there, ready to cheer me up with a coffee, drinks or amazing Belgian/Italian food. Thank you for giving me such good memories to remember, you have made this adventure so much more fun and have been, since the first day, a true friend to me.

Of course, I could have never finished this thesis without the support of my parents and my sister. Thank you for always being there for me, for helping and encouraging me through the distance and for making me feel at home when I most needed it. This wouldn't be possible without all your love and support.

To Carlo, there are not enough words to thank you for everything you have done for me during these (almost) four years. You have been strong and patient for both of us, being always there for me through endless calls (you have even become an expert in leukaemia and NMR), and you have made me happy even in the worst moments.

PUBLICATION CONTRIBUTIONS

- **Vilaplana Lopera, N.**, Almaghrabi, R., Papatzikas, G., Cunningham, A., Schnuetgen, F., Cazier, J. B., Schuringa, J. J., Reed, M., Garcia, P. and Günther, U. L. Crosstalk between AML and stromal cells triggers acetate secretion through the metabolic rewiring of stromal cells. *In preparation*.

- Wierenga, A.T.J., Cunningham, A.*, Erdem, A.*, **Vilaplana Lopera, N.***, Brouwers-Vos, A. Z., Pruis, M., Mulder, A. B., Günther, U. L, Martens J. H. A., Vellenga, E. and Schuringa J. J. HIF1/2-exerted control over glycolytic gene expression is not functionally relevant for glycolysis in human leukemic stem/progenitor cells. *Cancer Metab* **7,** 11 (2019). https://doi.org/10.1186/s40170-019-0206-y

  * *Equal contribution*

- Blakemore, D., Almaghrabi, R., **Vilaplana, N.**, Gonzalez, E., Moya, M., Murphy, G., Stewart, G., Gambus, A., Petermann, E. and Garcia, P. An ATM-MYBL2-CDC7 axis regulates replication initiation and prevents replication stress in pluripotent stem cells. *bioRxiv* 2020.06.04.131276. https://doi.org/10.1101/2020.06.04.131276

TABLE OF CONTENTS

LIST OF FIGURES

LIST OF TABLES

LIST OF ABBREVIATIONS

AA	Amino acid
ACLY	ATP citrate lyase
ACSS1	Acetyl-CoA synthetase 1
ACSS2	Acetyl-CoA synthetase 2
ACSS3	Acetyl-CoA synthetase 3
ALL	Acute lymphocytic leukaemia
AML	Acute myeloid leukaemia
ANGPT1	Angiopoietin 1
ASL	Argininosuccinate lyase
ASS1	Argininosuccinate synthetase-1
ASXL1	Additional sex comb-like
B2M	β2 microglobulin
BCAA	Branched-chain amino acid
BCAT1	Branched-chain amino acid transaminase 1
BIRD	Bilinear rotation decoupling
BSA	Bovine serum albumin
CAF	Cancer-associated fibroblasts
CAR	CXCL12-abundant reticular
CEBPA	CCAAT enhancer binding protein α
CFSE	Carboxyfluorescein succinimidyl ester
CLL	Chronic lymphocytic leukaemia
CLP	Common lymphoid progenitor
CML	Chronic myeloid leukaemia
CMML	Chronic myelomonocytic leukaemia
CMP	Common myeloid progenitor
CXCL12	CXC chemokine ligand 12
CXCL4	CXC-chemokine ligand 4
CXCR4	CXC chemokine receptor 4
DCFH-DA	2′,7′-Dichlorofluorescin diacetate
DHAP	Dihydroxyacetone phosphate

DKK1	Dickkopf-related protein 1
DMSO	Dimethyl sulfoxide
DNMT3A	DNA methyltransferase 3A
EDTA	Ethylenediaminetetraacetic acid
EGLN1	Egl-9 hypoxia inducible factor 1
FAB	French-American-British
FACS	Fluorescence-activated cell sorting
FADH2	Flavin adenine dinucleotide reduced
FBS	Foetal bovine serum
FDA	Food and Drug Administration
FDR	False discovery rate
FID	Free induction decay
FLT3	Fms-like tyrosine kinase 3
G6PD	Glucose-6-phosphate dehydrogenase
GAP	Glyceraldehyde 3-phosphate
G-CSF	Granulocyte colony-stimulating factor
GFP	Green fluorescent protein
GMP	Granulocyte-macrophage progenitor
GSEA	Gene Set Enrichment Analysis
HBSS	Hank’s Balanced Salt Solution
HIF	Hypoxia-inducible factor
HK2	Hexokinase-2
HMDB	Human metabolome database
HRP	Horseradish peroxidase
HSC	Haematopoietic stem cell
HSQC	Heteronuclear single quantum coherence
IDH	Isocitrate dehydrogenase
IGF-1	Insulin-like growth factor 1
IL	Interleukin
INEPT	Insensitive nuclei enhanced by polarisation transfer
LDHA	Lactate dehydrogenase A

LSC	Leukaemic stem cell
LT	Long-term
MACS	Magnetic-activated cell sorting
MCT	Mono-carboxylate transporter
MDS	Myelodysplastic syndrome
MEP	Megakaryocyte-erythrocyte progenitor
MLL	Multi lineage leukaemia
MPN	Myeloproliferative neoplasm
MPP	Multipotent progenitor
MS	Mass spectrometry
MSC	Mesenchymal stem cell
NAC	N-acetyl-L-cysteine
NAD+	Nicotine adenine dinucleotide oxidised
NADH	Nicotine adenine dinucleotide reduced
NCS	Newborn calf serum
NF-κβ	Nuclear factor-κβ
NK	Natural killer
NMR	Nuclear magnetic resonance
NOESY	Nuclear Overhauser effect spectroscopy
NPM1	Nucleophosmin 1
NTC	Non-targeted control
NUS	Non-uniform sampling
OXPHOS	Oxidative phosphorylation
PAGE	Polyacrylamide gel electrophoresis
PBMC	Peripheral blood mononuclear cells
PBS	Phosphate buffered saline
PC	Pyruvate carboxylase
PCA	Principal component analysis
PCR	Polymerase chain reaction
PD-1	Programmed death protein 1
PDH	Pyruvate dehydrogenase

PDK	Pyruvate dehydrogenase kinase
PD-L1	Programmed death-ligand 1
PDVF	Polyvinylidene difluoride
Pen/Strep	Penicillin-streptomycin
PEP	Phosphoenolpyruvate
PFG	Pulse field gradient
PKM2	Pyruvate kinase isoform 2
PlGF	Placental growth factor
PPP	Pentose-phosphate patway
PQN	Probabilistic quotient normalization
RF	Radio frequency
ROS	Reactive oxygen species
RT	Real time
RUNX	Runt-related transcription factor
SCC	Squamous cell carcinoma
SCF	Stem cell factor
SDS	Sodium dodecyl sulfate
sgRNA	Single guide RNA
ST	Short-term
TCA	Tricarboxylic acid
TCI	Triple resonance cryoprobe
TET	Ten-eleven translocation
TGF-β	Transforming growth factor-β
TMSP	Tetramethylsilylpropanoic acid
TNF-α	Tumour necrosis factor alpha
TP53	Tumour protein 53
TPM	Transcripts per million
TPO	Thromopoietin
UMCG	University Medical City Groningen
UoB	University of Birmingham
VCAM1	Vascular cell adhesion molecule-1

VEGF	Vascular endothelial growth factor
WHO	World Health Organisation

1. Introduction

1.1. Stem cells and leukaemia

1.1.1. HSCs and the haematopoietic system

Haematopoiesis is the process of formation of all the different types of blood cells through several commitment and differentiation steps. Haematopoiesis is fundamentally a hierarchical system, with more immature cells at the top of the hierarchy and mature functional cell types at the base.

The classic haematopoiesis model is presided by haematopoietic stem cells (HSCs), which have the potential to self-renew and differentiate towards the different blood lineages on demand. HSCs were first identified in 1961 by Till and McCulloch [1], when haematopoietic colonies were discovered in irradiated mice that were subjected to bone marrow transplantations. HSCs can be divided into two subpopulations: the long-term (LT)-HSCs, which are defined by their long-term capacity to repopulate the haematopoietic system for more than 3-4 months [2]; and the short-term (ST)-HSCs, which have a short-term reconstitution capacity of less than one month, and reduced self-renewal ability [3] (Figure 1.1). LT-HSCs differentiate into ST-HSCs, their immediate progeny, and ST-HSCs subsequently differentiate into multipotent progenitor (MPP) cells. MPP cells are characterised by the lack of the capacity to reconstitute the haematopoietic system or to self-renew, they are not lineage committed and can differentiate into the lineage-restricted progenitors, the common myeloid progenitor (CMP) [4] and the common lymphoid progenitor (CLP) [5], which give rise to the myeloid and lymphoid lineages of blood cells, respectively. Common myeloid progenitors subsequently differentiate into other progenitors which are: (i) the megakaryocyte-erythrocyte progenitors (MEPs), which give rise to megakaryocytes and erythrocytes; and (ii) the granulocyte-macrophage progenitors (GMPs),

which can generate granulocytes (basophils, neutrophils and eosinophils), macrophages and myeloid dendritic cells (Figure 1.1). The common lymphoid progenitors give rise to B-cells, T-cells and natural killer (NK) cells, as well as lymphoid dendritic cells. All these differentiation steps are grouped in a tree-like hierarchic model in which transcription factors and cytokines are required to conduct each step [6].

Over the past several years, new findings have challenged the hierarchical view of haematopoiesis, as reviewed in [7, 8]. Single cell assays have revealed that haematopoiesis is a complex process where more subtypes of stem and progenitor cells than the classical description exist. For example, megakaryocytes have been reported to skip the hierarchical differentiation and be directly derived from HSCs [9]. Alternative representations of haematopoiesis have been proposed using trajectory lines of differentiation for the different types of cells in the HSC compartment [7]. However, further investigation along with optimisation of single-cell techniques and refinement of computational analysis will bring more insights on the complex process of haematopoiesis.

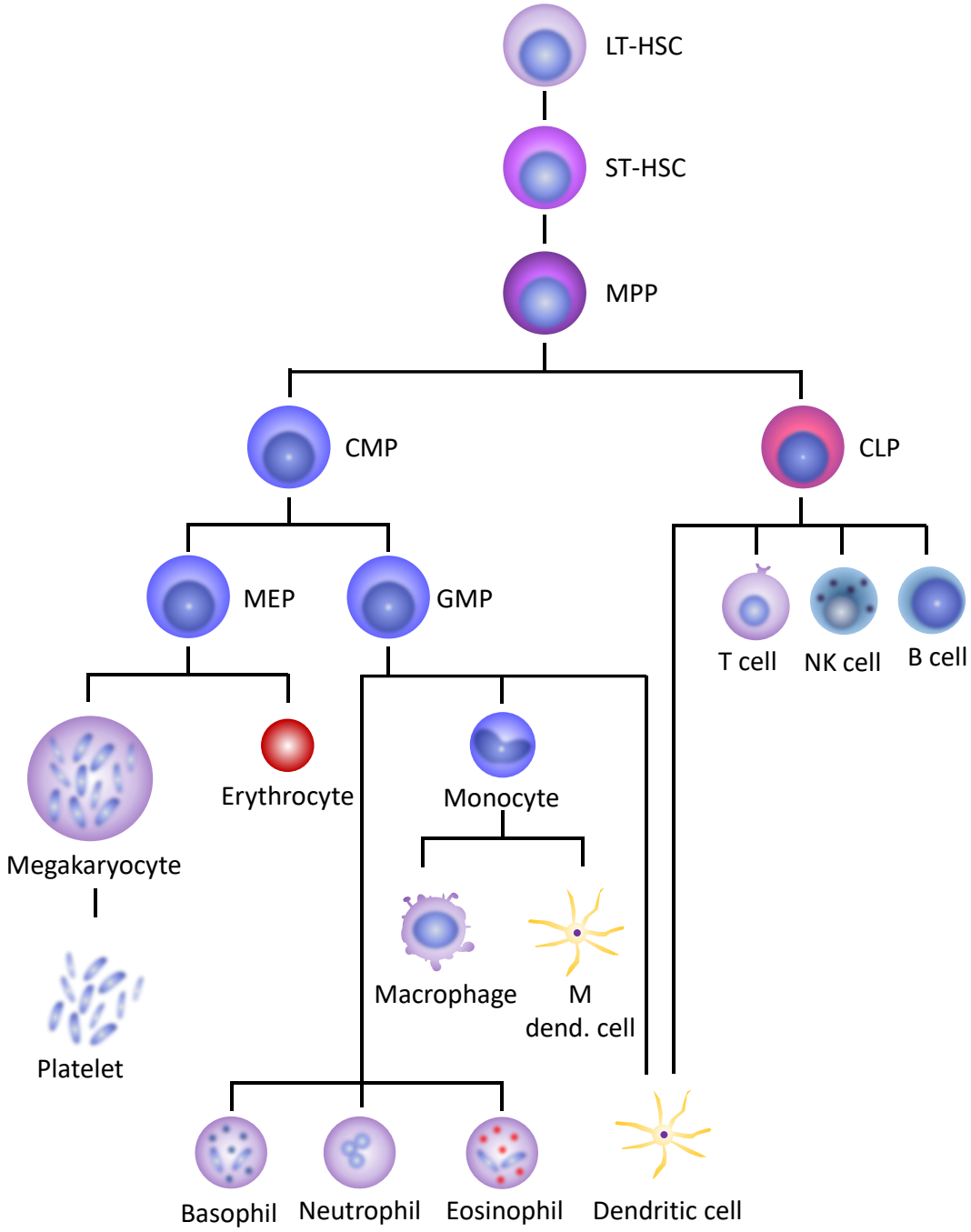

Figure 1.1 Scheme of differentiation in haematopoiesis.

Briefly, LT-HSCs differentiate into ST-HSCs and lose reconstitution potential and self-renewal capacities. ST-HSCs differentiate into the multipotent progenitors (MPP) which do not present self-renewal properties. MPPs differentiate into the common myeloid progenitor (CMP) and common lymphoid progenitor (CLP), which give rise to the myeloid and lymphoid lineages, respectively. The myeloid progenitor can differentiate into the megakaryocyte-erythrocyte progenitors (MEP), which give to megakaryocytes (and platelets) and erythrocytes, and the granulocyte-macrophage progenitors (GMP), which give rise to: basophils, neutrophils and eosinophils; macrophages and monocyte dendritic cells (M. dend. cell) through differentiation from monocytes; and dendritic cells. The CLP also gives rise to dendritic cells as well as T cells, natural killer (NK) cells and B cells.

In the adult stage and under normal conditions, HSCs remain in a quiescent state which ensures their capacity to repopulate the haematopoietic system and confers them protection from genotoxic insults [10]. The number of the different cell populations that conform the haematopoietic system needs to be tightly regulated, thus, the fate of HSCs into quiescence, self-renewal and differentiation must be finely tuned. HSC cells reside in the bone marrow surrounded by complex microenvironment composed of different cell types and extracellular elements. This microenvironment is broadly referred as the niche, and it has been shown to be responsible for regulating and maintaining blood production and immune cells. Components of the niche secrete various soluble factors and cytokines that regulate HSCs activity, as reviewed in [11, 12] and in section 1.2.1.1. Failure to this homeostasis would result in an imbalance on the proportion of HSCs leading to pathological conditions such as leukaemia.

1.1.2. Haematological malignancies: AML

Leukaemia can be defined as a group of haematological cancers that are characterised by a rapid proliferation and lack of differentiation of abnormal blood cells that impair normal haematopoiesis. Leukaemia can be classified according to: (i) the speed of progression, into acute or chronic forms; and (ii) the nature of the malignant cells found, into myeloid or lymphoid subtypes. This classification defines four subtypes of leukaemia: acute myeloid leukaemia (AML), chronic myeloid leukaemia (CML), acute lymphocytic leukaemia (ALL) and chronic lymphocytic leukaemia (CLL).

AML arises from the accumulation of genetic alterations in normal haematopoietic progenitor cells which lead to an excessive proliferation of a clonal population of aberrant immature myeloid cells that infiltrate the bone marrow, blood and organs severely impairing normal haematopoiesis. This malignant cell accumulation, along with the reduction of healthy and functional haematopoietic cells, results in a variety of symptoms including infection, bleeding, anaemia and organ infiltration [13]. AML can be acquired *de novo*, it can be derived from previous diseases such as myelodysplastic syndrome (MDS) or myeloproliferative neoplasm (MPN) (known as secondary-AML) or it can develop after treatment with cytotoxic agents (known as therapy-related AML) [14].

1.1.2.1. AML classification

There are two commonly used systems to classify AML: the French-American-British (FAB) classification and the World Health Organisation (WHO) classification. The FAB classification was proposed in the 1970's and it groups AML into 9 classes (M0 to M7) based on the cell type that originates the disease and the degree of maturity [15], as detailed in Table 1. The WHO classification was introduced in 1999 and includes other prognostic factors, such as

chromosome translocations and other molecular markers [16]. The WHO classification divides AML into six major subgroups (Table 2): AML with recurrent genetic abnormalities, AML with myelodysplasia-related changes, therapy-related myeloid neoplasms, AML not otherwise specified, myeloid sarcoma and myeloid proliferations of Down syndrome.

FAB classification of acute myeloid leukaemia

Subtype	Name
M0	Undifferentiated acute myeloblastic leukaemia
M1	Acute myeloblastic leukaemia with minimal maturation
M2	Acute myeloblastic leukaemia with maturation
M3	Acute promyelocytic leukaemia
M4	Acute myelomonocytic leukaemia
M4eos	Acute myelomonocytic leukaemia with eosinophilia
M5	Acute monocytic leukaemia
M6	Acute erythroid leukaemia
M7	Acute megakaryoblastic leukaemia

Table 1 French-British-American classification of acute myeloid leukaemia from 1976 [15].

WHO classification of acute myeloid leukaemia

Subtype	Genetic abnormalities
AML with recurrent genetic abnormalities	AML with t(8;21)(q22;q22);*RUNX1-RUNX1T1*
	AML with inv(16)(p13.1q22) or t(16;16)(p13.1;q22);*CFB-MYH11*
	APL with *PML-RARA*
	AML with t(9;11)(p21.3;q23.3);*MLLT3-KMT2A*
	AML with t(6;9)(p23;q34.1);*DEK-NUP214*
	AML with inv(3)(q21.3q26.2) or t(3;3)(q21.3;q26.2); *GATA2, MECOM*
	Megakaryoblastic AML with t(1;22)(p13.3;q13.3);*RBM15-MKL1*
	BCR-ABL1
	AML with mutated *NPM1*
	AML with biallelic mutations of *CEBPA*
	AML with mutated *RUNX1*
AML with myelodysplasia-related changes	
Therapy-related myeloid neoplasms	
AML not otherwise specified	AML with minimal differentiation
	AML without maturation
	AML with maturation
	Acute myelomonocytic leukaemia
	Acute monoblastic/monocytic leukaemia
	Pure erythroid leukaemia
	Acute magakaryoblastic leukaemia
	Acute basophilic leukaemia
	Acute panmyelosis with myelofibrosis
Myeloid sarcoma	
Myeloid proliferations related to Down syndrome	Transient abnormal myelopoiesis (TAM)
	Myeloid leukaemia associated with Down syndrome

Table 2 World Health Organization classification of acute myeloid leukaemia revised in 2016 [16].

1.1.2.2. Molecular and cellular heterogeneity in AML

The development of AML is linked with the acquisition of chromosomal rearrangements and gene mutations that result in increased proliferation and survival of an immature myeloid clonal population. Chromosomal translocations usually result in a loss of function of transcription factors that are crucial for normal haematopoietic development. However, the acquisition of chromosomal translocations is not sufficient to cause AML, and other activating mutations are necessary for aberrant cells to acquire proliferation and survival advantages. Therefore, the acquisition of genetic abnormalities in AML has been described as a two-hit event, where at least two classes of mutations need to take place for the development of AML [17]. The first class of mutations (Class I) are related to proliferation and survival whilst the second class of mutations (Class II) affect transcription factors and are related to the impairment of normal differentiation.

Some of the most common cytogenetic abnormalities found in AML include: monosomies or deletions in chromosomes 5 and 7; abnormalities in the long arm of chromosome 11 (11q); translocations in chromosomes, such as t(15;17), t(8;21) and t(9;11); rearrangements such as (q22;q22) and (q31;q22); and inversions such as inv(16) [18, 19].

The most frequent mutations found in AML include: disruption of nucleophosmin 1 protein (NPM1); the constitutive activation of Fms-like tyrosine kinase 3 (FLT3) due to internal tandem duplication in the juxtamembrane domain; alterations in DNA methyltransferases such as the DNA methyltransferase 3A (DNMT3A) and demethylases such as the ten-eleven translocation (TET) 2; mutations in the isocitrate dehydrogenase (IDH) 1 and 2; abnormalities in transcription factors such as the Runt-related transcription factor (RUNX) 1 and the CCAAT enhancer binding protein α (CEBPA); mutations in genes related to chromatin modification such as the

additional sex comb-like (ASXL1) and multi lineage leukaemia (MLL); deletions in the tumour protein 53 (TP53); and in several splicing factors such as *SRSF2*, *SF3B1*, *ZRSR2* and *U2AF* [20]. A summary of the listed mutations is depicted in Figure 1.2.

The pathogenesis and prognostic in AML are closely related to the types of chromosomal rearrangements and gene alterations acquired during the development of the disease. Some chromosomal translocations, such as t(8;21)(q22;22) or inv(16)(p13.1q22), are related with longer remission and survival, and others, such as alterations in chromosomes 5 and 7, are associated with poor prognosis and survival [21]. Other examples include patients with *NPM1* mutation and lack of *FLT3* mutation have a favourable prognosis whilst t(9;11) has been associated with a poor prognosis [22].

Although AML prognosis is related to genetic background, highly variable outcomes have been found between patients with the same cytogenetic and molecular profiles highlighting the presence of other sources of heterogeneity within cytogenetic/molecular AML subtypes [23]. This heterogeneity has been attributed to AML cells being organised hierarchically, with the presence of a subpopulation of self-renewing cells known as leukaemia stem cells (LSCs) at the apex of the hierarchy [24-26]. LSCs are functionally defined entities that do not necessarily derive from healthy HSCs, but their properties bear resemblance with HSCs. LSCs can self-renew, give rise to the non-LSC bulk AML cell population and remain quiescent [27]. All these features render LSCs more resistant to conventional therapies, which are focused on targeting the bulk of rapid proliferating cells. Therefore, to achieve long-term remission in AML, treatments must be aimed at targeting and eliminating the LSC population [28].

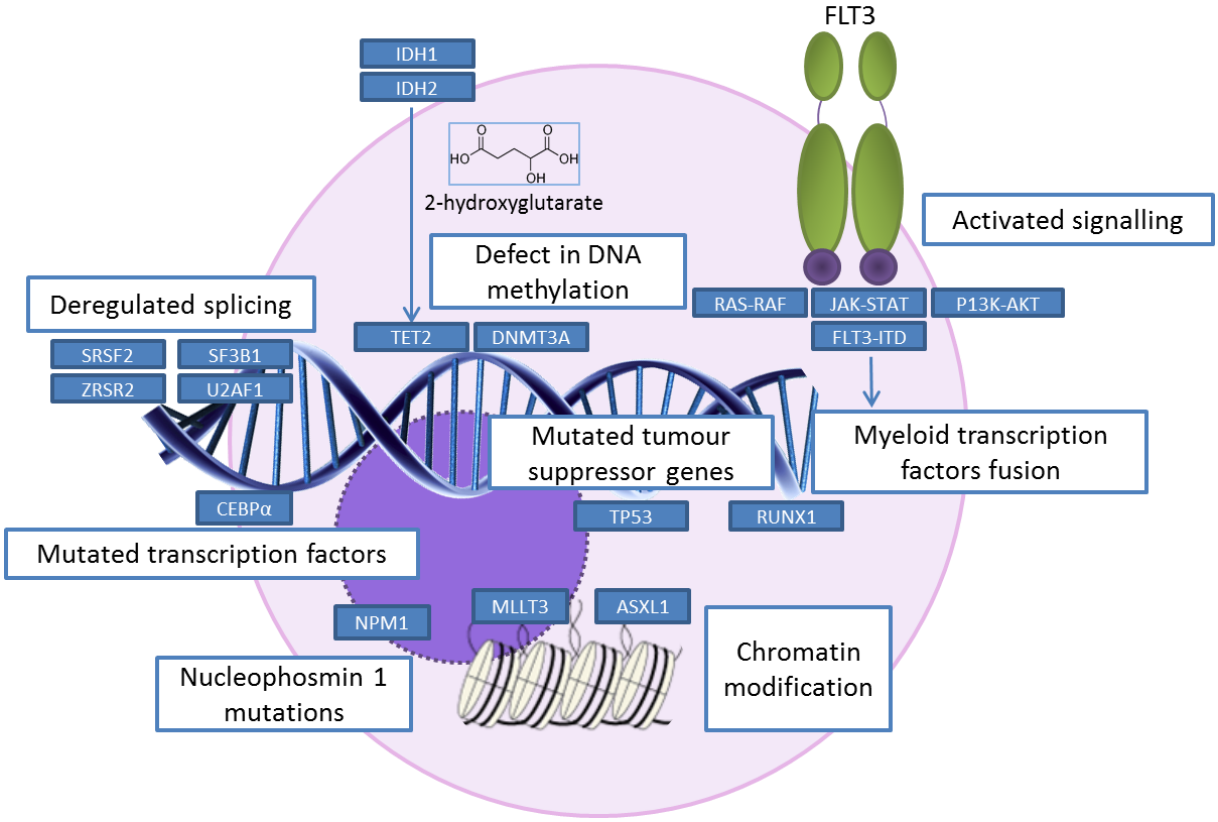

Figure 1.2 Most common genetic mutations (blue squares) in AML and their role.

1.1.2.3. AML treatment

AML treatment has remained mostly unchanged for decades since the induction chemotherapy and combination of anthracycline and cytarabine, also known as "7+3", was proposed in 1973 [29]. Initial treatment is often followed by allogeneic HSC transplantation to prevent relapse. Several attempts of improving the dosage of anthracycline and cytarabine followed during decades, with only a new agent (tretinoin) being approved for the treatment for the promyelocytic leukaemia in 1995 [30]. In the 2000, the Food and Drug Administration (FDA) approved a new agent, a drug-antibody conjugate against CD33 named gemtuzumab ozogamicin [31], for the treatment of old patients with relapsed CD33-positive AML. However, this treatment was withdrawn in 2010 due to lack of confirmatory trials. Hence, AML treatment remained mainly unchanged for more than 40 years and, thus, development of new therapies for AML seems crucial. Nonetheless, during 2017 and 2018, eight new treatments were approved by the FDA, including gemtuzumab ozogamicin at a new dose and schedule [32]. The other set of new agents are aimed at inhibiting FLT3, IDH1 and 2, at patients with comorbidities, and at patients with myelodysplasia related changes, as reviewed in [33].

Despite these improvements, new treatments are given to patients when not responding to the first line therapy "7+3", and, generally, only to patients that present specific mutations that can be targeted by the treatment. Therefore, improvements in AML therapy are necessary.

1.1.3. Metabolism in AML

Genetic alterations in leukaemic cells dictate how these malignant cells proliferate, differentiate and interact with the bone marrow microenvironment. Moreover, it has been shown that genetic alterations can also affect how AML cells obtain energy to fulfil proliferation and survival demands by presenting a reprogrammed metabolism. Altered metabolism is not only particular of AML cells but all cancer cells, and it is now considered one of the hallmarks of cancer [34]. Metabolic alterations in AML could be potentially exploited for the development of new therapies. In fact, this is not a new concept, as targeting of tetrahydrofolate metabolism with aminopterin, which was later substituted by methotrexate, was one the first successful trials using chemotherapy in ALL [35].

Aerobic glycolysis implies the conversion of glucose to lactate under normal oxygen conditions and fully functional mitochondria, and was first reported by Otto Warburg in the 1920s [36], where it was thought as a disfunction of mitochondrial metabolism rather than an ability of cancer cells. It is now clearer that, although it yields less energy than mitochondrial oxidative phosphorylation (OXPHOS) per round, aerobic glycolysis is an essential mechanism for cancer cells to grow. It has been proposed that not only cancer cells, but all proliferating cells utilise aerobic glycolysis to fulfil the demand for biomass, as the diverting pathways from glycolysis provide the necessary building blocks to incorporate nutrients into biomass. Additionally, aerobic glycolysis is 10 to 100 times faster than OXPHOS and, thus, can generate comparable amounts of energy [37].

AML metabolism, as many other cancers, is characterised by the utilisation of aerobic glycolysis [38] (Figure 1.3, green). Indeed, the glycolytic phenotype of AML cells was related to a worse prognosis [39], and the key genes in the synthesis of pyruvate and lactate, pyruvate

kinase isoform 2 (PKM2; *PKM2*) and lactate dehydrogenase A (LDHA; *LDHA*) respectively, were found to be critical for leukaemogenesis [40]. Moreover, FLT3 mutations were also linked with an increase in glycolysis due to upregulation of hexokinase-2 (HK2) [41]. Additionally, the enzyme that links glycolysis and PPP, glucose-6-phosphate dehydrogenase (G6PD), was also found indicative of adverse prognosis and its inhibition showed anti-leukaemic properties that synergised with the chemotherapeutic drug cytarabine [42]. This finding highlights the anabolic side of aerobic glycolysis, as the PPP is used to generate nucleotides (Figure 1.3, orange). Another interesting finding is that AML cells were found to use fructose to compensate for low glucose levels through the upregulation of the glucose transporter GLUT5 [43] (Figure 1.3, pink). Moreover, the study also reported that AML patients with high levels of GLUT5 were related to a worse prognosis, and the inhibition of GLUT5 was found to synergise with cytarabine.

AML cells rely on glycolysis (or fructolysis when glucose is scarce) to sustain their growth (Figure 1.3, green and pink). However, the activity of the tricarboxylic acid (TCA or Krebs cycle) cycle followed by the electron transport chain (Figure 1.3, blue), which provides energy through OXPHOS, is still essential for AML cells. Glutamine can be used as an alternative substrate to feed the TCA cycle, in a process known as glutamine anaplerosis or glutaminolysis [44] (Figure 1.3, yellow), and was reported to be crucial in AML [45-47]. Another alternative substrate to sustain the TCA and obtain energy are fatty acids. AML cells were reported to use fatty acids to obtain acetyl-CoA, flavin adenine dinucleotide reduced ($FADH_2$) and nicotine adenine dinucleotide reduced (NADH) through fatty acid β-oxidation [48-50] (Figure 1.3, purple). Acetyl-CoA can be further used for fluxing the TCA cycle and obtain energy through

OXPHOS. However, fatty acid synthesis was also reported to be high in AML and targeting fatty acid synthesis showed antileukaemic potential [51, 52].

The usage of OXPHOS in AML was found to be especially important in chemotherapy resistance. It was reported that chemo resistant AML cells displayed high levels of reactive oxygen species (ROS), which are generated as a by-product of the metabolism of oxygen, and an increase in mitochondrial mass, which were attributed to a high OXPHOS status [50]. In addition, targeting of the electron transport chain and, thus, OXPHOS metabolism [53-55] have shown potential in sensitising AML cells.

Restricting arginine levels was reported to reduce AML cell viability [56, 57], revealing that AML cells depend on this metabolite. Arginine is synthesised from citrulline by the argininosuccinate synthetase-1 (ASS1) and the argininosuccinate lyase (ASL) and is transported by the cationic amino acid transporters. It was reported that some AML cells lack ASS1 and can, therefore, depend on the import of arginine [57]. In another study, comparing the consumption of arginine in AML patients and healthy donors resulted in higher consumption by the AML patients [56]. Moreover, depletion of arginine intra- and extracellularly by using a human recombinant arginase (BCT-100) showed reduction of primary AML blasts and synergy with cytarabine [56].

Another potential dependence of AML cell is to branched-chain amino acids, as AML leukaemic stem cells were found to have the branched-chain amino acid (BCAA) pathway and BCAA transaminase 1 (BCAT1) upregulated [58]. In this study, knock-down of BCAT1 resulted in a growth and survival deficiency that was related to BCAA being responsible for oxoglutarate homeostasis, which acts as a cofactor of dioxygenase enzymes like the Egl-9 hypoxia inducible factor 1 (EGLN1) and TET family proteins.

Overall, AML metabolism relies on glycolysis and alternative fuels, such as fructose, glutamine and fatty acids, to fulfil the energetic demands and feed the TCA cycle and OXPHOS. However, other sources of carbon have been reported to be used by other types of cancer cells such as amino acids, lactate or acetate [59] and could also contribute to energy generation in AML cells. Metabolic studies in AML cells have opened new avenues for the development of novel therapeutic approaches. Nonetheless, studies of AML metabolism in the context of the haematopoietic niche are scarce [49, 60-62]. This type of studies are essential because AML cells are known to interact and modulate the niche into their own benefit through various mechanisms, including metabolism.

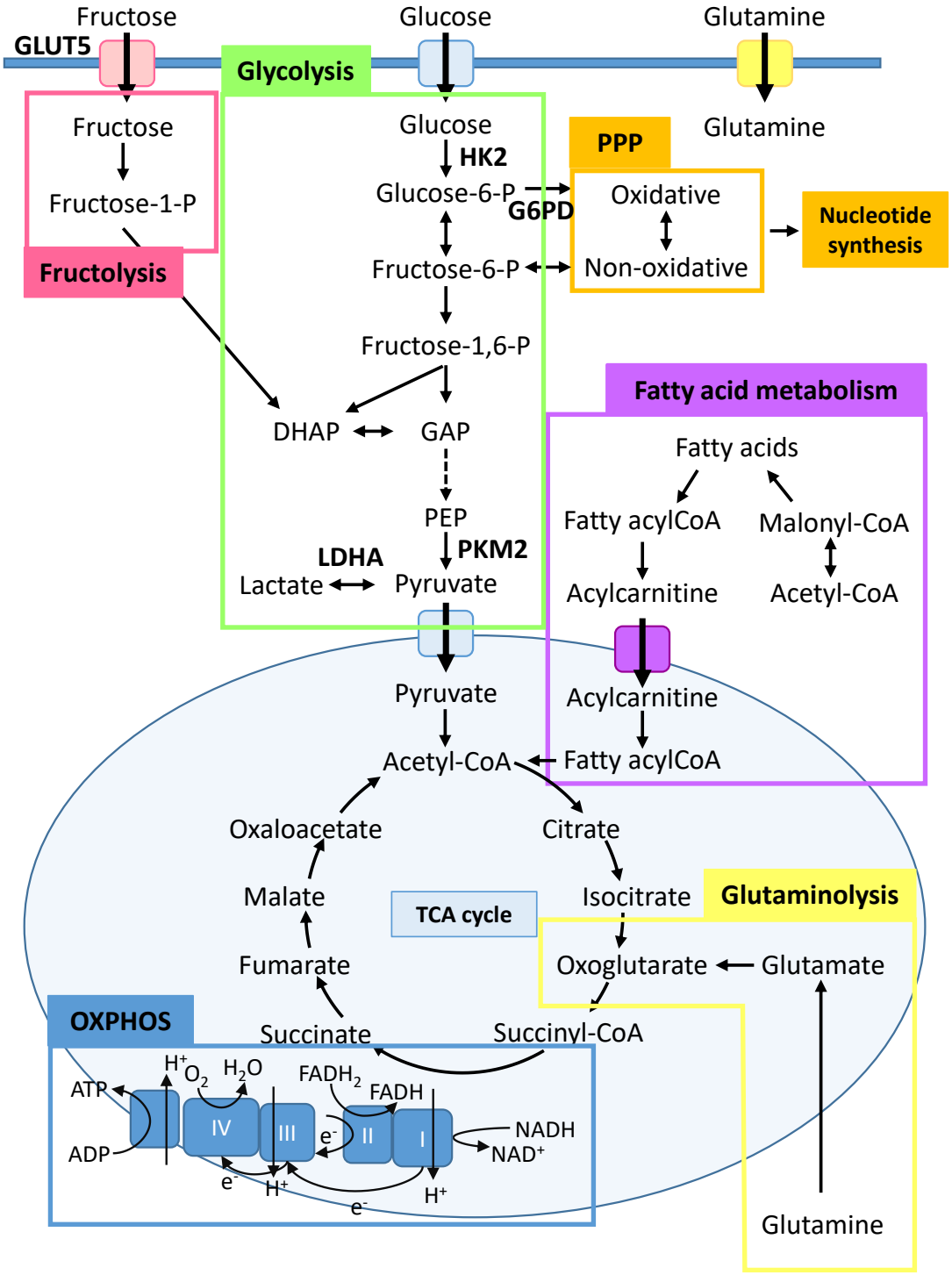

Figure 1.3 Scheme of metabolic pathways that are relevant in AML metabolism.

Simplified scheme of metabolic pathways that are relevant in AML metabolism. The name for each pathway is highlighted in each colour box. HK2, hexokinase 2; G6PD, glucose-6-phosphate dehydrogenase; PPP, pentose phosphate pathway; PKM2, pyruvate kinase M2; LDHA, lactate dehydrogenase A; DHAP, dihydroxyacetone phosphate; GAP, glyceraldehyde 3-phosphate; PEP, phosphoenolpyruvate; TCA, tricarboxylic acid; OXPHOS, oxidative phosphorylation. Based on [63].

1.2. The stem cell niche

HSC cells reside in the bone marrow surrounded by complex microenvironment composed of different cell types and extracellular elements. This microenvironment is broadly referred as the niche, and it has been shown to be responsible for regulating and maintaining blood production and immune cells [64].

Leukaemic cells bear resemblance with HSCs, including the interaction and dependence on bone marrow niches for proliferation, expansion and resistance to chemotherapy. Malignant haematological cells can interact with the niche transforming it into their own benefit via secretion of cytokines, soluble factors and extracellular vesicles, which results in an altered niche that cannot support HSCs and allows for the development of haematological diseases [65]. Moreover, there are several evidences pointing at the niche having a role in disease initiation and will be discussed below, in section 1.2.2.1.

1.2.1. The niche in health

HSCs are mainly located in the bone marrow where they exert the ability to self-renew, differentiate or stay quiescent. Despite HSCs being one of the most studied tissue specific stem cells, their maintenance and expansion *in vitro* is challenging, which has been attributed to the lack of signalling with the microenvironment, as reviewed in [12]. The first evidence for the importance of the niche as a regulator of the fate of HSCs was reported in 1978 by Ray Schofield [66], after observing that spleen HSCs were less able to regenerate haematopoietic cells in irradiated mice than bone marrow HSCs. Ever since, more evidence on HSCs interacting with the microenvironment, sustaining homeostasis in response to the needs of an organism for differentiation or preservation of the stem cell pool, has been gathered [65] and will be discussed below.

HSCs in the bone marrow reside in perivascular niches regulated by endothelial cells and mesenchymal stem cells (MSCs) [67]. Two anatomically distinct niches for HSCs have been proposed based on the proximity to the bone: the central niche [67] and the endosteal niche [68]. The central niche is situated in the inner bone marrow, accounting for more than 90% of the bone marrow volume, contains arterioles and sinusoids and includes 85% of all HSCs [69]. The endosteal niche locates proximal to the bone surface, contains the transition zone vessels [70] and includes approximately 15% of all HSCs.

It has been postulated that the functional role of both niches differs; the central niche is responsible for daily blood production of cells and is more susceptible to genotoxic damage by irradiation or myeloablation, whilst the endosteal niche is protected from these stresses and has been related to haematopoietic regeneration after chemotherapy [71]. HSCs migration from the endosteal to the sinusoidal niche is regulated by sympathetic nerves in the bone marrow [72]. Quiescence and haematopoietic lineage commitment were reported to be differentially regulated in the endosteal and sinusoidal niches. In the endosteal niche, quiescence is maintained by the secretion of several signals such as N-cadherin by N-cadherin^{+} bone-lining cells [71], CXC chemokine ligand 12 (CXCL12) by CXCL12-abundant reticular (CAR) cells [73] or granulocyte colony-stimulating factor (G-CSF) by osteoblasts [74], whilst in the sinusoidal niche, blood cells such as megakaryocytes have been reported to secrete factors to induce quiescence [75, 76]. Lineage commitment is biased towards the lymphoid lineage in the endosteal niches and towards the myeloid lineage in the sinusoidal niches, as evidenced by the loss of endosteal niches causing myeloid-biased differentiation during aging [77].

1.2.1.1. Niche regulation of HSC activity

Several niche components were found to be implicated in the regulation of the HSCs fate through the secretion of factors. Stromal-derived cells, such as osteoblasts, endothelial cells or adipocytes, and the HSCs' progeny, such as megakaryocytes, macrophages or T-cells, interchange a series of cytokines and soluble factors that are responsible for the maintenance, retention or quiescence of HSCs. A summary of the interactions between the niche and HSCs that regulate HSCs fate is depicted in Figure 1.4.

Osteolineage cells were the first niche cells that were proposed to present interactions with HSCs, as osteoblasts were found to be present in the endosteal region and it was reported that they could support the expansion of haematopoietic progenitors *in vitro* [74]. However, their role in regulating HSCs activity is controversial. Although osteoblasts were reported to secrete CXCL12 and stem cell factor (SCF), which are known to be related to HSC maintenance [73, 78], their deletion had little effect in the HSCs pool [79]. Osteoblasts secrete other molecules implicated in the preservation of HSCs such as osteopontin [80], thrombopoietin (TPO) [81] and angiopoietin 1 (ANGPT1) [82] that could regulate quiescence. However, it has been recently reported that megakaryocytes and leptin receptor-positive stromal cells are the main producers of ANGPT1 in the bone marrow of mice [83] and N-cadherin^{+} bone-lining cells have been reported to promote HSC maintenance by providing SCF [71].

Imaging of HSCs in their native microenvironment revealed that HSCs localised near sinusoids reside in perivascular niches [67]. Consequent studies reported that perivascular cells in the bone marrow express niche factors such as ANGPT1 [83], CXCL12, SCF, interleukin (IL) 7, vascular cell adhesion molecule-1 (VCAM1) and osteopontin [84], which were found to regulate the maintenance and attraction to the niche [85]. Moreover, the generation of a mouse

model expressing the GFP reporter under the control of the *Cxcl12* gene promoter revealed the existence of CAR cells located mainly around sinusoids [73].

Adipocytes were reported to impair the proliferation of haematopoietic progenitors through the secretion of the adiponectin protein [86]. Adipocytes were also suggested to act as negative regulators of HSC function due to several evidences: (i) lower density of haematopoietic progenitor cells in adipocyte-rich locations in the bone marrow [86]; (ii) higher HSC engraftment in mice with inhibited adipogenesis or genetically incapable of generating adipocytes [87]; and (iii) faster recovery after transplantation or chemotherapy when adipogenesis is inhibited [88].

Other cells that have been reported to have a role in the regulation of HSCs include endothelial cells, sympathetic nerve fibres and nonmyelinating Schwann cells. Endothelial cells, in the interior of blood vessels, secrete maintenance factors such as CXCL12 [89] and SCF [79], self-renewal factors such as Notch ligands [90] and pleiotrophin [91], and proliferation factors like E-selectin [92]. Sympathetic nerve fibres regulate HSCs migration [93, 94], and were related to HSCs' protection by activating recovery after genotoxicity through β-adrenergic signalling [95]. Nonmyelinating Schwann cells, which are glial cells that recover sympathetic fibres in the niche, were shown to promote HSC quiescence by secreting transforming growth factor-β (TGF- β) [96].

In addition to the regulation of HSCs by stromal niche components, haematopoietic progeny was shown to also regulate HSCs fate. Megakaryocytes were reported to regulate quiescence through the secretion of CXC-chemokine ligand 4 (CXCL4) [76], ANGPT1 [83] and TPO [75]. Depletion of macrophages was found to mobilize HSCs into the blood, through loss of osteoblasts responsible for HSCs retention in the niche [97]. Regulatory T cells have also been

recently reported to maintain HSC quiescence by generating adenosine that protects HSCs from oxidative stress [98]. Additionally, other factors that regulate HSCs can be generated from a distance, such as TPO, which has been reported to be a systemic factor secreted by the liver for maintaining HSCs [99].

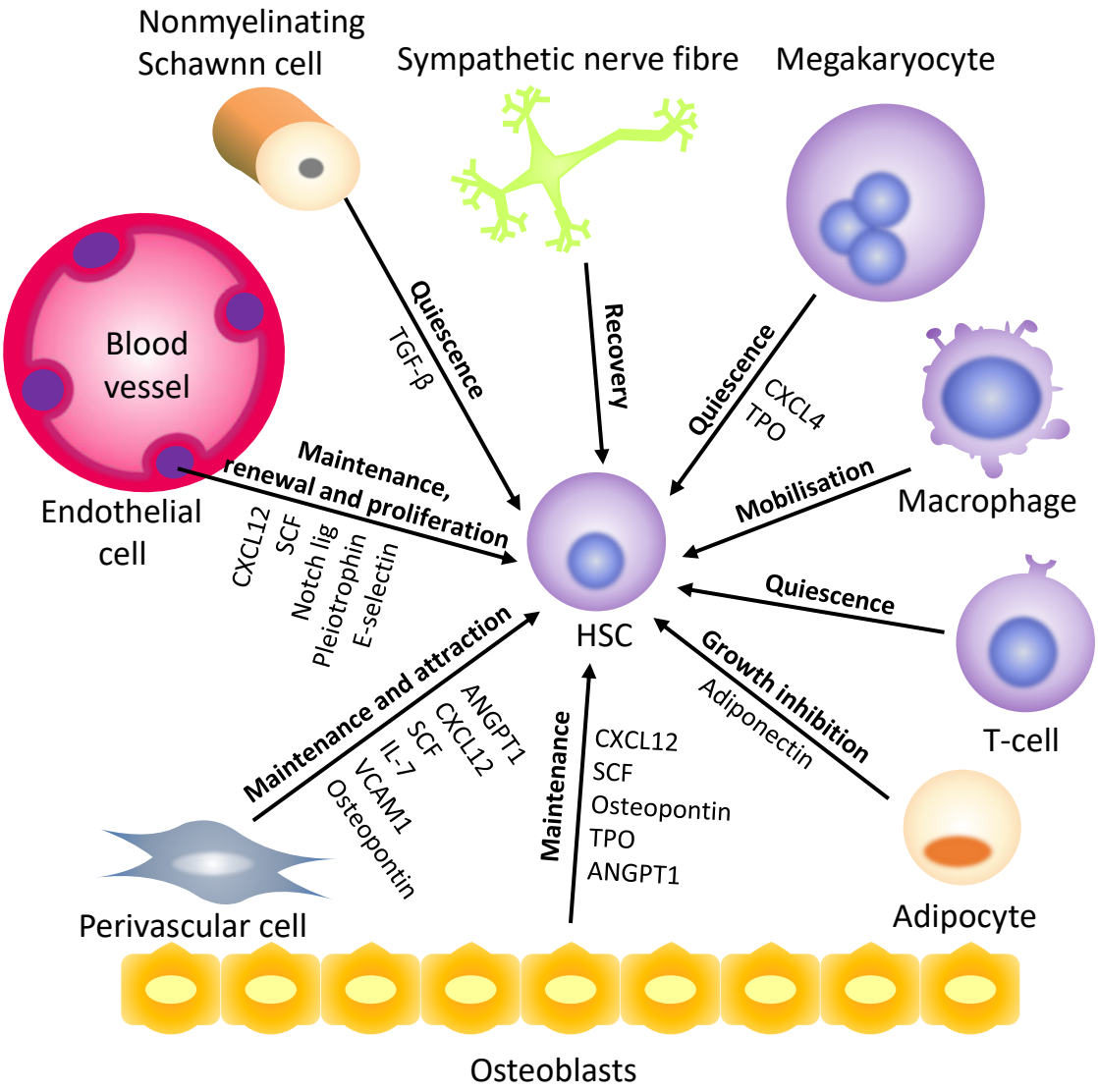

Figure 1.4 Summary of interactions between niche cells and HSCs.

HSCs reside within niches where other cell types regulate their function by secreting soluble factors and cytokines. Some of these interactions are direct and mediated by cytokines and soluble factors, such as the interactions with osteoblasts, adipocytes, megakaryocytes, nonmyelinating Schwann cells, endothelial cells and perivascular cells, whilst others, such as T-cells, macrophages and sympathetic nerve fibres, induce the secretion of soluble factors and cytokines by other cell types.

1.2.2. The malignant niche

The discovery of alterations in niche components during the development of haematological malignancies evidenced the cooperation between malignant and niche cells. Two non-mutually exclusive explanations have been proposed: (i) alterations in niche components can predispose or initiate the disease [100-102]; and (ii) malignant cells remodel the niche to facilitate invasion, progression and relapse [65].

1.2.2.1. The niche as an initiator of disease

Several studies have suggested that the niche could be the origin or could facilitate disease initiation. One of such evidences lies in rare cases where haematological malignancies derived from allogeneic HSC transplantation [103]. In those cases, it is thought that either the healthy donor cells carried mutations that originated the disease or healthy donor cells were transformed under the selective pressure of the recipient's niche becoming malignant.

An example of a possible role of the niche as an initiator of disease was reported in mice, where a deletion of the inhibitor-α of the nuclear factor-κβ (NF-κβ) specifically in non-haematopoietic cells led to the development of myeloproliferative malignancy [100].

Other examples of AML development from alterations in the niche include (i) the deletion of *Dicer1* in MSCs [101], which causes a myelodysplasia that can evolve to a secondary AML, and (ii) the activation of β-catenin in osteoblasts, which activates the Notch ligand jagged-1 and leads to AML development in mice [102].

1.2.2.2. Niche remodelling in haematological malignancies

Malignant cells are known to remodel the niche to promote their own survival. The mechanisms underlying malignant remodelling of the niche include inflammation, angiogenesis, cooperation with MSCs, aberrant osteogenic development, sympathetic nerve depletion and immune

evasion, as reviewed in [104] and discussed below. These alterations in the niche result in increased survival and proliferation, impairment of normal haematopoiesis and resistance to therapy and are mediated by a large set of cytokines and soluble factors released extracellularly as well as in extracellular vesicles, such as exosomes [105]. A summary of the interactions between AML and niche cells is depicted in Figure 1.5.

The link between the proliferation of malignant haematopoietic cells and inflammation was first established when it was discovered that individuals with chronic immune-stimulatory or autoimmune diseases presented higher risk of AML development [106, 107]. These studies suggested that the development of AML could be promoted by an aberrant pro-inflammatory cytokine expression. Since then, several reports have linked pro-inflammatory cytokines with haematological malignancies. For instance, it was reported that MSCs derived from MDS patients secreted higher levels of the inflammatory cytokines IL-6, IL-1β and tumour necrosis factor alpha (TNF-α) than normal MSCs [108, 109]. Moreover, IL-6 was reported to contribute to the development of CML [110, 111] and IL-1β was related to neural damage in the bone marrow in MPN [112].

Aberrant haematopoietic cells induce the secretion of angiogenic factors to increase the vascularisation of the niche and obtain oxygen, nutrients and other factors that help them survive [113]. The secreted angiogenic molecules include the family of vascular endothelial growth factors (VEGF) [114-116], including the placental growth factor (PlGF) [117], which is secreted by MSCs after the induction by CML cells. Additionally, it was reported that the transfer of VEGF could be mediated by exosomes [105]. The new vessels created by malignant cells present an abnormal morphology and are thought to cause vascular leakiness, which can lead to poor drug delivery, and increased hypoxia [118]. A new concept recently proposed is

that vasculature remodelling occurs differently in the central and endosteal niche. Intravital microscopy analysis of the calvarium bone marrow of a mouse model of AML revealed that AML cells secrete angiogenic factors in the central niche whilst, in the endosteal niche, AML cells secrete pro-inflammatory and anti-angiogenic cytokines that degrade the endosteal compartment impairing the support of the niche to healthy HSCs [119].

MSCs or stromal cells were found to increase the proliferation and survival of AML cells, and mediate the chemo resistance of AML through various mechanisms. Co-culturing AML with MSCs showed inhibition of drug-related apoptosis [120, 121]. Several mechanisms for the protective role of MSCs have been proposed, such as the secretion of soluble factors such as TGF-β and CXCL12 [122], mitochondrial transfer [61, 62] or gap junctions [123]. MSCs derived from AML patients have been recently shown to have a tendency to differentiate to adipocytes [124], which were found to feed AML cells back with fatty acids [60]. Moreover, MSCs derived from AML patients were reported to be aberrant and not able to support normal haematopoiesis [125]. Additionally, MSCs were found to protect and retain AML cells via the CXC chemokine receptor 4 (CXCR4)/CXCL12 axis, and its disruption increased the sensitivity of AML cells to chemotherapy [126, 127].

Alterations in the osteogenic compartment were also reported in haematological malignancies. For example, the osteoblast counts in human MDS and AML patients was found to be 55% lower than in healthy patients and depletion of osteoblasts in a murine AML mouse model was found to enhance disease development [128]. Moreover, aberrant osteogenic development was characterised by single-cell RNA sequencing in an AML mouse model [129]. Similarly, a loss of mature osteoblasts was reported in a mouse model of human T-ALL, resulting in a less efficient support of HSCs [130]. Additionally, exosomes secreted by AML cells were found to

induce the expression of the Dickkopf-related protein 1 (DKK1) in MSCs, which blocked osteolineage development and bone formation [131].

AML cells were also found to disrupt the sympathetic nerves on the bone marrow niche to promote disease progression and impair HSCs maintenance [132]. In this study, ablation of adrenergic nerves in mice resulted in a higher infiltration of AML stem cells and acceleration of the disease.

Finally, the immune system was also reported to have a role in the development of AML. AML cells can create an immunosuppressive microenvironment and dysregulate both the innate and adaptive immune responses, as reviewed in [133]. For instance, one of the mechanisms that AML cells use to escape the antitumour function of T cells is the upregulation of the programmed death-ligand 1 (PD-L1) which binds to the programmed death protein 1 (PD-1) of activated T cells [134]. Another mechanism proposed for immune evasion from T cells was mediated indirectly by the generation of acidic and hypoxic conditions through AML metabolism [135, 136], which is primarily glycolytic, as reviewed in section 1.1.3.

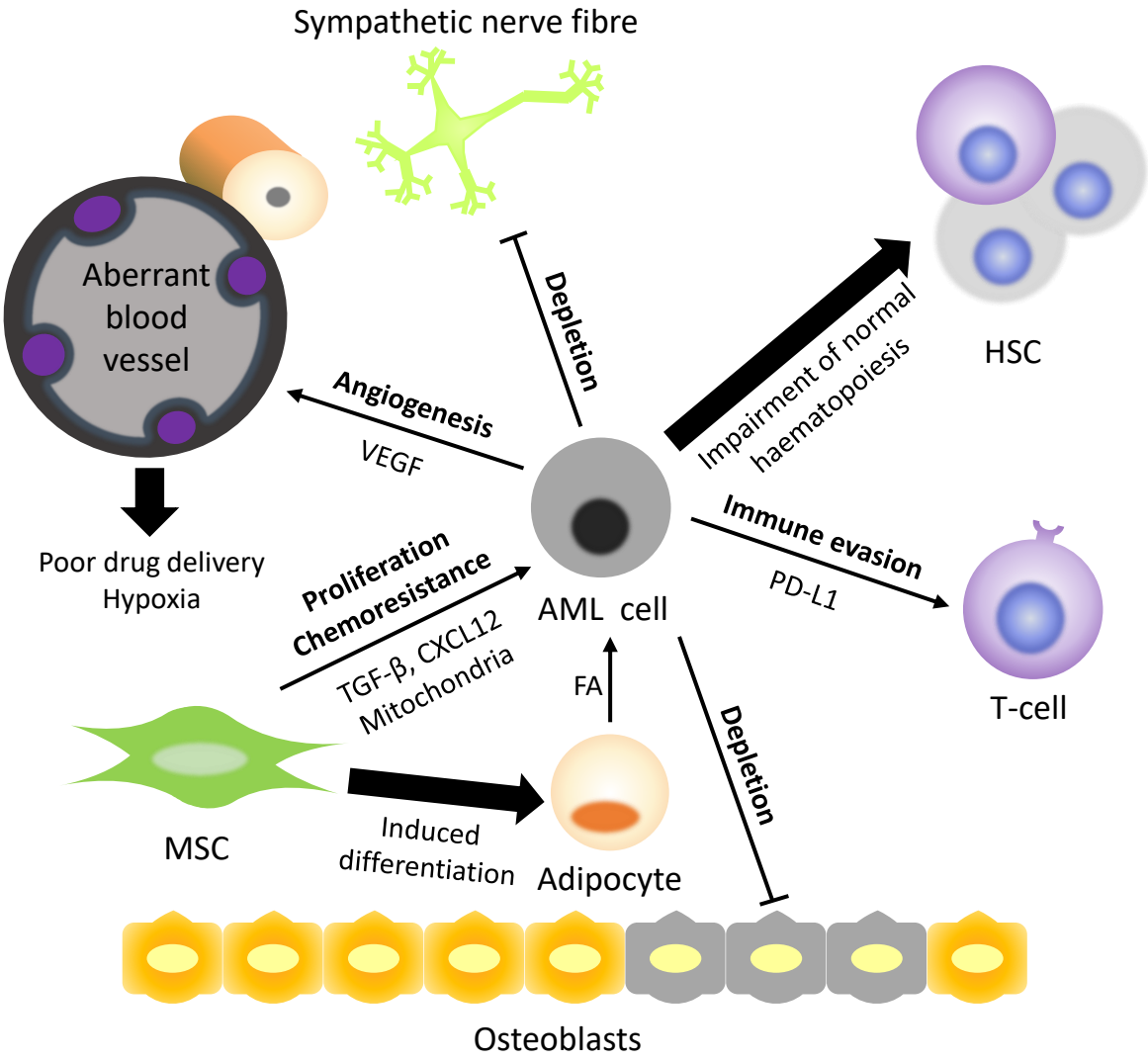

Figure 1.5 Summary of interactions between AML cells and niche cells.

AML cells invade the haematopoietic niches and modify several cell types into their own benefit via the secretion of soluble factors and cytokines. Some of these interactions are direct (thin arrows), such as the secretion of the proliferation factors TGF-β and CXCL12 by MSCs, and some others are indirect and result from other interactions (thick arrows), such as the poor drug delivery and hypoxia in the niche (which derive from aberrant vascularisation). FA, fatty acids.

1.2.3. Metabolic interactions in the leukaemic niche

One type of communication between malignant and niche cells with growing importance is that of metabolic interactions and crosstalk mediated by metabolites. Metabolites are small molecules that can be easily transported from one cell type to another to overcome the limitations in nutrients and obtain energy.

Metabolic interchange between niche cells and cancer cells has been reported in several types of cancer, as reviewed in [137]. Niche cells can be reprogrammed by cancer cells into secreting metabolites to the extracellular medium that can later fulfil nutrient necessities of cancer cells. For instance, in pancreatic ductal adenocarcinoma, stroma-associated stellate cells have been reported to secrete alanine which is later consumed by cancer cells and is used to fulfil metabolic requirements such as non-essential amino acids, TCA and lipid biosynthesis [138].

In the context of haematopoietic disorders, AML-adipocyte crosstalk has started to gain importance in the recent years. AML cells have been reported to induce fatty acid secretion in adipocytes in co-cultures of patient samples *in vitro* and in patient-derived xenograft models [60]. The mechanism involves the induction of lipolysis in adipocytes followed by a subsequent secretion of fatty acids. AML cells benefit from the secreted fatty acids by metabolising them through β-oxidation to obtain energy. Similarly, another study showed that adipocytes can protect AML cells from apoptosis and ROS by secreting fatty acids, which increases fatty acid β-oxidation in AML cells [49]. Moreover, an increase in adipogenic potential was found in stromal cells derived from AML patients [124].

Similarly, it was found that CML cells can reside in gonadal adipose tissue, where they induce lipolysis and secretion of fatty acids which were used to fulfil their energetic needs and evade chemotherapy [139].

Another metabolic interchange occurring between niche and leukaemic cells was reported in CLL, where primary CLL cells used stromal cells to obtain cysteine and promote glutathione synthesis and be protected against drug cytotoxicity [140]. In this study, it was characterised that CLL cells presented limited ability to import cystine and further synthesise glutathione using its antioxidant properties to reduce ROS levels. Stromal cells converted cystine into cysteine and secreted cysteine to the extracellular medium; CLL cells consumed the secreted cysteine, enhancing drug resistance. Similar results were also reported in ALL [141], where, in addition to characterising stromal uptake of cystine and conversion to cysteine, the pharmacological depletion of cysteine resulted in a decrease in ALL survival and chemoresistance.

Finally, a crosstalk between stromal and AML cells not directly involving metabolites but mitochondria was reported by two different studies [61, 62]. Both studies reported that AML cells have the capacity to induce stromal cell secretion of mitochondria and increase their mitochondrial mass. It was reported that the mitochondrial transfer occurred through tunnelling nanotubes, as a response to oxidative stress, and that this transfer was enhanced by some chemotherapeutic agents.

1.2.4. The niche as a therapeutic target

The main purpose of studying the niche and the interactions with malignant cells is to design new therapies targeting elements of the niche or specific interactions between those elements and malignant cells. New therapies could be used in conjunction with existing treatments to increase the overall survival and minimize the downside effects of current treatments.

Several new therapies have been developed aiming at the detachment and mobilisation of aberrant haematopoietic cells from the niche to increase the efficacy of chemotherapy. One of such therapies was aimed at inducing the entrance of AML stem cells into the cell cycle by G-CSF treatment and resulted in increased apoptosis and elimination of AML stem cells in a mouse model of human AML [142]. Another approach was based on targeting the CXCR4/CXCL12 axis with an antagonist named plerixafor in combination with chemotherapy yielded positive results in refractory AML [143] and multiple myeloma [144] in phase I/II clinical studies. Additionally, an alternative inhibitor of CXCR4, named BL-8040, was tested in AML blasts *in vitro* and in a mouse model of human AML showing increased apoptosis [145]. Following a similar strategy, targeting of e-selectin, a membrane protein responsible for homing in the niche that binds to the hyaluronic acid receptor CD44 [146], with an antagonist (GM-1271) was also tested in multiple myeloma [147] and CML cell lines and mouse models [148] resulting in reduced chemoresistance and improved outcome, respectively. Likewise, a CD44 monoclonal antibody showed reduction of the leukaemic population in a mouse model of AML [149].

Targeting of angiogenesis with a monoclonal antibody against VEGF (bevacizumab), which is commonly used to treat several types of cancer such as colorectal cancer, metastatic breast cancer and glioblastoma (reviewed in [150]), in conjunction with chemotherapy was also tested

in relapsed or refractory AML patients with moderate results [151], although further tests in a different cohort of relapsed and refractory AML patients [152] and in elder patients [153] did not show any significant antileukemic activity.

Another strategy that has been recently proposed is based on targeting leukaemic cells by using a hypoxia-activated prodrug (TH-302) [154], which in the presence of oxygen undergoes redox cycling but under hypoxia is reduced to a DNA crosslinking alkylating agent able to target the leukaemic cells. This hypoxia-activated prodrug, as well as others (PR-104 [155] and evofosfamide [156]) are under clinical testing.

Other promising targets that have been proposed involve targeting nitric oxide production to reduce vascular permeability [118] and the inhibition of the fibroblast growth factor 2 [157], which is secreted via exosomes to protect leukaemia cells from tyrosine kinase inhibitors.

Therapies aiming at metabolic vulnerabilities in AML have also been proposed, such as the inhibition of fatty acid β-oxidation using etoxomir, which impairs the entry of fatty acids into the mitochondria by blocking the enzyme carnitine palmitoyltransferase 1 (CPT1), or ranozaline, which partially inhibits the final enzyme in the fatty acid β-oxidation pathway (3-ketoacyl CoA thiolase) to disrupt the interaction between AML and adipocytes [48, 49].

Overall, several therapies are currently being developed targeting interactions between leukaemic cells and the niche. However, AML treatment has barely changed for decades and, while new drugs are being tested in clinical trials, new treatments and strategies for targeting AML cells are crucial. Metabolism provides an exciting avenue as some aspects of cancer metabolism are ubiquitous to all cancer types and specific metabolic alterations can occur similarly in other diseases, thus, allowing for the repurpose of already existing drugs. For instance, the previously mentioned ranozaline, which partially inhibits fatty acid β-oxidation

and can interfere in the interaction between AML cells and adipocytes, is a currently used as a treatment for heart-related chest pain (angina) [158]. Therefore, a better understanding on how leukaemic cells communicate and benefit from metabolic interactions in the niche is crucial to find targets and develop novel treatments.

1.3. NMR as a tool to study metabolism

Metabolomics and metabolic tracing studies give insight on the intracellular and extracellular metabolite concentrations in biological systems to characterise cellular processes, the physiological state of the system or the response to stimuli. Metabolomics studies are focused on studying the dynamic concentrations of metabolites, whilst metabolic tracing studies involve the tracing of specifically labelled metabolites to model the usage of the metabolic pathways within a cell [159]. As metabolite levels and pathway flux information are complementary, complete metabolic understanding is best achieved by combining both approaches.

The main technical approaches in metabolic studies are mass spectrometry (MS) and nuclear magnetic resonance (NMR) spectroscopy as both techniques allow for the detection of various metabolites simultaneously. In MS, the identification and quantification of metabolites is based on their mass-to-charge ratio after ionisation. In metabolomics, MS is often coupled to a separation step prior to ionisation, which is usually liquid or gas chromatography. The sensitivity of MS allows to quantify metabolites at very low concentrations (femtomolar to attomolar) [160]. In NMR spectroscopy, the magnetic properties of atomic nuclei are used to provide structural information that allows to identify and quantify metabolites. Despite NMR spectroscopy not being as sensitive as MS, it is quantitative and reproducible, it allows for the analysis of positional isotopomer distributions, as well as, the isotope-filtering of a selection of molecules in a mixture, it does not require additional sample processing and it is non-destructive, thus, samples can be used for further analysis [161]. Moreover, NMR spectroscopy can be applied in the dynamic analysis of metabolism in tissues from living organisms.

1.3.1. NMR spectroscopy basic principles

NMR spectroscopy is an analytical technique that uses the magnetic properties of nuclei to obtain structural information of molecules. Nuclear magnetic resonance involves the excitation of nuclei, positioned in a constant and strong magnetic field, using oscillating electromagnetic fields that generate a resonance which results in the induction of a current in a receiver coil. The detected signal provides information on the chemical environment of the nuclei and can be interpreted in terms of structural and dynamic information allowing for the identification and quantification of molecules.

Rotating objects are characterised by an angular momentum which describes the tendency of a rotating object to continue to spin. If a rotating object is charged, its rotation will lead to the generation of a magnetic field. Although nucleons (protons and neutrons) are not classically spinning, they present an intrinsic angular moment known as the spin (*S*) which can be visualised by a vector pointing along the axis of rotation of a particle. The overall spin of the nucleus of an atom is described by the spin quantum number (*I*), which can be an integer or a half-integer. Some basic rules for establishing the spin quantum number include: (i) in atoms where the number of protons and neutrons are both even these vectors are paired against each other resulting in no overall spin, termed $I = 0$; (ii) if the number of protons and neutrons are both odd, the nucleus has an integer spin different from 0 (i.e. 1, 2, 3); and (iii) if the number of protons plus neutrons is odd, the nucleus has a half-integer spin (i.e. ½, 3/2, 5/2). Nuclei with ½ spin are broadly used in NMR spectroscopy, the most common ones being ^{1}H, ^{13}C, ^{31}P and ^{15}N [162].

Particles with spin have a corresponding magnetic moment which has been termed spin angular momentum. The size of the magnetic moment is characterised by the gyromagnetic ratio, which

is a property of individual nuclei (Equation 1) [163]. The gyromagnetic ratio is the constant of proportionality; it is measured in $rad^{-1}T^{-1}$ and is characteristic of each nucleus.

Equation 1

$$\mu = \gamma S$$

The magnetic moments associated with nuclear spins with spin I can have $2I + 1$ orientations. Therefore, the magnetic moments associated with a ½ nuclear spin, such as ^{1}H or ^{13}C, will present two possible orientations. In the absence of a magnetic field, the magnetic moments associated to ½ spin nuclei are randomly distributed. However, when a magnetic field of strength B_0 is applied in the z-axis, the magnetic moments orient with (α) or against the field (β), thus, generating two different energetic spin states (Figure 1.6A). The population of these states is determined by a Boltzmann distribution that depends on the strength of the magnetic field (B_0), the gyromagnetic ratio (γ) and Planck's constant (h) (Equation 2), where N_α and N_β are the number of nuclei in the α and β energy states, respectively. The distribution in both states is slightly biased towards the α state, leaving a net magnetisation vector in the direction of the external magnetic field (Figure 1.6B). [163]

Equation 2

$$\frac{N_\beta}{N_\alpha} = exp\left(-\frac{\gamma\ h\ B_0}{2\pi\ k\ T}\right)$$

When a radio frequency (RF) pulse, of a certain frequency and length, is applied in a different direction than the magnetic field, the magnetisation vector can be manipulated to shift towards the new field. The magnetisation vector then rotates around the external magnetic field axis following a precession movement at a certain frequency, which is known as the Larmor frequency and is specific to each nucleus (Figure 1.6C). The applied RF pulse is a small magnetic field that oscillates precisely at the Larmor frequency to be in resonance with the

nucleus. Therefore, even if the strength of the RF pulse is considerably lower than the strength of the external magnetic field, the RF pulse is able to shift the magnetisation vector [164].

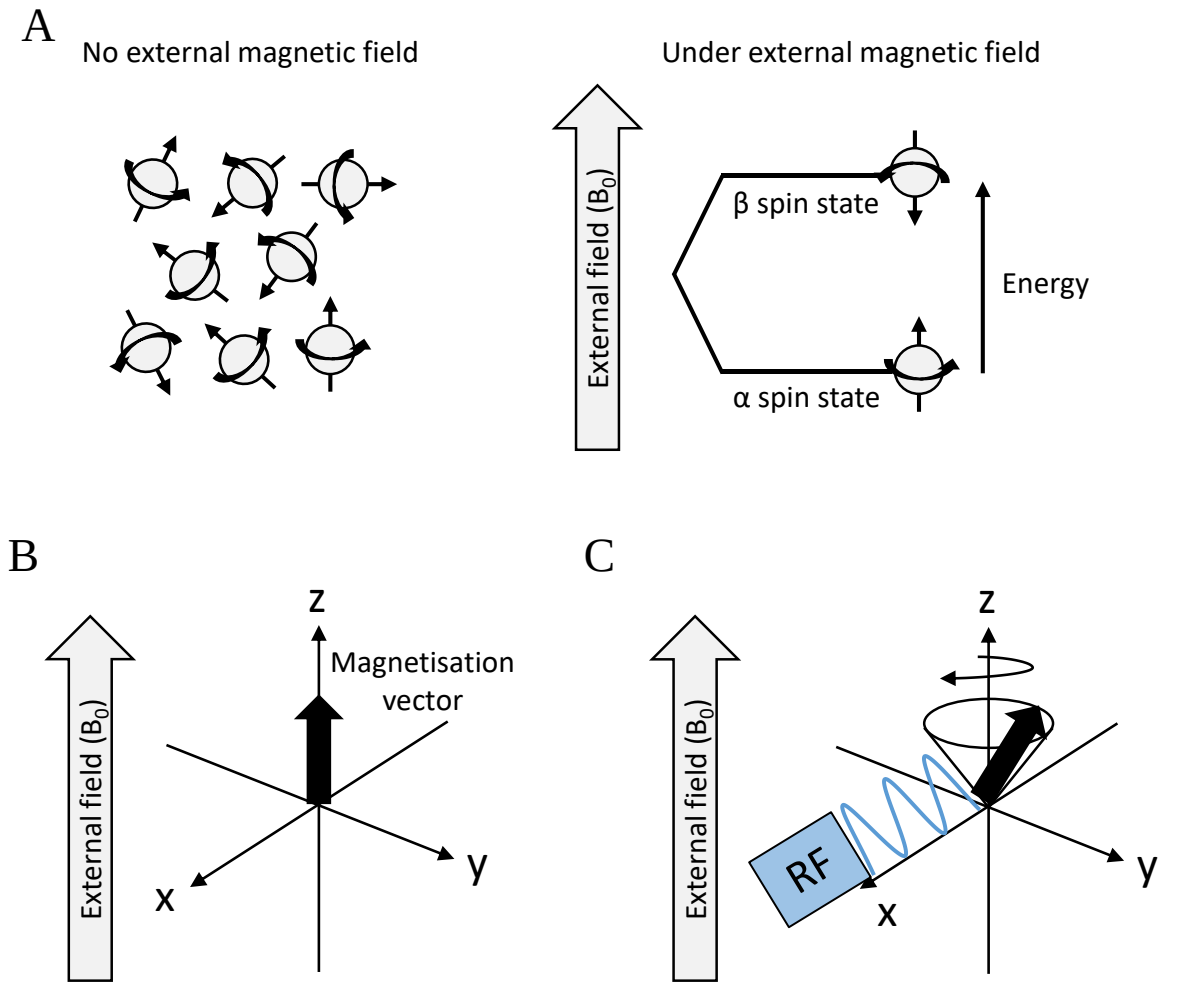

Figure 1.6 Schematic representations of the orientation of nuclear spins and the magnetisation vector under a magnetic field.

A) Schematic representation of the orientation of ½ nuclear spins with and without external magnetic field in equilibrium. Briefly, spins are randomly oriented when no magnetic field is present but tend to orient in favour (α) or against (β) the field when an external magnetic field is applied. The difference between both states is proportional to the gyromagnetic ratio (γ), the strength of the magnetic field (B_0) and Planck's constant (h). B) The α spin state is slightly more populated than the β spin state due to stability creating a net magnetisation vector in the direction of the external magnetic field. C) When a radio frequency pulse is applied from a different axis than the external field the magnetisation vector precesses around the axis of the external magnetic field.

The precession movement of the nuclei in the transverse plane (x, y) can be detected using a receiver coil where the nuclei induce an alternating electrical current. The recorded signal presents as a decaying complex exponential wave shape and is known as the free induction decay (FID).

When the RF pulse is stopped, the magnetisation returns to its equilibrium state in a process called relaxation. Relaxation can be divided into two different processes: a loss of signal intensity, expressed with the time constant T_1, and related to the magnetisation components that are parallel to the main field; and the second one associated with a broadening of the signal, with a time constant T_2, and related to the magnetisation components that are perpendicular to the main field.

The FID signal is the recorded observable NMR signal over time that is converted to a frequency-domain spectrum with a Fourier transformation. Frequencies in the spectrum are then converted to chemical shifts (δ), in parts per million (ppm), using a signal of a reference compound such as tetramethylsilane or tetramethylsilylpropanoic acid (TMSP) as indicated in Equation 3, where υ is the frequency of a signal, $\upsilon_{reference}$ is the signal of the reference compound and $\upsilon_{spectrometer}$ is the frequency of operation of the spectrometer. This standardisation allows to compare the frequencies in spectra obtained from different spectrometers that operate at different external magnetic field strength frequencies [163].

Equation 3

$$\delta = \frac{\upsilon - \upsilon_{reference}}{\upsilon_{spectrometer}} \times 10^6$$

Nuclei that present different chemical environments will resonate at different frequencies and, thus, be observed at different positions or chemical shifts within the spectrum. The chemical shift depends on the shielding of the external field (B_0) performed by the atom's neighbouring

electrons, where more shielded nuclei close to higher electron densities appear at lower chemical shifts (higher field) whilst less shield nuclei resonate at higher chemical shifts (lower field). As an example, the expected chemical shift ranges in ^{1}H-NMR are depicted in Figure 1.7.

Nuclei from the same molecule that are connected by chemical bonds can give rise to *J*-couplings. *J*-couplings arise from the interaction of two nuclear spins mediated by surrounding electrons giving rise to the signal splitting into multiple resonance lines. This multiple resonance lines appear because adjacent spins can have different orientations resulting in different energies. These multiple resonance signals distribute the signal intensity in smaller peaks, the multiplicity of those peaks gives information of the number of spins coupled to the signal of interest [164]. The intensity ratios of the multiple resonance signals can be predicted by Pascal's triangle. The magnitude of the *J*-coupling, known as the coupling constant, gives information about the proximity of the coupled nuclei and can be measured as the distance between the signals [163]. Coupling constants are measured in Hz and are independent of the strength of the external magnetic field. Couplings can occur between the same type of nuclei (e.g. ^{1}H-^{1}H) or between different types (e.g. ^{1}H-^{13}C) and can be supressed by selective radio frequency irradiation, in a process known as decoupling [165].

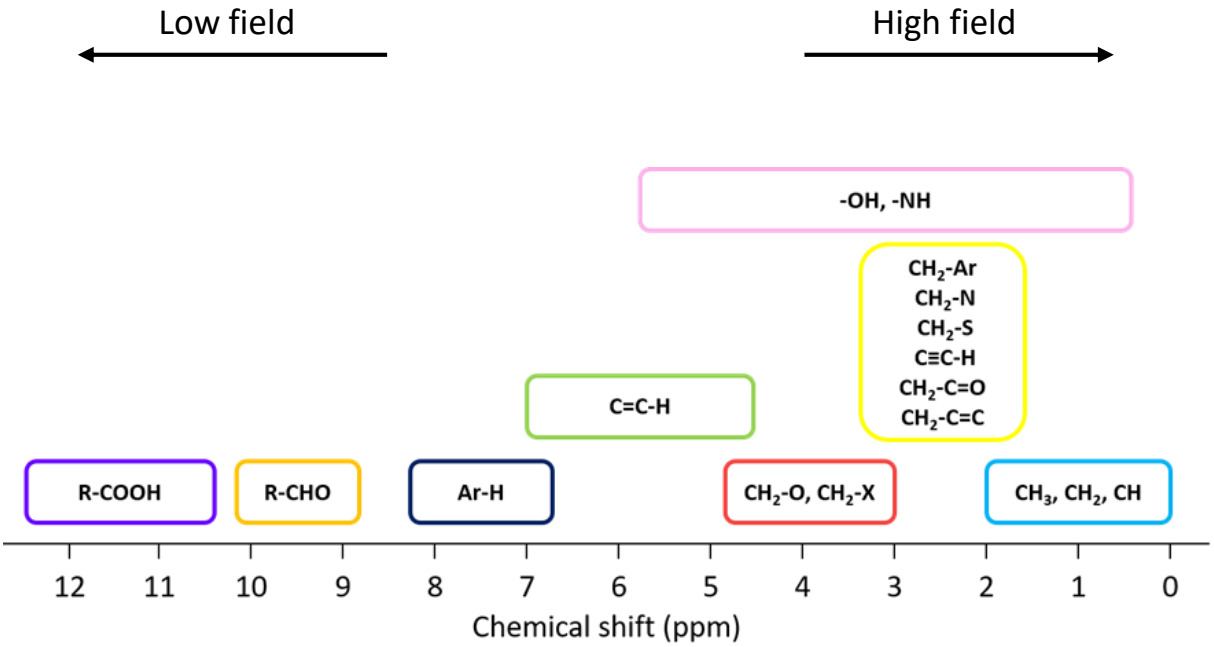

Figure 1.7 Schematic representation of ^{1}H expected chemical shift ranges of protons close to different functional groups.

Based on Paula Bruice's [166] book.

1.3.2. 1D and 2D NMR interpretation

The NMR spectrum contains structural and quantitative information about the molecule or molecules analysed. In metabolomics and metabolic studies, several types of experiments have been used to characterise intra- and extracellular metabolites and assess, for example, variations in metabolic pathways, production and consumption of metabolites or pH changes [167].

One of the approaches that can be used to obtain information about the composition and concentration in a mixture is 1D NMR spectroscopy, the most common type being ^{1}H-NMR spectroscopy [168]. In ^{1}H-NMR spectroscopy, magnetisation of ^{1}H nuclei is created by applying a series of radio frequency pulses and delays followed by the acquisition of the signal. In this type of experiment, samples are usually prepared in aqueous solutions and the experiment pulse sequence includes pre-saturation pulses to saturate and supress the water signal that would otherwise dominate the spectrum [169].

^{1}H-NMR spectra provide information about the metabolic composition and concentration in a sample. Metabolites can be identified according to the chemical shift and multiplicity of their signals. As an example, lactate has been assigned in a ^{1}H-NMR spectrum of medium from a cell line in Figure 1.8. The chemical shift of both signals appears at the expected regions, according to Figure 1.7, the proton at C2 (green) appears at a higher chemical shift than the methyl protons of C3 (blue) because the hydroxyl group in C2 reduces the shielding shifting the signal (green) to a higher chemical shift (lower field). The multiplicity of the signals depends on the *J*-coupling and, in the case of the protons in C3 (blue), appears as a doublet because the protons couple with the proton in C2 (green), which can only have two orientations, splitting the signal once into a doublet. In the case of the proton in C2 (green), the coupling occurs with the three equivalent protons in C3, each one having two possible orientations,

splitting the signal three times with the same separation or *J*-coupling (because the three protons are equivalent) and creating a quadruplet. The intensity ratios can be predicted by Pascal's triangle, for 3 adjacent protons there are 8 possible combinations (ααα, αββ, ββα, βαβ, βαα, αβα, ααβ, βββ) where two groups of 3 are degenerate (αββ, ββα, βαβ and βαα, αβα, ααβ) leading to a signal with intensities 1331.

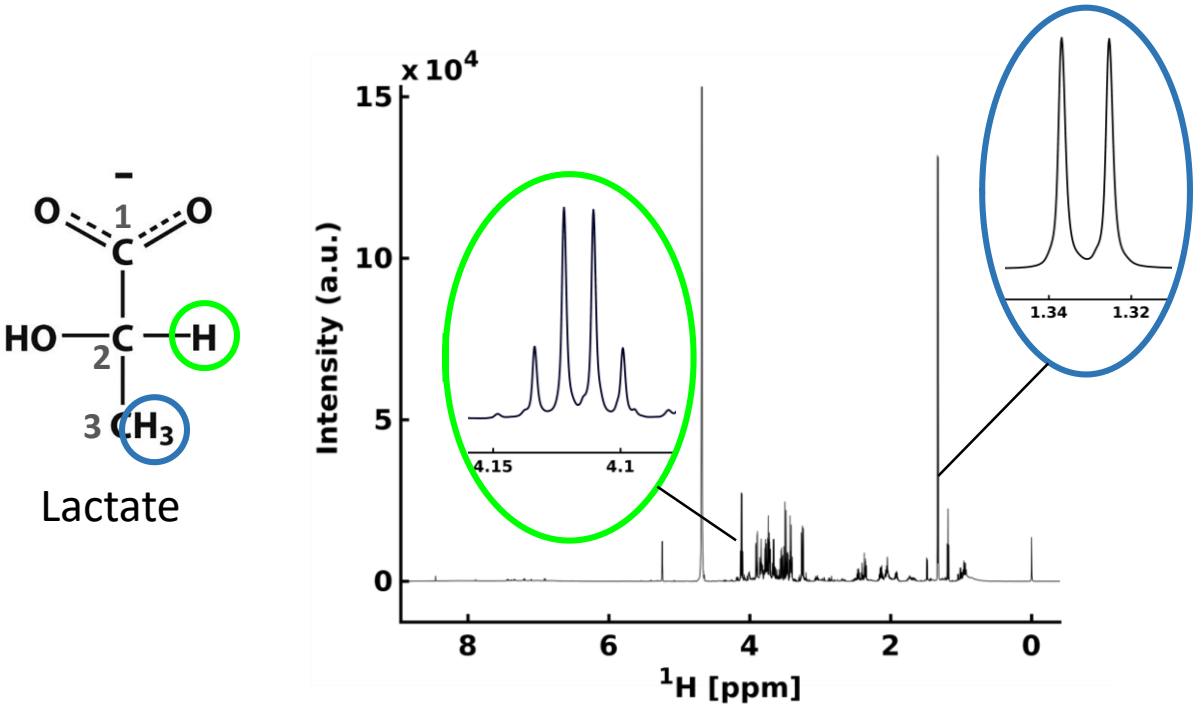

Figure 1.8 Example of a ^{1}H-NMR spectrum of a medium sample where the ^{1}H signals in lactate have been assigned.

^{1}H-NMR spectrum of a medium sample from SKM-1 cells in RPMI medium after 24 hours of incubation. The signals for lactate have been assigned: doublet corresponding to the protons in the methyl group in C3 at 1.33 ppm and the proton next to the hydroxyl group in C2 at 4.12 ppm.

Two-dimensional spectra can correlate two nuclei to obtain molecular information about connectivity either through chemical bonds, with experiments such as the heteronuclear single quantum coherence (HSQC), or through space, with experiments such as the nuclear Overhauser effect spectroscopy (NOESY). In such 2D NMR spectroscopy two types of nuclei are analysed simultaneously by adding additional RF pulses that transfer the magnetisation from one nucleus to the other before an evolution period followed by the detection of the signal. The signal is allowed to evolve yielding a series of FIDs that, after being transformed to frequencies, conform a 2D frequency spectrum. In a 2D spectrum, the chemical shifts of each type of nuclei are represented in an axis and the intensity is represented as a contour. These experiments are especially useful to resolve signals that overlap in 1D spectra [170].

One of the 2D NMR experiments used in this thesis is the 2D-HSQC NMR spectroscopy [171]. In a ^{1}H-^{13}C-HSQC spectrum each signal indicates the presence of a ^{13}C bound to a ^{1}H and allows to see coupling between ^{1}H-^{1}H, as in ^{1}H-NMR spectroscopy, and ^{13}C-^{13}C. An example of a ^{1}H-^{13}C-HSQC from intracellular metabolites of cells incubated with uniformly labelled glucose ([U-^{13}C] glucose) is shown in Figure 1.9A, where lactate signals have been assigned. It is important to note that lactate derived from uniformly labelled glucose through glycolysis can present all the carbons labelled, because all positions remain labelled in glycolysis when glucose is split into DHAP and GAP. The chemical shift of both signals in the ^{1}H dimension correlates with the ^{1}H-spectrum from Figure 1.8. In the ^{13}C dimension the chemical shift of C2 (green) is higher than C3 (blue) due to a de-shielding effect from the carboxylic group in C1. The C3 signal (blue) has a triplet multiplicity which can be explained by the sum of singly labelled C3, which may represent the natural abundance ^{13}C, (central signal, blue) and the coupling to C2 which splits the signal in a doublet (outer peaks, blue). The C2 signal (green) is

coupled to both C3 and C1 but, as both carbons are not equivalent, the *J*-coupling is different for each coupling splitting the signal twice and generating a doublet of doublets (green).

Obtaining label incorporations from HSQC spectra is not trivial as the natural abundance of ^{13}C (1.1%) can lead to a misinterpretation of the total amount of labelling in a sample. Several approaches have been proposed, one of them being the combination NMR spectroscopy and MS analysis, using simulations of the *J*-couplings combined with the mass isotopologues [172]. Another approach using NMR spectroscopy exclusively, which was used in this thesis, is to analyse an unlabelled reference sample, which only contains natural abundance ^{13}C, together with the labelled sample [173]. In this approach, the ^{13}C from the unlabelled reference sample is then subtracted to the labelled sample to obtain the total label incorporation. The advantage of this approach is that only one technique (NMR spectroscopy) is needed. However, there are a couple of disadvantages to this approach: (i) generating exact same samples, labelled and unlabelled, is not possible with biological samples and, therefore, an approximation is made; and (ii) if the intensity of a signal is too low in the reference unlabelled sample the metabolite cannot be assigned due to lack of sensitivity.

An alternative NMR-approach that does not require the usage of an unlabelled sample that has been recently reported is the use of ^{13}C-edited [174] and ^{13}C-filtered [175] spectra. In these filtered experiments, the pulse sequences use gradient bilinear rotation decoupling (BIRD) [176], tailored to filter the ^{13}C-bound protons yielding only the ^{12}C-bound protons [175]. Moreover, another spectrum with the total pool of protons (bound to ^{12}C and ^{13}C) is also obtained, allowing for the obtention of the ^{13}C-labelled fraction by subtraction of the ^{12}C-fraction from the total proton spectrum. In the ^{13}C-edited experiments [174], another mechanism, using similar spectral filters, is applied to obtain the ^{13}C-bound fraction.

In both cases acquiring a spectrum with the total carbons (^{12}C and ^{13}C) bound to protons allowing for the quantification of label incorporation in a range of metabolites, by obtaining the fraction of ^{13}C-labelled protons of the total pool of protons.

The advantage of this experimental approach is a higher sensitivity compared to an HSQC spectrum, as only the labelled sample is needed, but at the cost of lacking a second dimension which is often needed to resolve overlapping signals, which results in the identification of a smaller subset of metabolites.

An example of the different ^{1}H-spectra obtained in a ^{13}C-filtered experiment are depicted in Figure 1.9B. To determine the label incorporation the area of the signal of a certain metabolite in the ^{13}C-bound ^{1}H-spectrum (blue) is divided by the area of such metabolite in the total C-bound ^{1}H-spectrum (green).

Alternative approaches for metabolic tracing have been described including: (i) 1D ^{13}C-NMR spectroscopy [177], which enables an easy analysis of the ^{13}C distribution in a sample but is less sensitive than ^{1}H-based spectroscopy; (ii) 2D-^{1}H,^{1}H TOCSY spectroscopy [178], which allows for quantification of the ^{13}C percentages in ^{13}C-labelled samples but requires long acquisition times and is subject to spectral overlapping; and (iii) the previously discussed combination of NMR and MS data to obtain isotopomer contributions [172], which overcomes the problem of spectral overlapping and increases data consistency due to the usage of two orthogonal techniques.

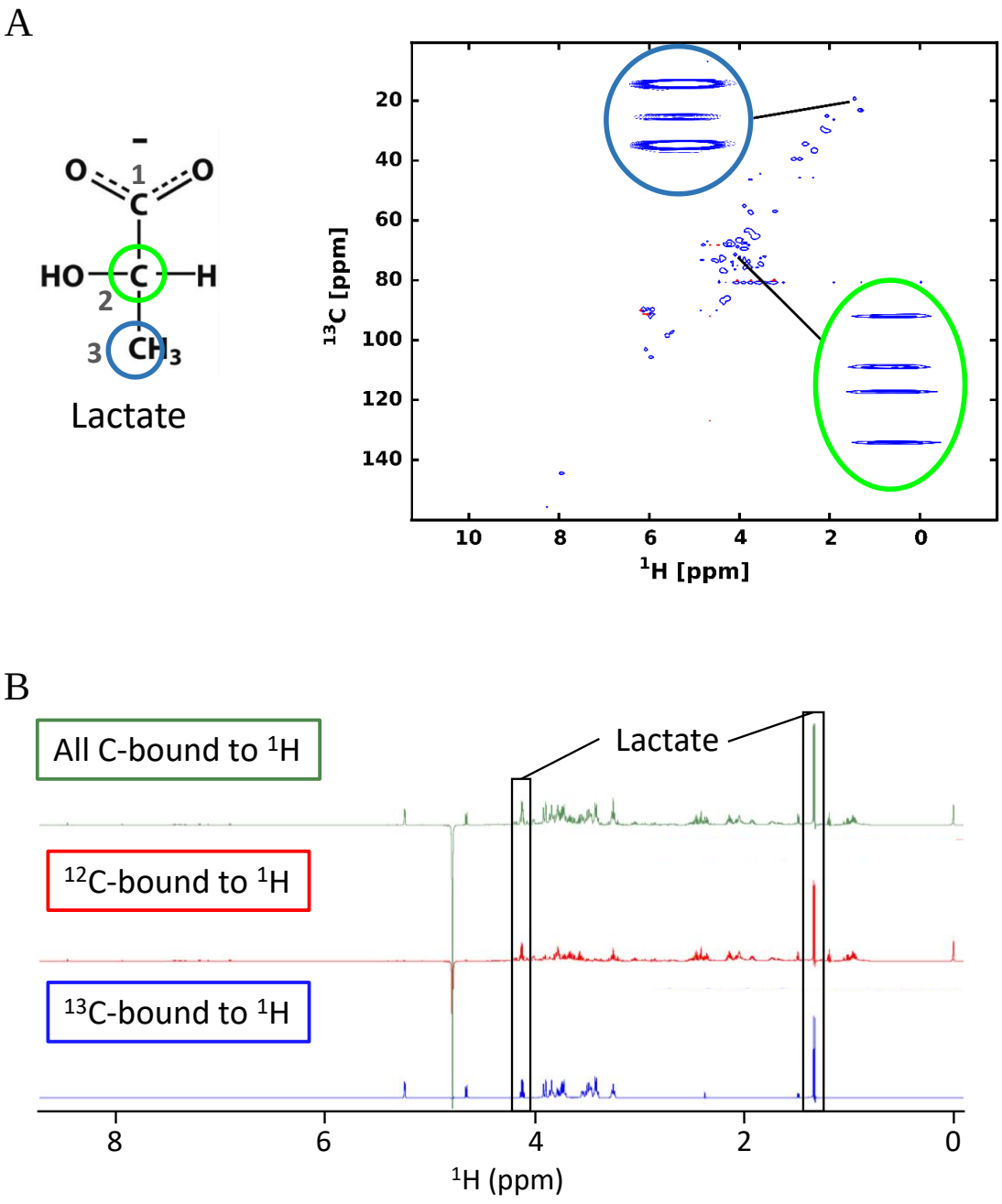

Figure 1.9 Examples of ^{1}H-^{13}C-HSQC and ^{13}C-filter NMR spectra where lactate has been assigned.

A) ^{1}H-^{13}C-HSQC spectrum of intracellular metabolites from MS-5 cells grown in U-^{13}C-glucose for 8 hours. Lactate signals have been assigned for C3 at 1.33 ppm (^{1}H dimension) and 22.9 ppm (^{13}C dimension) and for C2 at 4.11 ppm (^{1}H dimension) and 71.3 ppm (^{13}C dimension). B) Set of spectra of a medium sample from SKM-1 cells cultured with U-^{13}C-glucose for 24 hours. In green a ^{1}H-NMR spectrum of the sample which includes all the carbons (^{12}C + ^{13}C) bound to protons. In red the ^{13}C-filter spectrum which results in a spectrum with only the ^{12}C bound to protons. In blue the subtraction of the ^{13}C-filter spectrum to the ^{1}H-NMR spectrum resulting in a spectrum with the ^{13}C bound to protons. Lactate signals at 1.33 and 4.11 ppm (^{1}H dimension) are marked in black.

1.3.3. NMR instrumentation

NMR spectrometers typically consist of a sample holder contained inside of a superconducting magnet and a probe with a radio frequency emitter/receiver coil that can be tuned and matched (Figure 1.6). Superconducting magnets are used to generate the strong, stable and highly homogenous external magnetic field B_0. These magnets are made of superconducting solenoid immersed in liquid helium (4 K) and are surrounded by a liquid nitrogen (77 K) compartment to minimise the loss of helium. Superconducting magnets are necessary as the strength of the magnetic field is related to the distribution of spin populations and, thus, related with the sensitivity and resolution of NMR spectra [179, 180].

NMR spectrometers present a cylindrical shape with a bore in the centre and in the direction of the vertical axis where samples are placed, in a cylinder named probe. The probe contains the equipment to control sample temperature and the RF coils for excitation (transmission) of nuclei as well as recording the signal (receiver), which can be tuned to specific frequencies for each type of nuclei. Probes are designed specifically for different nuclei and can also have different sample size, 3 and 5 mm being the most common. A lock coil is also included in the probe to keep a constant magnetic field and to compensate for the drift of the magnet over time and other instabilities by monitoring the deuterium signal. Hence, deuterium oxide is added to samples before the acquisition of the NMR experiment.

In order to adjust the homogeneity of the external magnetic field, a set of coils termed shims apply smaller magnetic fields on top the main magnetic field [181]. The values of the shims need to be optimised to improve the magnetic field homogeneity which is required to minimise the line width of the resonances in spectra.

Finally, the radio frequency emitter generates the precise frequency required to excite the nuclei of the sample by applying pulses.

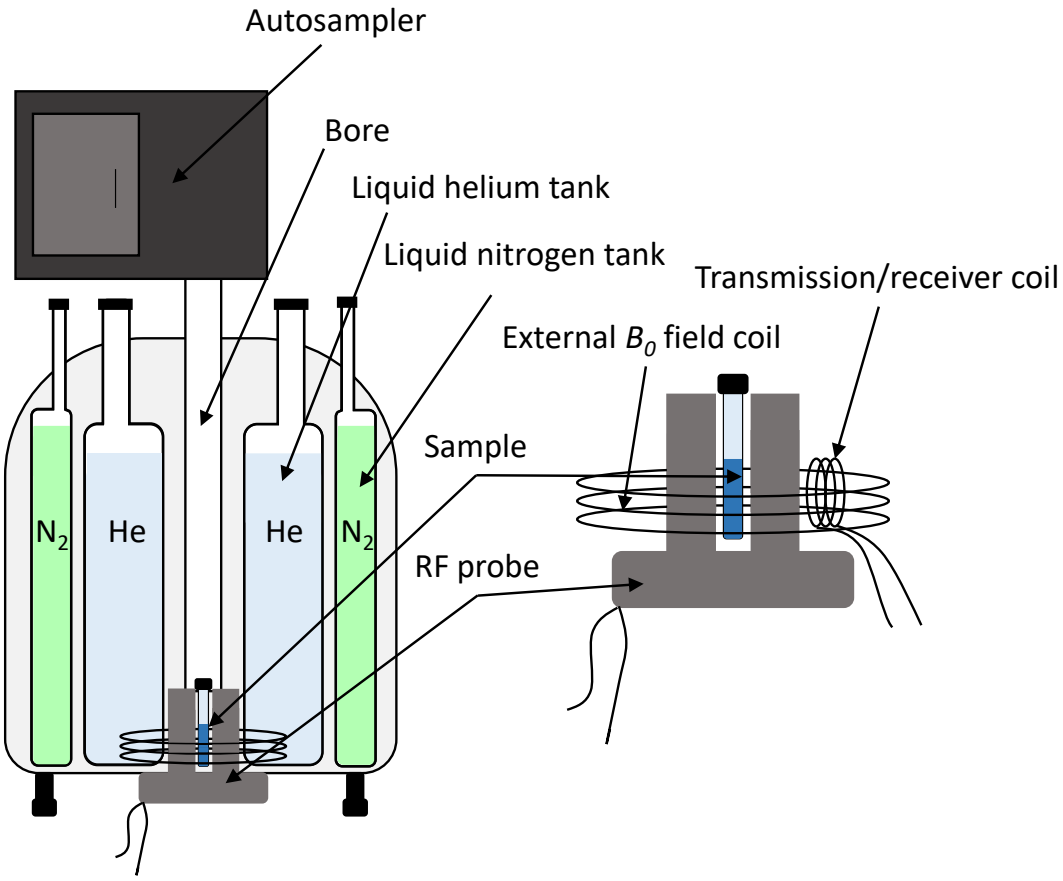

Figure 1.10 Schematic representation of an NMR spectrometer.

The sample is introduced in the bore by the autosampler and slowly placed in the bore using an air cushion for insertion and release. The probe contains several coils to generate the external magnetic field (superconducting coil in liquid helium), the radio frequency coils for excitation of nuclei (transmission) as well as recording of the NMR signal (receiver). The superconducting magnet in helium is protected from heat transmission by liquid nitrogen containers.

1.4. Aims of the thesis

AML cells reside in the bone marrow surrounded by complex microenvironment comprising several different cell types. AML cells are known to interact and reprogram niche components, by secreting cytokines and soluble factors, into their own benefit [65]. MSCs or stromal cells are known to support AML cells during disease development and can facilitate chemotherapy resistance [120, 121]. There is evidence that AML cells can modulate the metabolism of niche cells to their own advantage, such as the reprogramming of adipocytes into secreting fatty acids [49, 60]. Therefore, it was hypothesised that AML and stromal cells could establish a metabolic crosstalk that could be exploited by AML cells.

The aims of this thesis were:

- To characterise and compare the metabolism of AML and stromal cells cultured alone and in co-culture, in various settings, to identify and explore potential metabolic interactions.
- To use primary samples from AML patients and healthy donors and compare their metabolism in co-culture with stromal cells to find target metabolic variations that only occur in AML.
- To compare the transcriptome of AML and stromal cells cultured alone and in co-culture to determine whether specific genes or pathways are activated or downregulated by co-culture, with a special focus on metabolism.
- To use different techniques, such as flow cytometry, tracer-based NMR spectroscopy and consumption assays, to unravel the mechanisms by which AML and stromal cells interact in co-culture.
- To functionally block the possible metabolic interactions between AML and stromal cells.

2. Materials and methods

2.1. Cells and culture conditions

2.1.1. Cell culture

All cell lines (SKM-1, Kasumi-1, HL-60, MS-5, HS-5 and HeLa, Table 3) were cultured in RPMI 1640 media (Gibco) supplemented with 15% (v/v) heat inactivated foetal bovine serum (FBS) (Sigma-Adlrich), 2 mmol/L L-glutamine (Gibco) and 100 U/mL penicillin-streptomycin (Pen/Strep) (Gibco). Cells were kept in a humidified incubator at 37°C and 5% CO_2. Cells were periodically tested for mycoplasma contamination with the MycoAlert™ mycoplasma detection kit (LT07-218, Lonza).

Cell line name	Cell type	Obtained from	Catalogue number
SKM-1	Human AML (M5) derived from MDS	DMSZ – German Collection of Microorganisms and Cell Cultures	ACC 547
Kasumi-1	Human AML (M2)	Prof. Constanze Bonifer's group	-
HL-60	Human AML (M2)	ATCC – American Type Culture Colection	CCL-240
MS-5	Mouse stromal	Prof. Jan Jacob Schuringa's group	-
HS-5	Human stromal	Prof. Hubert Serve's group	-
HeLa	Human cervical cancer	ATCC	CCL-2

Table 3 Cell lines used with information on the cell type and source.

AML cell lines (SKM-1, Kasumi-1, HL-60) were passaged every 2-3 days to maintain cells in exponential growth. Adherent cell lines (MS-5, HS-5 and HeLa) were routinely subcultured every 2-3 days or when they reached 80% confluency. Briefly, detachment was carried out by removing the cell culture medium, washing with 1 volume of phosphate buffered saline (PBS)

(Thermo Fisher Scientific) and incubating cells with 1-2 ml of 0.25% trypsin 1 mM ethylenediaminetetraacetic acid (EDTA) (Thermo Fisher Scientific) for 5 min at 37°C. After the incubation, cells were gently tapped, and complete detachment was assessed under the microscope. 5-10 ml of fresh media were added to inactivate trypsin, cells were spun, and the corresponding dilution was performed.

2.1.2. Co-cultures

Co-cultures consisted of AML cell lines (SKM-1, Kasumi and HL-60), presenting a round morphology, cultured over monolayers of adherent cells (MS-5, HS-5 or HeLa). Adherent cells were grown until confluency before each experiment to prevent growth. Co-cultures were plated in a 4:1 AML-stroma ratio and 750.000 cells/ml density, unless differently indicated (see section 5.2.2). Co-cultures were maintained under the same conditions of cell culture media, temperature and $\%CO_2$ as for the separate cultures. For hypoxia experiments, cells were kept in a humidified incubator at 37°C, 5% CO_2 and 5% O_2.

In co-cultures of AML and stromal cells, AML cells mainly float on top of the monolayer of stromal cells except for a minor population that sits and adheres to the monolayer. This adherent fraction of AML cells attached to the stromal monolayer cannot be removed by pipetting or washing with PBS. As this fraction of cells could contaminate the stromal cell fraction when separating both cell types, a clean-up was necessary before detaching the stromal cell fraction.

The clean-up method to separate residual AML cells from the stromal fraction was adapted from a previously described protocol to separate AML and adipocytes [60]. Briefly, suspension AML cells were removed, and the unwashed stromal cell layer was washed with PBS before adding a 1:5 dilution of 0.25% trypsin 1 mM EDTA in PBS to detach the remaining AML cells. Detachment was observed under the microscope to ensure all AML cells were removed (usually

1-2 min). Media was then rapidly added to quench trypsin and the mixture was discarded. The stromal fraction was washed with PBS and was completely detached from the support following the method described in the previous section.

2.1.3. Culture of primary healthy and AML samples obtained from the Martini Hospital and cultured in The University Medical City Groningen (Groningen, The Netherlands)

2.1.3.1. Isolation of haematopoietic stem and progenitor cells from healthy and AML samples

Mononuclear AML and healthy samples had been previously isolated from peripheral blood and bone marrow samples of Martini Hospital patients and stored in liquid nitrogen by the Experimental Hematology department of the University Medical City Groningen.

Mononuclear AML samples (Table 4) were thawed, added to newborn calf serum (NCS) (Sigma-Aldrich) and spun at 450 g for 5 min. The cell pellet was resuspended in 6 mL of prewarmed NCS with 4µM of $MgSO_4$ (Sigma-Aldrich), 20 U/mL DNase I (11284932001, Roche) and 5 U/mL heparin (Ziekenhuis Apotheek Midden-Brabant), and incubated at 37°C for 15 min. Cells were spun at 450 g for 5 min and were resuspended in 6 mL of supplemented PBS (with 4µM of $MgSO_4$, 20 U/mL of DNase I and 5 U/mL of heparin) and were incubated with FcR block (130-059-901, Miltenyi Biotec) on ice for 15 min, according to manufacturer's protocol. Cells were then washed with supplemented PBS.

Peripheral blood mononuclear cells (PBMC) samples from healthy donors were thawed in a 37°C water bath, diluted 1:10 in supplemented PBS (with 4µM of $MgSO_4$, 20 U/mL of DNase I and 5 U/mL of heparin) and incubated at 37°C for 15 min.

2.1.3.2. Cell sorting of CD34+ and CD38+/CD38- by Flow cytometry

Several AML samples (AML1, AML2 and AML3) and a healthy donor sample (PBMC1) were sorted by fluorescence-activated cell sorting (FACS) according to CD34 and CD38 expression. A small fraction of cells was used as a control for sorting (unstained, CD38 single stain, CD34 single stain and DAPI single stain). 10 µL of anti-CD38 FITC (555459, BD Biosciences) and 10 µL of anti-CD34 APC (560940, BD Biosciences) per 10 million cells, according to manufacturer's protocol, were added to the bulk of cells and were incubated on ice for 30 min. Cells were washed with supplemented PBS and passed through a cell strainer to achieve single cell suspension. 10 µL of DAPI (D1306, Thermo Fisher Scientific) per 10 million cells were added to each sample before sorting for CD34+CD38+ and CD34+CD38- cells using a Sony SH800S (Sony) or a MoFlo XDP (Beckman Coulter).

2.1.3.3. Isolation of CD34+ cells by magnetic-activated cell sorting

For one of the AML (AML4) and one of the healthy donor (PBMC2) samples magnetic-activated cell sorting (MACS) was used to sort CD34+ cells. Briefly, cells were incubated with 10 µL of anti-CD34 microbeads (130-046-702, Miltenyi) per million of expected CD34 cells for 30 min at 4ºC. Cells were then washed and resuspended in 1 mL of PBS-EDTA (PBS with 2 mM EDTA). Pre-separation filter and MS MACS column (Miltenyi) were loaded to a MACS separator (Miltenyi) and equilibrated with 1 mL of PBS-EDTA before the cell suspension was loaded into the pre-separation filter. Once the cell suspension had run through, 1 mL of PBS-EDTA was added to the pre-separation filter and column three times before removing the column from the separator, adding 1 mL of PBS-EDTA and ejecting the CD34-positive cells with the plunger. CD34-positive cells were then washed with PBD-EDTA.

Patient	Tissue of origin	Type of AML (FAB)	Karyotype	Other mutations	Risk
AML1	BM	M4	46,XX,inv(16)(p13.1q22)[10]	CBFβ-MYH11	Int
AML2	PB	M5	inv(16)(p13q22)/t(16;16)(p13;q22)	CBFβ-MYH11	Adv
AML3	PB	M5	Normal	FLT3-ITD; NPM1; DNMTA3; IDH2	Adv
AML4	PB	M1	Unknown	-	Adv

Table 4 Primary AML patient information on tissue of origin, type of AML, karyotype, mutations and risk for the samples obtained from the Martini Hospital in Groningen.

BM, bone marrow; PB, peripheral blood; int, intermediate; and adv, adverse.

2.1.3.4. Primary AML and healthy donor samples' culture conditions

Primary AML cells were cultured in Gartner's medium (α-MEM (Gibco) with 12.5% (v/v) FCS (Sigma-Aldrich), 1% (v/v) Pen/Strep (Thermo Fisher Scientific), 12.5% (v/v) Horse serum (Invitrogen), 0.4% (v/v) β-mercaptoethanol (Merck Sharp & Dohme BV) and 0.1% hydrocortisone (H0888, Sigma-Aldrich) with 0.02 µg of IL-3 (Sandoz), 0.02 µg NPlate (Amgen) and 0.02 µg of G-CSF (Amgen).

Healthy donor cells were washed with supplemented PBS and were sorted by FACS and MACS as described previously. After sorting, cells were cultured in Gartner's medium with 0.3 µg/ml of human SCF (255-SC, Novus Biologicals), 0.3 µg/ml of NPlate, 0.3 µg/ml of FLT3 ligand (Amgen) and 20 ng/ml of IL-3.

Co-cultures were plated with a 4:1 leukaemic/healthy patient to stromal cells ratio and 500.000 cells/mL density in the supplemented Gartner's medium (see AML or healthy for the different supplement). Samples of AML and MS-5 cells cultured alone in the same number as in co-

culture were also cultured in Gartner's medium as a control. Samples of medium were collected at 0, 24 and 48 hours.

2.1.4. Culture of primary healthy and AML samples obtained from the University Hospital Birmingham, NHS Foundation Trust and cultured in the University of Birmingham (Birmingham, UK)

Peripheral blood samples from AML and chronic myelomonocytic leukaemia (CMML)[1] patients were obtained from the University Hospital Birmingham NHS Foundation Trust (Birmingham). All subjects read the patient information sheet and signed a consent form. Peripheral blood from a healthy volunteer was extracted by an experienced phlebotomist from the Institute of Biomedical Research in the University of Birmingham. The study was conducted according to Good Clinical Practice guidelines, consistent with the principles described in the Declaration of Helsinki. The study was approved by the West Midlands – Solihull Research Ethics Committee (10/H1206//58).

2.1.4.1. Isolation of haematopoietic stem and progenitor cells from healthy and AML samples

AML/CMML and healthy donor cells were obtained in heparin-coated vacutainers. Mononuclear cells were isolated using Ficoll Paque™ PLUS (GE LifeScience) density gradient centrifugation. Briefly, heparinized blood was diluted 1:1 with RPMI 1640 medium before being added in a 3:4 dilution to ficoll. The mixture was centrifuged for 30 min at room temperature and 300 g with low acceleration and brake. The intermediate mononuclear cell

[1] Samples were obtained from MDS patients after progression to AML. However, one of the patient samples was diagnosed as CMML after collecting and performing the co-culture experiments.

layer was extracted from the mixture and washed twice with RPMI 1640 medium supplemented with 10% (v/v) FBS. Mononuclear cells were then counted, resuspended in freezing medium (FBS with 10% (v/v) dimethyl sulfoxide (DMSO)) and stored at -80°C.

2.1.4.2. Isolation of CD34+ cells by magnetic-activated cell sorting and culture conditions

Cells were thawed and kept in culture for 16-24 hours in Stem Span H3000 media (STEMCELL Technologies) supplemented with 50 µg/ml ascorbic acid (Sigma-Aldrich), 50 ng/ml human SCF (255-SC-010, R&D Systems), 10 ng/ml human IL-3 (203-IL-010, R&D Systems), 2 units/ml human-erythropoietin (100-64, PeproTech), 40 ng/ml insulin-like growth factor 1 (IGF-1) (100-12, PeproTech), 1 µM dexamethasone (D2915, Sigma-Aldrich) and 100 µg/ml primocin (ant-pm-2, Invivogen). $CD34^+$ $cKit^+$ cells were purified using magnetic microbeads (130-046-702 (CD34) and 130-091-332 (CD117), Miltenyi Biotec). Briefly, cells were resuspended in 100 µL of separation buffer (2 mM EDTA, 0.1% (w/v) bovine serum albumin (BSA) in PBS) and 30 µL of FcR blocking reagent (Miltenyi Biotec) were added. 30 µL of each CD34 and CD117 (c-Kit) microbeads were added and the sample was incubated for 30 min at 2-8°C. Cells were washed with 500 µL of separation buffer and were resuspended in 500 µL of fresh separation buffer. Magnetic MS columns (Miltenyi Biotec) were loaded in a magnetic cell separator (Miltenyi Biotec) and were rinsed with 500 µL separation buffer. Cell suspension was applied onto the column and the column was washed with 500 µL of separation buffer twice. The column was flushed with 500 µL of separation buffer and the collected cells were washed with 500 µL of separation buffer. Cells were then counted and centrifuged before being cultured in the supplemented Stem Span media for 24 hours.

Co-cultures were plated with a 4:1 leukaemic/healthy patient to stromal cells ratio and a density of 300.000 cells/mL in the supplemented Stem Span media. Samples of leukaemic/healthy cells and MS-5 cells alone were also cultured in supplemented Stem Span media as controls. Media samples were collected at 0, 24, 48 and 72 hours.

Patient	Tissue of origin	Type of disease	Karyotype	Other mutations
AML5	PB	Secondary AML from MDS	46,XY	TET2; SRSF2; RUNX1; CEBPA; ASXL1
AML6	PB	Secondary AML from MDS	46,XY	NPM1 neg FLT3 neg
CMML	PB	CMML type 2 derived from single lineage dysplasia	46,XX	-

Table 5 Primary AML/CMML patient information on tissue of origin, type of disease, karyotype and mutations for the samples obtained from the University Hospital Birmingham NHS Foundation Trust in Birmingham.

PB, peripheral blood.

2.2. Cell treatments

2.2.1. ROS-related treatments with H_2O_2 and NAC

A 1 mM H_2O_2 stock solution was prepared by diluting a 30% (v/v) H_2O_2 solution (Merck) in water. N-acetyl-L-cysteine (NAC) (106425, Merck) was diluted in cell culture medium to a final stock concentration of 20 mM. Stocks were added to cell culture medium to a final concentration of 50 µM H_2O_2 or 5 mM NAC. SKM-1 and MS-5 cells cultured alone and in co-culture were incubated for 24 hours in 50 µM H_2O_2 complete cell culture medium, 5 mM NAC complete cell culture medium or control medium. Samples of medium were collected at 0 and 24 hours.

2.2.2. ACSS2 inhibitor

ACCS2 inhibitor was reconstituted in DMSO to a final stock concentration of 5 mM. Aliquots of the inhibitor in DMSO were kept at -20°C and a fresh aliquot was used for every experiment. The ACSS2 inhibitor was added to complete cell culture medium to a final concentration of 20 µM, the choice of working concentration was based on previous publications [182, 183]. The inhibitor was used with MS-5 cells cultured alone or in co-culture with SKM-1 cells where samples of medium were collected at 0, 4, 8 and 24 hours. The ACSS2 inhibitor was also used in HL-60 cells incubated with 4 mM [2-^{13}C] acetate culture medium for 24 hours before extraction of polar metabolites.

2.3. Cellular assays

2.3.1. Proliferation analysis using CFSE

The CellTrace™ carboxyfluorescein succinimidyl ester (CFSE) Cell Proliferation Kit (C34570, Invitrogen) was used to assess proliferation of AML cells in co-culture. A single use vial of dry CellTrace CFSE dye was resuspended in DMSO to a final concentration of 5 mM. AML cells were stained in a 1:1000 dilution of the 5 mM CFSE dye in PBS for 5 min at room temperature. Cells were washed twice with complete culture medium. A small aliquot of cells was reserved to be analysed by flow cytometry (sample for 0 hours) and the rest of the cells were divided to be cultured alone and in co-culture with MS-5 cells for 48 hours. Small aliquots of cells after 24 and 48 hours were analysed by flow cytometry.

Flow cytometry analysis was carried out in a CyAn ADP flow cytometer (Beckman Coulter). Data analysis was performed using the FlowJo software package (BD). Gating on live cells was applied and cell number was fixed to be equal for each sample in the experiment. Histograms with fluorescence intensity per cell count were generated and the geometric mean for each population and time point were calculated using the same software.

2.3.2. Cellular ROS measurements using DCFH-DA

2′,7′-Dichlorofluorescin diacetate (DCFH-DA) (D6883, Sigma-Aldrich) was dissolved in DMSO to a final stock concentration of 20 mM. MS-5 cells were cultured alone and in co-culture with SKM-1 cells for 24 hours prior to being washed with PBS. Cells were then incubated with a working concentration of 100 μM DCFH-DA in Hank's Balanced Salt Solution (HBSS) (Thermo Fisher Scientific) at 37°C for 30 min protected from light. Cells were detached and washed twice with PBS 2% (v/v) FBS before being resuspended in PBS 2% (v/v) FBS for flow cytometry analysis (as described in the previous section 2.3.1).

2.4. NMR spectroscopy

2.4.1. Tracer-based experiments

^{13}C-labelled glucose

[U-^{13}C] glucose (CC860P1, CortecNet) or [1,2-^{13}C] glucose (453188, Sigma-Aldrich) was added to RPMI 1640 medium without glucose (11879020, Merck) to a final concentration of 11 mM (as in the complete cell culture medium). The medium was supplemented with 15% (v/v) FBS (Sigma-Aldrich), 2 mmol/L L-glutamine (Gibco) and 100 U/mL Pen/Strep (Gibco). The medium was prepared fresh and was filtered with a 0.2 µm syringe filter (Sartorius) before each experiment. Cells were incubated in the labelled medium for the time indicated for each experiment whilst samples of medium were collected. Control unlabelled samples were prepared for 2D-NMR experiments and were cultured in normal complete cell culture media (with glucose) under the same conditions as the labelled samples.

^{13}C-labelled acetate

Sodium [2-^{13}C] acetate (279315-1G, Sigma-Aldrich) was added at different concentrations (0.25, 1, 3 and 4 mM) to complete cell culture medium. Acetate labelled medium was prepared fresh and was filtered with a 0.2 µm syringe filter before each experiment. Cells were incubated for each experiment (2 and 24 hours) before separation of cells and/or metabolite extraction. Control unlabelled samples were prepared for 2D-NMR experiments by adding unlabelled sodium acetate trihydrate (1.37012, Merck) to the same final concentration as in the corresponding isotope-labelled sample. Unlabelled samples were cultured under the same conditions as the labelled ones serving as a control.

2.4.2. Metabolite extraction

For intracellular metabolite extraction, already separated suspension cells and detached adherent cells were centrifuged at 300 g for 5 minutes. The supernatant was discarded, and cells were washed with 1 ml PBS (Sigma-Aldrich), centrifuged at 4°C and 10000 g for 30 seconds. The supernatant was discarded, and the pellet was rapidly resuspended in 400 µl of HPLC grade methanol (Merck) pre-chilled on dry ice. Samples were transferred to glass vials for further extraction. 325 µl Milli-Q water and 400 µl HPLC grade chloroform (Merck) were added and samples were vortexed for 30 seconds. Samples were incubated for 10 min on ice and then centrifuged at 4°C and 1300 g for 15 minutes without brake. Samples were rested for 10 minutes and 400 µl of the polar phase (upper phase) were collected and placed in a new tube. Polar phase samples were evaporated in a speed vacuum concentrator. Dry samples were kept at -80°C.

2.4.3. Media samples collection

Samples of medium for extracellular metabolite analysis were collected and directly stored at -80°C.

2.4.4. 1D ^{1}H-NMR

Dried polar phases were reconstituted in 50 µL of 0.1 M phosphate buffer with 3 mM NaN_3, 0.5 mM 3-(Trimethylsilyl) propionic-2,2,3,3-d_4-acid sodium salt (TMSP) and 10% (v/v) D_2O (all from Sigma-Aldrich). Samples were sonicated for 10 min and transferred to 1.7 mm NMR tubes (CortecNet) using the Micro Pipet System 1.7 (New Era Enterprises).

Medium samples obtained from cultures of cell lines were diluted with a 10% (v/v) of 1 M phosphate buffer with 3 mM NaN_3 and 5 mM TMSP in 100% D_2O. Medium samples from primary AML and healthy donors were diluted 1:1 with D_2O and then mixed with the D_2O

phosphate buffer (as the medium samples from cell lines). Buffered samples were transferred to 3 mm NMR tubes (CortecNet) using glass pipettes.

All samples were prepared within 24 hours before the acquisition and were kept at 4°C.

All NMR data was acquired at Bruker 600MHz spectrometers equipped with Avance-III consoles using a cooled Bruker SampleJet autosampler. For cell extracts, a triple resonance cryoprobe (TCI) 1.7mm z-axis pulsed field gradient (PFG) cryogenic probe was used, and for media samples, a 5mm TCI z-PFG cryogenic probe was used. Probes were equipped with a cooled SampleJet autosampler (Bruker) and automated tuning and matching. Spectra were acquired at 300K using 1D ^{1}H-NOESY (Nuclear Overhauser effect spectroscopy) pulse sequence with pre-saturation water suppression (noesygppr1d, standard pulse sequence from Bruker). The spectral width was 12 ppm, the number of data points was TD 32,768, the interscan delay was d1 4 sec and the NOE mixing time was d8 10 msec. The ^{1}H carrier was set on the water frequency and the ^{1}H 90^{o} pulse was calibrated at a power of 0.256 W and had a typical length of ca 7-8 µs. For polar extracts and primary medium samples 128 transients and 8 steady state transients were acquired, and for medium samples from cell lines 64 transients and 8 steady state transients were acquired. The experimental time for polar extracts and primary media samples was 14 min and for media samples from cell lines was 7.5 min.

2.4.5. Data processing: 1D ^{1}H-NMR

Spectra were processed using the *MetaboLab* [184] software within the MATLAB environment (MathWorks). FID signals were multiplied by 0.3 Hz exponential window function and zero-filling up to 131,072 data points was applied prior to Fourier transformation. Chemical shift was calibrated by referencing the TMSP signal to 0 ppm and spectra were manually phase corrected. The baseline was corrected by applying a spline baseline correction. The TMSP,

water and edge regions of the spectra were excluded before scaling the spectra using a probabilistic quotient normalization (PQN). Chenomx 7.0 software (Chenomx Inc.) and the human metabolome database (HMDB) were used to assign the metabolites present in the acquired spectra. Peak intensities were obtained directly from the spectra. The intracellular metabolite measurements are presented as relative peak intensities.

Relative metabolite changes over 24 or 48 hours were calculated by obtaining the peak intensities of each metabolite at 0 and 24 or 48 hours, the initial intensity (0 hours) was deducted from the final intensity (24 or 48 hours) and the result was divided by the initial intensity.

In order to compare data from different cell lines, in some cases acetate intensities were converted to concentrations using a calibration curve shown in Figure 5.1B. For primary cells, data was normalised to the control medium sample obtained at initial time (0 hours).

2.4.6. ^{13}C-filtered ^{1}H-NMR

[U-^{13}C] Glucose labelled medium samples were analysed with ^{13}C-filtered ^{1}H-NMR spectroscopy as described in [175]. Samples were prepared as described in section 2.4.4, and were analysed in the Bruker 600 MHz with a 5mm TCI z-PFG cryogenic probe. Spectra were acquired at 300 K using a double gradient BIRD filter pulse sequence developed in-house [175]. A pulse program combining the ^{1}H[^{12}C] and the all-^{1}H experiments in scan-interleaved mode was used. The difference between the two FIDs gave the ^{1}H[^{13}C] signal. The spectral width was 12 ppm, the number of data points was 16,384 in each dimension and the relaxation delay was 5.3 sec. 256 transients with 64 steady state transients were acquired and the experimental time was 15 min.

2.4.7. Data processing: ^{13}C-filtered ^{1}H-NMR

^{13}C-filtered ^{1}H-NMR spectra were processed in *Topspin 4.0.5* (Bruker). Spectra were zero filled to 32,768 data points before Fourier transformation. Phase correction was applied to the ^{1}H[-^{12}C] and the all-^{1}H spectra and the difference ^{1}H[^{13}C] spectrum was obtained by aligning on chemical shift. Metabolites were picked in the ^{1}H[^{13}C] spectrum and integrated in all the spectra (^{1}H[^{12}C], ^{1}H[^{13}C] and all-^{1}H) using the *Topspin 4.0.5* (Bruker) integral tool. Label incorporations for each metabolite were obtained by dividing the corresponding peak area in the ^{1}H[^{13}C] spectrum by the peak area in the all-^{1}H spectrum.

2.4.8. 2D ^{1}H-^{13}C HSQC

Labelled and unlabelled dried polar phases from tracer-based experiments were reconstituted in 50 µL of 0.1 M phosphate buffer in 100% D_2O with 3 mM NaN_3 and 0.5 mM TMSP. Samples were sonicated for 10 min and transferred to 1.7 mm NMR tubes with the Micro Pipet System 1.7. Samples were prepared fresh before the acquisition.

Samples were analysed in the Bruker 600 MHz with a 5mm TCI z-PFG cryogenic probe at 300K using a modification of the hsqcgphprsp from Bruker (Appendix 8.2), with additional gradient pulses during the insensitive nuclei enhanced by polarisation transfer (INEPT) echo periods and using soft 180º pulses for ^{13}C. For the ^{1}H dimension, the spectral width was 13.018 ppm with 1024 complex points. For the ^{13}C dimension, a spectral width of 160 ppm with 2048 complex points. 2 transients were acquired per spectra and with an interscan delay of 1.5 sec. A non-uniform sampling (NUS) of 25% sampling schedule was generated using the Wagner's schedule generator (Gerhard Wagner Lab, Harvard Medical School) with a tolerance of 0.01 and default values for the other parameters. The total experimental time was 4 hours.

2.4.9. Data processing: 2D ^{1}H-^{13}C HSQC

^{1}H-^{13}C HSQC spectra were processed and phase corrected with *NMRPipe* (National Institute of Standards and Technology of the U.S.) [185] (Appendix 8.1). *MetaboLab* was used to reference using the signal for the methyl group of L-lactic acid, at 1.31/22.9 ppm in the ^{1}H and ^{13}C dimensions, respectively. Identification of metabolites in 2D spectra was carried out using the *MetaboLab* software which includes a chemical shift library for ca. 200 metabolites. Intensities were obtained from signals in the spectra, as shown in Figure 2.1. A ^{1}H-NMR spectrum was acquired per each sample and the total area of this spectrum was obtained from *MetaboLab* to normalize the 2D data for differences in cell number. To obtain the % of ^{13}C in a metabolite, the normalized intensity of a certain carbon in the labelled sample was divided by the normalized intensity of the same carbon in the unlabelled sample and was multiplied by the natural abundance of ^{13}C (1.1%).

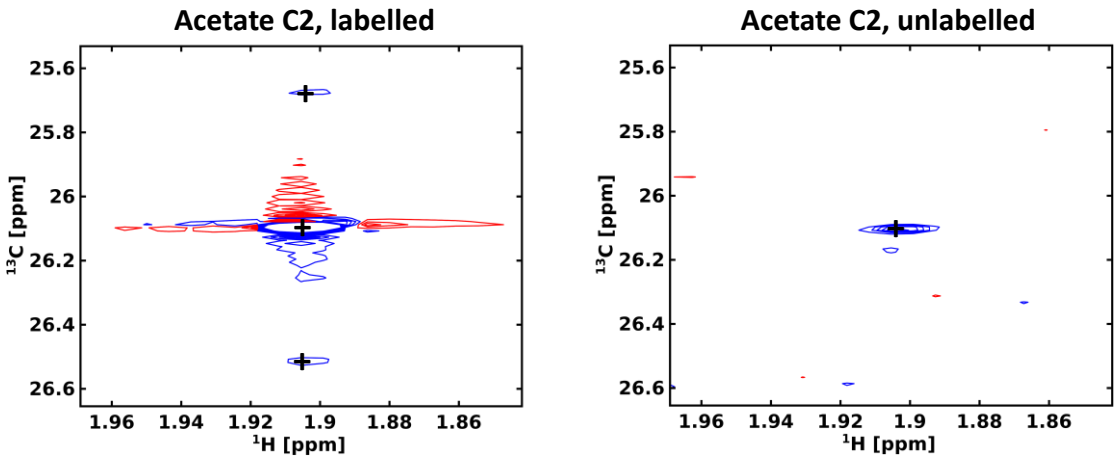

Figure 2.1 Example of how intensities are obtained from 2D ^{1}H-^{13}C-HSQC spectra.
C2 of acetate signal picking in a labelled (left) vs unlabelled (right) ^{1}H-^{13}C-HSQC spectra from SKM-1 cells incubated with [2-^{13}C] acetate for 2 hours. The black plus sign indicates the exact chemical shift where the intensity has been picked.

2.5. Molecular biology

2.5.1. RNA extraction

Cells were washed with PBS and were resuspended in 500 µL of Trizol (Invitrogen). To facilitate cell lysis, cells were pipetted up and down for 30 sec. Cell lysates were divided into 2 tubes of 250 µL and were stored at -80°C.

Before extraction, samples were thawed and centrifuged for 5 min at 12,000 g and 4°C to eliminate the excess of fat content, according to the manufacturer's instructions. The clear supernatant was transferred to new tubes and 50 µL of chloroform (VWR chemicals) were added to each tube. Tubes were shaken vigorously and incubated at room temperature for 3 minutes. The mixture was centrifuged for 15 min at 12,000 g and 4°C before transferring the aqueous phase containing the RNA to a new tube. RNA was precipitated by adding 125 µL of isopropanol (VWR chemicals) to the aqueous phase. The mixture was incubated for 10 min at room temperature and was centrifuged for 10 min at 12,000 g and 4°C. The supernatant was discarded, and the RNA pellet was washed with 250 µL of 75% (v/v) ethanol (VWR chemicals). The tubes were briefly vortexed before being centrifuged for 5 min at 7,500 g and 4°C. The supernatant was discarded, and the RNA pellet was air dried for 5 min. The RNA pellet was resuspended in 20 µL of RNAse-free water (Thermo Fisher Scientific) and was incubated in a water bath at 55-60°C for 10 min.

The RNA yield was determined by measuring the absorbance at 260 and 280 nm in a Nanodrop 2000c spectrophotometer (Thermo Fisher Scientific) and samples were stored at -80°C.

2.5.2. cDNA synthesis

For cDNA synthesis, 2 µg of RNA for each sample were used and were topped up with RNAse-free water until a total of 12 µL. 0.5 µg of oligo dT (Promega) were added and the mixture was

incubated for 5 min on ice. 2 µL of 10 mM dNTP mix (Invitrogen), 1 µL of 40U/µL RNaseOUT (Invitrogen), 1 µL of 200U/µL M-MLV reverse transcriptase (Promega), 5 µL of 5X M-MLV Reaction Buffer containing 250 mM Tris-HCl (pH 8.3), 375 mM KCl, 15 mM $MgCl_2$, 50 mM DTT and 3 µL of DEPC water. The mixture was incubated at 42°C for 1 hour. Samples were stored at -20°C.

2.5.3. Real time q-PCR

Real time quantitative polymerase chain reaction (qPCR) was performed to analyse the cDNA samples. The reaction mix for SYBR green real time qPCR contained 1 µL of cDNA, forward oligo at 450 nM concentration, reverse oligo at 450 nM concentration, 10 µL of 2X SYBR™ Green PCR Master Mix Reagent (Invitrogen, 4309155) and was topped up to 20 µL with water. The reaction mix for TaqMan real time qPCR contained 1 µL of cDNA, 0.3 µL of 60 nM β2-microglobulin forward oligo, 0.4 µL of 80 nM β2-microglobulin reverse oligo, 0.875 µL of 175 nM TaqMan™ probe, 10 µL of TaqMan™ Universal Master Mix II (both from Thermo Fisher Scientific) and 7.4 µL of water.

Each reaction was performed in triplicate as technical replicates. The real time qPCR was performed in a Stratagene Mx3005P (Agilent Technologies). The qPCR program for the SYBR qPCR included a denaturation step of 95°C for 1 min, 40 amplification cycles (95°C for 30 sec, 60°C for 1 min, 72°C for 1 min) and a dissociation cycle (95°C for 1 min, 60°C for 30 sec and 95°C for 30 sec). The qPCR program for the TaqMan qPCR included a denaturation step (50°C for 2 min, 90°C for 10 min), 40 amplification cycles (95°C for 15 sec, 60°C for 1 min).

C_t values were used to calculate the relative expression of a panel of genes compared to β2 microglobulin (B2M) (human and mouse, respectively) following the $2^{(-\Delta\Delta C_t)}$ method [186]. The list of oligonucleotide of human and mouse genes used can be seen in Table 6.

Oligo type	Species	Gene	Gene ID	RefSeq ID	Exons
KiCqStart™ primers KSPQ12012 (Sigma-Aldrich)	Human	*ACSS1*	H_ACSS1_1	NM_001252677	10-12
		ACSS2	H_ACSS2_1	NM_001242393	16-18
		B2M	H_B2M_1	NM_004048	2-3
		HIF1A	H_HIF1A_1	NM_001243084	12-14
		HK1	H_HK1_1	NM_000188	15-16
		VEGFA	H_VEGFA_1	NM_001204384	4-6
	Mouse	*Hk2*	M_Hk2_1	NM_013820	4-5
		Pdhx	M_Pdhx_1	NM_175094	9-10
		Pdk1	M_Pdk1_1	NM_172665	8-10
		Pdk2	M_Pdk2_1	NM_133667	7-9
		Vegfa	M_Vegfa_1	NM_001025257	3-5
TaqMan® assays (Thermo Fisher Scientific)	Mouse	*B2m*	Mm00437762_m1	NM_009735.3	1-2

Table 6 Oligonucleotides and primer sets for the genes analysed by qPCR.

2.5.4. Generation of ACCS1 and ACSS2 CRISPR KO HL-60 cell lines

The HL-60 ACSS1 and ACSS2 KO cell lines were generated by Dr Frank Schnütgen in the University of Frankfurt as part of a collaboration within the HaemMetabolome ITN.

Acetyl-CoA synthetase 1 and 2 (ACSS1 and ACSS2) knockouts were generated in a Cas9 coding HL-60 cell line generated previously in the lab of Dr Frank Schnütgen in the University of Frankfurt. The ACSS1 and ACSS2 lentivirus were produced by transfecting 293T cells with the psPAX2 (Addgene), pMD2.G (Addgene) and pLentiCRISPRv2-DeltaCas-EGFP and -E2Crimson (using the pLentiCRISPRv2 from Addgene as template). The single guide RNA (sgRNA)s for ACSS1 and ACSS2 were cloned in the EGFP and E2Crimson plasmids, respectively. The sequences for the sgRNAs used are listed in Table 7.

Target	Name	Sense	Sequence
ACSS1	hACSS1 1	s	CACCGgggcatgtagatggcaaca
	hACSS1 1	as	AAACtgttgccatctacatgcccC
	hACSS1 2	s	CACCGtgagcctggaacggaagtg
	hACSS1 2	as	AAACcacttccgttccaggctcaC
ACSS2	hACSS2 1	s	CACCGtgatggtatgtgatctgag
	hACSS2 1	as	AAACctcagatcacataccatcaC
	hACSS2 2	s	CACCGttctggggagacattgcca
	hACSS2 2	as	AAACtggcaatgtctccccagaaC

Table 7 sgRNA sequences targeting ACSS1 and ACSS2 genes

Transfected HL-60-Cas9 cells were sorted according to vector used and frozen before shipped to the University of Birmingham. The list of cell lines produced can be seen in Table 8.

Cell line name	sgRNA used
11	hACSS1 1
12	hACSS1 2
21	hACSS2 1
22	hACSS2 2
1121	hACSS1 1 + hACSS2 1
1221	hACSS1 2 + hACSS2 1
1122	hACSS1 1 + hACSS2 2
1222	hACSS1 2 + hACSS2 2
NTC	Empty vector

Table 8 List of KO HL-60 cell lines and sgRNAs used to generate them

2.5.5. Determining protein levels by Western blotting

2.5.5.1. Protein extraction

Cells were cultured in fresh cell culture media for 24 hours before harvesting 10 million cells of each type. Cells were washed with PBS before being resuspended in 150 µL of protein lysis buffer (Table 9) and incubated on ice for 30 min. Samples were centrifuged for 10 min at 600 g and 4°C and the supernatant from each sample was transferred to a fresh tube. Samples were snap frozen by introducing them in a container with dry ice and 100% ethanol before being stored at -80°C.

Protein lysis buffer

Reagent	Concentration
Tris-HCl pH 7.4	20 mM
EDTA	10 mM
NaCl	100 mM
Triton-100	1% (v/v)
NaF	1 mM
β-glycerophosphate	1 mM
Ethylene glycol tetra-acetic acid (EGTA)	1 mM
Polypropiolate sodium (PPNa)	5 mM
Phenylmethylsulfonyl fluoride (PMSF) (Sigma-Aldrich, P7626)	1 mM
Sodium orthovanadate (Na_3VO_4) (Sigma-Aldrich, S6508)	100 µM
Protease inhibitor cocktail set III (Calbiochem, 539134)	1X

Table 9 Protein lysis buffer composition

2.5.5.2. Protein quantification

To determine the concentration of protein of each sample, a Bradford absorption assay was perfomed. A range of BSA concentrations (0, 1, 2, 4, 6, 8 and 10 µg/µL) were prepared from 1µg/µL stock solution of BSA (Sigma-Aldrich, 1076192) in 800 µL of water with 200 µL of protein assay dye reagent (Bio-Rad, 5000006). 1 µL of each sample of protein was also resuspended in 800 µL of water with 200 µL of Bradford reagent. Absorbance of all samples was measured with the Nanodrop 2000c spectrophotometer at 595 nm and a linear regression was automatically applied to the range of BSA solutions. The absorbance of the protein samples was automatically interpolated to the standard curve to determine the protein concentration.

2.5.5.3. SDS-PAGE and Western blotting

40 µg of protein per sample were resuspended in 4X Laemmli buffer (40% (v/v) Glycerol, 8% (v/v) sodium dodecyl sulfate (SDS), 0.04% (w/v) bromophenol blue and 5% (v/v) β-mercaptoethanol in 240 mM Tris/HCl pH 6.8). Proteins were denaturalised by incubation for 8 min at 95°C. Proteins and a protein ladder (P7719, New England Biolabs) were loaded to a Mini-PROTEAN® TGX™ Precast Gel (Bio-Rad) and were subjected to SDS-Polyacrylamide gel electrophoresis (PAGE) for approximately 3 hours at 100 V. A semi-dry transfer system (Trans-Blot Turbo, Bio-Rad) was used to transfer the proteins to a polyvinylidene difluoride (PDVF) membrane (Millipore) at 25 V for 30 min. Protein transfer was checked after by incubating the membrane with Ponceau S staining (P7170, Sigma-Aldrich).

The membrane was cut at 50 kDa before being blocked in 5% (w/v) BSA in TTBS (50 mM Tris-HCl pH 7.6, 150 mM NaCl and 0.1% (v/v) Tween20) for 1 hour. After blocking, the upper part of the membrane was incubated with 1:100 dilution of ACSS1 primary antibody (D-7, sc-377149, Mouse, Santa Cruz BioTechnology) in TTBS for 2.5 hours at room temperature and

the lower part was incubated with the housekeeping protein antibody β-actin horseradish peroxidase (HRP) conjugated (CST 5125, Rabbit, Cell Signalling Technology) overnight at 4°C. The upper part of the membrane was lightly washed by incubating three times with TTBS for 30 sec before being incubated with the anti-mouse HRP secondary antibody (NXA931, Amersham) at 1:5000 dilution in TTBS for 1 hour at room temperature. After, the upper part of the membrane was lightly washed three times with TTBS for 30 sec and incubated with Novex™ ECL Chemiluminescent Substrate Reagent Kit (Invitrogen) for 2 min before developed onto photographic film. The lower part of the membrane, after being incubated overnight, was washed three times with TTBS for 10 min followed by incubation with the ECL chemiluminescent kit and developed with the same method as with the upper part.

The upper part of the membrane was reused to blot the ACSS2 protein. To strip the membrane, the membrane was incubated for 45 min with a stripping buffer (2% (v/v) SDS, 0.7% (v/v) β-mercaptoethanol, 62.5 mM Tris-HCl pH=6.8 in water) warmed up at 50°C before being washed four times with TTBS. The membrane was blocked in 5% (w/v) BSA in TTBS for 30 min before being incubated overnight at 4°C with a 1:1000 dilution of the ACSS2 antibody (PA5-52059, Rabbit, Thermo Fisher Scientific) in TTBS. The membrane was washed 3 times with TTBS for 5 min before being incubated with a 1:5000 dilution of the anti-rabbit HRP secondary antibody (NA9340, Amersham) in TTBS for 2 hours at room temperature. The membrane was washed three times with TTBS for 5 min before incubated with the ECL chemiluminescent kit for 3 min and developed with the same method described previously.

2.6. RNA sequencing

2.6.1. RNA extraction and purification

RNA samples of SKM-1 and MS-5 cells cultured alone and in co-culture extracted using Trizol (as described in section 2.5.1) were purified using the RNeasy Plus Micro kit (Qiagen) as follows. RNA samples were resuspended in 350 µL of buffer RLT before transferring to gDNA eliminator spin columns placed in 2 mL collection tubes. Samples were centrifuged for 30 sec at 8,000 g twice before discarding the columns. 350 µL of 70% (v/v) ethanol were added to the flow-through samples before directly transferring to RNeasy MinElute spin columns placed in 2 mL collection tubes. The spin columns and collectors were centrifuged for 15 sec at 8,000 g and the flow-through was discarded. To wash the columns, 700 µL of buffer RW1 were added to each column and the columns were centrifuged for 15 sec at 8,000 g. The flow-through was discarded and a second wash with 500 µL of buffer RPE was applied to each column before centrifuging for 15 sec at 8,000 g. A third wash was performed by adding 500 µL of 80% (v/v) ethanol to each column and centrifuging the columns for 2 min at 8,000 g. The flow-through was discarded and the columns were centrifuged with the lids open for 5 min at 12,000 g. The columns were placed in new collection tubes and 15 µL of RNase-free water were added directly to the centre of the spin column membranes. Columns were centrifuged for 1 min at 12,000 g to elute the RNA.

The quality of the RNA extracted and purified was assessed using the Tapestation system from the genomics service of the University of Birmingham. The RNA integrity number (RIN) and sample concentration were determined for every sample and are shown in Table 10. As the RIN values were approximately 10 for all samples, the extracted RNA had the high quality needed for sequencing.

To prepare the samples for transportation, 1 µL of 3M sodium acetate (pH 7-8) and 20 µL of 100% ethanol were added to 10 µL of each RNA sample.

Samples were sent to Theragen Etex Co., LTD. (www.theragenetex.net) for transcriptome analysis. cDNA libraries were prepared with the TruSeq Stranded mRNA Sample Prep Kit (Illumina) and RNA sequencing was performed in a HiSeq2500 platform (Illumina).

Sample	Replicate	RNA concentration (ng/µL)	RNA integrity number (RIN)
SKM-1 only	1	364	9.3
	2	388	10
	3	466	9.7
SKM-1 co-culture	1	720	10
	2	501	10
	3	670	10
MS-5 only	1	491	10
	2	552	10
	3	601	10
MS-5 co-culture	1	708	10
	2	622	10
	3	696	10

Table 10 Quality control of RNA samples of SKM-1 and MS-5 cells cultured separately and in co-culture for RNA sequencing

2.6.2. RNA sequencing data analysis

Transcriptomic data generated by Theragen Etex Co., LTD. was analysed by Grigorios Papatzikas as part of a collaboration within the HaemMetabolome ITN.

Quality control metrics were obtained with *FastQC 0.11.7* software (Babraham Bioinformatics). To quantify transcript abundances using the *Kallisto 0.43.0* software (Patcher Lab), read counts were aligned to the GRCh36 human reference genome cDNA index (Ensembl

rel.99) and the GRCm38 mouse reference genome cDNA index (Ensembl rel.67). Gene-level differential expression analysis was carried out with the R statistical package *Sleuth 0.30.0* comparing the expression of cells cultured alone vs co-culture. Differentially expressed genes were calculated using the Wald statistical test, correcting for multiple testing with the Benjamin-Hochberg method. The false discovery rate (FDR) threshold was set at 1% (q-values < 0.01). *Ensembl* gene transcripts were annotated to Entrez IDs and official gene symbols with the R statistical package *BioMart 2.40.3*. To normalise for sequencing depth and gene length, transcripts per million (TPM) expression values were calculated.

Gene Set Enrichment Analysis (GSEA) was performed with the R statistical package *fgsea 1.10.0*. The collection of hallmark gene sets from the Molecular Signature Database was used for the GSEA, setting the FDR threshold at 5%.

2.7. Statistics

All statistical analyses, except for transcriptomic data analysis (see section 2.6.2), were performed in *GraphPad Prism v8* (GraphPad Software Inc.). t-Student tests were performed not assuming equal variance applying Welch's correction. Linear regression and interpolation to the linear regression were automatically calculated by the software.

The statistical analysis was assessed by the CRUK Birmingham's bioinformatician Yi Pan.

3. Characterising metabolic alterations in AML and stromal cells in co-culture

3.1. Introduction

AML cells in the bone marrow are surrounded by a complex microenvironment composed of a variety of other cell types, soluble factors and extracellular matrix, known as the niche [187]. It is known that AML cells can interact and modulate components of the niche into their own support and it has been suggested that changes in the niche network lead to malignant transformation and favour disease progression, as reviewed in [84, 188, 189]. Crosstalk between AML and stromal cells has been described to be mediated via exosomes [131] and mitochondria [61, 62]. For both cases, stromal cells act as a support for AML cells and provide them with chemotherapy resistance [190]. Metabolism in HSCs and AML cells has been broadly investigated, as reviewed in [191-193]. Nonetheless, there are few studies covering metabolic alterations related to the interaction between stromal and AML cells.

In this chapter, a comparison of the metabolism of AML and stromal cells cultured alone or in co-culture is presented. Several AML and stromal cell lines were analysed using different experimental designs to identify common metabolic alterations. Moreover, the metabolism of AML patient samples and healthy donor samples were also analysed in co-culture to determine whether the metabolic changes observed in established cell lines can be recapitulated in primary cell cultures.

3.2. Results

3.2.1. Is AML and stromal metabolism altered in co-culture?

To characterise how co-culture affects the metabolism of AML and stromal cells, an experimental design allowing clear metabolic comparison was crucial. Thus, AML and stromal cells were cultured separately and in co-culture with the same cell culture medium and vessel, cell density and cell number. The AML-stromal ratio used was 4:1, to maintain AML cells in their optimal density and have a confluent monolayer of stromal cells. To identify extracellular metabolites, media was sampled at different time points; and, to study intracellular metabolite levels, cells were detached or collected and quenched prior to metabolite extraction (Figure 3.1).

The first experiments were performed using a secondary AML cell line, SKM-1, and a mouse stromal bone marrow-derived cell line, MS-5. I decided to use this particular mouse stromal cell line since it is extensively used as growth support in co-cultures with primary human AML cells [194, 195]; therefore, interactions between both cell types could be expected. SKM-1 and MS-5 cells were cultured separately and in co-culture for 24 hours before metabolite extraction. Polar intracellular metabolite samples were analysed by ^{1}H-NMR spectroscopy and 24 metabolites could be assigned and quantified, an example of a spectrum with the signals assigned can be seen in Figure 3.2.

The intracellular metabolite levels characterised in SKM-1 cells showed unaltered levels of branched-chain amino acids and other amino acids in co-culture (Figure 3.3A). Glycolysis-related metabolites (Figure 3.3B) seemed to present higher levels in co-culture with significant increases in acetate and nicotine adenine dinucleotide oxidised (NAD^{+}) and a slight increase in lactate. TCA cycle metabolites were largely unchanged by co-culture except for asparagine that

showed a significant decrease in comparison with SKM-1 cells cultured alone (Figure 3.3C). The rest of the metabolites analysed showed no significant alterations, except for a decrease in phosphocholine (Figure 3.3D).

In MS-5 cells, the detected intracellular metabolites remained unaltered by co-culture except for aspartate, which presented with significantly lower levels in co-culture, as can be observed in Figure 3.4. This result suggests that, contrary to SKM-1 cells, the metabolism of MS-5 remained mostly unchanged in co-culture, at the intracellular level.

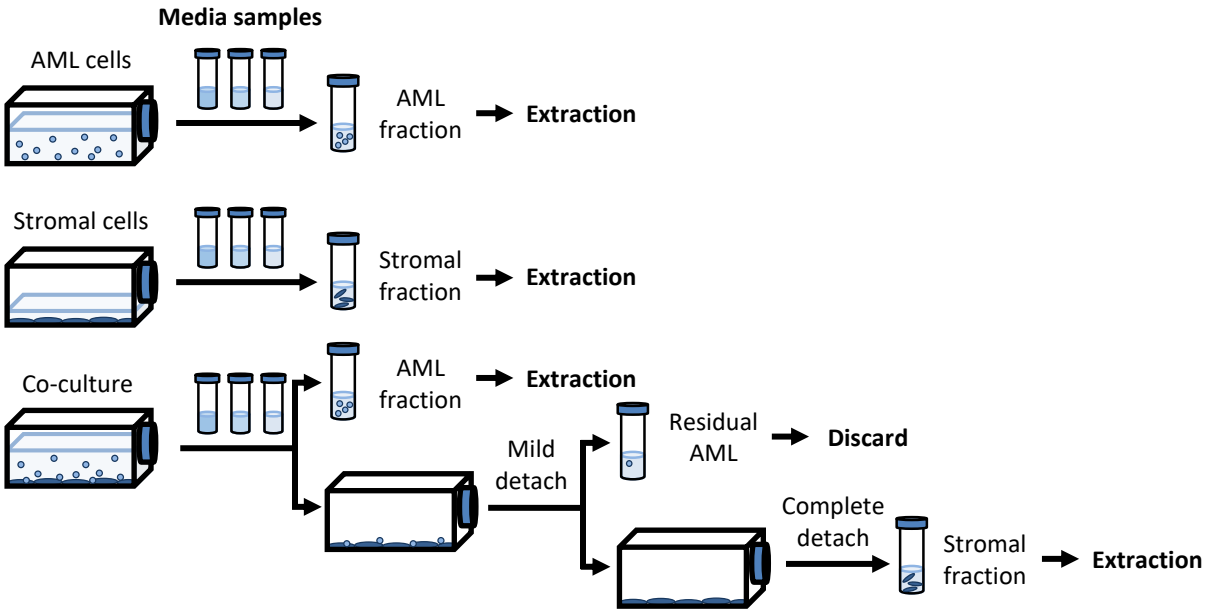

Figure 3.1 Co-culture experimental design.

Schematic representation of experimental design used for co-culture experiments. In brief, AML and stromal cells were cultured in separated flasks and in co-culture in direct contact under the same conditions (cell culture medium, cell number and density), medium samples were collected for different time points. After a selected time, AML and stromal cells were separated and/or collected and intracellular metabolites were extracted. For cells in co-culture, AML cells in suspension were collected and extracted and the adherent stromal fraction was treated to mildly detach residual AML cells. After quenching the mild detachment, residual AML were discarded, and stromal cells were complete detached and extracted.

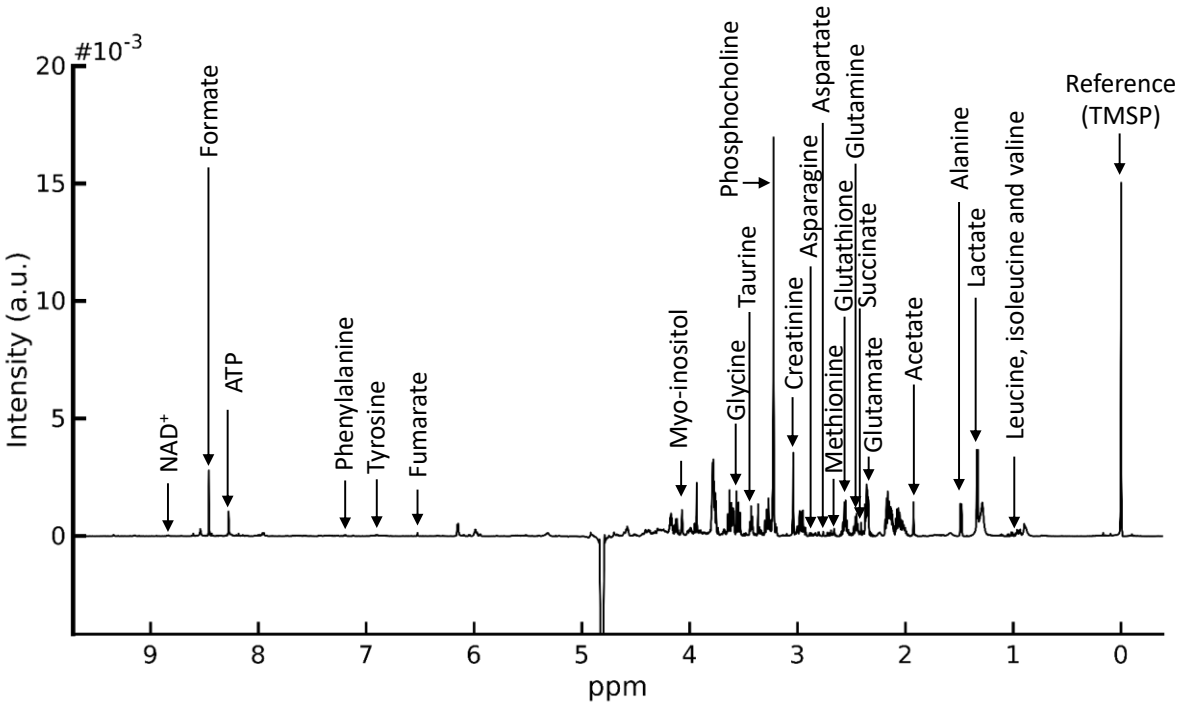

Figure 3.2 Metabolites assigned in polar extracts ^{1}H-NMR.

Example of a ^{1}H-NMR spectrum from a polar extract of SKM-1 cells. 24 metabolites could be assigned after processing the spectrum (referencing the TMSP signal to 0 ppm, phasing and correcting the baseline). The exact chemical shifts used to quantify each metabolite are: TMSP, 0 ppm; leucine, 0.975 ppm; isoleucine, 1.020 ppm; valine, 1.040 ppm; lactate, 1.340 ppm; alanine, 1.490 ppm; acetate, 1.925 ppm; glutamate, 2.375 ppm; succinate, 2.410 ppm; glutamine, 2.450 ppm; glutathione, 2.555 ppm; methionine, 2.645 ppm; aspartate, 2.800 ppm; asparagine, 2.885 ppm; creatinine, 3.040 ppm; phosphocholine, 3.225 ppm; taurine, 3.430 ppm; glycine, 3.570 ppm; myo-inositol, 3.555 ppm; fumarate 6.525 ppm; tyrosine, 7.190 ppm; phenylalanine, 7.435 ppm; ATP, 8.275 ppm; formate, 8.460 ppm; and NAD^{+}, 8.850 ppm.

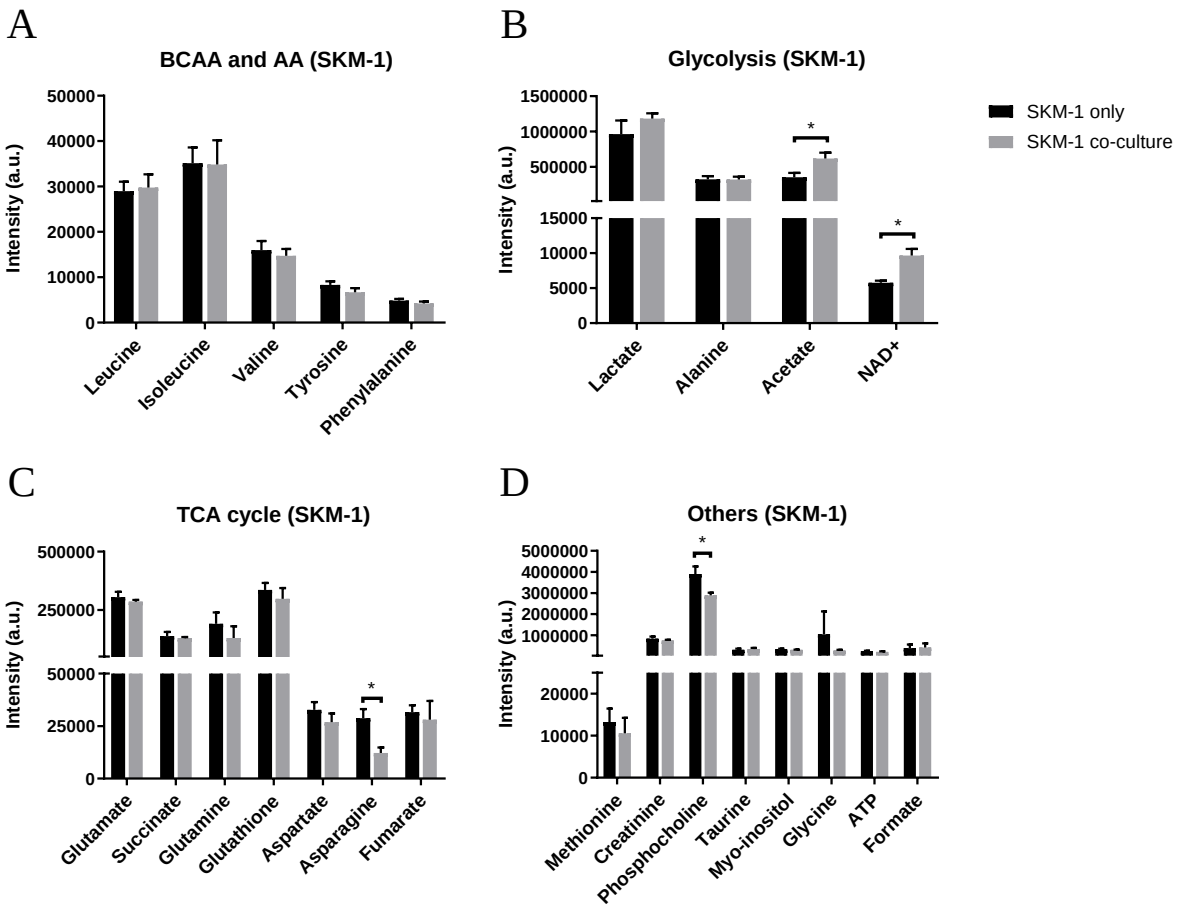

Figure 3.3 Intracellular metabolite levels in SKM-1 cells in co-culture.

Intracellular metabolite levels detected in SKM-1 cells cultured alone or in co-culture with MS-5 cells for 24 hours. A: Branched chain amino acids (BCAA) and other amino acids (AA), B: Glycolysis-related metabolites, C: TCA cycle-related metabolites and D: Other metabolites. Cells were separated and polar metabolites extracted before ^{1}H-NMR spectra were acquired. Bars represent the mean of n=3 independent experiments and error bars represent standard deviation. An unpaired t-student test was applied for each metabolite and p-values were represented as * for p-value<0.05, ** for p-value<0.01 and *** for p-value<0.001.

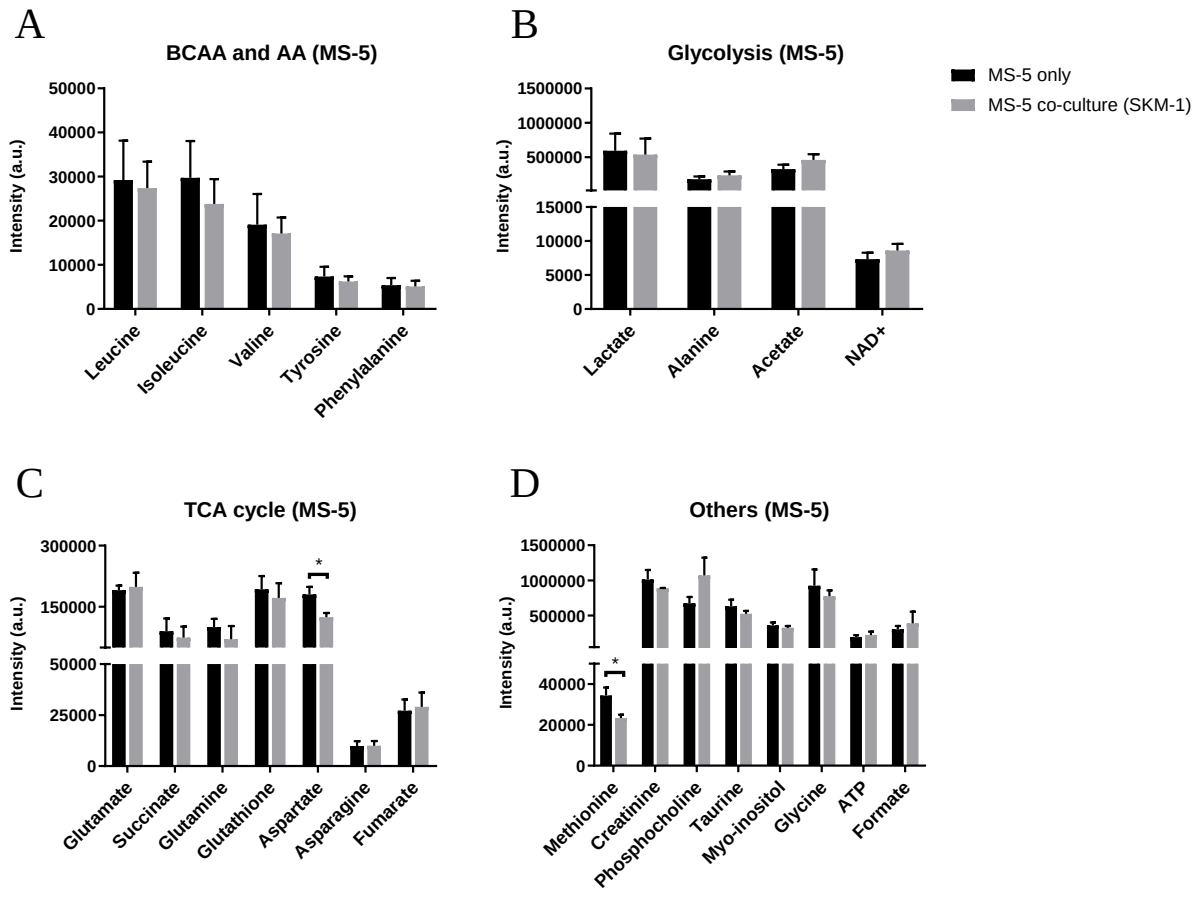

Figure 3.4 Intracellular metabolite levels in MS-5 cells in co-culture.

Intracellular metabolite levels detected in MS-5 cells cultured alone or in co-culture with SKM-1 cells for 24 hours. A: Branched chain amino acids (BCAA) and other amino acids (AA), B: Glycolysis-related metabolites, C: TCA cycle-related metabolites and D: Other metabolites. Cells were separated and polar metabolites were extracted before acquiring ^{1}H-NMR spectra. Bars represent the mean of n=3 independent experiments and error bars represent standard deviation. An unpaired t-student test was applied for each metabolite and p-values were represented as * for p-value<0.05, ** for p-value<0.01 and *** for p-value<0.001.

After intracellular metabolite changes caused by co-culture were established, media samples of SKM-1 and MS-5 cells cultured alone or in co-culture were collected at 0 and 24 hours to characterise their extracellular pool of metabolites. 13 extracellular metabolites were assigned and quantified by ^{1}H-NMR spectroscopy, as can be seen in Figure 3.5. The measured levels were converted into relative changes over 24 hours; with positive values indicating production and negative values indicating consumption of a metabolite.

Proliferative cells and especially cancer cells rely on glycolysis, where glucose consumption and lactate production are the main metabolic activity measured extracellularly [196]. The analysis for these metabolites in SKM-1 and MS-5 cells revealed that cells in co-culture consumed more glucose and produced more lactate than when cultured alone (Figure 3.6A). The relative consumption/production over 24 hours for both glucose and lactate in co-culture were approximately the sum of the relative consumption/production of glucose and lactate for each cell type cultured alone, respectively. This result seemed to suggest that both AML and stromal cells did not present an altered glycolysis rate in co-culture. Alanine can also be a by-product of glycolysis and was found to present with a slight increase in the relative production in co-culture (Figure 3.6A), mimicking the tendency observed for lactate.

The most striking differences were found in acetate and pyruvate. The production of these two metabolites was 10 times higher than any other metabolite analysed (Figure 3.6B). Acetate was slightly consumed by SKM-1 cells and was produced by MS-5 cells alone (Figure 3.6B). However, in co-culture, the relative production of acetate was almost twice that of MS-5 cells alone. Pyruvate followed a similar tendency, although it was produced by SKM-1 cells alone and to a minor degree by MS-5 cells alone, being secreted at a higher rate in co-culture (Figure 3.6B). These results revealed that co-culture had a strong effect in the metabolism of these cells

resulting in a remarkable increase of acetate and pyruvate secretion. Interestingly, intracellular acetate levels in SKM-1 were higher in co-culture. Both this finding and the observation that SKM-1 alone did not secrete any acetate seemed to indicate that these cells could be consuming acetate that was most likely secreted by MS-5 cells.

As shown in Figure 3.6C, glutamine and glutamate relative consumption/production levels over 24 hours were very similar for SKM-1 cells alone and in co-culture. This result was difficult to interpret but could be suggesting that, due to availability, these metabolites were consumed and produced at a lower rate by both cell types.

Moreover, aspartate and asparagine relative changes revealed that MS-5 cells were mainly responsible for the secretion of acetate and consumption of asparagine from the extracellular medium (Figure 3.6C). Interestingly, SKM-1 cells also consumed aspartate when cultured alone although at a lower rate than MS-5 cells. This result suggested that aspartate could be a potential crosstalk metabolite, being secreted by MS-5 cells and consumed by SKM-1 cells. Moreover, SKM-1 cells also had lower levels of intracellular levels of asparagine, which could be caused by a higher usage of asparagine which, in turn, could be generated from aspartate.

Branched-chain amino acids and formate presented a similar tendency to glutamine and glutamate suggesting that cells consumed them according to their availability (Figure 3.6D).

Overall these results confirmed that co-culture had an effect in the metabolism of both SKM-1 and MS-5 cells at the intra and extracellular level.

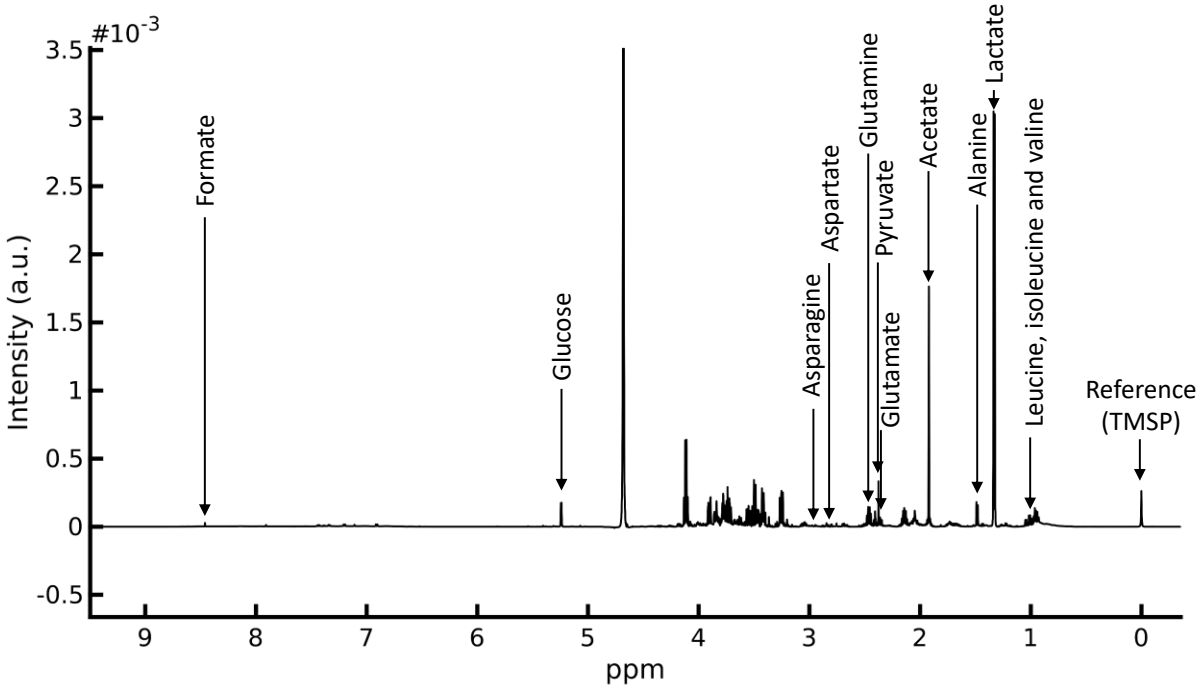

Figure 3.5 Metabolites assigned in ^{1}H-NMR spectra from media samples.

Example of a 1H-NMR spectrum from a medium sample of SKM-1 and MS-5 cells in co-culture after 20 hours. 13 metabolites could be assigned after processing the spectrum (referencing the TMSP signal to 0 ppm, phasing and correcting the baseline). The exact chemical shifts used to quantify each metabolite are: TMSP, 0 ppm; leucine, 0.975 ppm; isoleucine, 1.020 ppm; valine, 1.050 ppm; lactate, 1.335 ppm; alanine, 1.490 ppm; acetate, 1.920 ppm; glutamate, 2.345 ppm; pyruvate, 2.375 ppm; glutamine, 2.480 ppm; aspartate, 2.805 ppm; asparagine, 2.950 ppm; glucose, 5.245 ppm; and formate, 8.460 ppm.

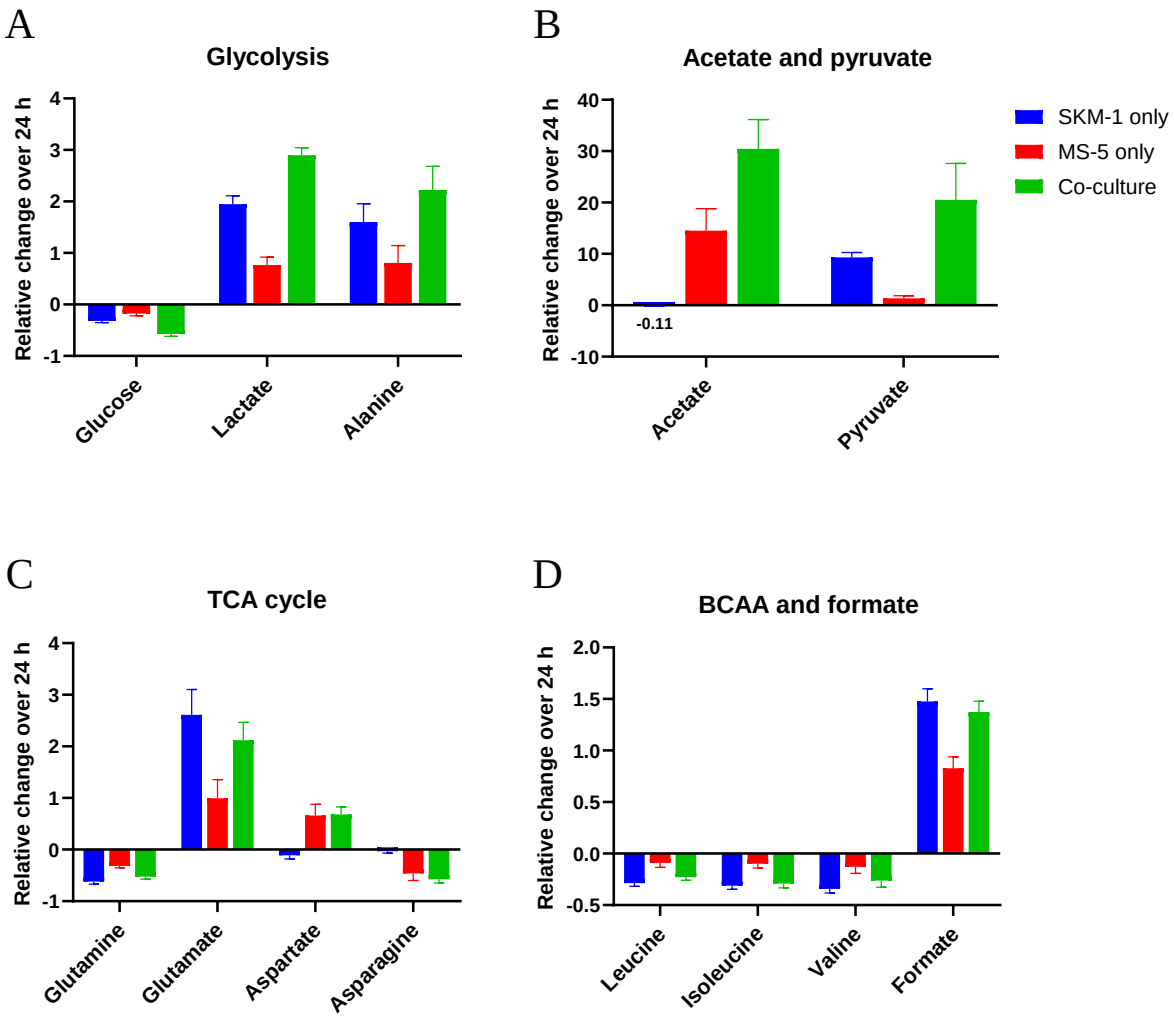

Figure 3.6 Relative change over 24 hours of extracellular metabolites in SKM-1 and MS-5 cells alone and in co-culture.

SKM-1 and MS-5 cells were cultured alone and in co-culture under the same conditions for 24 hours. Samples of medium at time 0 and 24 hours were analysed by ^{1}H-NMR spectroscopy and converted into rates of production or consumption. A: Glycolysis-related metabolites, B: Acetate and pyruvate C: TCA cycle-related metabolites and D: Branched chain amino acids (BCAA) and formate. Bars represent the mean of n=3 independent experiments and error bars represent standard deviation. Metabolites that have been produced are represented by positive values and metabolites that are consumed are represented by negative values.

3.2.2. Common metabolic alterations in AML-MS-5 co-cultures

Next, I decided to characterise whether other leukemic cell lines would present similar metabolic alterations to those found for SKM-1 in co-culture. I used the Kasumi and HL-60 cell lines and co-cultured them with MS-5 cells to characterise their metabolism and identify common metabolic differences in co-culture.

Intracellular metabolic alterations that were found to be common in the three AML cell lines used (SKM-1, Kasumi and HL-60) are depicted in Figure 3.7. Compared to cells cultured alone, all AML cell lines tested presented significantly lower levels of intracellular asparagine and higher of intracellular NAD^+ in co-culture (Figure 3.7A, B). MS-5 cells cultured with the three AML cell lines showed a decrease in intracellular aspartate (Figure 3.7C). In the AML cells in co-culture, asparagine levels were reduced by approximately a half compared to cells alone (grey bars, Figure 3.7A). In MS-5 cells in co-culture, the decrease in aspartate was not so pronounced (grey bars, Figure 3.7C). The lower levels of these metabolites seemed to indicate that an interchange involving aspartate and asparagine could occur in co-culture. The interpretation of the increased levels of NAD^+ found was not straightforward and could be related to various processes such as cellular redox homeostasis or the result of overall cellular metabolism.

There was one co-culture induced extracellular metabolic alteration found in all three cell lines: an increase in acetate secretion (Figure 3.8). After 24 hours, acetate secretion was significantly higher in co-cultures with the three AML cell lines than in AML and MS-5 cells cultured alone, reaching more than double of the amount for SKM-1 (Figure 3.8A) and HL-60 (Figure 3.8C). Kasumi cells in co-culture presented an increase in acetate secretion that was not as severe as that for SKM-1 and HL-60. This finding is remarkable, as changes in the extracellular medium

are more interesting because they can be followed over time and usually involve changes at the intracellular level.

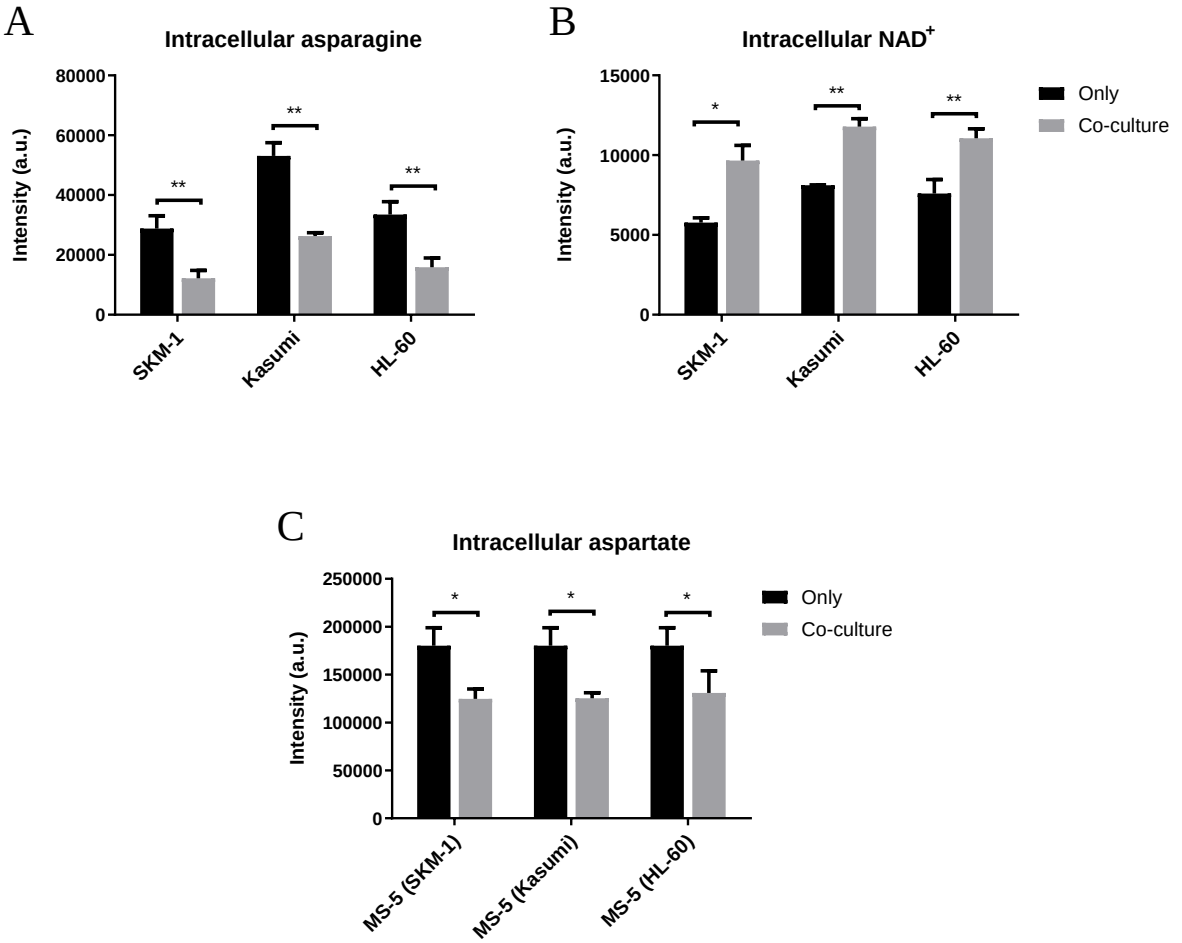

Figure 3.7 Common intracellular metabolites altered in co-cultures with AML cell lines.

SKM-1, Kasumi and HL-60 cells were cultured alone or with MS-5 cells for 24 hours before extraction of polar metabolites and ^{1}H-NMR spectroscopy analysis. A: Asparagine in AML cell lines, B: NAD^{+} in AML cell lines and C: Aspartate in MS-5 cells. Metabolites that were significantly altered in co-culture for the three AML cell lines tested are presented. Bars represent the mean of n=3 independent experiments and error bars represent standard deviation of arbitrary intensity units. An unpaired t-student test was applied for each metabolite and p-values were represented as * for p-value<0.05, ** for p-value<0.01 and *** for p-value<0.001.

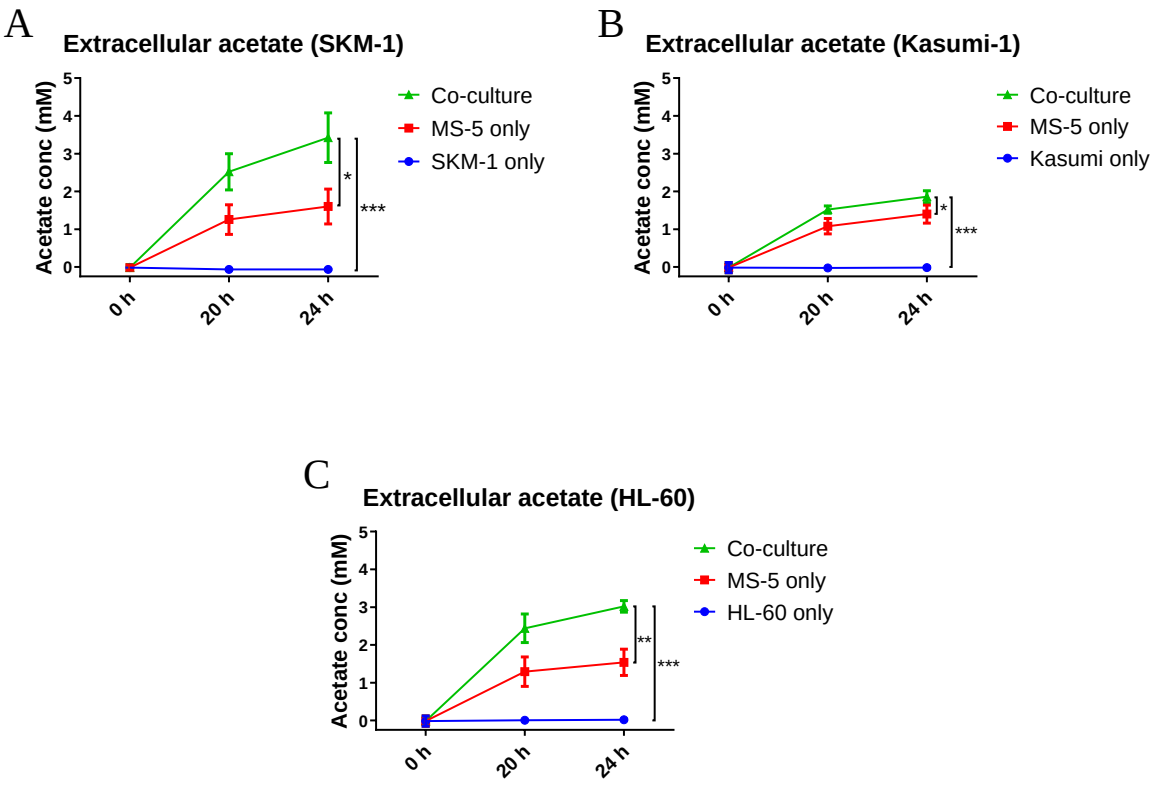

Figure 3.8 Common extracellular metabolites altered in co-cultures with AML cell lines.

SKM-1 (A), Kasumi (B) and HL-60 (C) cells were cultured alone or with MS-5 cells for 24 hours. Samples of media were collected at 0, 20 and 24 hours and were analysed by ^{1}H-NMR spectroscopy. Acetate presented significantly different levels in co-culture for the three AML tested. Each point represents the mean of n=3 independent experiments and error bars represent standard deviation. An unpaired t-student test was applied at time point 24 hours for each condition and p-values were represented as * for p-value<0.05, ** for p-value<0.01 and *** for p-value<0.001.

3.2.3. Is proliferation of AML cells affected by co-culture with stromal cells?

The metabolic changes observed in AML-MS-5 co-cultures could be attributed to increased proliferation under these conditions. To test this possibility, I decided to use carboxyfluorescein succinimidyl ester (CFSE). CFSE is a fluorescent staining dye that is incorporated into cells and is not transferred to adjacent cells (MS-5 cells in this case) after being stained. When stained cells duplicate, their fluorescence is halved, allowing to track proliferation. A proliferation test was not performed with MS-5 cells as they were kept confluent for co-culture experiments and thus their growth was contact inhibited.

AML cell lines (SKM-1, Kasumi and HL-60) were stained with CFSE and their fluorescence intensity was assessed by flow cytometry at time 0. Cells were then divided into two groups, to grow them alone or in co-culture with MS-5 cells, and were cultured for 48 hours. Samples of cells were collected at 24 and 48 hours and were analysed by flow cytometry. A histogram with the results is shown in Figure 3.9.

The analysis revealed that SKM-1 cells in co-culture after 48 hours showed a slightly slower rate of proliferation (Figure 3.9A). However, the proliferation rate at 48 hours was not significantly different from SKM-1 cells cultured alone. Moreover, none of the AML cell lines presented differences in proliferation rates in co-culture at any time point (Figure 3.9B and C). This result indicates that the metabolic alterations found in co-culture were caused by a mechanism that did not involve changes in proliferation for at least a short time frame of up to 48 hours.

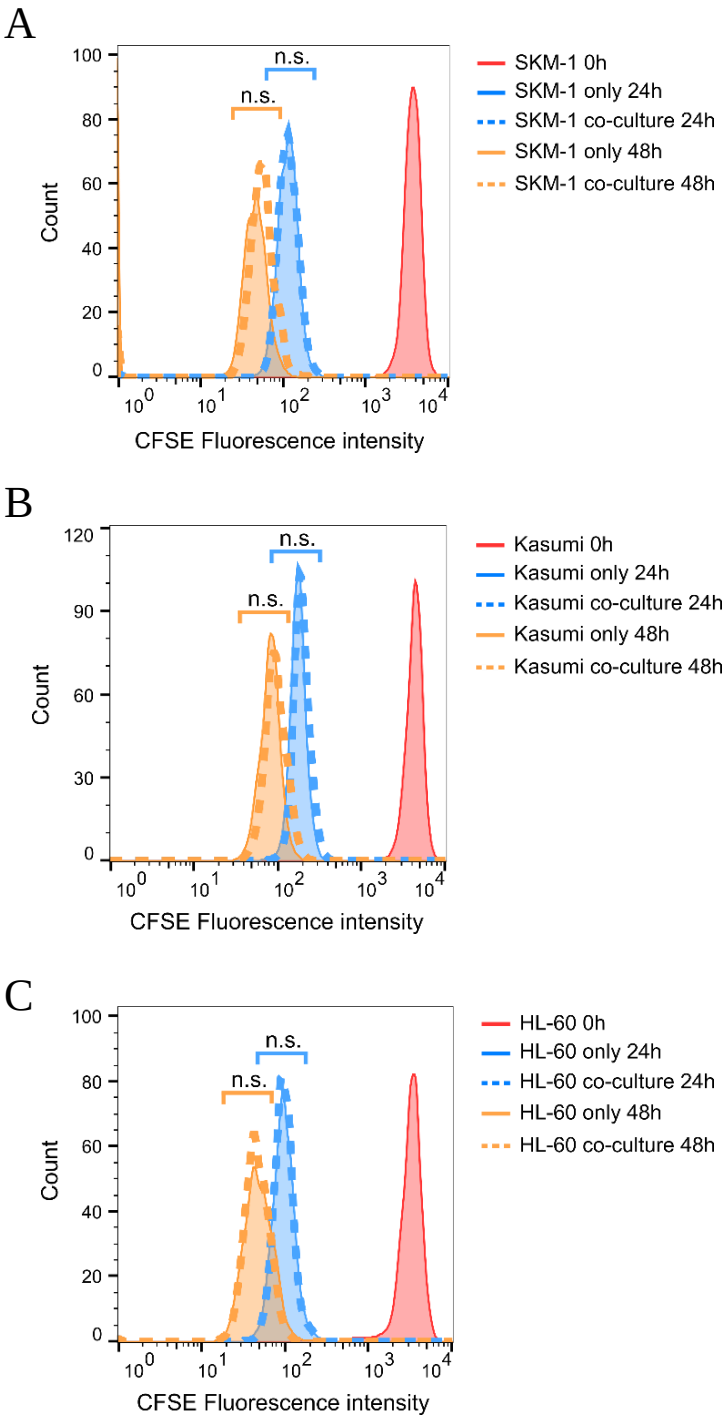

Figure 3.9 Cell proliferation analysis by flow cytometry using CFSE in SKM-1, Kasumi and HL-60 alone or in co-culture.

Analysis was carried out with FlowJo software. The population of living cells was gated and 1500 cells for each condition were randomly selected and plotted. The geometric mean for each population and time point was compared between cells alone or in co-culture by performing an unpaired unpaired t-student test and p-values were represented as n.s. for not significant. Each histogram is representative of n=3 independent experiments.

3.2.4. Is contact affecting the metabolic interaction in AML-stroma co-cultures?

Cell-to-cell contact has been reported to have a role in several interactions between AML and stromal cells [197]. Therefore, I decided to investigate the effect of preventing the cell-cell contact in co-cultures by separating cells with a permeable membrane. The size of the permeable membrane used (0.4 μm) allowed cells to share metabolites, cytokines and extracellular vesicles but it prevented the formation of tunnelling nanotubes (TNTs) as well as mitochondrial trafficking.

Co-cultures were performed as indicated in the scheme in Figure 3.10A. SKM-1, Kasumi and HL-60 cells were cultured alone and in co-culture with MS-5 cells for 24 hours before polar metabolite extraction. Samples of media were collected at time 0, 20 and 24 hours. ^{1}H-NMR spectroscopy was performed on the polar extracts and samples of media.

The analysis of intracellular metabolite levels revealed that the only common significant variation was a decrease in asparagine levels in the AML cell lines in co-culture Figure 3.10B. I also measured NAD^+ levels (Figure 3.10C) in AML cell lines and aspartate (Figure 3.10D) in MS-5 cells as they were altered in co-culture in direct contact. As can be seen in Figure 3.10C and D, NAD^+ and aspartate levels in co-culture followed a similar trend as with direct contact but were not always significantly different for the three AML cell lines. This result suggests that contact could be exacerbating the metabolic differences caused by co-culture.

The analysis of extracellular metabolites revealed that increased acetate secretion did not occur when cells were not in direct contact (Figure 3.11) evidencing that contact is crucial for acetate secretion. Moreover, co-cultures presented a lower level of extracellular acetate than MS-5 cells alone for all AML cell lines (SKM-1, Kasumi and HL-60) (Figure 3.11A, B and C,

respectively), suggesting that leukemic cells could be consuming acetate generated from MS-5 cells.

From this moment, I decided to continue investigating only the increased acetate secretion in co-culture as it seemed more interesting than the intracellular metabolite changes. There were several reasons to further investigate acetate increase, including the magnitude of the differences found in co-culture, the fact that it involved extracellular changes, and acetate being widely described to play a role in cancer metabolism and in the epigenetic landscape of cancer cells.

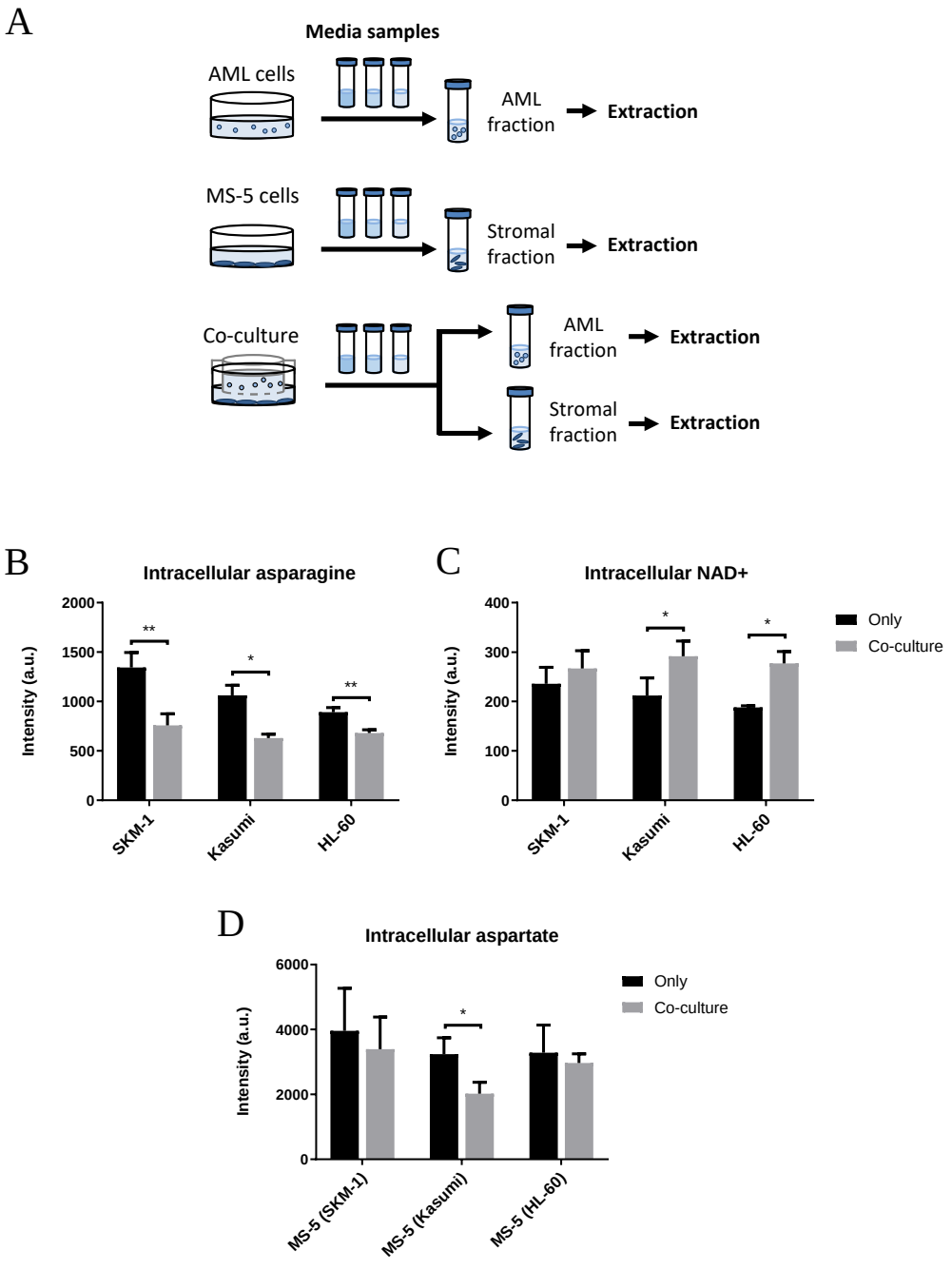

Figure 3.10 Co-cultures separated by a permeable membrane: experimental design and intracellular metabolite levels.

A) Schematic representation of experimental design used for co-culture with a permeable membrane experiments. In brief, AML and stromal cells were cultured separately as well as in co-culture separated by a permeable membrane under the same conditions (cell culture medium, cell number and density), samples of medium were collected at certain time points and cells were separated and extracted. B) Intracellular metabolite levels detected in SKM-1 cells cultured alone or in co-culture with MS-5 cells for 24 hours. Cells were separated and polar metabolites were extracted before performing ^{1}H-NMR spectroscopy. Bars represent the mean of n=3 independent experiments and error bars represent standard deviation. An unpaired t-student test was applied for each metabolite and p-values were represented as * for p-value<0.05, ** for p-value<0.01 and *** for p-value<0.001.

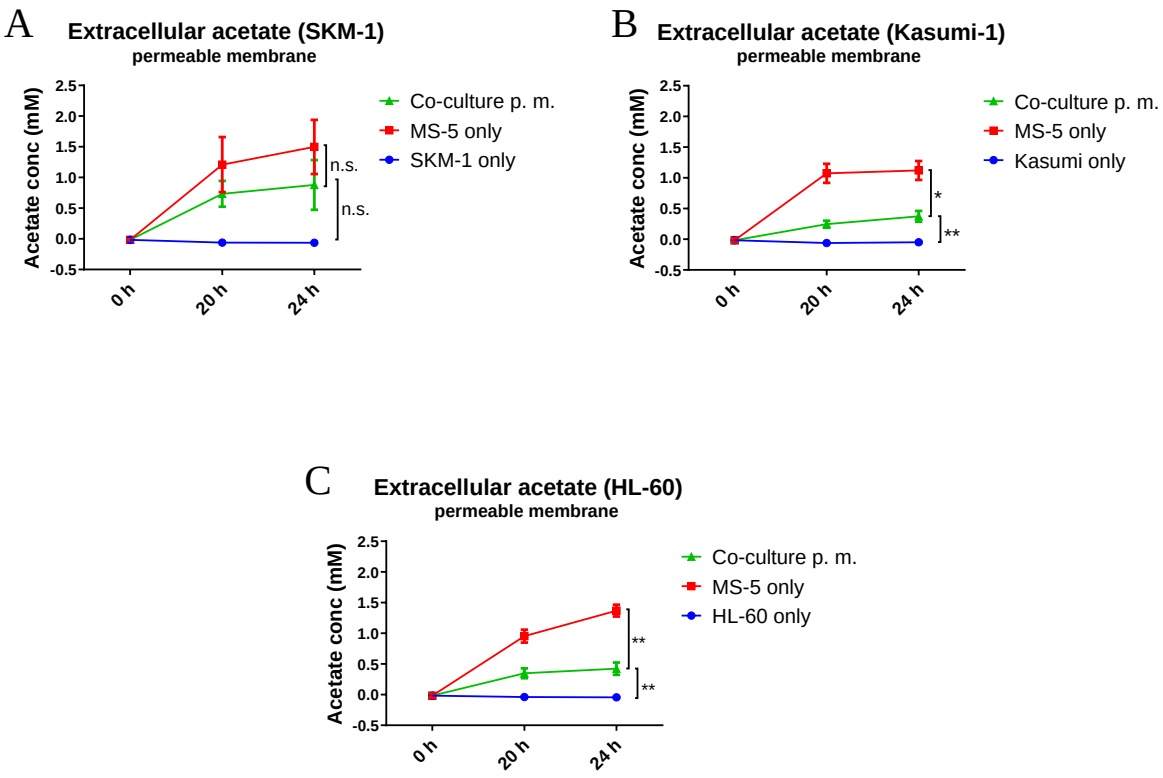

Figure 3.11. Extracellular acetate in co-cultures separated by a permeable membrane.

SKM-1, Kasumi and HL-60 cells were cultured alone or with MS-5 cells separated by a permeable membrane for 24 hours. Samples of media were collected at 0, 20 and 24 hours and were analysed by ^{1}H-NMR spectroscopy. Acetate levels were analysed and are represented in this figure. Each point represents the mean of n=3 independent experiments and error bars represent standard deviation. An unpaired t-student test was applied at time point 24 hours for each condition and p-values were represented as * for p-value<0.05, ** for p-value<0.01 and *** for p-value<0.001.

3.2.5. Co-culture of AML cells with unrelated adherent cells and another stromal cell line does not yield increased acetate secretion

Next, I sought to determine whether the increased acetate secretion in co-culture was specific of the interaction of AML and stromal cells or it could occur with other unrelated cells. To answer this, I selected the cervical cancer cell line HeLa as an unrelated cell line because of its adherent properties and similar morphology to MS-5 cells. The same experimental set up as previous co-cultures was performed: HeLa cells were grown until confluence and then cultured alone and with SKM-1 cells. Media samples were collected and analysed by ^{1}H-NMR spectroscopy.

HeLa cells did not secrete acetate in any of the studied conditions, as can be seen in Figure 3.12A. This result suggests that the increased acetate secretion could be specific to stromal cells.

To corroborate the previous hypothesis, the same experiment was performed using another stromal cell line, the human stromal cell line HS-5, following the same experimental set up. The NMR data obtained from the collected medium samples (Figure 3.12B) did not show any acetate secretion by HS-5 cells or in co-culture. Altogether, these results suggests that the increased acetate secretion could be particular of MS-5 cells.

A

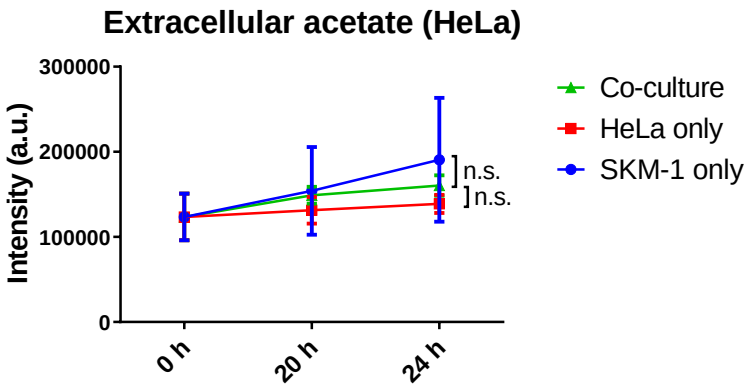

B

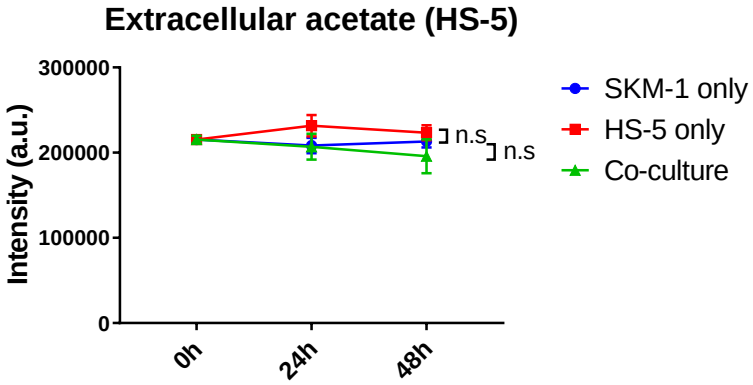

Figure 3.12 Extracellular acetate levels in co-cultures with unrelated adherent cells and human stromal cells.

A) SKM-1 cells were cultured alone or with HeLa cells for 24 hours. Samples of media were collected at 0, 20 and 24 hours and were analysed by ^{1}H-NMR spectroscopy. Acetate levels are represented in this figure. B) SKM-1 cells were cultured alone or with HS-5 cells for 48 hours. Samples of media were collected at 0, 24 and 48 hours and were analysed by ^{1}H-NMR spectroscopy. Acetate levels are represented in this figure. For A and B, each point represents the mean of n=3 independent experiments and error bars represent standard deviation. An unpaired t-student test was applied at time point 24 hours for each condition and p-values were represented as n.s. for not significant * for p-value<0.05, ** for p-value<0.01 and *** for p-value<0.001.

3.2.6. Do primary AML and healthy donor samples present increased acetate secretion in co-culture?

Work in this section was carried out in the University Medical City of Groningen (UMCG) in Groningen, The Netherlands as a placement. I performed the experiments in collaboration with Alan Cunningham (from Prof. Schuringa's lab) as a collaborative work within the HaemMetabolome-ITN (675790).

Previous results in this chapter indicated that AML cell lines directly co-cultured with MS-5 cells presented a significant increase in acetate secretion. I sought to investigate whether primary AML patient samples would present an increased acetate secretion in co-culture and whether healthy donor samples would present a similar behaviour or whether acetate secretion could be specific of AML cells.

A panel of four AML and two healthy peripheral blood samples was used. Mononuclear cells obtained from Martini Hospital in Groningen (The Netherlands) had been previously isolated by density gradient and kept frozen. In order to study differences in stemness, mononuclear cells were thawed and sorted into CD34+ CD38- and CD34+ CD38+ (Figure 3.13), where CD34+ CD38- cells have commonly been recognised as the AML stem cell population with self-renewal properties and CD34+ CD38+ is the committed myeloid progenitor population [25]. After sorting, when enough cell numbers were obtained, cells were directly plated with MS-5 alone and in co-culture and samples of media were collected at 0, 24 and 48 hours. ^{1}H-NMR spectroscopy was performed, and glucose, lactate and acetate extracellular levels were analysed.

The first two primary AML samples analysed, AML1 and AML2 (Figure 3.14), did not substantially consume glucose or secrete lactate when cultured alone. In co-culture, glucose

consumption and lactate secretion were very similar to MS-5 cells alone suggesting that AML cells did not metabolise them. The lack of glucose and lactate metabolism was contrary to data obtained from the AML cell lines tested previously. This result seems to strongly indicate that these primary AML cells had an extremely slow metabolism or were not metabolically active.

Acetate levels did not show any substantial difference between groups. Additionally, there was no difference between the CD38 positive and negative cells.

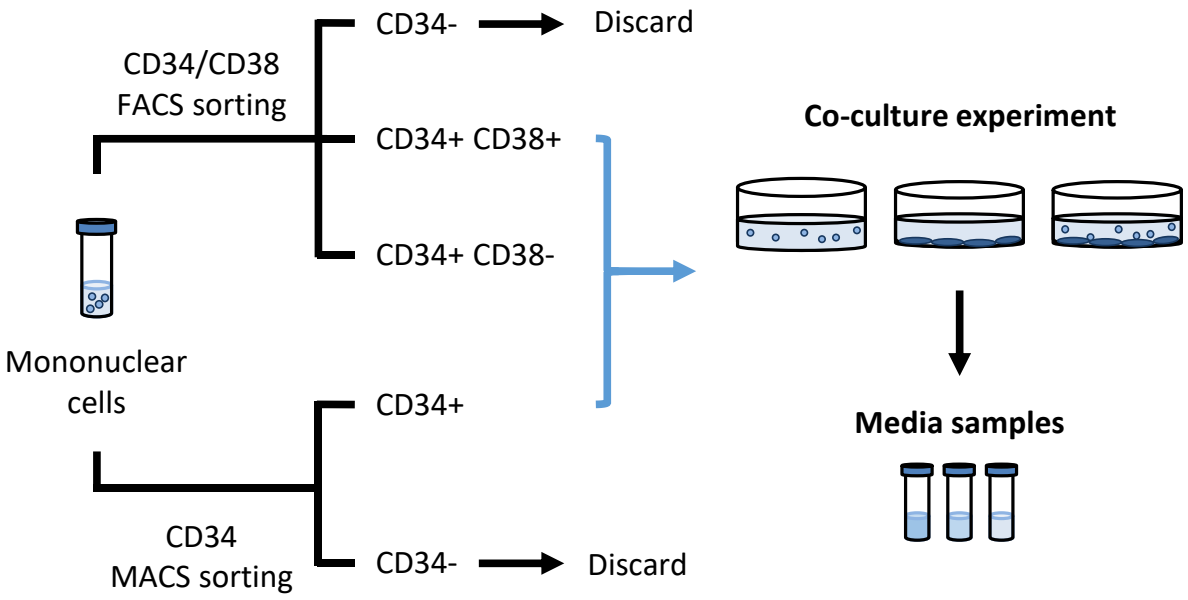

Figure 3.13 Experimental design for primary samples isolation and co-culture (UMCG).

In brief, mononuclear cells where either CD34/CD38 FACS sorted or CD34 MACS sorted. For CD34/CD38 FACS sorting, CD34- cells were discarded and CD34+ CD38+ and CD34+ CD38- cells where cultured alone and co-cultured with MS-5 cells as previously described in this chapter. For CD34 MACS sorting, CD34- cells were discarded and CD34+ cells where cultured alone or co-cultured with MS-5 cells as previously described in this chapter. Samples of media where collected at 0, 24 and 48 hours.

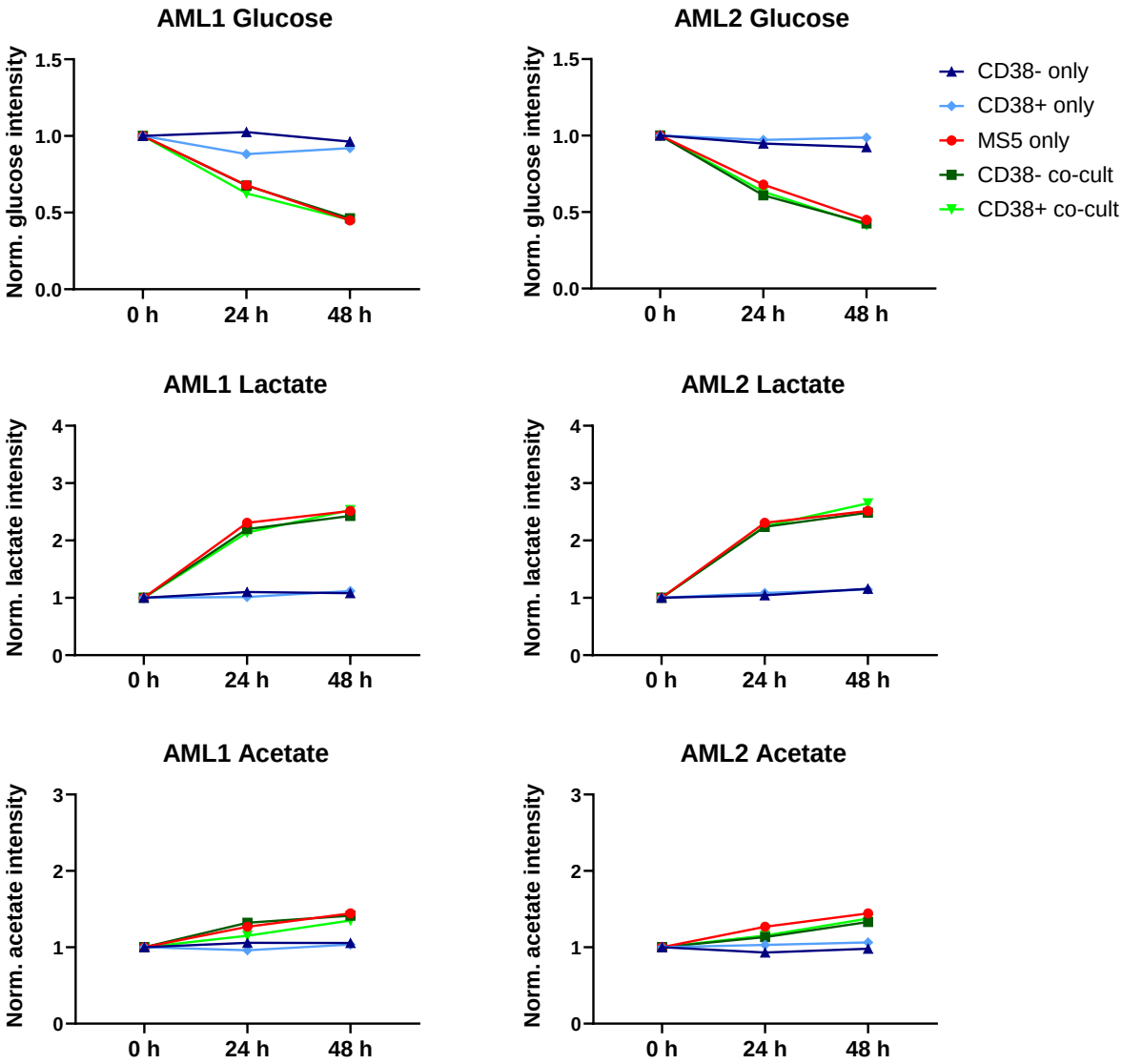

Figure 3.14 Extracellular metabolites in primary AML samples 1 and 2.

Primary AML mononuclear cells were thawed and sorted selecting the CD34+ CD38- and CD34+ CD38+ populations. For AML1, only one replicate of AML cells alone and in co-culture could be used (500,000 cells per condition) due to cell number availability after sorting. One replicate of MS-5 cells alone was prepared. For AML2, only one replicate of CD38- and three replicates of CD38+ AML cells were used. One replicate of MS-5 cells alone was prepared. AML and MS-5 cells were cultured in separated plates and in co-culture in direct contact under the same conditions (cell culture medium, cell number and density) for 48 hours. Samples of media were collected at 0, 24 and 48 hours and analysed by ^{1}H-NMR spectroscopy. Statistical analysis could not be applied for patient cells due to insufficient replicates.

The following samples, AML3 and AML4, were used with only one population of AML cells. For AML3, FACS sorting resulted in a majority of CD34+ CD38- cells. Moreover, the number of CD34+ CD38+ cells obtained was too low to perform an experiment and, therefore, only CD34+ CD38- cells were used. For AML4, MACS sorting was used to obtain CD34+ cells, CD38 status was not tested.

AML3 and AML4 (Figure 3.15) showed slight glucose consumption and lactate secretion when cultured alone. However, a substantially higher rate of glucose and lactate turnover was found in co-culture compared to MS-5 cells alone. Therefore, these primary cells were considered to be metabolically active.

AML3 alone (Figure 3.15, left, blue dots) and in co-culture (Figure 3.15, left, green triangles) consumed acetate and did not mimic the increased acetate secretion found in co-cultures with AML cell lines. This result reveals that AML cells can consume acetate suggesting that a crosstalk mediated by acetate could be occurring in co-culture. AML4 did not consume or secrete acetate when cultured alone (Figure 3.15, right, blue dots). However, an increased acetate secretion in co-culture (Figure 3.15, right, green triangles), compared to MS-5 cells alone (red squares), was detected. This result agrees with the AML cell line data from previous sections supporting the notion that acetate is a crucial metabolite in co-culture.

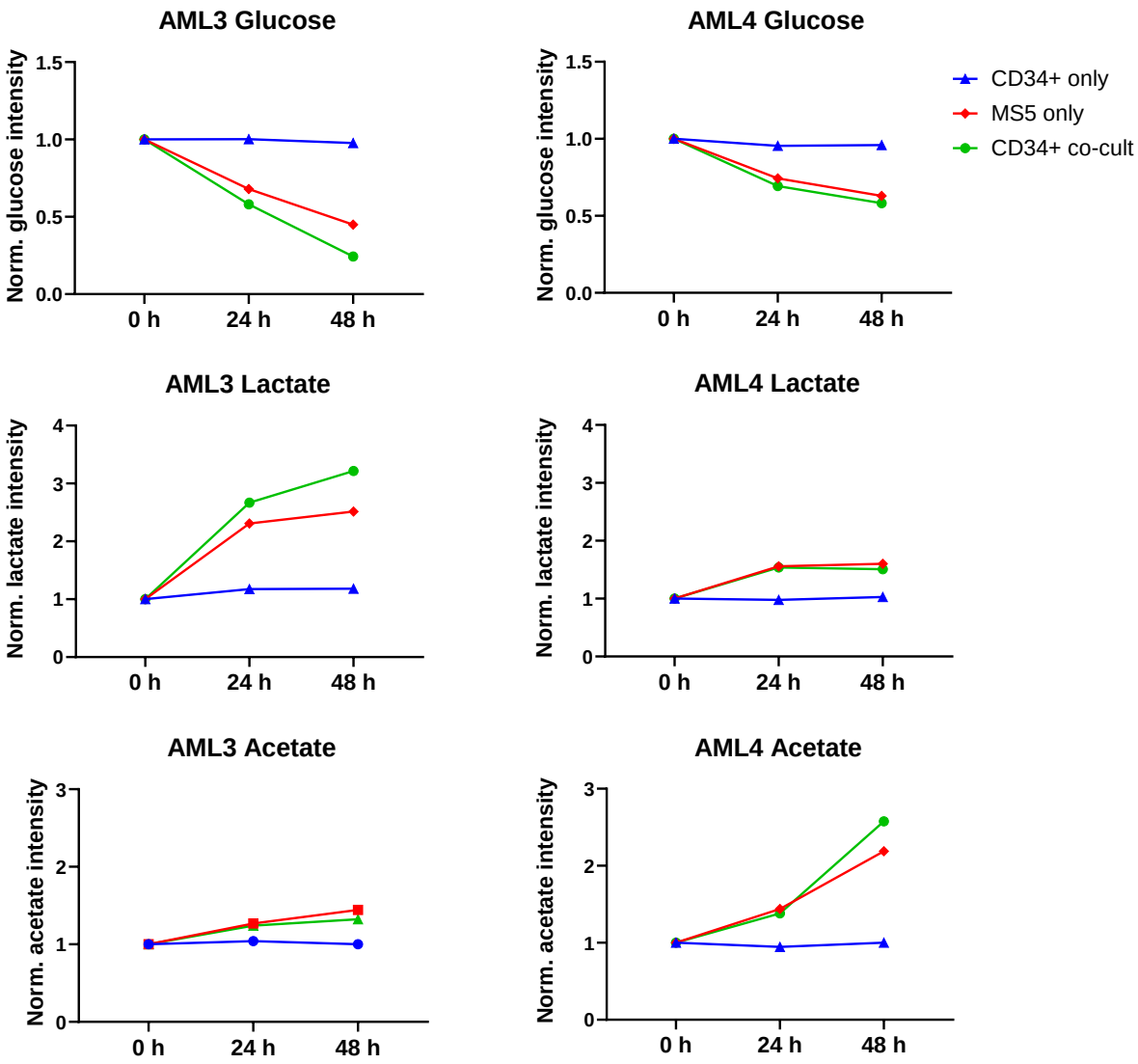

Figure 3.15 Extracellular metabolites in primary AML samples 3 and 4.

For AML3, mononuclear cells were thawed and sorted selecting the CD34+ CD38- and CD34+ CD38+ populations. Only CD34+ CD38- cells were found. Three replicates of AML cells alone and in co-culture (500,000 cells per condition) and one replicate of MS-5 cells alone were prepared. For AML2, mononuclear cells were thawed and CD34+ cells were sorted with MACS. Three replicates of CD34+ AML cells were used. For both, AML and MS-5 cells were cultured in separated plates and in co-culture in direct contact under the same conditions (cell culture medium, cell number and density) for 48 hours. Samples of media were collected at 0, 24 and 48 hours and analysed by ^{1}H-NMR spectroscopy. Statistical analysis could not be applied for patient cells due to insufficient replicates.

In addition to assessing the metabolism of primary AML cells in co-culture, two peripheral blood mononuclear cells (PBMC) samples from healthy donors were analysed to determine whether AML cells behave differently. For PBMC1, FACS sorting yielded both CD34+ CD38- and CD34+ CD38+ populations. For PBMC2, MACS sorting was used obtaining CD34+ cells and not testing differences between CD38+ and CD38-.

Both PBMC1 and PBMC2 consumed glucose and secreted lactate when cultured alone (Figure 3.16, blue). They also consumed and secreted more glucose and lactate, respectively, in co-culture (Figure 3.16, green) compared to MS-5 alone (red). Moreover, PBMC1 CD38+ in co-culture at 48 hours had consumed all the available glucose. Thus, these PBMC cells were considered metabolically active. In co-culture (Figure 3.16, green), both samples did not induce an increased acetate secretion. These results reveal that healthy samples did not behave like AML cells and did not induce an increase in acetate secretion. Additionally, PBMC1 CD38+ cells (Figure 3.16, light blue) showed acetate consumption at the latest time point. This result could be explained by cells being starved due to the low levels of glucose.

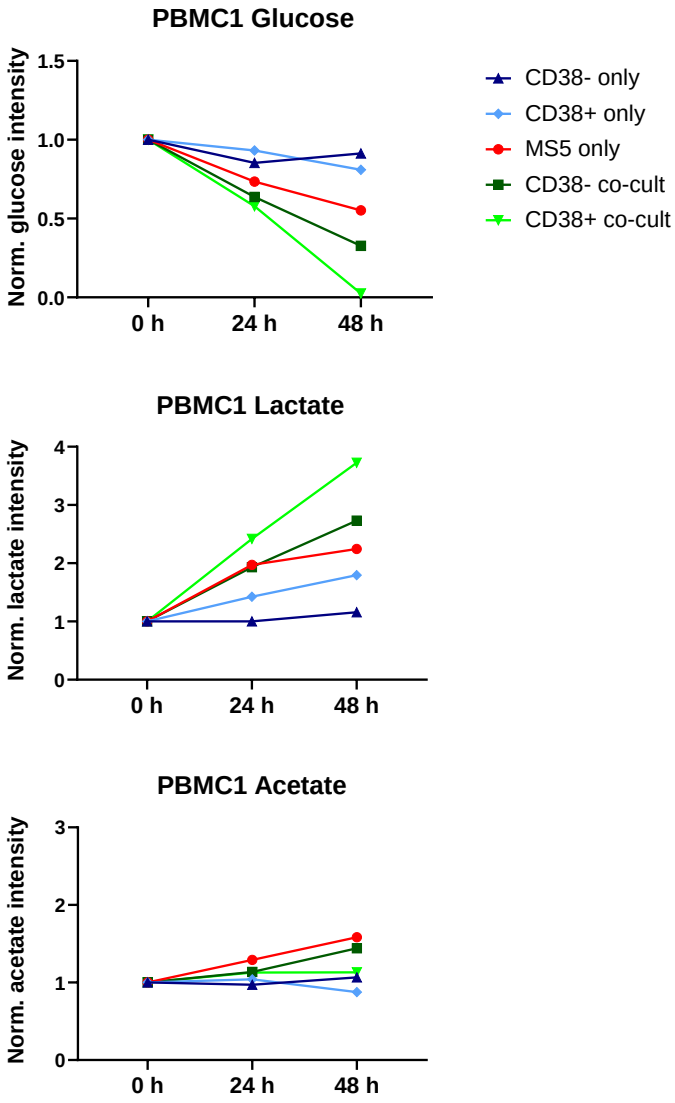

Figure 3.16 Extracellular metabolites in healthy peripheral blood mononuclear cell sample 1.

Healthy peripheral blood mononuclear cells were thawed and FACS sorted selecting the CD34+ CD38- and CD34+ CD38+ populations. Three replicates of healthy PBMC cells alone and in co-culture (500,000 cells per condition) and one replicate of MS-5 cells alone were used. Healthy PBMCs and MS-5 cells were cultured in separated plates and in co-culture in direct contact under the same conditions (cell culture medium, cell number and density) for 48 hours. Samples of media were collected at 0, 24 and 48 hours and analysed by ^{1}H-NMR spectroscopy. Statistical analysis could not be applied for patient cells due to insufficient replicates.

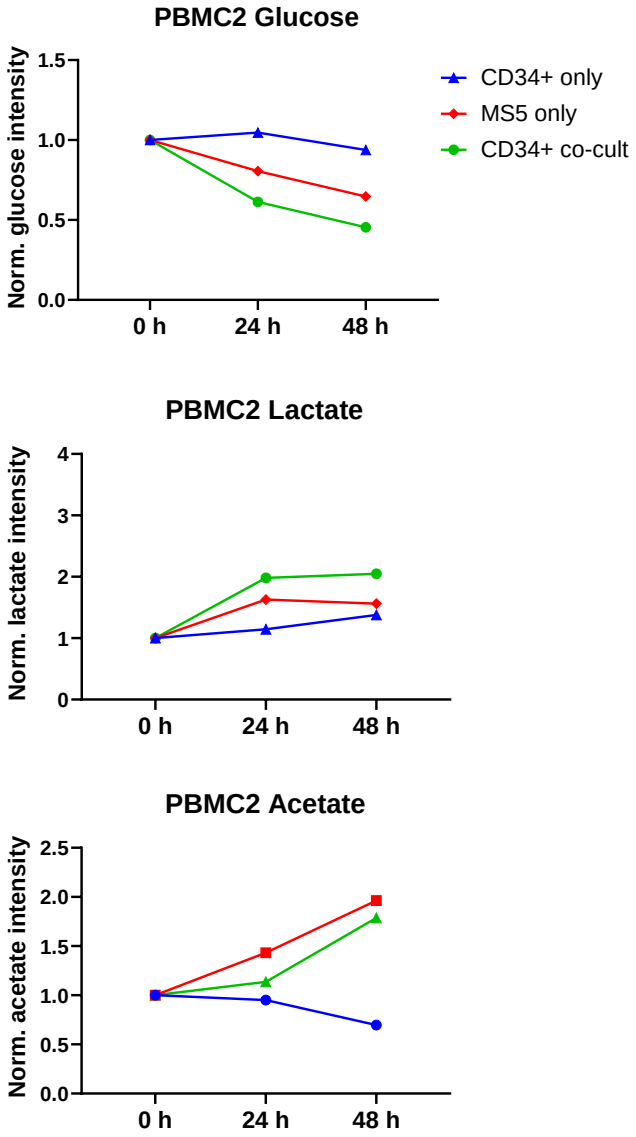

Figure 3.17 Extracellular metabolites in healthy peripheral blood mononuclear cell sample 2.

Healthy peripheral blood mononuclear cells were thawed and MACS sorted, selecting CD34+ cells. Three replicates of healthy PBMC cells alone and in co-culture (500,000 cells per condition) and one replicate of MS-5 cells alone were used. Healthy PBMCs and MS-5 cells were cultured in separated plates and in co-culture in direct contact under the same conditions (cell culture medium, cell number and density) for 48 hours. Samples of media were collected at 0, 24 and 48 hours and analysed by ^{1}H-NMR spectroscopy. Statistical analysis could not be applied for patient cells due to insufficient replicates.

The summary of these preliminary results led to the realisation of several factors that were key for obtaining meaningful data: the metabolic stage of the cells; sorting strategy and good viability. Thus, taking advantage of culture-conditions already established in Dr Garcia's lab in the University of Birmingham (UoB), I performed additional metabolic analysis in other 4 samples obtained from the Queen Elisabeth Hospital in Birmingham and from a UoB healthy donor.

A panel of three AML and one healthy peripheral blood samples was analysed. Mononuclear cells had been previously isolated by density gradient and frozen down. Cells were thawed and incubated for 24 hours in a CD34+ expansion medium following an in-house protocol (Figure 3.18) before CD34+ sorting with MACS. Sorted CD34+ cells were plated with MS-5 alone and in co-culture. Samples of media were collected at 0, 24, 48 and 72 hours, and ^{1}H-NMR spectroscopy was performed. Glucose and lactate levels were analysed to determine if cells were metabolically active.

As it can be seen in Figure 3.19, AML5 did not uptake glucose and neither secreted lactate when cultured alone (blue dots). However, in co-culture (green triangles), it consumed glucose and secreted lactate at a higher level than MS-5 cells alone (red squares). This result suggests that AML5 cells were only metabolically active in co-culture. AML6 (Figure 3.19) consumed glucose when cultured alone (blue dots) but did not secrete lactate. In co-culture (green triangles), it consumed more glucose and secreted more lactate than MS-5 cells cultured alone (red squares). Hence, AML6 cells in co-culture were considered metabolically active.

In both cases acetate levels in co-culture after 72 hours were substantially higher than in MS-5 cells alone. Moreover, after 48 hours, acetate levels in AML5 cells in co-culture (green triangles) were already higher than in MS-5 cells alone (red squares). These results resemble

the previous findings in co-cultures with AML cell lines, where increased acetate secretion was found.

Another observation that drew attention was that increased acetate secretion in co-culture occurred at the latest time points, which coincided with higher glucose consumption and lactate productions. This result could be attributed to cells recovering from thawing and sorting and becoming more metabolically active.

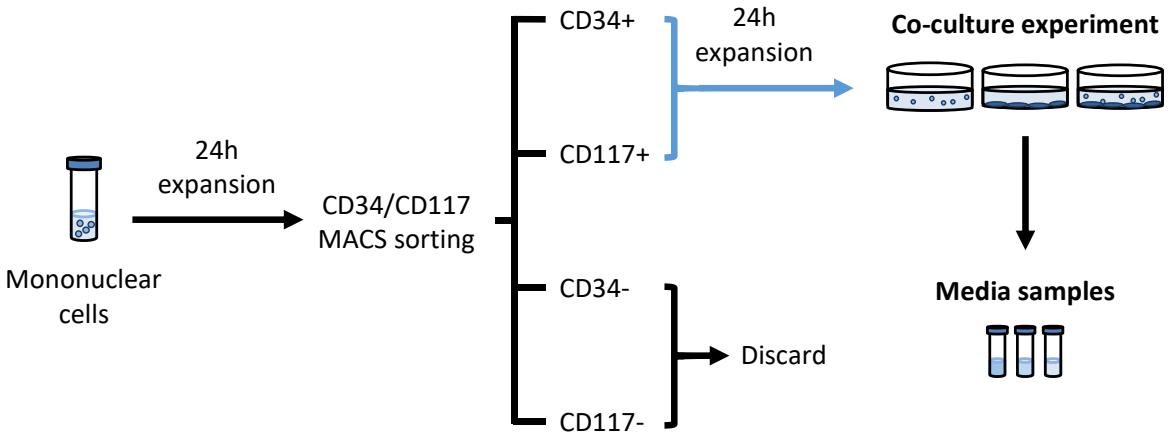

Figure 3.18. Experimental design for primary samples isolation and co-culture (UoB).

Schematic representation of experimental design used for co-cultures with primary samples. In brief, mononuclear cells are expanded for 24 hours prior to CD34/CD117 MACS sorting. CD34+ and CD117+ cells were expanded for 24 hours and cultured alone or co-cultured with MS-5 as previously described. Samples of media where collected at 0, 24, 48 and 72 hours.

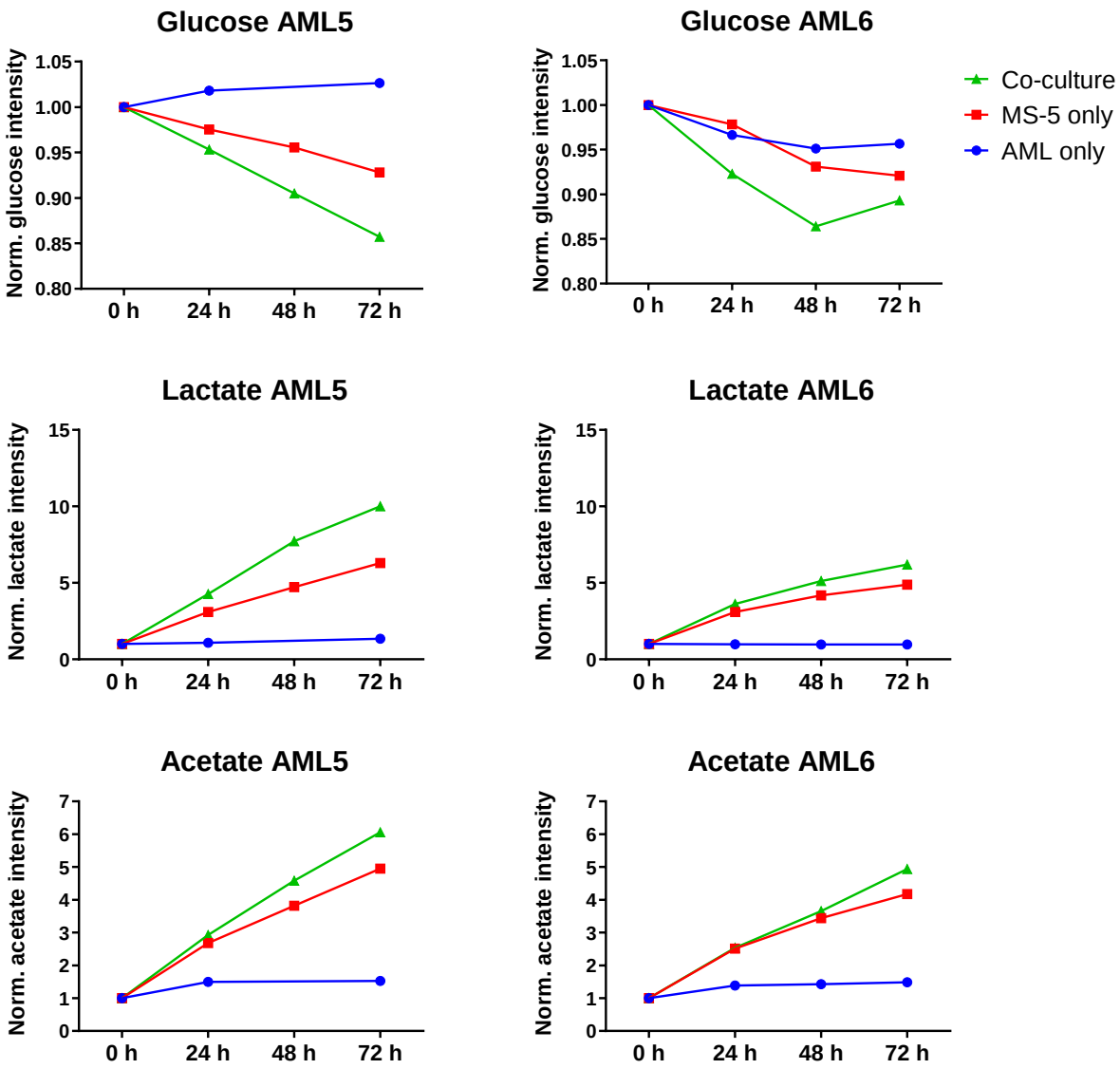

Figure 3.19 Extracellular metabolites in AML patient samples 5 and 6.

Primary AML mononuclear cells were thawed and MACS sorted as described in the experimental design. For AML5, two replicates of AML cells alone and in co-culture could be used (500,000 cells per condition) due to cell number availability after sorting. For AML6, only one replicate of AML cells alone and in co-culture could be used. Three replicates of MS-5 cells alone were prepared for both experiments. AML and MS-5 cells were cultured in separated plates and in co-culture in direct contact under the same conditions (cell culture medium, cell number and density) for 72 hours. Samples of media were collected at 0, 24, 48 and 72 hours and analysed by ^{1}H-NMR spectroscopy. Statistical analysis could not be applied for patient cells due to insufficient replicates.

A sample from a chronic myelomonocytic leukaemia (CMML) patient was also included, as it was first categorised as AML and was later diagnosed as CMML. This sample (Figure 3.20, left) consumed low levels glucose when cultured alone (blue dots) but did not secrete lactate. Moreover, it did consume low amounts of lactate. In co-culture (green triangles), it consumed glucose at a slightly higher rate than MS-5 cells alone but did not secrete more lactate than MS-5 cells alone (red squares). When cultured alone (Figure 3.20, left, blue dots), it consumed acetate but there were no differences between CMML in co-culture (green triangles) and MS-5 cells alone (red squares). The low glucose consumption and absence of lactate secretion suggest that these cells could either present a slow metabolism or not be metabolically active.

Finally, a healthy peripheral blood sample PBMC3 was analysed (Figure 3.20, right). Glucose consumption in this sample, in all cases, did not present a linear decrease over time. However, PBMC3 cells cultured alone (Figure 3.20, right, blue dots) consumed glucose, and they also consumed more glucose in co-culture than MS-5 cells cultured alone (red squares). Lactate secretion also occurred in cells alone and in co-culture (blue dots and green triangles, respectively). Therefore, the sample was considered to be metabolically active. Co-culture acetate levels (Figure 3.20, right, green triangles) were very similar to MS-5 cells alone (red squares), there was not an increase in acetate secretion in co-culture. This result agrees with the healthy donor data from PBMC1 and PBMC2, suggesting that healthy samples do not induce increased acetate secretion in co-culture.

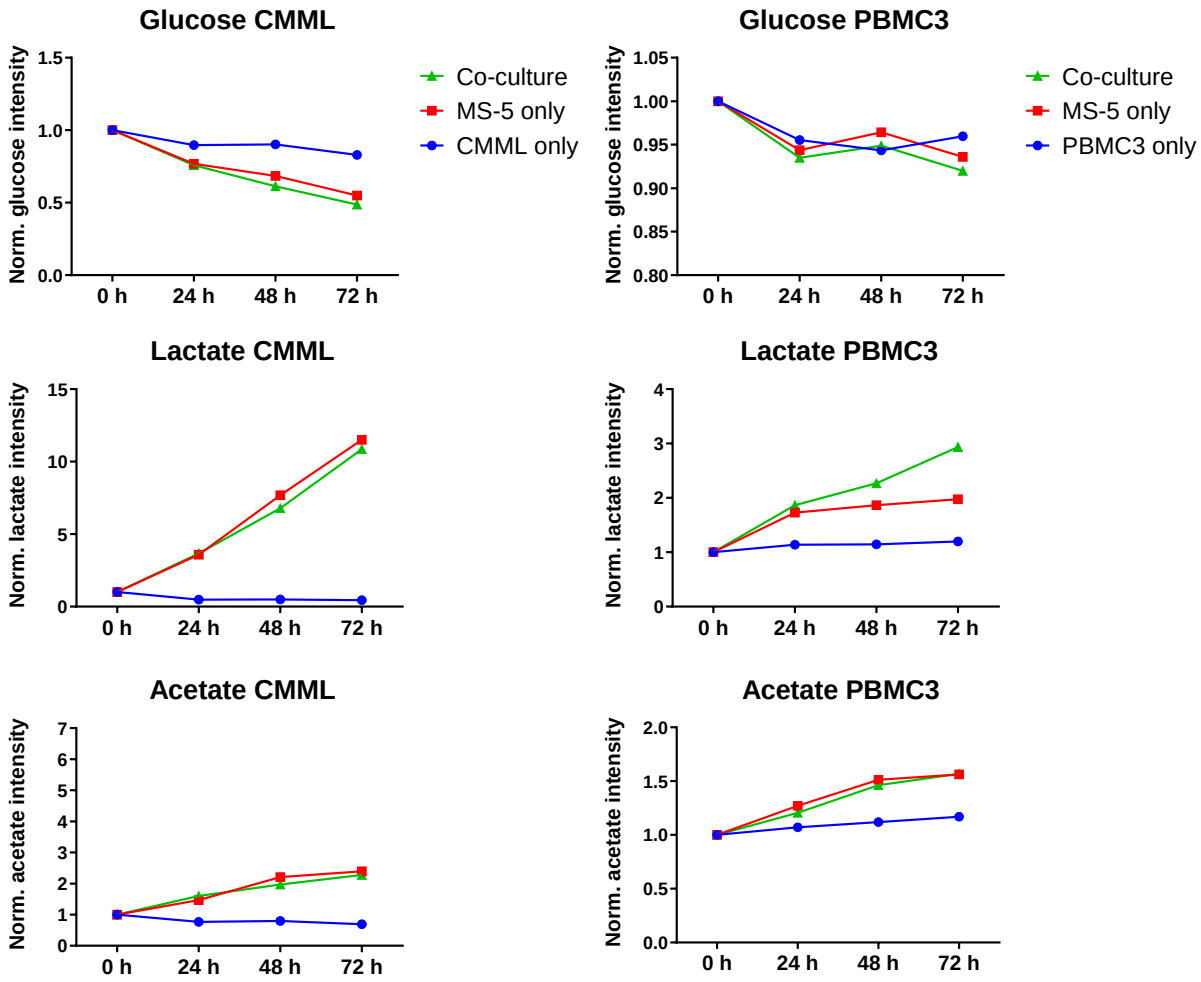

Figure 3.20 Extracellular metabolites in a primary CMML sample and the healthy peripheral mononuclear cell sample 3.

For the CMML sample, primary CMML mononuclear cells were thawed and MACS sorted selecting the CD34+ population. One replicate of CMML cells alone and two replicates of CMML cells in co-culture could be used (500,000 cells per condition) due to cell number availability after sorting. Primary healthy mononuclear cells were isolated by density gradient from peripheral blood and MACS sorted selecting the CD34+ population. Two replicates of healthy PBMC cells alone and in co-culture were used. For both samples, two replicates of MS-5 cells alone were prepared. CMML/healthy PBMC and MS-5 cells were cultured in separated plates and in co-culture in direct contact under the same conditions (cell culture medium, cell number and density) for 72 hours. Samples of media were collected at 0, 24, 48 and 72 hours and analysed by ^{1}H-NMR spectroscopy. Statistical analysis could not be applied for patient cells due to insufficient replicates.

Out of six primary AML samples analysed in this chapter, four were metabolically active (one of them only in co-culture) and three presented an increased acetate secretion when co-cultured with MS-5 cells. A CMML sample was also analysed and did not yield an increased acetate secretion. However, it was unclear whether this CMML sample was metabolically active. All the healthy donor samples analysed were metabolically active and none of them presented differences in acetate production in co-culture in comparison to MS-5 cells alone. These results suggested that increased acetate secretion in co-culture: (i) was specific of AML cells; (ii) was related to the metabolic state of cells; and (iii) did not occur with all AML samples.

	Metabolically active?		Acetate secretion?
	Alone	**Co-culture**	
AML1	✗	✗	✗
AML2	✗	✗	✗
AML3	✓	✓	✗
AML4	✓	✓	✓
AML5	✗	✓	✓
AML6	✓	✓	✓
CMML	?	?	✗
PBMC1	✓	✓	✗
PBMC2	✓	✓	✗
PBMC3	✓	✓	✗

Table 11 Summary of results obtained with primary AML/CMML patient samples and healthy donors in co-culture.

3.3. Discussion

3.3.1. Designing co-culture studies to characterize metabolite interactions by ^{1}H-NMR spectroscopy

The overall aim of this chapter was to determine whether AML and stromal cells would present a metabolic interaction in co-culture. For this, it was pivotal to establish an experimental design that would enable the interaction as well as the later separation of cell types for NMR spectroscopy analysis. It was also essential to establish controls to compare the metabolism of each cell type cultured alone and in co-culture. Moreover, characterising the role of other factors, such as proliferation, in the metabolism of cells in co-culture was essential.

First, it was crucial to establish robust controls to be able to compare metabolic levels in co-culture. To assure comparisons were valid, cells were cultured alone and in co-culture under the same conditions of cell culture medium, cell culture vessel, cell number and density [173]. Cells were incubated for the same amount of time and samples of medium were collected at different time points.

Another important point to produce comparable and reliable data, was to use an optimum method to stop metabolism and extract intracellular metabolites. Thorough washing whilst avoiding intracellular leakage, and quick quenching of the metabolism was fundamental [198]. A method that had been developed in-house for rapid metabolite extraction was used [173] ensuring clean and immediate quenching of metabolism and optimized extraction of polar metabolites.

An AML cell line, SKM-1, and a mouse stromal cell line, MS-5, were chosen for the first co-culture experiments. Co-cultures of SKM-1 and MS-5 cells were performed by allowing MS-5 cells to attach to the bottom as a confluent monolayer and adding SKM-1 cells as a suspension.

A population of SKM-1 cells adhered to the MS-5 monolayer. Adhesion of AML cells to stroma was expected as it had been reported since very early AML-stroma studies [199]. AML cells attached to the monolayer of stroma could impede proper separation of cells in co-culture, as if only suspension cells were taken off together and the monolayer was detached and extracted, those remaining AML cells attached would contaminate the stromal extracts. Therefore, separation and clean-up of the stromal cells were necessary. A mild trypsinisation protocol, previously described in the literature to detach AML cells from adipocytes [60], was used. As the protocol could leave remaining AML cells or detach some stromal, the procedure was timed, and every step was checked under the microscope to ensure a correct separation.

Proliferation could be a critical factor altering metabolism that could mask the interactions found in co-culture. Higher rates of proliferation would be translated into faster exhaustion of nutrients and increase in waste by-products in the medium altering the metabolism of the present cells [196]. Therefore, I analysed the rate of proliferation of AML cells cultured alone compared to in co-culture. I decided to use CFSE, instead of bromodeoxyuridine assays or colorimetric assays (such as resazurin), because it can be incorporated into the AML cells before performing co-cultures and it is not perturbed by the adjacent cells (MS-5). No differences in proliferation were found for any of the three AML cell lines tested (Figure 3.9) indicating that metabolic changes characterised can be attributed entirely to interactions occurring in co-culture and not to effects derived from variations in proliferation.

3.3.2. Isolation and culture of primary AML and healthy donor samples for performing co-culture experiments

One of the objectives of this chapter was to characterise whether the metabolic alterations found in co-cultures with cell lines, especially increased acetate secretion, also occurred in primary AML and healthy donor co-cultures with MS-5 cells. Moreover, I also wanted to characterise whether the degree of stemness of primary AML and healthy donors would have a metabolic effect in co-culture.

Firstly, co-culture experiments comparing the population with self-renewal properties (CD34+ CD38-) from the population of myeloid progenitors (CD34+ CD38+) [25], did not yield different metabolic outcomes in primary AML cells (Figure 3.14). In healthy donor samples, CD38+ cells showed faster metabolic rates for glucose consumption and lactate secretion (Figure 3.16). This result suggests that a higher proliferation of this population took place and allows the conclusion that, in this case, CD38 status had no effect in the metabolism of cells in co-culture.

Another important consideration for primary co-cultures was the ratio between AML/Healthy CD34+ cells and MS-5 cells. Even though cell number was reduced, due to primary cell availability being extremely limited, the 4:1 AML-stroma ratio was kept to have comparable results to those obtained with cell lines.

Finally, primary co-culture experiments revealed that not all primary cells were metabolically active. Several primary AML samples (Figure 3.14) did not show any glucose consumption and lactate secretion. The lack of basal metabolism could be caused by cells kept frozen for long periods and/or bad recovery after thawing or sorting. The in-house protocol with expansion times after thawing and sorting seemed to yield better recovery of cells. However, a CMML

sample was processed following this protocol and, although it was not clear, it seemed to not be metabolically active, as it consumed extremely low levels of glucose and did not secrete lactate (Figure 3.20).

3.3.3. Glycolysis in co-culture

All proliferating cells present a glycolytic metabolism where glucose is utilised to produce lactate and secrete it to the extracellular medium [196]. Cancer cells rely on glycolytic metabolism because, even it is not optimal for energy scavenging, it provides them with the necessary biomass for proliferation [37]. In the first case analysed, using SKM-1 and MS-5 cells in co-culture, increased glucose consumption and lactate secretion compared to cells cultured alone were detected. The relative consumption/production of glucose and lactate coincided with the sum of the relative consumption/production of glucose and lactate of cells alone (Figure 3.6A), respectively. Intracellular levels of glucose were not detected, probably because glucose is quickly metabolised. Lactate levels intracellularly did not vary in both SKM-1 and MS-5 cells (Figure 3.3B and Figure 3.4B, respectively), possibly because it presented an overflow metabolism, where lactate is secreted as it is generated intracellularly. No significant differences in glucose or lactate metabolism were found in the other AML cell lines tested in direct contact or separated by a permeable membrane. These results suggest that glycolysis is not altered in co-culture.

In contrast to my results, in a similar study using leukaemic cell lines and primary MSCs, an increase in glycolysis was found [200]. Almost all the AML cells tested in co-culture in this study did not consume more glucose than when cultured alone and secreted more lactate revealing an increase in glycolysis. However, this study also reported that HL-60 cells in co-culture with primary MSCs did not present increased glycolysis, which agrees with my results using the HL-60 cell line. One of the other conflicting points is that primary MSCs alone were reported to secrete negligible levels of lactate. This result is in contrast with my findings as MS-5 cells did secrete lactate at a comparable level to any AML cell line.

3.3.4. Aspartate/Asparagine in co-culture

The combination of all metabolic data obtained suggested that an aspartate-mediated communication between MS-5 and AML cells was possible. MS-5 cells were found to secrete aspartate and asparagine, whilst AML cells were found to consume aspartate (Figure 3.6C). Moreover, all AML cells in co-culture presented lower levels of intracellular asparagine (Figure 3.7A). These results could indicate that MS-5 cells could be secreting aspartate that AML cells could uptake. AML cells could convert aspartate to asparagine to further use it to generate proteins or as an amino acid exchange factor [201]. However, as the relative aspartate secretion in MS-5 cells alone and those found in co-culture were similar, this hypothesis would imply that MS-5 cells in co-culture presented an increased aspartate secretion that could be counteracted by AML cells consumption. This idea could be supported by MS-5 cells presenting lower levels of intracellular aspartate (Figure 3.4C) in co-culture, which could indicate that aspartate is secreted faster or to a higher extent by MS-5 cells in co-culture. However, this hypothesis needs corroboration. Similar intracellular tendencies in aspartate and asparagine, although not significant, were found in co-cultures using a permeable membrane (Figure 3.10B and D), suggesting that this effect could also be taking place at a lower extent and not require direct contact.

An aspartate-mediated metabolic crosstalk was recently reported between squamous cell carcinoma (SCC) cells and cancer-associated fibroblasts (CAF) [202]. Bertero et al reported a communication involving aspartate and glutamate, where aspartate was secreted by CAF cells and consumed by cancer cells while cancer cells secreted glutamate to feed CAFs back. Aspartate sustained the proliferation of SCC cells and glutamate balanced the redox state of CAFs. This data exemplifies how aspartate can be exchanged between cancer cells and

fibroblasts and supports the hypothesis of an aspartate-mediated communication between AML and stromal cells found in this thesis. However, the mechanism for the aspartate exchange between AML and stromal cells did not seem to involve glutamate as MS-5 cells cultured alone did not consume glutamate but secreted it (Figure 3.4C). With the available data, it is unclear whether an aspartate-mediated crosstalk could be taking place in AML-stromal co-cultures. More experiments including transcriptional data and tracer-based NMR spectroscopy could clarify whether there these cells could be exchanging aspartate.

Additionally, another explanation for the significant decrease of intracellular aspartate in MS-5 cells could be related to lower pyruvate availability, which could be caused by pyruvate being converted to acetate and being secreted. Aspartate can be synthesised from pyruvate through the conversion of pyruvate to oxaloacetate by the pyruvate carboxylase (PC) enzyme and further transformation of oxaloacetate to aspartate by transamination by an aspartate aminotransferase enzyme (encoded by *GOT1* or *GOT2*) [203]. Hence, a decrease in aspartate could be caused by the lack of pyruvate, which could be being primarily converted to acetate. In order to corroborate this hypothesis, determining whether acetate is derived from pyruvate, for example using ^{13}C-labelled glucose, would be necessary.

3.3.5. Acetate in co-culture

The major metabolite variation characterised in co-culture was increased acetate secretion. It was found in co-cultures with the three AML cell lines tested (Figure 3.8) and with several primary AML patient samples (Figure 3.15 and Figure 3.19). MS-5 cells alone secreted acetate in a significantly higher degree than AML cells alone. SKM-1 and Kasumi cells consumed acetate when cultured alone and HL-60 produced a minor amount.

Interestingly, although acetate is not part of the formulation of the RPMI medium, SKM-1 and Kasumi cells were found to consume acetate. This is probably explained by the presence of FBS in the medium, as it was shown that acetate can be present in FBS in a range from 100-300 μM [204].

I decided to perform the same co-culture experiments using a permeable membrane to test the effect or lack of cell contact on acetate production. Cell-to-cell contact had already been reported to play a role in the interactions between leukaemic and stromal cells, as reviewed by Gruszka et al [197]. Several examples include: mitochondrial transfer only occurred in co-cultures in direct contact [62]; short-term proliferation, viability and colony formation were higher in co-cultures and apoptosis was reduced to a higher degree in direct contact compared to co-cultures with a permeable membrane [121]; and chemotherapy resistance to etoposide was also higher in direct contact than with a permeable membrane [205]. Increased acetate secretion did not occur in co-cultures separated by a permeable membrane (Figure 3.11) indicating that direct contact between the stromal and AML cell lines is an important factor in acetate secretion in co-culture.

Co-cultures using unrelated adherent cells such as HeLa did not lead to increased acetate secretion (Figure 3.12A). This finding suggests that the increase in extracellular acetate detected could be specific of stromal cells.

Co-cultures with a human stromal cell line (HS-5) did not result in increased acetate secretion (Figure 3.12B). However, as opposed to MS-5 cells, HS-5 cells did not secrete acetate when cultured alone. This result may suggest that this alteration only occurs in acetate-secreting cells and co-culture is boosting the production of acetate. Nevertheless, it would be interesting to expand these results by testing co-cultures with other stromal cell lines such as HS-27A [206] or SR-4987 [207]. Furthermore, a comparison between co-cultures with primary MSCs derived from AML and healthy donors could also unravel differences between the interaction of AML cells with AML-derived and healthy stroma.

Co-cultures with primary AML and healthy cells revealed that acetate secretion occurs in some AML co-cultures but not in any healthy donor samples. Taking into account only the AML cells that were metabolically active, three out of four AML samples and none of the healthy samples analysed presented increase acetate secretion.

It is also important to remark that the AML sample that was metabolically active and did not present increased acetate secretion in co-culture (Figure 3.15, AML 3) had lower intramolecular levels of acetate in co-culture compared to MS-5 cells alone suggesting that AML cells could be consuming acetate in co-culture. Moreover, the same sample showed acetate consumption when cultured alone. This finding suggests that acetate could be key in AML-stromal metabolic interactions: its secretion is increased in some co-cultures whilst it is being consumed by AML cells in co-culture in others.

The sum of these results indicates that a potential acetate-mediated communication could be taking place between AML and MS-5 cells. Acetate has not been reported as a metabolite transferred from supporting cells to cancer cells in co-culture previously. However, other mono-carboxylate metabolites such as lactate and alanine were found to be part of crosstalk between stromal and cancer cells [138, 208, 209].

One of the examples of communication of stromal and cancer cells via metabolites was reported in breast cancer [208], where cancer-associated fibroblasts presented a glycolytic metabolism phenotype and produced lactate to nourish cancer cells. Fibroblasts exposed to breast cancer cells present an upregulation of the expression of mono-carboxylate transporter (MCT) 4, which was caused by oxidative stress [208]. MCT4 allowed them to secrete lactate that was consumed by breast cancer cells using MCT1.

In a different study [209], oxidative cancer cells from several types of cancer (human cervix squamous carcinoma, lung carcinoma and human colorectal adenocarcinoma) were reported to uptake lactate derived from glycolytic tumour cells and use it to fulfil their energy demands. Consequently, oxidative cancer cells spared glucose that diffused into the tumour to feed glycolytic cells. Lactate influx and efflux were mediated by MCT1 and MCT4, as in the previous case. These findings resemble the acetate data obtained and, as acetate can also be transported via MCTs [210, 211], further investigation into these transporters will be carried out in the following chapters.

Another example was found in pancreatic ductal adenocarcinoma, where stroma-associated pancreatic stellate cells provided alanine to cancer cells [138]. Alanine was used by cancer cells to flux the TCA cycle and fulfil non-essential amino acid and lipid requirements.

Overall this data anticipates that crosstalk mediated by acetate is occurring between AML and stromal cells. I decided to focus this thesis mainly in the interchange of acetate because of several reasons. The first one is the magnitude of the increase of acetate secretion, being significantly higher in all the AML cell lines tested and having characterised it in primary AML co-cultures. Secondly, changes in extracellular medium require intracellular processes to be altered to a great extent, as the concentrations of metabolites extracellularly are higher than intracellularly, involving a more pronounced metabolic rewiring. Finally, acetate has gained increasing importance in cancer metabolism as it has been extensively reported as a carbon source alternative [212, 213], as an epigenetic promoter of lipid synthesis [214] and as a nutritional source under stress conditions [215].

In this section, metabolism in AML-stromal co-cultures has been studied. Several metabolic alterations have been found highlighting possible acetate-mediated crosstalk that occurs with AML and MS-5 cells in direct contact. How this additional acetate is generated, by which cell type and what internal genetic alterations are involved are questions that will be addressed in the next chapter.

4. Defining how the metabolism of AML and stromal cells is altered in co-culture

4.1. Introduction

In the previous chapter, the metabolism of AML and stromal cells in co-culture was studied using several cell lines and primary patient and healthy donors. The majority of AML-stroma co-cultures yielded an increased acetate secretion to the extracellular medium. Moreover, the increased acetate secretion was found for MS-5 stromal cells co-cultured with AML cell lines or primary AML patient samples but did not occur with peripheral blood mononuclear cells from healthy donors.

In this chapter, experiments were focused on understanding the mechanism of metabolic rewiring leading to acetate secretion in co-culture. In particular, I sought to determine: (i) which cell type is responsible for the increased acetate secretion; (ii) from which precursors is the secreted acetate derived; (iii) which metabolic pathways are altered in co-culture; and (iv) what is the mechanism that leads to acetate secretion. A combination of several metabolic experiments, including tracer-based approaches, and transcriptomic data will serve as a framework to gain a deeper understanding of the results from the previous chapter.

4.2. Results

4.2.1. Separating AML and MS-5 cells after being in co-culture reveals that MS-5 cells might be responsible for increased acetate secretion

In the previous chapter, the metabolism of AML and stromal cells in co-culture was characterised. Acetate was revealed as the major metabolic variation in co-cultures with AML and MS-5 cells. When AML cell lines and primary patient samples were co-cultured with MS-5 cells an increase in acetate secretion compared to cells cultured alone was detected. However, MS-5 cells did produce acetate to a minor extent when cultured alone. These results suggested that MS-5 cells could be responsible for the extra acetate found in co-cultures. To determine whether MS-5 cells secreted more acetate in co-culture and whether the metabolic changes imposed during co-culture could be maintained, I decided to separate AML and MS-5 cells after co-culture and keep them in the used medium to measure the levels of acetate at different time points.

Three AML cell lines (SKM-1, Kasumi and HL-60) were co-cultured with MS-5 cells for 24 hours before being separated and cultured individually in the same used medium containing the acetate secreted in co-culture, for another 24 hours (Figure 4.1A). Samples of medium were collected at 0, 24 and 48 hours and were analysed by ^{1}H-NMR spectroscopy. Acetate levels at different time points can be seen in Figure 4.1B, C and D.

MS-5 cells that had previously been co-cultured with SKM-1 cells presented significantly higher levels of acetate than after 24 hours of co-culture (Figure 4.1B), suggesting that MS-5 cells continued secreting acetate at a similar rate. SKM-1 cells cultured alone after being in co-culture with MS-5 cells also exhibited significantly higher levels of acetate than after 24 hours of co-culture (Figure 4.1B, green triangle). However, the increase in acetate at 48 hours was

considerably lower than in MS-5 cells (Figure 4.1B, red square) suggesting that SKM-1 cells are not causing the increased acetate secretion found in co-culture.

In the case of co-cultures of Kasumi and MS-5 cells, results showed that MS-5 cells after co-culture continued secreting acetate with a similar trend than in co-culture (Figure 4.1C, green triangle). Kasumi cells after co-culture did not present differences in extracellular acetate levels (Figure 4.1C, red square) suggesting that Kasumi cells are not responsible for acetate secretion in co-culture.

MS-5 cells cultured alone after being in co-culture with HL-60 cells presented significantly higher levels of acetate than when co-cultured for 24 hours (Figure 4.1D, green triangle). HL-60 cells after co-culture had similar levels of acetate than in co-culture (Figure 4.1D, red square) suggesting that, as the other cell types, HL-60 cells do not seem to be responsible for acetate secretion in co-culture.

Overall these results suggest that MS-5 cells might be responsible for the increased acetate secretion found in co-culture. In addition, these results seem to indicate that the metabolic reprogramming that MS-5 cells exhibit in co-culture lasts after being separated for at least 24 hours.

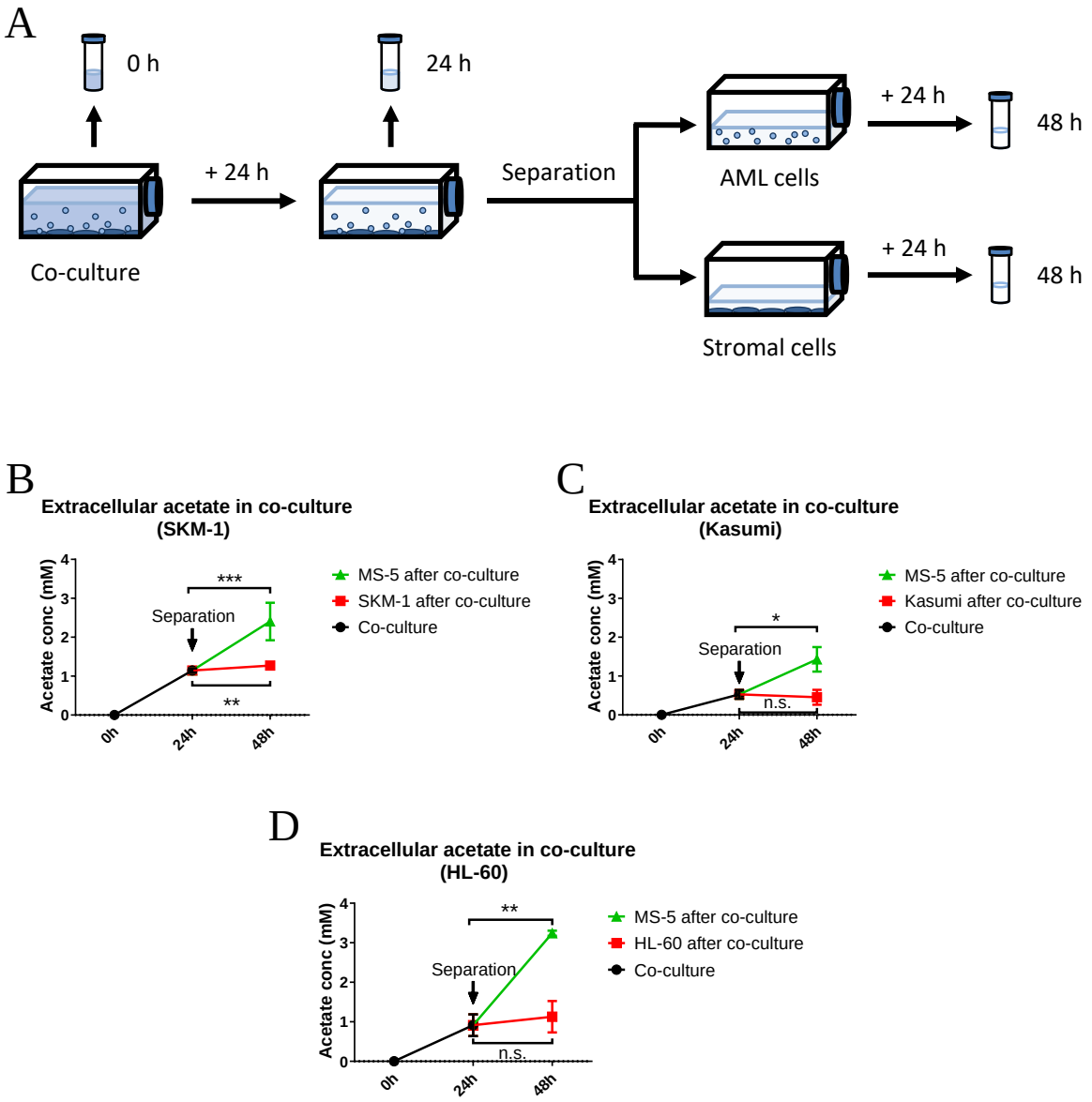

Figure 4.1 AML and MS-5 cells cultured separately after being in co-culture: experimental design and extracellular acetate levels.

A) Schematic representation of experimental design used for co-cultures of AML and MS-5 cells prior to separation and culture of AML and MS-5 cells. In brief, AML and stromal cells were co-cultured for 24 hours before separating both cell types and culturing AML and MS-5 cells separately in the used medium for 24 hours. Samples of medium were collected at 0, 24 and 48 hours. B, C and D) Extracellular acetate levels in AML cell lines (SKM-1 B, Kasumi C and HL-60 D) and MS-5 cells in co-culture for 24 hours and after being separated and cultured alone for 24 hours detected by ^{1}H-NMR spectroscopy. Each point represents the mean of n=3 independent experiments and error bars represent standard deviation. An unpaired t-student test was applied for each cell type and p-values were represented as n.s. for not significant * for p-value<0.05, ** for p-value<0.01 and *** for p-value<0.001.

4.2.2. What is the metabolic precursor for the secreted acetate found in co-culture?

Next, I sought to determine the metabolic precursor for the secreted acetate found in co-culture. Acetate can be derived mainly from three metabolic sources: pyruvate through glycolysis, lipids through fatty acid oxidation and histone deacetylation [216]. Firstly, I decided to determine whether acetate could be derived from pyruvate by performing tracer-based analysis using [U-^{13}C] glucose.

Three AML cell lines (SKM-1, Kasumi and HL-60) and MS-5 cells were cultured alone and in co-culture for 24 hours in [U-^{13}C] glucose labelled medium. Samples of medium were collected after 24 hours and analysed using a ^{13}C-filtered ^{1}H-NMR pulse sequence, that allows to determine the percentage of label incorporation in metabolites using labelled samples only [175]. The percentages of label incorporation found in pyruvate and pyruvate-related metabolites (acetate, alanine and lactate) are shown in Figure 4.2.

The three AML cell lines presented similar label incorporation percentages for all the metabolites analysed (Figure 4.2A, B and C). The label incorporation in extracellular pyruvate and acetate in co-culture was significantly higher than in AML and MS-5 cultures alone for all the cell lines tested (Figure 4.2A, B and C, green vs blue and red bars). These results indicate that the secreted acetate is generated through the metabolism of glucose. Moreover, these results suggest that acetate in co-culture most likely derives from pyruvate arising from glycolysis. For lactate and alanine, a tendency for higher label incorporation in co-culture was detected for all the cell lines used (Figure 4.2A, B and C, green vs blue and red bars), with alanine being significantly higher in co-culture between MS-5 and HL-60 compared to HL-60 grown alone

(Figure 4.2C). Higher label incorporations in lactate and alanine could be in line with increased glycolysis and pyruvate metabolism.

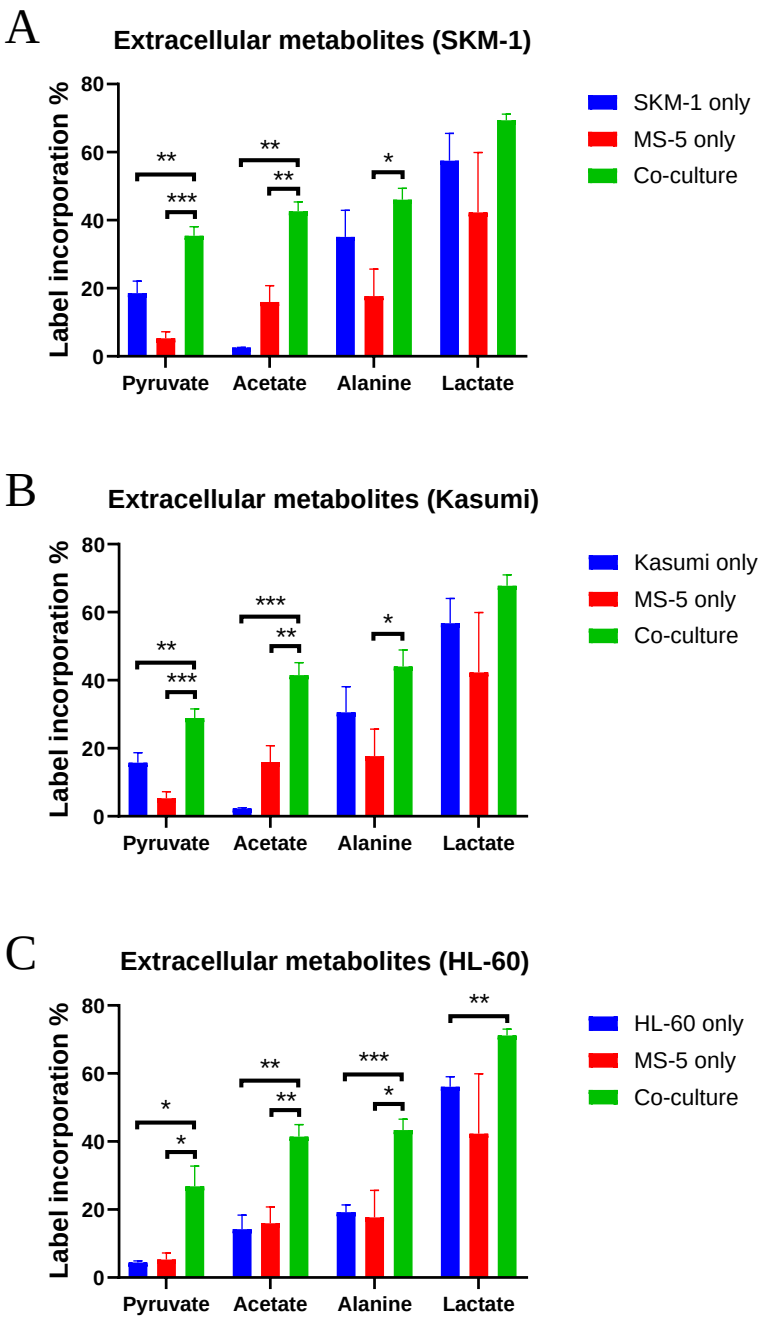

Figure 4.2 Label incorporation from [U-^{13}C] glucose into extracellular metabolites in AML and MS-5 cells cultured alone or in co-culture.

Three AML cell lines (SKM-1, Kasumi and HL-60) and MS-5 cells were cultured alone or in co-culture in a [U-^{13}C] glucose labelled medium for 24 hours. Samples of medium were collected at 24 hours and the ^{13}C label incorporation was quantified using a ^{13}C-filtered ^{1}H-NMR pulse sequence. Label incorporation is expressed in percentage. Bars represent the mean of n=3 independent experiments and error bars represent standard deviation. An unpaired t-student test was applied for each metabolite and p-values were represented as * for p-value<0.05, ** for p-value<0.01 and *** for p-value<0.001.

4.2.3. How is the transcriptome of MS-5 cells altered in co-culture?

Previous results indicated that co-culture enhanced acetate secretion in MS-5 cells and that the secreted acetate was likely to be derived from glucose. To gain a deeper understanding of the mechanisms underlying this metabolic reprogramming, I decided to acquire transcriptomic data of MS-5 and SKM-1 cells cultured alone and in co-culture. For MS-5 cells, the aim was to identify possible pathways that could lead to increased acetate production, the mechanism of secretion and the signalling that could be triggering this effect.

MS-5 cells were cultured alone and in co-culture with SKM-1 cells with the same experimental design described in the previous chapter. After 24 hours, cells were separated, RNA was extracted and purified. RNA was sequenced by Theragen and bioinformatics analysis of the raw output data and gene-level differential expression analysis was performed by Grigorios Papatzikas, as part of a collaboration within the HaemMetabolome-ITN.

Principal component analysis (PCA) of the gene expression data for MS-5 cells demonstrated that the triplicates for MS-5 cells alone (MO, red triangles) and for MS-5 cells in co-culture (MC, blue dots) clustered together (Figure 4.3A). This result indicates that MS-5 cells cultured alone and in co-culture present a distinct transcriptomic profile.

Next, differential gene expression analysis was performed, revealing 587 genes differentially expressed in MS-5 cells in co-culture with a q-value below 0.1 (Figure 4.3B). 476 genes were upregulated in co-culture (red Z-scores) and 111 genes were downregulated in co-culture (blue Z-scores). These results suggest that there are many significant differences in the transcriptome of MS-5 cells cultured alone or in co-culture and that most of these changes lead to upregulated gene expression.

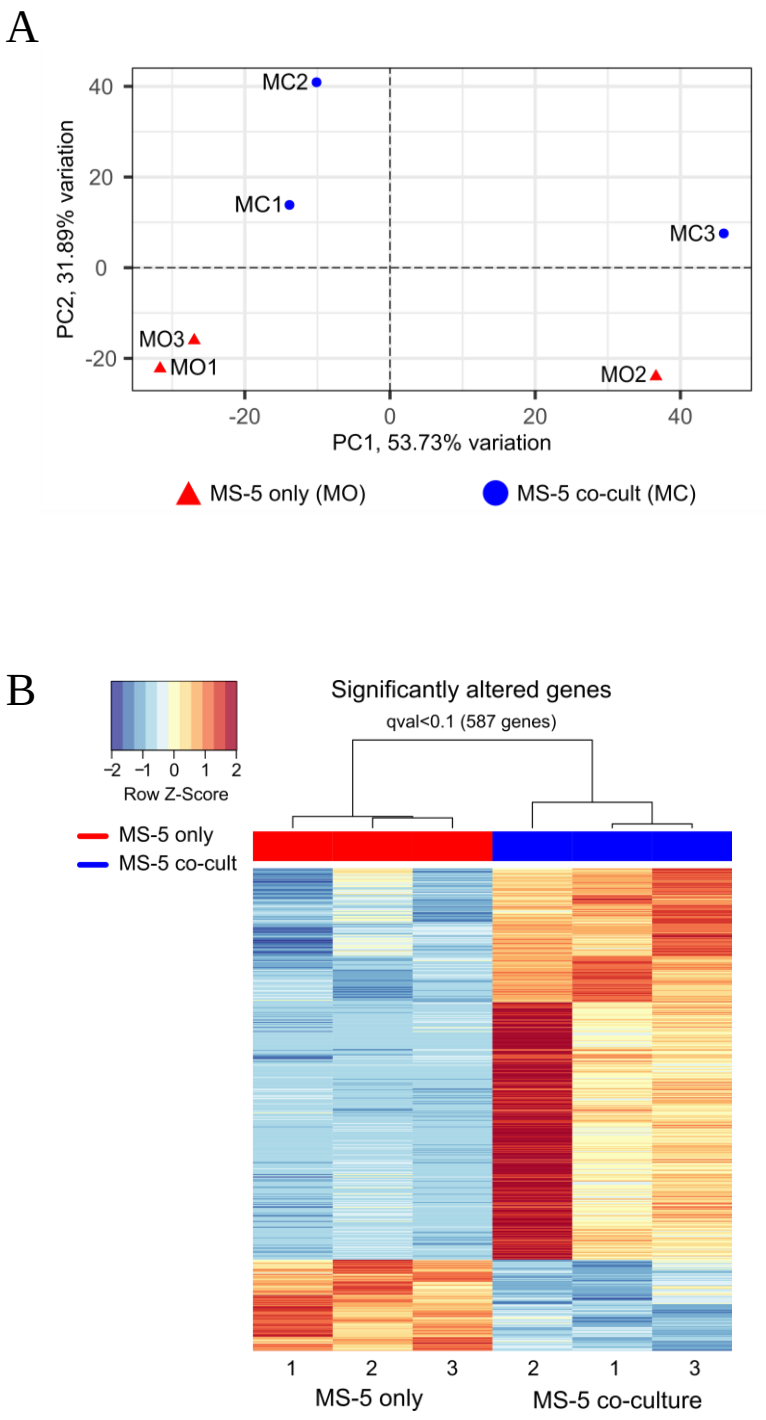

Figure 4.3 Principal component analysis (PCA) and heat map of the differentially expressed genes in MS-5 cells cultured alone vs in co-culture with SKM-1 cells.

A) PCA plot showing the clustering of individual samples of MS-5 cells cultured alone (MO) and MS-5 cells in co-culture (MC). The x and y axis values represent the variation between the sample groups. B) Heat map of differentially expressed genes in MS-5 only (red) vs MS-5 co-culture (blue) calculated using the Wald statistical test, correcting for multiple testing comparison employing the Benjamini-Hochberg method using a false discovery rate threshold of 1% (q-value<0.01). PCA analysis and heat map were generated by Grigorios Papatzikas using Sleuth 0.30.0 R statistical package.

Following initial differential gene expression analysis, a gene set enrichment analysis (GSEA) [217] was carried out. The hallmark gene set list with the 25 highest ranked gene sets according to expression can be seen in Figure 4.4A. The main metabolic pathways that appeared in the list were glycolysis and reactive oxygen species (ROS), both upregulated in co-culture. The enrichment scores for these pathways are presented in Figure 4.4B.

To gain insight on the specifics of the mechanism by which MS-5 cells in co-culture upregulate acetate secretion, I decided to look at the individual expression values of the genes involved in glycolysis, pyruvate metabolism and MCTs. An overview scheme of the genes involved in the aforementioned pathways can be seen in Figure 4.5A.

Glucose transporters (*Slc2a1* and *Slc2a4*) and most glycolytic enzymes (*Pgm1*, *Hk2*, *Gpi1*, *Pfkl*, *Gapdh*, *Pgk1*, *Pgam1-2*, *Eno1-1b-2* and *Pkm*) were found to be upregulated in co-culture (Figure 4.5B, left). Moreover, *Pfkfb3*, which codes for 6-phosphofructo-2-kinase/fructose-2,6-biphosphatase 3 (PFKFB3) and is known to upregulate glycolysis by generating fructose-2,6-bisP which activates 6-phosphofructokinase-1 (*Pfkl*) [218, 219], was also found to be upregulated. These results suggest that glucose should be transported and metabolized to a higher extent in MS-5 cells in co-culture.

Data from pyruvate metabolism (Figure 4.5B, centre) indicates that pyruvate transport (*Mpc1-2*) and several pyruvate dehydrogenase (PDH) complex-related genes (*Pdha1*, *Pdhb* and *Pdhx*), which are involved in the conversion of pyruvate to acetyl-CoA, were slightly downregulated. Moreover, the pyruvate dehydrogenase kinases (PDKs) (*Pdk1*, *Pdk2* and *Pdk4*), which inhibit the activity of the PDH complex, were upregulated (Figure 4.5B, centre). Alternatively, pyruvate can be converted to oxaloacetate via pyruvate carboxylase (*Pcx*), to lactate by lactate dehydrogenase (*Ldha*) and to alanine via alanine transaminase (*Gpt*) (Figure 4.5A). The

expression values for these genes in co-culture (Figure 4.5B, centre) indicated that only *Ldha* was upregulated in co-culture. The acetyl-CoA synthetase genes, *Acss2* and *Acss3*, were also found to be slightly upregulated in co-culture.

Transcriptomic levels of MCTs (Figure 4.5B, right) suggested upregulation of *Slc16a3* and *Slc16a10*, the first one being the highest. The *Slc16a3* gene encodes for MCT4 and could be related to acetate export, and *Slc16a10* encodes for an aromatic amino acid transporter [220].

Overall the transcriptomic data for MS-5 cells in co-culture suggests that these cells present an upregulation of glycolysis and ROS pathways as well as PDH downregulation/inhibition, and an increase in the expression of MCT4.

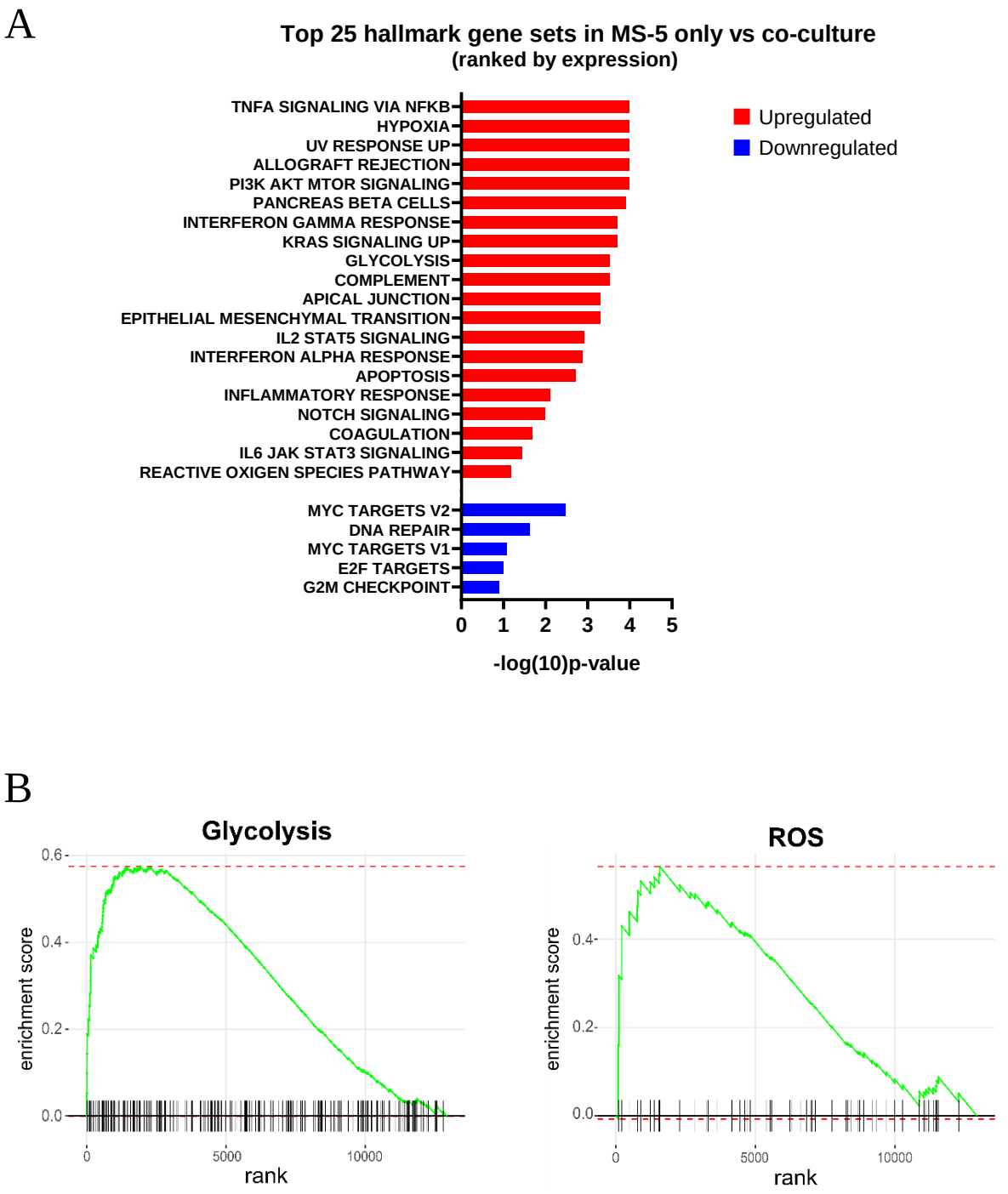

Figure 4.4 GSEA top hallmark gene sets in MS-5 only vs co-culture and GSEA enrichment scores for glycolysis and ROS pathways.

RNA-seq data from MS-5 cells cultured alone and in co-culture was analysed by GSEA using the collection of hallmark gene sets from Molecular Signature Database with a false discovery rate threshold at 5% by Grigorios Papatzikas. A) Top 25 GSEA hallmark gene sets ranked by expression in MS-5 only vs co-culture. P-values for each pathway are presented as –log(10)p-value. B) GSEA enrichment score plots of glycolysis and ROS generated by Grigorios Papatzikas.

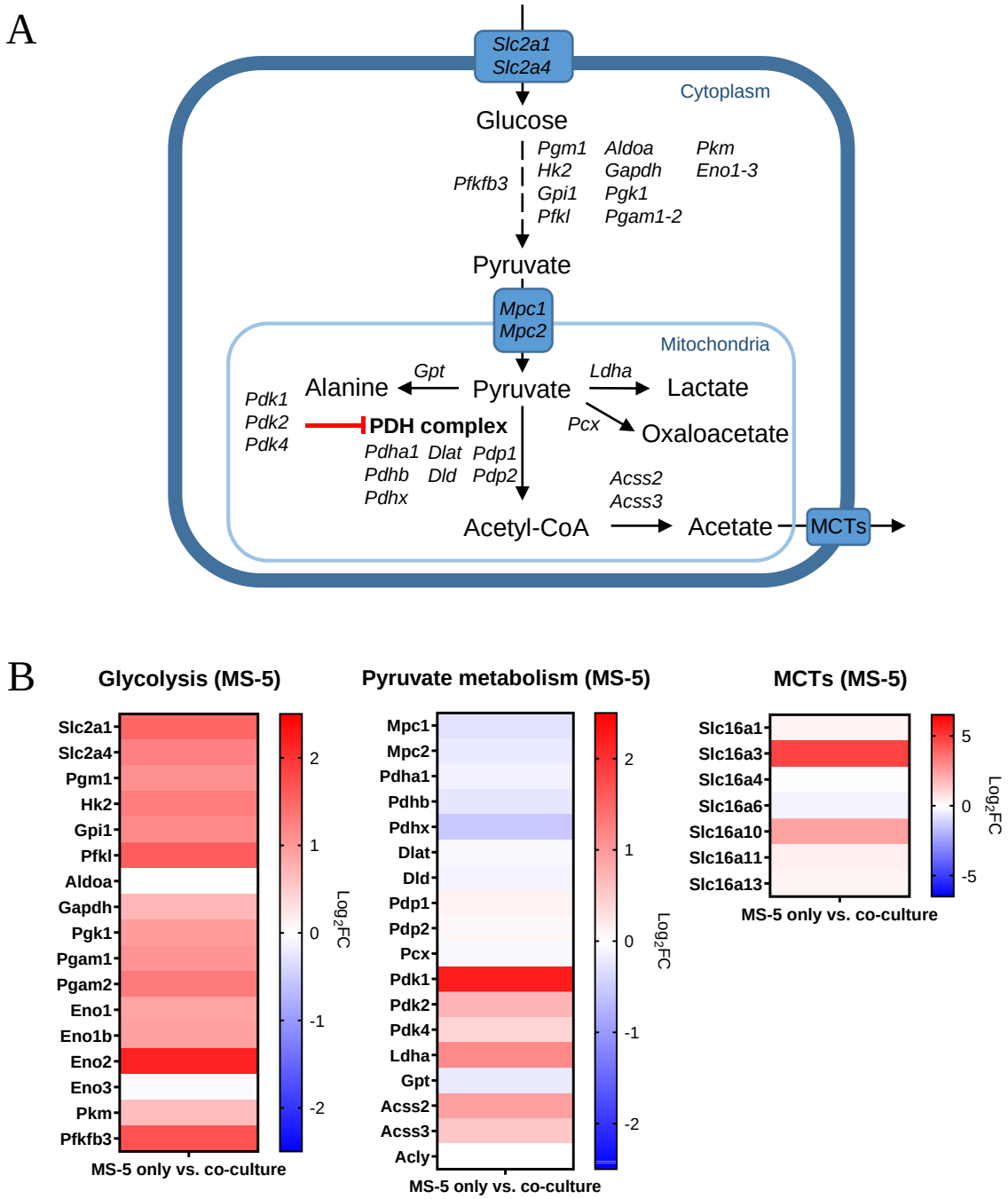

Figure 4.5 Glycolysis and pyruvate metabolism overview and fold change values in MS-5 cells only vs co-culture.

A) Scheme of metabolic enzyme genes, transporter genes (blue rectangles) and metabolites involved in glycolysis and pyruvate metabolism pathways. PDKs inhibit the pyruvate dehydrogenase complex (red sign). B) Fold change values of detected gene transcripts (TPMs) of glycolysis, pyruvate metabolism and MCTs. FC values are represented as log_2FC, red values indicate upregulation and blue values indicate downregulation in MS-5 cells in co-culture.

4.2.4. How is the transcriptome of SKM-1 cells altered in co-culture?

After analysing the transcriptomic data of MS-5 cells in co-culture and having found that several metabolic pathways were altered in these cells in co-culture, it seemed relevant to study how the transcriptome of AML cells can be altered by co-culture. The analysis was focused on finding metabolic alterations that could be linked to data from the previous chapter, in particular, related to acetate metabolism.

SKM-1 cells were cultured for 24 hours alone or in co-culture with MS-5 cells. Cells were separated before RNA extraction and purification. These samples were obtained simultaneously with the MS-5 samples alone and in co-culture presented in the previous section. RNA was sequenced by Theragen and bioinformatics analysis of the raw output data and gene-level differential expression analysis was performed by Grigorios Papatzikas as described in the methods section.

PCA on the genome expression data for SKM-1 cells demonstrated that the triplicates for SKM-1 cells alone (SO, red triangles) and for SKM-1 cells in co-culture (SC, blue dots) clustered together (Figure 4.6A). This result indicates that SKM-1 cells cultured alone and in co-culture present a distinct transcriptomic profile.

Differential gene expression analysis was performed, revealing that 1635 genes were differentially expressed in SKM-1 cells in co-culture with a q-value below 0.1 (Figure 4.6B) 1270 genes were upregulated in co-culture (red Z-scores) and 365 genes were downregulated in co-culture (blue Z-scores). These results indicate that there were several significant differences in the transcriptome of SKM-1 cells cultured alone or in co-culture and that most of these changes lead to upregulated gene expression.

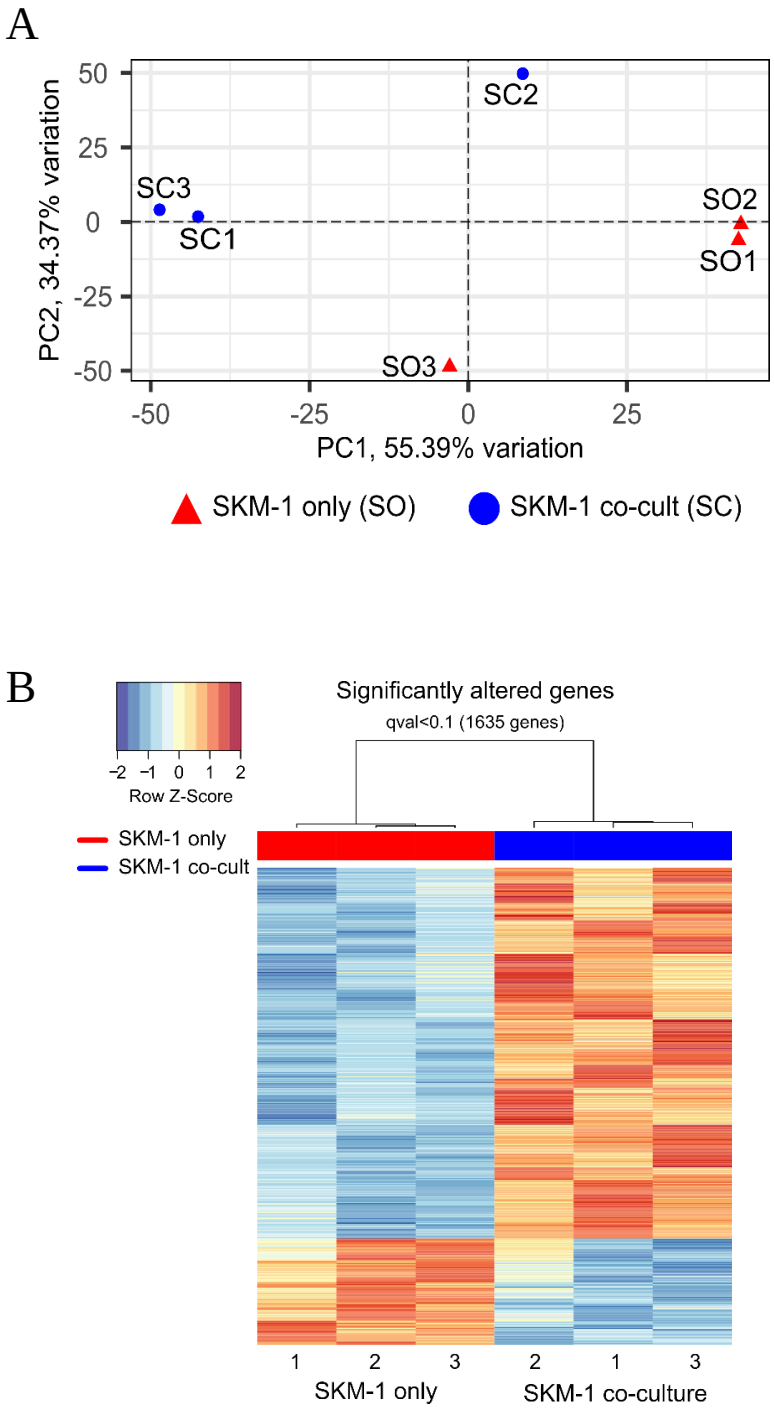

Figure 4.6 Principal component analysis (PCA) and heat map of the differentially expressed genes in SKM-1 cells cultured alone vs in co-culture with MS-5 cells.

A) PCA plot showing separate clusters for SKM-1 cells cultured alone (SO) and SKM-1 cells grown in co-culture (SC). The x and y axis values represent the variation between the sample groups. B) Heat map of differentially expressed genes in SKM-1 only (red) vs SKM-1 co-culture (blue) calculated using the Wald statistical test, correcting for multiple testing comparison employing the Benjamini-Hochberg method using a false discovery rate threshold of 1% (q-value<0.01). PCA analysis and heat map were generated by Grigorios Papatzikas using Sleuth 0.30.0 R statistical package.

Next, GSEA was performed as described in the methods section. Figure 4.7A contains the hallmark gene set list for the 25 highest ranked gene sets according to their expression. Several signalling pathways were found to be upregulated in SKM-1 in co-culture. No metabolic pathways were found in the top 25 list except for xenobiotic metabolism, which is not relevant for this study. However, the hypoxia pathway appeared at the fourth position of upregulated genes on the hallmark gene set list (Figure 4.7A).

Hypoxia is well-known to alter the metabolism of cells by direct mechanisms, such as down-regulation of oxidative phosphorylation and fatty acid oxidation, and indirect mechanisms involving stabilization of the hypoxia-inducible factors (HIFs) [221]. I, therefore, decided to check whether HIF-1 signalling pathway could be also upregulated in SKM-1 cells in co-culture. A heat map of the differentially expressed genes (q-value<0.1) in the HIF-1 signalling pathway can be seen in Figure 4.7B. 21 genes were found to be significantly altered in SKM-1 cells in co-culture compared to cultured alone. 20 of the significantly altered genes were upregulated, suggesting increased HIF-1 activity in SKM-1 cells in co-culture.

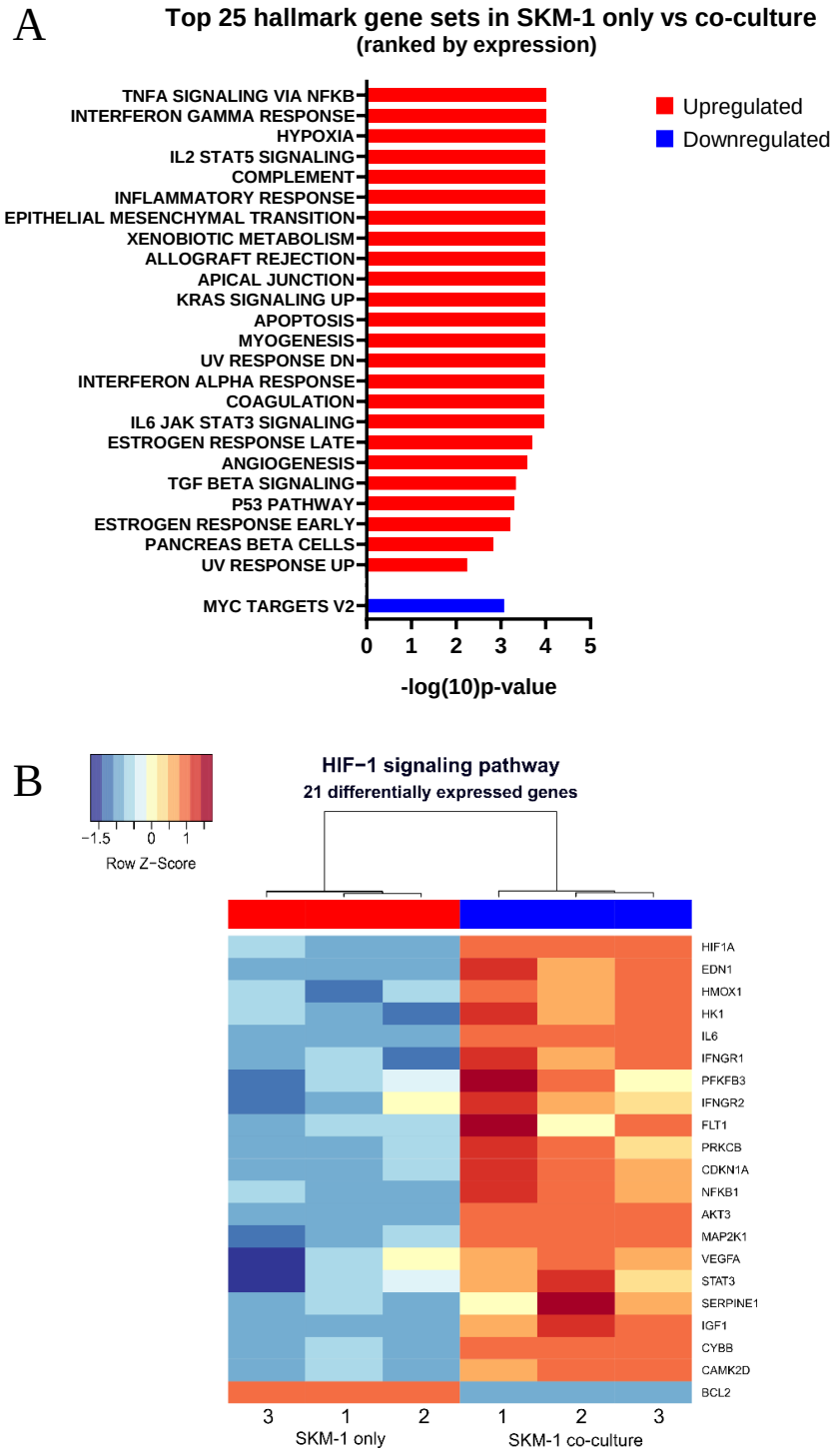

Figure 4.7 GSEA top hallmark gene sets in SKM-1 only vs co-culture and HIF-1 signalling pathway expression heatmap.

RNA-seq data from SKM-1 cells cultured alone and in co-culture was analysed by GSEA using the collection of hallmark gene sets from Molecular Signature Database with a false discovery rate threshold at 5% by Grigorios Papatzikas. A) Top 25 GSEA hallmark gene sets ranked by expression in SKM-1 only vs co-culture. P-values for each pathway are presented as –log(10)p-value. B) Differentially expressed genes in the HIF-1 signally pathway generated by Grigorios Papatzikas.

One of the aims of performing transcriptomic analysis on SKM-1 cells in co-culture was to find whether acetate metabolism was upregulated; thus, I decided to compare gene expression values in acetate-related pathways in cells cultured alone vs co-culture.

Acetate uptake and metabolism remained mainly unchanged in co-culture with only a slight upregulation in *SLC16A3* (Figure 4.8A, left). The *SLC16A3* gene codes for MCT4, which has been suggested to be involved in acetate transport [222], and was also found to be one of the genes upregulated in MS-5 cells in co-culture in the RNA-seq analysis. Interestingly, the acetyl-CoA synthetase genes were not altered and *ACSS1* was slightly downregulated (Figure 4.8A, left). These results suggest that acetate import and conversion to acetyl-CoA were not different in SKM-1 cells alone and in co-culture. There were no differences in the TCA cycle-related genes (Figure 4.8A, middle) between cells alone and co-culture. This result was also similar when examining fatty acid metabolism and histone acetylation-related genes (Figure 4.8A, right). These results indicate that SKM-1 cells in co-culture did not present a different acetate metabolism and did not present a differential usage of the TCA cycle, fatty acid synthesis or histone acetylation.

Finally, it had been reported that leukaemic cells could be communicating with stromal cells via Gap junction [123]. Therefore, I decided to evaluate the gene expression values of Gap junction-related genes in SKM-1 and MS-5 cells in co-culture vs cultured alone. *GJA1* and *GJC1* were upregulated in SKM-1 cells in co-culture whilst *GJD3* was downregulated. In MS-5 cells in co-culture, a general slight upregulation was found in the Gap junction genes. These results suggest that it is possible that SKM-1 and MS-5 cells could establish a contact communication mediated by Gap junction.

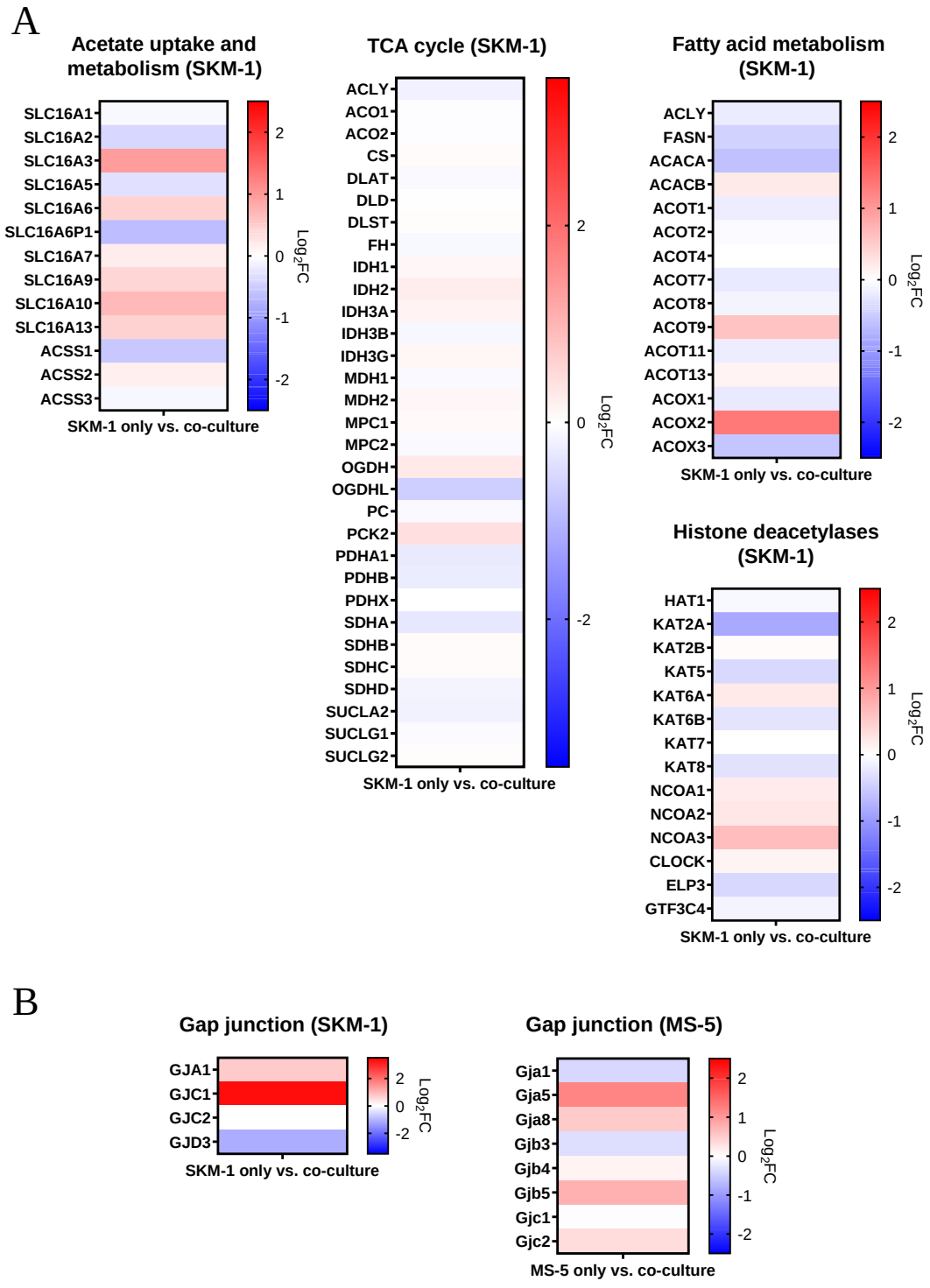

Figure 4.8 Acetate metabolism-related pathways in SKM-1 only vs co-culture and Gap junction expression in SKM-1 and MS-5 cells in co-culture.

Fold change values of detected gene transcripts (TPMs) of A) acetate uptake and metabolism, TCA cycle, fatty acid metabolism and histone deacetylases B) Gap junction-related genes. FC values are represented as log_2FC, red values indicate upregulation and blue values indicate downregulation of SKM-1 or MS-5 cells in co-culture.

4.2.5. RNA sequencing validation by quantitative PCR

Transcriptomic data for SKM-1 and MS-5 cells in co-culture was presented in the previous sections. I decided to use quantitative PCR (qPCR) as an independent technique to validate the RNA sequencing data. Several genes that were found to be involved in relevant altered pathways in the transcriptomic data analysis were selected and their expression was analysed by real time qPCR in SKM-1 and MS-5 cells cultured alone vs co-culture.

SKM-1 and MS-5 cells were cultured alone and in co-culture for 24 hours prior to separation and RNA extraction. RNA samples were reverse transcribed into cDNA and analysed by real time qPCR. *HIF-1A*, *HK1*, *VEGFA*, *ACSS1* and *ACSS2* genes were selected for quantification in SKM-1 cells and *Hk2*, *Pdhx*, *Pdk1*, *Pdk2* and *Vegfα* were chosen for MS-5 cells.

The messenger RNA (mRNA) expression values for the set of genes selected for SKM-1 cells are shown in Figure 4.9A. *HIF-1A*, *HK1* and *VEGFA* are part of the HIF-1 signalling pathway and were found to be upregulated, as shown in Figure 4.7B. *HK1* and *VEGFA* mRNA expression values from real time qPCR were significantly higher in SKM-1 cells in co-culture compared to cultured alone (Figure 4.9A, red bars). However, *HIF-1A* did not show any differences in mRNA expression which is not in agreement with the RNA sequencing results. The expression for *ACSS1* and *ACSS2* was found to be significantly lower for *ACSS1* and similar for *ACSS2* in co-culture (Figure 4.9A, red bars). These results are in agreement with the RNA sequencing data presented in Figure 4.8A (left) and suggest that SKM-1 did not upregulate the activation of acetate by the acetyl-CoA synthetases in co-culture.

The real time qPCR results for the selected genes in MS-5 cells are shown in Figure 4.9B. All the analysed genes are related to the glycolytic pathway. There was a significant upregulation of *Hk2 Pdk1*, *Pdk2* and *Vegfα* mRNA expression and a significant downregulation of *Pdhx*

mRNA expression. These results are in agreement with the transcriptomic data obtained for MS-5 cells and indicate that MS-5 cells present a reprogrammed glycolytic metabolism in co-culture.

Overall, the expression values obtained in the real time qPCRs for SKM-1 and MS-5 recapitulate the results found in the RNA sequencing data.

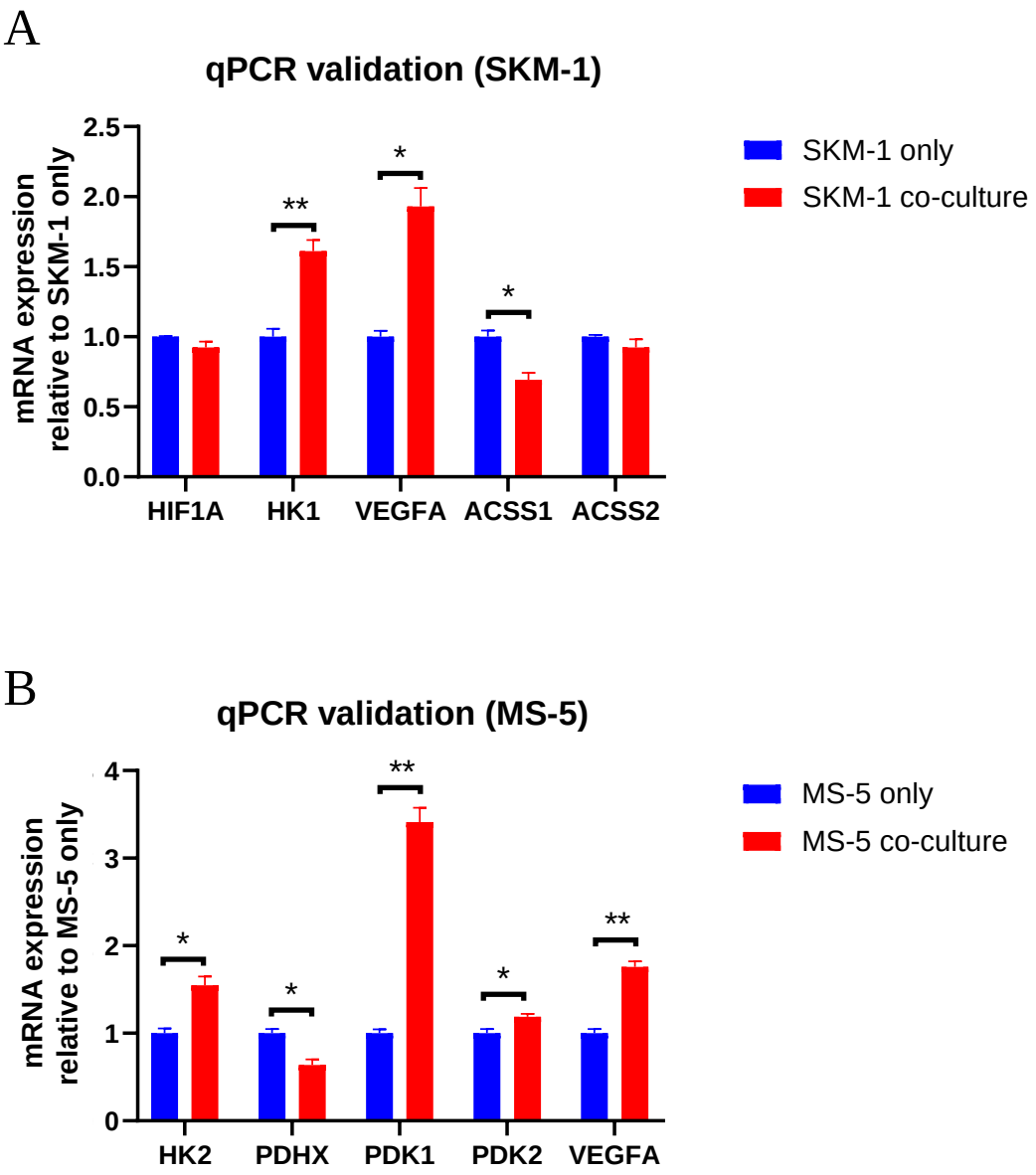

Figure 4.9 Quantitative PCR mRNA expression values for RNA sequencing validation in SKM-1 and MS-5 cells cultured alone vs in co-culture.

SKM-1 and MS-5 cells were cultured alone and in co-culture for 24 hours before RNA extraction and purification. Real time qPCR was performed for a set of genes A) *HIF-1A*, *HK1*, *VEGFA*, *ACSS1* and *ACSS2* for SKM-1 and B) *Hk2*, *Pdhx*, *Pdk1*, *Pdk2* and *Vegfα* for MS-5 cells. mRNA quantification was normalized to *B2m* house-keeping gene. Each plot is representative of three independent experiments. Bars represent the mean and error bars represent the SEM. An unpaired t-student test was applied for each gene and p-values were represented as * for p-value<0.05, ** for p-value<0.01 and *** for p-value<0.001.

4.2.6. Is pyruvate entry into the TCA cycle affected in MS-5 cells in co-culture?

Transcriptomic data revealed that the expression of PDH in MS-5 cells was slightly lower in co-culture and that the expression of PDKs, which act as inhibitors of PDH, was upregulated. I sought to determine if these genomic alterations would lead into an overall lower PDH activity or could imply differences in PC activity.

To study the PDH vs PC activity, I decided to use [1,2-^{13}C] glucose and analyse the isotopic distribution of glutamate and aspartate in MS-5 cells cultured alone or in co-culture. [1,2-^{13}C] Glucose metabolized through the glycolysis pathway yields [2,3-^{13}C] pyruvate that can be converted to [U-^{13}C] acetyl-CoA via PDH activity or to [2,3-^{13}C] oxaloacetate through PC activity (Figure 4.10). If pyruvate enters the TCA cycle via PDH, [1,2-^{13}C] acetyl-CoA and non-labelled oxaloacetate can flux the TCA and be further metabolized into [4,5-^{13}C] glutamate and [1,2-^{13}C] or [3,4-^{13}C] aspartate. A second round of the TCA cycle with PDH entry starting with non-labelled acetyl-CoA would lead to [1,2-^{13}C] glutamate and [3-^{13}C] glutamate; and starting with labelled PDH-derived [1,2-^{13}C] acetyl-CoA would lead to [1,2,4,5-^{13}C] or [3,4,5-^{13}C] glutamate, respectively. If pyruvate enters the TCA cycle via PC, PC-derived [2,3-^{13}C] oxaloacetate can be fluxed to the TCA cycle giving rise to [2,3-^{13}C] glutamate or can be directly converted to [2,3-^{13}C] aspartate (see Figure 4.10).

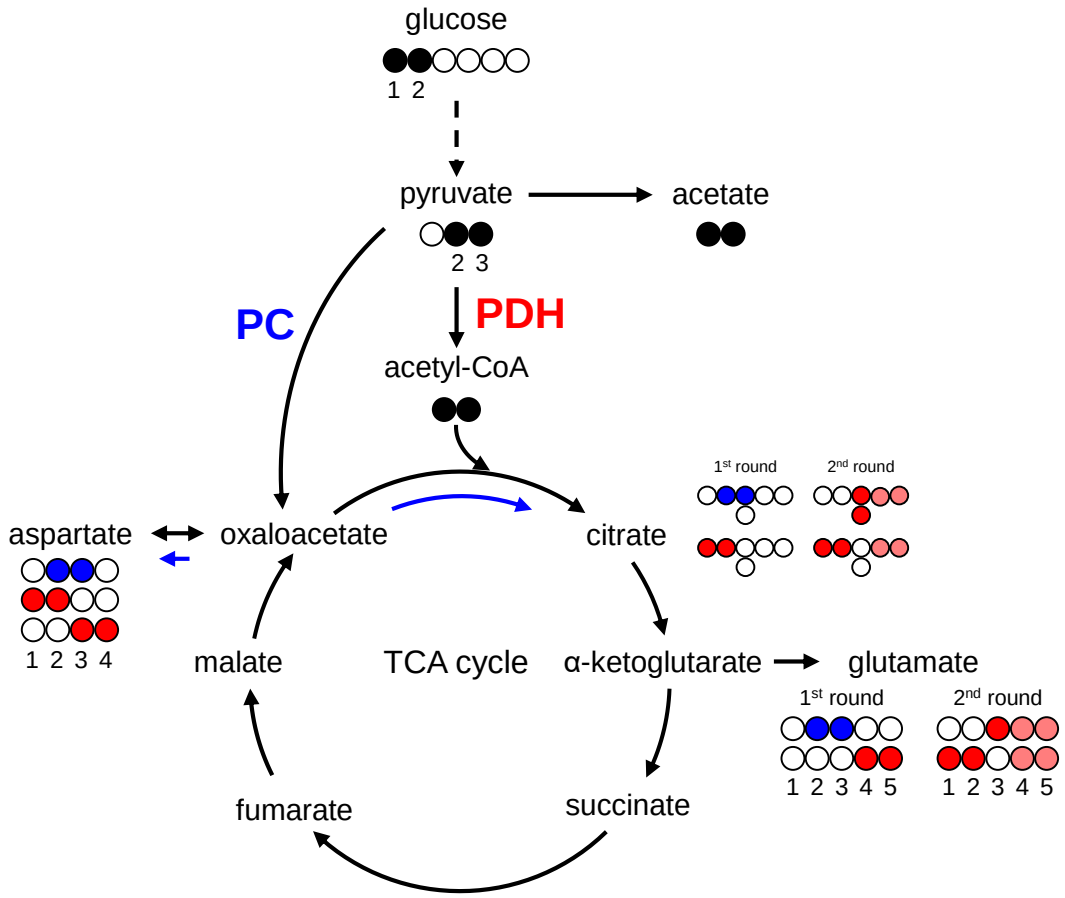

Figure 4.10 Scheme of labelling patterns expected in TCA cycle-related metabolites from [1,2-^{13}C] glucose.
In brief, [1,2-^{13}C] glucose is converted into [2,3-^{13}C] pyruvate through glycolysis. Pyruvate can enter the TCA cycle via pyruvate dehydrogenase (red) or pyruvate carboxylase (blue) activities. After the first round of the TCA cycle, different labelling patterns in aspartate and glutamate can be used to discern between PDH and PC activities. Labelling patterns derived from the second round of the TCA cycle have also been included. Light red carbons in citrate and glutamate indicate positions that would be labelled if labelled PDH-derived oxaloacetate is fluxed to a second round of TCA cycle.

The experimental design followed was to culture MS-5 cells alone and in co-culture with SKM-1 cells for 24 hours before replacing the medium with [1,2-^{13}C] glucose medium. Cells were cultured with [1,2-^{13}C] glucose medium for 8 hours before separation and extraction of MS-5 cells. Metabolites were analysed with ^{1}H-^{13}C-HSQC NMR spectroscopy. Detected carbons from aspartate and glutamate can be seen in Figure 4.11 and Figure 4.12, respectively.

The *J*-couplings for each carbon in aspartate were measured and assigned to PDH or PC-derived activity by comparison with predicted data, shown in Table 12. For example, the C2 of aspartate in MS-5 only (Figure 4.11A) presented 5 signals in the carbon dimension (y-axis). The central signal corresponds to singly labelled C2. The two faint middle signals that are closer to the central peak separated by 36.8 Hz correspond to labelled C2 next to another labelled carbon. This other carbon seems to be C3 as the coupling constant detected (36.8 Hz) is very similar to the predicted one for ^{13}C2-^{13}C3 which is 36.4 Hz. Therefore, as only PC activity can generate [2,3-^{13}C] aspartate these signals can be assigned to PC activity. Similarly, the two outer signals separated by 54.5 Hz seem to correspond to [1,2-^{13}C] aspartate and might be derived from PDH activity, as the predicted coupling constant between ^{13}C2 and the carboxylic acid ^{13}C1 which is 54.2 Hz. The coupling constant of the ^{13}C1-^{13}C2 is higher than the ^{13}C2-^{13}C3 because C1 is a carboxylic acid whilst C2 and C3 are methyl carbons and *J*-coupling in CH_x-COOH is higher than the *J*-coupling in CH_x-CH_x.

As can be seen in Figure 4.11A, ^{1}H-^{13}C-HSQC carbon sections in aspartate suggest that there was higher PC activity in MS-5 cells in co-culture as the PC-derived peaks are more intense for both C2 and C3 from aspartate.

In order to quantify the PDH and PC contributions in aspartate, both C2 and C3 carbons could be used as the coupling constants for the PDH and PC-derived labelling patterns are distinct

enough: for C2, the PDH product would present a predicted ^{13}C2-^{13}C1 coupling constant of 53.8 Hz and the PC product would present a ^{13}C2-^{13}C3 predicted coupling constant of 36.8 Hz (Table 12); for C3, the PDH product would present a predicted ^{13}C3-^{13}C4 coupling constant of 50.8 Hz and the same ^{13}C2-^{13}C3 predicted coupling of 36.8 Hz (Table 12). In this case, C2 intensities were used to obtain percentages of PDH or PC activities in aspartate.

The percentage of PDH contribution to the multiplet in MS-5 only and co-culture was in both cases of 53% and was not significantly different in co-culture (Figure 4.11B, left). However, PC contribution to the multiplet was significantly different in co-culture. PC activity in MS-5 cells cultured alone was of 5% whereas in MS-5 in co-culture it was of 15% (Figure 4.11B, right). These results indicate that PDH activity did not vary in MS-5 cells in co-culture compared to MS-5 cells cultured alone but PC activity was significantly increased by a factor of three in co-culture, suggesting that pyruvate entry to the TCA cycle in MS-5 cells was affected by co-culture.

	Aspartate			**Glutamate**		
	Interaction	Predicted $^{1}J_{CC}$ (Hz)	Detected $^{1}J_{CC}$ (Hz)	Interaction	Predicted $^{1}J_{CC}$ (Hz)	Detected $^{1}J_{CC}$ (Hz)
PDH only (1st round TCA)	C1-C2	54.2	54.5	C4-C5	51.3	52
	C3-C4	50.8	-			
PC only	C2-C3	36.4	36.8	C2-C3	34.8	35.4
PDH only (2nd round TCA)	-	-	-	C3-C4-C5	Mult	Mult
				C3-C4	34.5	35.4
				C1-C2	53.4	54.5
				C4-C5	51.3	52

Table 12 Predicted [223] and detected ^{13}C-^{13}C *J*-couplings in aspartate and glutamate carbons, classified by PDH or PC-derived activities.

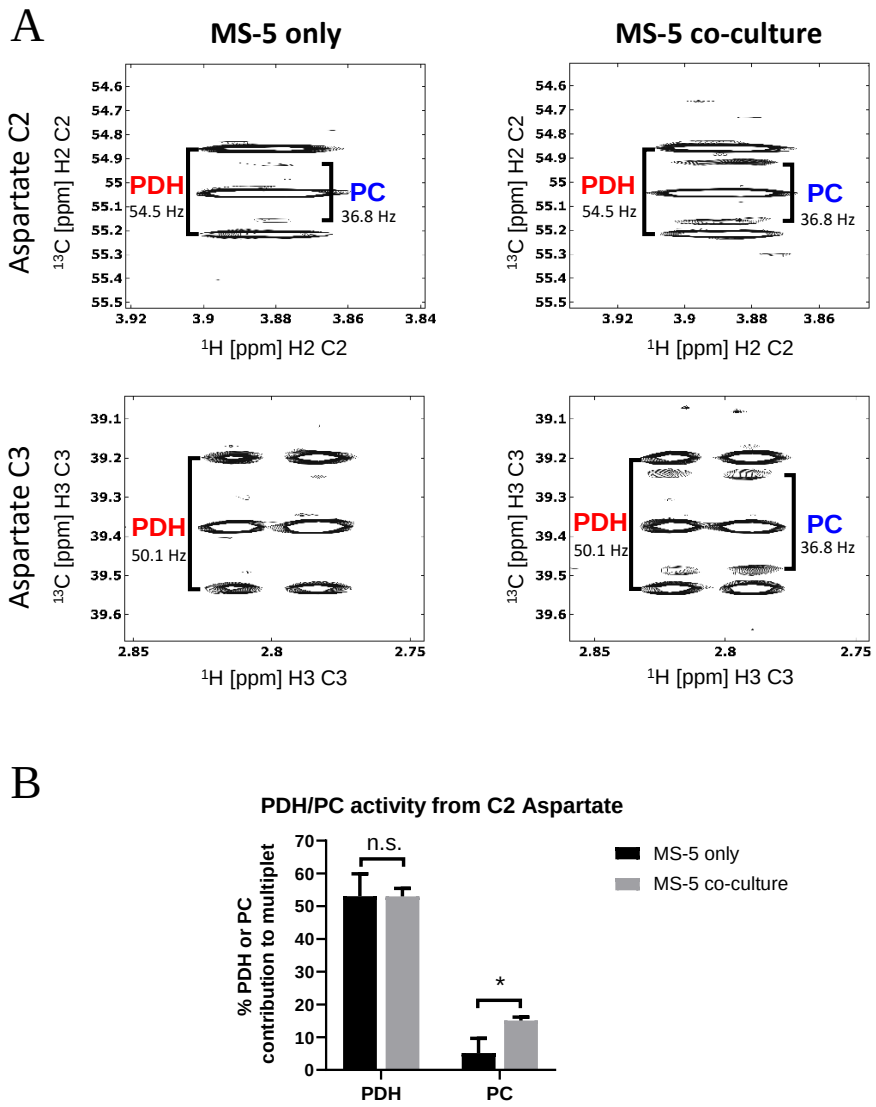

Figure 4.11 Aspartate sections from ^{1}H-^{13}C-HSQC and PDH/PC activity contributions to the signals detected.

MS-5 cells were cultured alone and in co-culture with SKM-1 cells for 24 hours before medium replacement for [1,2-^{13}C] glucose medium and culture for 8 more hours. Cells were separated, extracted and analysed by ^{1}H-^{13}C-HSQC NMR spectroscopy. A) Sections from ^{1}H-^{13}C-HSQC on C2 and C3 from aspartate. *J*-couplings indicated were used to assign PDH and PC-derived signals (red and blue, respectively). Sections are representative of three independent experiments. B) Aspartate C2 was used to quantify the contributions of PDH and PC activities to the multiplet, as indication of the PDH/PC activities in MS-5 cells alone and in co-culture. Bars represent the mean of n=3 independent experiments and error bars represent standard deviation. An unpaired t-student test was applied and p-values were represented as n.s. for not significant * for p-value<0.05, ** for p-value<0.01 and *** for p-value<0.001.

For glutamate, *J*-couplings were measured for each carbon section of ^{1}H-^{13}C-HSQC data, compared to the predicted values (Table 12) and assigned to the correspondent activity (PC or PDH) as previously exemplified. Glutamate C2 sections, depicted in Figure 4.12A, present extra couplings associated to PC activity that are not detected in MS-5 cells cultured alone, suggesting that only MS-5 cells in co-culture have PC-derived glutamate.

The *J*-coupling value detected in the C3 section of glutamate in MS-5 cells in co-culture could be attributed to the C2-C3 coupling linked to PC activity. However, it could also be caused by C3-C4 coupling derived from a second round of TCA via PDH as the predicted couplings for C2-C3 (34.8 Hz) and C3-C4 (34.5 Hz) are very similar (Table 12).

C4 section of glutamate in MS-5 cells in co-culture slightly displayed a complex multiplet pattern that was not found in MS-5 cells cultured alone. This pattern could be attributed to C3-C4-C5 being labelled and it could be explained by both PC-derived [2,3-^{13}C] oxaloacetate being combined with labelled acetyl-CoA and by PDH-derived [4,5-^{13}C] oxaloacetate combined with labelled [U-^{13}C] acetyl-CoA in a second round of the TCA cycle.

As PDH and PC activities could generate glutamate with the same labelling patterns in C3 and C4, only C2 could be used to quantify the PDH/PC contributions in glutamate. PDH and PC contributions in glutamate C2 can be seen in Figure 4.12B. The percentage of PDH contribution to the multiplet was not significantly different in co-culture. PDH activity contributions to the multiplet in both MS-5 only and co-culture were of 53 and 51%, respectively (Figure 4.12B, left). MS-5 cells cultured alone did not show any PC activity whereas MS-5 cells in co-culture presented a 19% of PC contribution to the multiplet. These results indicate that PDH activity was almost not altered by co-culture and PC activity only seemed to occur in co-culture.

Overall, ^{1}H-^{13}C-HSQC data on aspartate and glutamate suggests that pyruvate entry into the TCA cycle is altered in co-culture due to an increase in PC activity that produces aspartate and fluxes the TCA cycle.

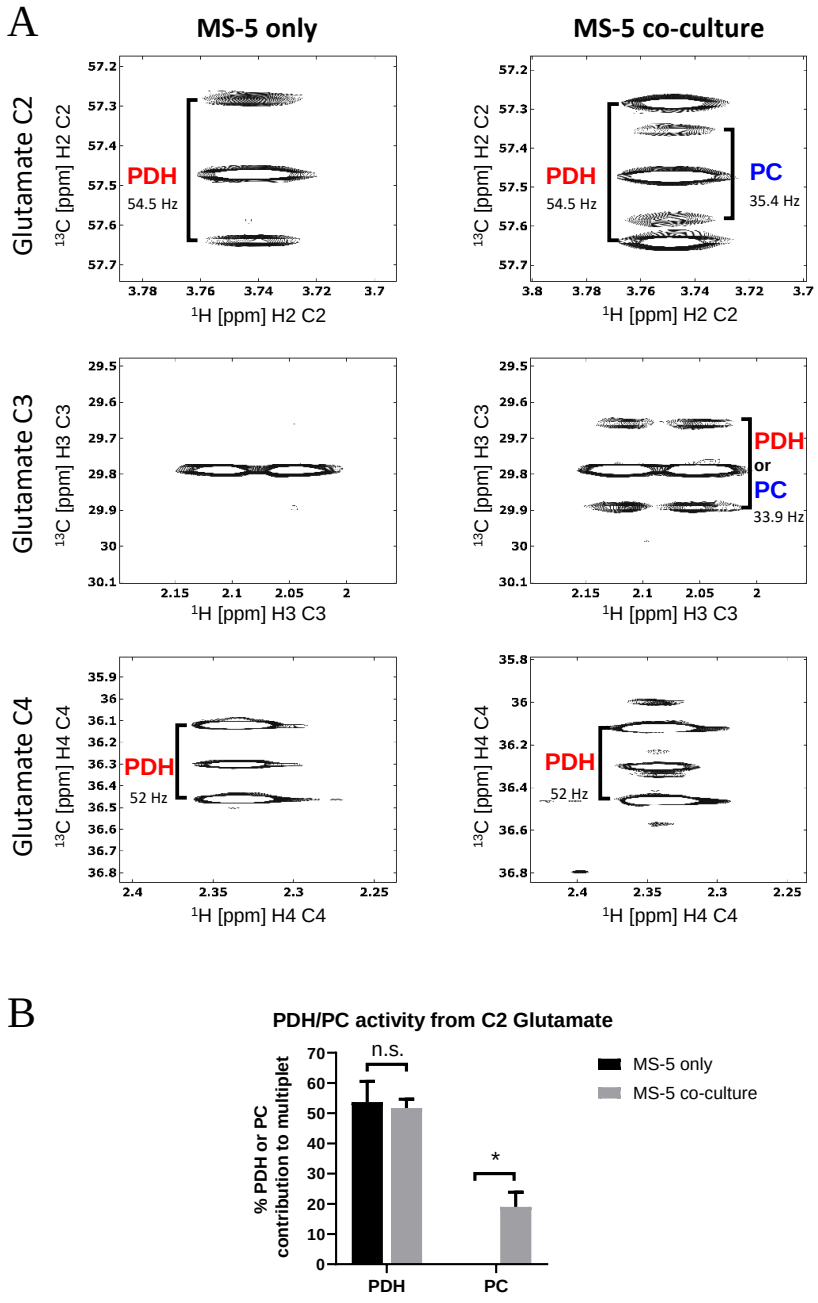

Figure 4.12 Glutamate sections from ^{1}H-^{13}C-HSQC and PDH/PC activity contributions to the signals detected.

MS-5 cells were cultured alone and in co-culture with SKM-1 cells for 24 hours before medium replacement for [1,2-^{13}C] glucose medium and culture for 8 more hours. Cells were separated, extracted and analysed by ^{1}H-^{13}C-HSQC NMR spectroscopy. A) Sections from ^{1}H-^{13}C-HSQC on C2, C3 and C4 from glutamate. *J*-couplings indicated were used to assign PDH and PC-derived signals (red and blue, respectively). Sections are representative of three independent experiments. B) Glutamate C2 was used to quantify the contributions of PDH and PC activities to the multiplet, as indication of the PDH/PC activities in MS-5 cells alone and in co-culture. Bars represent the mean of n=3 independent experiments and error bars represent standard deviation. An unpaired t-student test was applied, and p-values were represented as n.s. for not significant * for p-value<0.05, ** for p-value<0.01 and *** for p-value<0.001.

4.2.7. Is ROS responsible for acetate secretion in co-culture?

The ROS pathway was found to be upregulated in MS-5 cells in co-culture compared to MS-5 cells cultured alone in the transcriptomic data analysed in previous sections. ROS has been reported to be involved in the spontaneous decarboxylation of pyruvate into acetate [224, 225]. Therefore, I sought to determine whether ROS could have a role in the increased acetate secretion by MS-5 cells in co-culture. I decided to measure the intracellular levels of ROS and test whether acetate levels would increase with higher ROS levels or decrease when using a ROS scavenger.

I first decided to characterise the intracellular levels of ROS in MS-5 cells cultured alone and in co-culture with SKM-1 cells. Cells were cultured for 24 hours before being stained with 2',7'-dichlorofluorescin diacetate (H_2DCFDA). H_2DCFDA is a cell-permeable stain that turns fluorescent upon oxidation by ROS [226, 227]. After staining, cell fluorescence was measured by flow cytometry.

As can be seen in Figure 4.13A, MS-5 cells in co-culture had significantly higher levels of ROS measured by H_2DCFDA compared to MS-5 cells cultured alone. This result suggests that MS-5 cells presented higher levels of ROS when co-cultured with SKM-1 cells.

After knowing that MS-5 cells in co-culture presented higher levels of ROS, I decided to determine whether the levels of secreted acetate would vary by increasing and decreasing the levels of ROS. As previously reported [61, 228], H_2O_2 was used to increase the levels of ROS and N-acetyl-L-cysteine (NAC), a ROS scavenger [229], was used to decrease ROS levels. SKM-1 and MS-5 cells where cultured alone and in co-culture in a control medium, medium with 50 µM H_2O_2 and medium with 5 mM NAC.

SKM-1 cells cultured with H_2O_2 or NAC medium did not show differences in consumption or production of acetate (Figure 4.13B, left). MS-5 cultured alone did not show an increase in acetate secretion when treated with H_2O_2 (Figure 4.13B, centre). However, acetate production when MS-5 cells alone were treated with NAC was lower than in the control medium. In co-culture (Figure 4.13B, right), acetate production was increased with H_2O_2 and decreased when treated with NAC. Moreover, the acetate production in co-culture cells treated with NAC was comparable to MS-5 cells cultured alone in the control medium. These results suggest that acetate secretion in co-culture could be ROS dependent as H_2O_2 activated the production of acetate and NAC restored it to the level of MS-5 cells control. It is unclear whether acetate secretion in MS-5 cells cultured alone could be also ROS-driven, as NAC can diminish the rate of production but H_2O_2 does not yield a higher production.

Based on the previous results, I decided to use increasing concentrations of H_2O_2 to test whether the increase of acetate production could be dose dependent.

As can be seen in Figure 4.13C (left), acetate secretion in MS-5 cells cultured alone did not vary significantly with increasing concentrations of H_2O_2. However, acetate secretion in co-culture did increase significantly with H_2O_2 in a dose dependent manner (Figure 4.13C, right). These results suggest that an increase in ROS levels influenced acetate secretion only in co-culture in a dose-dependent manner.

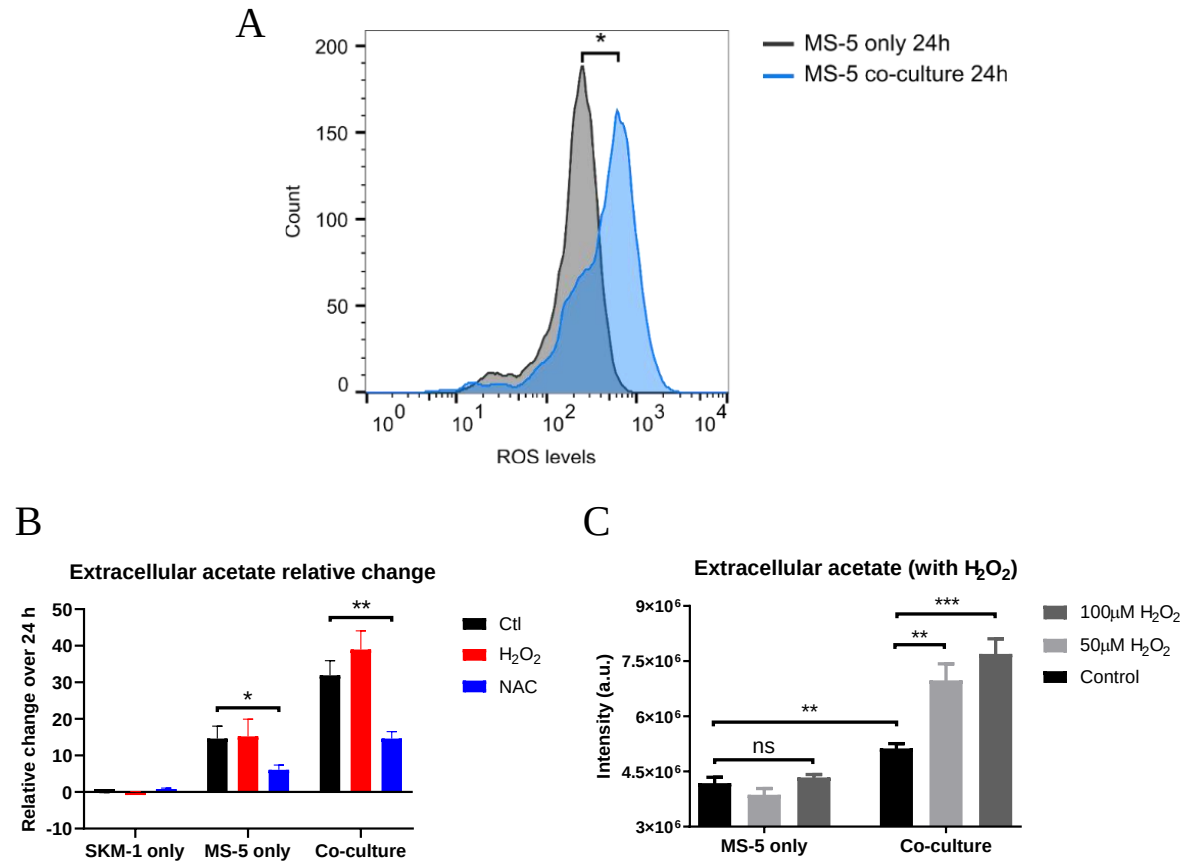

Figure 4.13 ROS plays a role in acetate secretion in co-culture.

A) Intracellular ROS levels measured by flow cytometry in MS-5 cells cultured alone and in co-culture with SKM-1 cells. In brief, MS-5 cells were cultured alone or in co-culture with SKM-1 cells for 24 hours prior to H_2DCFDA staining and fluorescence measurement by flow cytometry. Analysis was carried out with FlowJo software. The population of living cells was gated and 1500 cells for each condition were randomly selected and plotted. The geometric mean for each population and time point was compared between cells alone or in co-culture by performing an unpaired unpaired t-student test. The histogram is representative of n=3 independent experiments. B) Extracellular acetate relative change in SKM-1 and MS-5 cells cultured alone and in co-culture for 24 hours in a control medium (black), medium with 50 µM H_2O_2(red) and medium with 5 mM NAC (blue). Samples of medium at 0 and 24 hours were collected, ^{1}H-NMR spectroscopy was performed and metabolite levels were converted to relative change over 24 hours. Bars represent the mean of n=3 independent experiments and error bars represent standard deviation. C) Extracellular acetate levels in MS-5 cells alone or in co-culture with SKM-1 cells in a control medium, medium with 50 µM H_2O_2 and with 100 µM H_2O_2. Samples of medium were collected after 24 hours and ^{1}H-NMR analysis was performed. Bars represent the mean of n=3 independent experiments and error bars represent standard deviation. An unpaired t-student test was applied for each condition in all the experiments and p-values were represented as * for p-value<0.05, ** for p-value<0.01 and *** for p-value<0.001.

4.3. Discussion

4.3.1. MS-5 cells are responsible for increased acetate secretion in co-culture

The overall aim of this chapter was to investigate the mechanisms behind increased acetate secretion in co-culture. Several questions were left open in the previous chapter such as which cell type was responsible for acetate secretion, what metabolic pathways were involved in acetate secretion and how were they altered. In order to answer whether AML or MS-5 cells were responsible for acetate secretion in co-culture, several experiments were carried out including studying the metabolism of both cell types cultured separately after being in co-culture, tracer-based NMR spectroscopy studies and transcriptome analysis.

MS-5 cells cultured separately, after being in co-culture with AML cells, continued secreting acetate; with significantly higher levels 24 hours after being cultured separately compared to acetate levels in co-culture conditions (Figure 4.1B, C and D). These results suggest that MS-5 cells could be responsible for acetate secretion in co-culture and, additionally, that the metabolic reprogramming that MS-5 cells suffer in co-culture is not quickly reverted once they are separated from co-culture and cultured alone.

It was also noted that SKM-1 cells slightly secreted acetate after co-culture (Figure 4.1B, red squares). This result was unexpected as it is contrary to the data from the previous chapter (Figure 3.6B and Figure 3.8A), where SKM-1 cells did not secrete acetate when cultured alone. Moreover, Kasumi and HL-60 cells separated after co-culture did not secrete acetate and maintained similar levels as the ones in co-culture. These results suggest that, as not all AML cell lines secreted acetate after co-culture, the increase in extracellular acetate found in SKM-1 cells was not caused by a metabolic switch triggered by co-culture. It is possible that acetate secretion by SKM-1 cells could be caused by contamination from MS-5 cells.

Several publications pointed out that acetate can be derived from glucose through the conversion of glucose into pyruvate which can be further oxidised to acetate [182, 224, 230]. Data obtained from [U-^{13}C] glucose labelling experiments in AML and MS-5 cells in co-culture revealed significantly higher label incorporations from glucose into acetate for all the AML cell lines tested (Figure 4.2A, B and C). This result suggests that the extra acetate found in co-culture was derived from glucose and is in agreement with the aforementioned studies.

Labelling experiments also revealed that MS-5 cells cultured alone are capable of generating labelled acetate from [U-^{13}C] glucose (Figure 4.2A, B and C, red bars). This finding implies that the mechanisms for acetate production from glucose and later secretion are already implemented in MS-5 cells alone. Moreover, even though HL-60 cells revealed a similar label incorporation in acetate from glucose, SKM-1 and Kasumi cells did not show any label incorporation in acetate. Therefore, MS-5 cells seem more likely to be responsible for acetate secretion in co-culture.

Transcriptomic data from SKM-1 and MS-5 cells in co-culture revealed that glycolysis was upregulated in MS-5 cells in co-culture (Figure 4.4A and B; Figure 4.5B, left) but not in SKM-1 cells (Figure 4.7A). Hence, considering that the extra acetate in co-culture was found to be derived from glucose, the upregulation of glycolysis only occurring in MS-5 cells in co-culture supports the hypothesis that MS-5 cells were responsible for acetate secretion.

4.3.2. MS-5 cells present a reprogrammed metabolism characterised by an increase in glycolysis

Transcriptomic data on MS-5 cells revealed that glycolysis was one of the top upregulated hallmark gene sets in co-culture (Figure 4.4). Moreover, most of the genes involved in glycolysis were also found to be upregulated in co-culture, including glucose transporters and glycolytic enzymes (Figure 4.5). The downregulation of the expression of PDH and upregulation of the PDKs, which inhibit PDH, further corroborated that glucose was not utilised to feed the TCA cycle. Overall, these results indicated that MS-5 cells presented an altered metabolism where glycolysis was upregulated at the expense of TCA cycle. This result is in agreement with several studies in other types of cancer, where stromal cells in co-culture with cancer cells presented higher glycolytic rates [231-233].

How glycolysis was upregulated in MS-5 cells is not clear. One possibility could involve AML cells secreting the vascular endothelial growth factor (VEGF). AML cells are known to promote angiogenesis by secreting angiogenic factors to the bone marrow microenvironment, as reviewed in [234], where one of such factors is VEGF [235, 236]. VEGF has been recently reported to participate in the upregulation of glycolysis in niche cells mediated by AML-derived exosomes [105]. The mechanism described involved the transfer of VEGF and VEGF-receptor messenger RNA from AML to endothelial cells and resulted in higher glycolysis, proliferation and migration of endothelial cells conferring chemoresistance to AML cells. Additionally, the upregulation of glycolysis by VEGF was reported to be mediated by the upregulation of PFKFB3 [237], which is encoded by the gene *Pfkfb3* in mouse. PFKFB3 is known to act as a positive regulator of glycolysis, through the generation of fructose-2,6-bisphosphate which activates 6-phosphofructokinase-1 [218, 219]. A similar mechanism could be taking place

between SKM-1 and MS-5 cells as they both presented significantly higher mRNA expression of *VEGFA*/*Vegfa* gene in co-culture (Figure 4.9), and MS-5 cells presented higher mRNA expression of *Pfkfb3* (Figure 4.5). Using the anti-VEGF monoclonal antibody bevacizumab [151] in co-culture or overexpressing VEGF in MS-5 cells could clarify whether VEGF is involved in the increase in glycolysis observed in MS-5 cells.

Interestingly, VEGF forms part of the HIF signalling pathway, and is transcriptionally activated by *HIF1A* [238]. The HIF signalling pathway was found to be upregulated in SKM-1 cells in co-culture (Figure 4.7). Despite *HIF1A* was found to be highly differentially expressed in the RNA sequencing data, the upregulation of the transcript could not be confirmed by real time qPCR. Nonetheless, the differential expression of other genes within the HIF signalling pathway, such as *VEGFA* and *HK1*, in SKM-1 co-culture conditions, were confirmed to be upregulated by real time qPCR (Figure 4.9, A). This data supports the hypothesis that the HIF signalling pathway could be upregulated in co-culture. Furthermore, the hypoxia pathway, which is also related to the activation of VEGF [239], was found to be one of the top 3 upregulated pathways in both cell types (Figure 4.4 and Figure 4.7). However, although hypoxia and HIF signalling could play a role in the reprogramming of MS-5 cells in co-culture, it is yet unclear how AML cells could transfer or exert this type of signalling. Alternatively, *HIF1A* could also be activated, independently of hypoxic conditions, by the activation of the mammalian target of rapamycin (mTOR) [240, 241]. This is supported by the transcriptomic data on MS-5 cells, which showed an upregulation of the mTOR pathway (Figure 4.4). Further experiments such as co-culturing cells under hypoxia or characterising whether mTOR is activated in MS-5 cells in co-culture could help elucidate the mechanism behind glycolysis activation.

4.3.3. Pyruvate metabolism is altered in MS-5 cells in co-culture

In the previous section, an upregulation of the glycolytic pathway in MS-5 cells in co-culture was found. [U-^{13}C] Glucose labelling revealed that acetate in co-culture was derived from glucose and transcriptomic data indicated that glycolysis was upregulated.

Pyruvate labelling from [U-^{13}C] glucose was found to be significantly higher in cells in co-culture than when cultured alone, mimicking the label distribution found in acetate (Figure 4.2). A similar tendency was found in alanine and lactate, where higher labelling from [U-^{13}C] glucose was present in cells in co-culture (Figure 4.2). As acetate, lactate and alanine can be generated from pyruvate, these results suggest that an accumulation of pyruvate probably linked to an increase in the glycolytic rate could be taking place in MS-5 cells in co-culture.

Transcriptomic data on pyruvate metabolism revealed that pyruvate transport and several components of the PDH complex were slightly downregulated whilst the pyruvate dehydrogenase kinases, which inhibit the activity of the PDH complex, were upregulated (Figure 4.5B, centre and Figure 4.9B). Alternative paths for pyruvate remained unaltered, in the case of alanine transaminase and pyruvate carboxylase, and upregulated in the case of lactate dehydrogenase (Figure 4.5B, centre). These results suggest that pyruvate accumulation in co-culture could be taking place. Results also seem to suggest that MS-5 cells in co-culture could be exploiting alternative pathways to PDH.

Tracer-based NMR spectroscopy using [1,2-^{13}C] glucose as a precursor was used to test whether MS-5 cells in co-culture could be activating PC to flux pyruvate into the TCA cycle, as previously established in-house for another leukaemia cell line [242] and as others have used for mass isotopomer analysis [243]. Aspartate labelling on C2 revealed that PDH activity remained unaltered but PC activity increased by a factor of three in co-culture. The analysis on

glutamate C2 also indicated that PDH activity was unaltered by co-culture. In glutamate, PC activity was only detected in MS-5 cells in co-culture. These results did not agree with the transcriptomic data on MS-5 cells in co-culture, where a decrease in PDH activity was expected and no variations were expected for PC activity. One of the possible explanations for these results is that the flux of pyruvate is higher in co-culture leading to its accumulation and further usage of all the possible pathways for pyruvate, including PC. Another possibility is that PC activation is caused by an accumulation of acetyl-CoA, which is known to be a potent activator of PC [244]. Both possibilities could occur simultaneously.

4.3.4. Acetate secretion could be mediated by ROS

The mechanism for the generation of acetate from glucose should involve the breakdown of glucose into pyruvate and the chemical conversion of pyruvate into acetate prior to secretion. Glucose is broken down into pyruvate through glycolysis, pyruvate can then be converted directly into acetate [224, 225] or to acetyl-CoA to be further down metabolized into acetate [245].

One of the aforementioned mechanisms for acetate secretion in stromal cells is acetyl-CoA conversion to acetate mediated by the acetyl-CoA synthetases. This mechanism would involve pyruvate being converted to acetyl-CoA via PDH activity or by the ATP citrate lyase (ACLY) prior to conversion to acetyl-CoA by the acetyl-CoA synthetases. Transcriptomic data revealed that the acetyl-CoA synthetases, encoded by *Acss2* and *Acss3* were upregulated in co-culture (Figure 4.5B, centre). However, ACLY expression remained unaltered in co-culture, the PDH complex (*Pdha1*, *Pdhb*, *Pdhx*, *Dlat*, *Dld*, *Pdp1* and *Pdp2*) was mainly downregulated and the PDKs (*Pdk1*, *Pdk2* and *Pkd4*), which inhibit PDH, were found to be upregulated (Figure 4.5B, centre). These results suggest that some acetate might be generated from acetyl-CoA derived from glycolysis. Nonetheless, as acetate secretion in co-culture is significantly large, alternative mechanisms for acetate synthesis must be active in MS-5 cells in co-culture.

It has been recently reported that mammals can synthesize acetate from pyruvate in a non-enzymatic conversion that involves ROS [224, 225]. This conversion has been linked to cells prone to overflow metabolism where high rates of glycolysis and excess of pyruvate occur [230]. I decided to investigate whether this conversion could occur in MS-5 cells in co-culture and could be the main reaction for generating acetate. GSEA analysis of transcriptomic data in MS-5 cells in co-culture revealed that the ROS signalling pathway was included in the top 25

upregulated pathways (Figure 4.4A and Figure 4.4B, right), suggesting that ROS could be a potential mediator in acetate secretion in co-culture.

ROS levels in MS-5 cells in co-culture with SKM-1 cells were significantly higher than in MS-5 cells cultured alone (Figure 4.13A). Treatment with H_2O_2 increased the rate of acetate secretion in co-culture but not in MS-5 cells cultured alone (Figure 4.13B). Moreover, H_2O_2 increased the level of extracellular acetate in co-culture in a dose dependent manner whilst it did not alter the level of extracellular acetate in MS-5 cells cultured alone (Figure 4.13C). Addition of NAC decreased the rate of acetate secretion in cells in co-culture and cultured alone. The rate of acetate secretion in NAC treated cells in co-culture was almost equal to untreated MS-5 cells alone suggesting that NAC treatment can recover the control phenotype. Altogether, these results suggest that ROS could play an important role in acetate secretion and the most probable mechanism for this ROS-mediated acetate secretion involves an increase in glycolysis leading to high concentrations of pyruvate that are converted to acetate via ROS.

A crosstalk between haematopoietic stem cells and stromal cells involving ROS was previously reported [246], revealing that HSCs were able to transfer ROS to bone marrow stromal cells via gap junction to prevent senescence. The transfer was mediated by connexin-43 which is a component of gap junction that has also been reported to provide chemoresistance to AML cells [123]. Gap junction transcriptomic data in SKM-1 and MS-5 in co-culture indicated that several gap junction genes were upregulated in both cell types (Figure 4.8B). Connexin-43 is encoded by *Gja1*, which was found to be slightly upregulated in SKM-1 cells in co-culture. However, connexin-45, encoded by *Gjc5*, was the highest upregulated gene found in SKM-1 cells in co-culture in the gap junction family. MS-5 cells in co-culture had several gap junction-related genes upregulated, with the highest upregulated gene being *Gja5*, which encodes for connexin-

40. These results suggest that it is possible that AML cells could be transferring ROS to MS-5 cells through gap junction. Additional experiments confirming the formation of gap junctions between SKM-1 and MS-5 cells could include testing ROS levels in AML and stromal cells before and after co-culture; using a ROS scavenger and checking the expression of GAP junction genes; and treating co-cultures with a gap junction disruptor such as carbenoxolone, used previously in other AML-stromal co-cultures [123, 247].

Another question that arose in the previous chapter was how acetate was being secreted to the extracellular medium. Transcriptomic data from MS-5 cells in co-culture revealed that two genes related to MCTs were upregulated. The highest upregulated MCT gene was *Slc16a3*, which encodes for MCT4. This transporter has been suggested to be one of the main transporters of acetate together with MCT1 [222] and has been reported to transport acetate in astrocytes [248] and in colorectal cancer cells [211]. Interestingly, this transporter had been reported to be upregulated in hypoxia [249] which is one of the top 25 hallmark upregulated pathways in MS-5 cells in co-culture (Figure 4.4A).

4.3.5. Transcriptome data reveals that SKM-1 cells in co-culture are not adapted to efficiently use acetate

The intersection analysis of metabolic and transcriptomic data for MS-5 cells indicated that these cells in co-culture had several metabolic pathways altered that resulted in increased acetate secretion. Acetate can be used as an alternative fuel to glucose by cancer cells [59, 212]. Therefore, it could be possible that AML cells would rewire their metabolism into using acetate.

Transcriptomic data on SKM-1 cells in co-culture vs alone was analysed focusing on the transport, activation and further metabolism of acetate. Acetate transport mediated by monocarboxylate transporters remained unaltered except for a slight upregulation in *SLC16A3* (Figure 4.8A, left). As mentioned in the previous section, *SLC16A3* encodes for MCT4 and has been related to acetate transport [211, 222, 248], although other studies suggest that MCT1 is responsible for acetate import [210]. The upregulation of the *SLC16A3* gene could be related with an increase in acetate import in co-culture. However, the activation of acetate by conversion into acetyl-CoA through the acetyl-CoA synthetases (*ACSS1* and *ACSS2*) was not found to be upregulated in co-culture (Figure 4.8A, left).

Acetyl-CoA could be further metabolized into the TCA cycle, fatty acid synthesis and histone acetylation [222]. However, none of these pathways seemed to have a major upregulation in SKM-1 cells (Figure 4.8A) suggesting that SKM-1 cells do not rewire their metabolism in co-culture to effectively use acetate. This result tallies with acetate generated by MS-5 cells in co-culture accumulating in the extracellular medium, which implies that AML cells are not extensively importing acetate. However, the fact that the transcriptome of SKM-1 cells is not altered in co-culture to effectively use acetate does not imply that AML cells are not using

acetate at all. Further investigation including acetate consumption experiments using labelled and unlabelled acetate could clarify whether acetate is being consumed and to what extent.

As previously mentioned, transcriptomic data in both MS-5 and SKM-1 cells indicated that hypoxia is one the highest upregulated pathways in co-culture. Apart from the increase in expression of the speculated acetate transporter MCT4 [249], hypoxia can increase the usage of acetate by cancer cells [215] and the contribution to the acetyl-CoA pool [204]. Moreover, acetate has been reported to function as an epigenetic metabolite under hypoxia, acetylating histone H3 resulting in an increase of lipid synthesis and, thus, acetate metabolism [214]. Additional experiments under hypoxia, including acetate measurements and acetate consumption in AML cells alone and in co-culture, could give insight on whether AML cells utilise the acetate secreted to the extracellular medium in hypoxia and how they use it.

In this section, the mechanism of how metabolism is altered in co-culture has been studied. MS-5 cells have been suggested to be responsible for acetate secretion in co-culture through upregulation of glycolysis and deregulation of pyruvate metabolism. Pyruvate accumulation in MS-5 cells in co-culture and ROS have been suggested to be the major causes for acetate secretion. The transcriptome of SKM-1 cells have not shown important upregulation of metabolic pathways, especially related to acetate metabolism. Whether AML cells are able to use acetate, how and why do they use it in co-culture are the next questions that will be discussed in the following chapter.

5. Understanding how AML cells use acetate in co-culture

5.1. Introduction

In the previous chapter, MS-5 cells were identified as responsible for the increased acetate secretion found in co-cultures with AML cells. The suggested mechanism of acetate secretion involved: (i) upregulation of glycolysis; (ii) deregulation of pyruvate metabolism; (iii) transfer of ROS probably through gap junction; and (iv) ROS-mediated decarboxylation of pyruvate.

One of the questions that arose in the previous chapters was whether AML cells could benefit from acetate secretion. Transcriptomic data on SKM-1 cells in co-culture did not reveal any major metabolic alterations related to acetate import or utilisation. However, these cells could still import and use acetate without presenting an adapted transcriptome.

Acetate has been reported to be an alternative to glucose in cancer cells under stress conditions of low oxygen concentration and lipid depletion [214, 215, 245]. Acetate can be metabolised intracellularly by being activated by ligation to the coenzyme-A by acetyl-CoA synthetases, yielding acetyl-CoA. There are three acetyl-CoA synthetases capable of synthesizing acetyl-CoA from acetate: ACSS1, ACSS2 and, with lower affinity, the acetyl-CoA synthetase 3 (ACCS3) [250]. ACSS1 and ACSS3 localised in the mitochondria [251] and ACSS2 in the cytoplasm and nucleus [252]. After the addition of CoA, it can be used in the TCA cycle, fatty acid synthesis and histone acetylation, as reviewed in [222].

In this chapter, I sought to determine: (i) whether AML cells consume acetate in co-culture; (ii) how is it metabolised by AML cells; and (iii) how to prevent acetate activation and usage. Acetate consumption studies, oxygen-modulating experiments, tracer-based NMR spectroscopy approaches, and the CRISPR-Cas9 technology were combined to address the above-mentioned questions.

5.2. Results

5.2.1. Can SKM-1 cells consume and use acetate?

In the previous chapters, metabolism in co-culture and the mechanisms underlying metabolic reprogramming in co-culture were studied. Acetate secretion was found to be the major metabolic alteration in co-culture and was attributed to an increase in glycolysis and ROS in MS-5 cells. Interestingly, the transcriptome of SKM-1 cells was not found to be adapted to efficiently utilise acetate in co-culture. However, whether SKM-1 cells can utilise acetate, independently of their transcriptome presenting a specific reprogramming, remains unclear. To determine whether SKM-1 cells consume acetate in co-culture, it was first necessary to assess whether SKM-1 cells can consume and metabolise acetate, to what extent and how it compares to the consumption and use of acetate by MS-5 cells.

First, it seemed crucial to determine the concentration of acetate generated and present in the extracellular medium in co-culture after 24 hours. To determine the concentration of acetate in co-culture, a calibration curve was prepared by preparing samples of fresh medium adding increasing concentrations of acetate to analyse them by ^{1}H-NMR spectroscopy. Samples of extracellular medium from SKM-1 and MS-5 co-cultured for 24 hours were also analysed and interpolated into the calibration curve to obtain the concentration of acetate in co-culture.

Cell culture medium was prepared by adding increasing concentrations of acetate (0, 0.25, 1, and 4 mM). Samples of extracellular medium of SKM-1 and MS-5 cells after 24 hours of co-culture were collected. All samples were analysed by ^{1}H-NMR spectroscopy.

The acetate signal in the ^{1}H-NMR spectra, corresponding to the methyl group of acetate at 1.92 ppm, for the control medium samples (0, 0.25, 1, and 4 mM acetate, grey scale) and co-culture (red) are shown in Figure 5.1A. It has been reported that some acetate can be found in the cell

culture medium due to the presence of FBS [204]. However, in the sample of medium with no added acetate (0 mM), the level of acetate detected was within the range of the noise in the spectrum and was not possible to quantify.

The intensities for the control samples were fitted to a linear regression and the concentration of acetate present in the co-culture sample was estimated by interpolating the intensity (Figure 5.1B). The estimated concentration of acetate after 24 hours of co-culture was 3.09 mM.

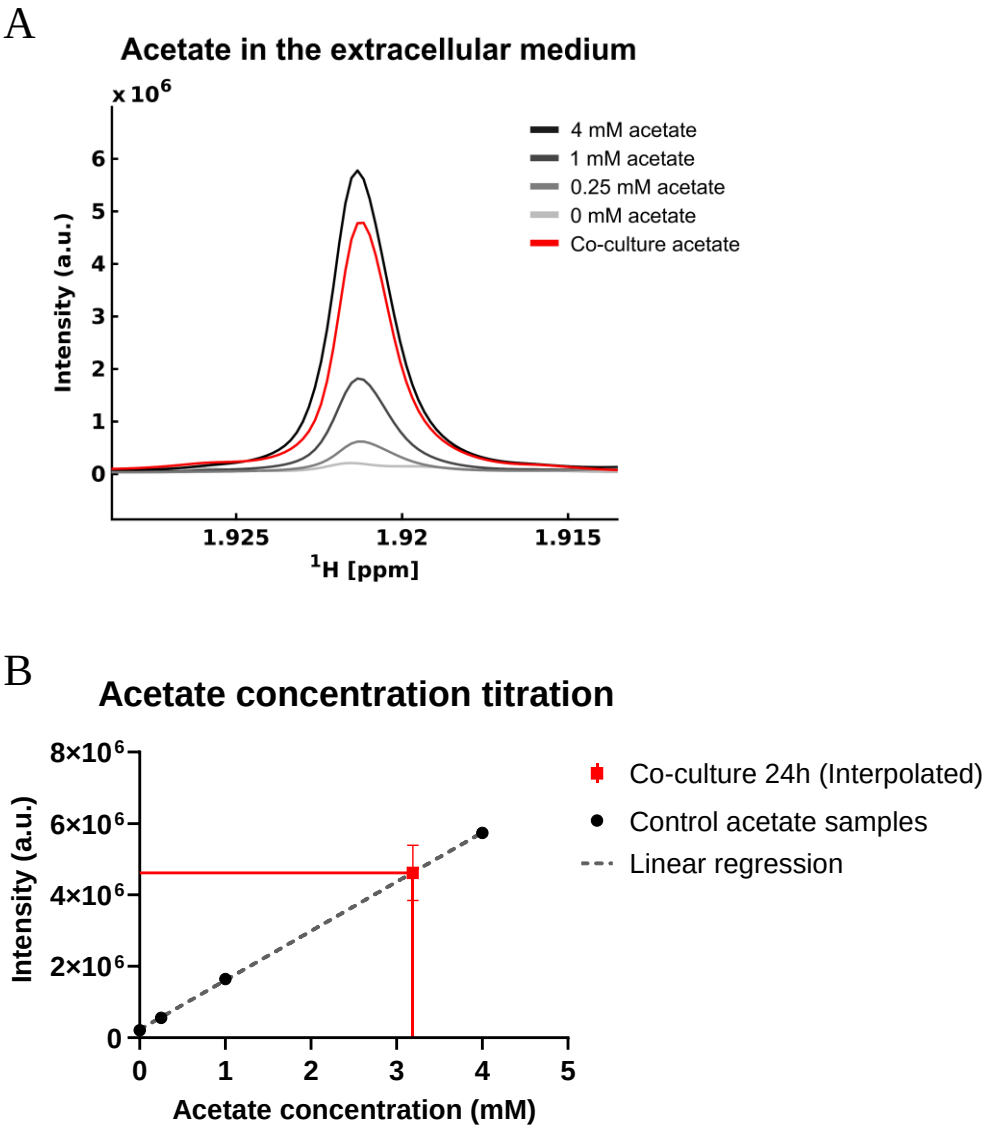

Figure 5.1 Determination of acetate concentration in co-culture.

Samples of extracellular medium with increasing concentrations of acetate and samples from SKM-1 and MS-5 cells in co-culture after 24 hours were prepared and analysed by ^{1}H-NMR spectroscopy. A) Acetate signal in ^{1}H-NMR spectra of control medium samples with increasing concentrations of acetate (grey scale) and SKM-1 and MS-5 co-culture (red). Representative of n=3 independent experiments. B) Linear regression of acetate concentrations and detected intensities in ^{1}H-NMR spectra (Intensity=$1.38 \cdot 10^{6} \pm 1.6 \cdot 10^{4}$ x Acetate concentration + $2.27 \cdot 10^{5} \pm 3.3 \cdot 10^{4}$; R^{2}=0.9987). The intensities detected in samples of co-culture were interpolated to obtain the estimate acetate concentration in co-culture (3.09 mM). Each point represents the mean of n=3 independent experiments and error bars represent standard deviation.

Once the concentration of extracellular acetate generated after 24 hours of co-culturing SKM-1 and MS-5 cells was estimated, the consumption of acetate by SKM-1 cells was assessed by culturing them in medium with two different acetate concentrations: co-culture (3 mM) and physiological (0.25 mM) [214, 253]. SKM-1 cells were cultured in acetate culture medium (3 or 0.25 mM) for 48 hours and samples of medium were collected at 0, 24 and 48 hours. Samples were analysed by ^{1}H-NMR spectroscopy.

As can be seen in Figure 5.2A, after 24 hours, SKM-1 cells significantly consumed acetate in physiological conditions and showed a similar tendency, although not significant, in co-culture conditions. After 48 hours, a significant consumption was detected for both conditions. These results suggest that SKM-1 cells consume acetate under co-culture and physiological conditions.

Another question that arose from this data was how quickly acetate could potentially be consumed by SKM-1 in co-culture. I decided to calculate the relative consumption over time of acetate, glucose and glutamine in SKM-1 cells cultured in 3 mM acetate medium after 48 hours. The consumption levels of both glucose and glutamine were significantly higher than the consumption of acetate (Figure 5.2B). This result indicates that acetate was being consumed at a significantly slower rate than glucose and glutamine. The fact that acetate was consumed at such slow rate could be a possible explanation to acetate being accumulated in the extracellular medium in co-culture.

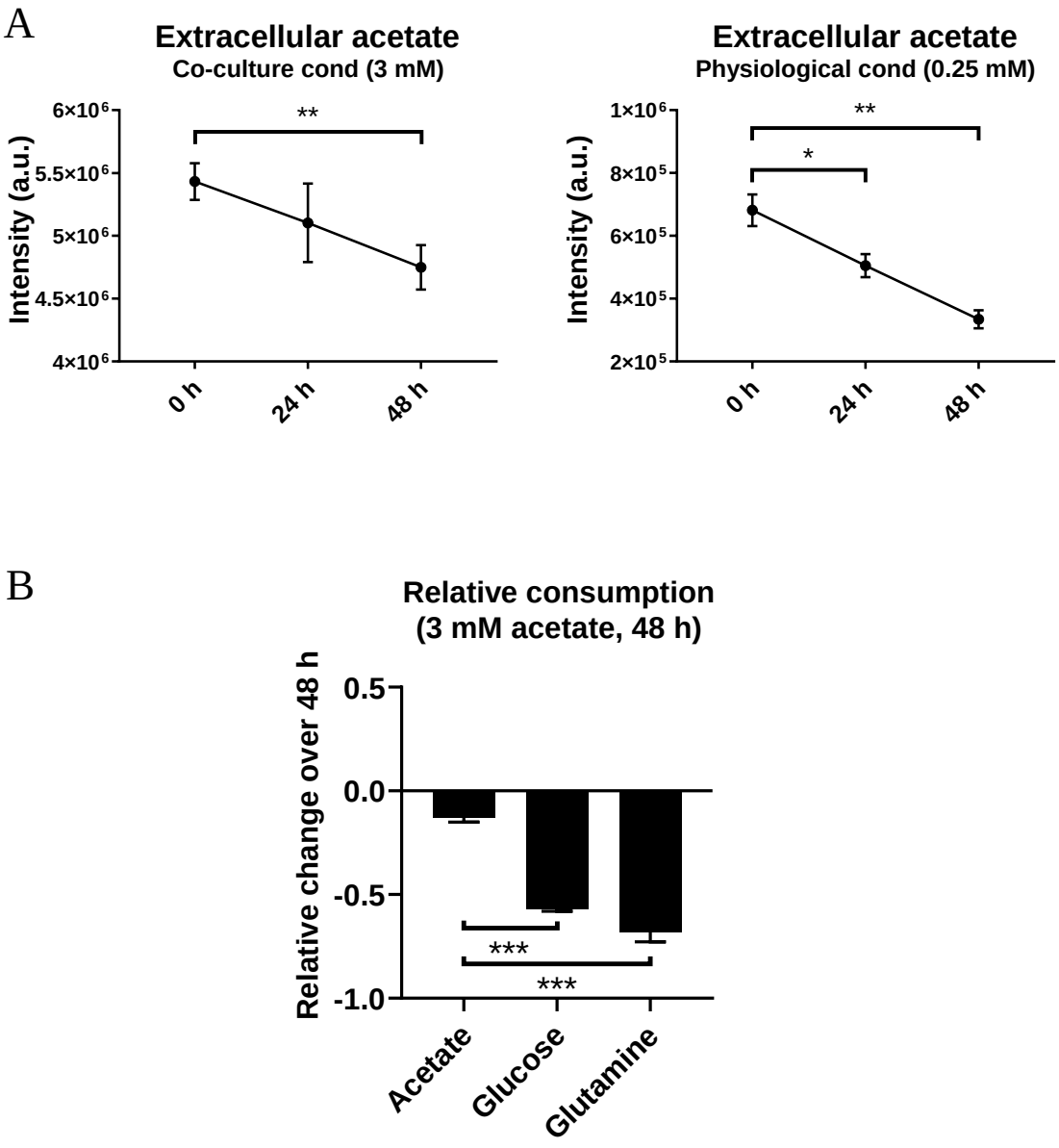

Figure 5.2 Acetate consumption in SKM-1 cells.

A) Extracellular acetate levels in SKM-1 cells cultured with 0.25 mM and 3 mM acetate medium after 0, 24 and 48 hours obtained by ^{1}H-NMR spectroscopy. Each point represents the mean of n=3 independent experiments and error bars represent standard deviation. B) Relative acetate, glucose and glutamine consumption of SKM-1 cells cultured for 48 hours in 3mM acetate medium. Metabolite levels for acetate (data in A), glucose and glutamine were converted to relative metabolite changes over 48 hours where negative values represent consumption of a certain metabolite. Bars represent the mean of n=3 independent experiments and error bars represent standard deviation. For both A) and B) an unpaired t-student test was applied for each condition and p-values were represented as * for p-value<0.05, ** for p-value<0.01 and *** for p-value<0.001.

Next, I decided to use isotopically labelled [2-^{13}C] acetate in SKM-1 and MS-5 cells to assess if both cell types can import and metabolise acetate. SKM-1 and MS-5 cells were cultured alone in 4 mM sodium [2-^{13}C] acetate (labelled) medium and in 4 mM unlabelled sodium acetate medium for 2 hours. Cells were collected and intracellular metabolites were extracted and analysed with ^{1}H-^{13}C-HSQC NMR spectroscopy. Percentages of ^{13}C were calculated by dividing the intensities found in the labelled samples by the corresponding unlabelled sample and multiplied by the natural abundance of ^{13}C (1.1%). The expected label distributions in intracellular metabolites that can be detected and identified by ^{1}H-^{13}C-HSQC NMR spectroscopy are shown in Figure 5.3A.

^{13}C percentages of intracellular metabolites in SKM-1 and MS-5 can be seen in Figure 5.3B, and a 2D example spectrum of SKM-1 cells incubated with labelled acetate, including the metabolites assigned can be seen in Figure 5.4. Both cell types seemed to be importing acetate as 57% and 27% of ^{13}C were detected in SKM-1 and MS-5 cells, respectively (Figure 5.3B). However, only SKM-1 cells presented label incorporation in other metabolites (see aspartate, acetylcarnitine, citrate, glutamate, oxoglutarate, glutathione, malate and proline). These results suggest that both cell types are capable of importing acetate but only SKM-1 cells can metabolise acetate.

Several metabolites that incorporated label from acetate in SKM-1 are involved or linked to the TCA cycle (aspartate, citrate, glutamate, oxoglutarate and malate) (Figure 5.3B), suggesting that a probable role for acetate in SKM-1 cells could be to feed the TCA cycle. Other metabolites, such as glutathione and proline, are derived from glutamate and, thus, also linked to TCA activity. The metabolite that presented the highest label incorporation from acetate in SKM-1 cells was acetylcarnitine (Figure 5.3B). Acetylcarnitine was reported to be produced by

cells when large amounts of acetyl-CoA are present in the mitochondria [254, 255], which correlates with the high concentration of acetate (4 mM) to which SKM-1 cells were exposed.

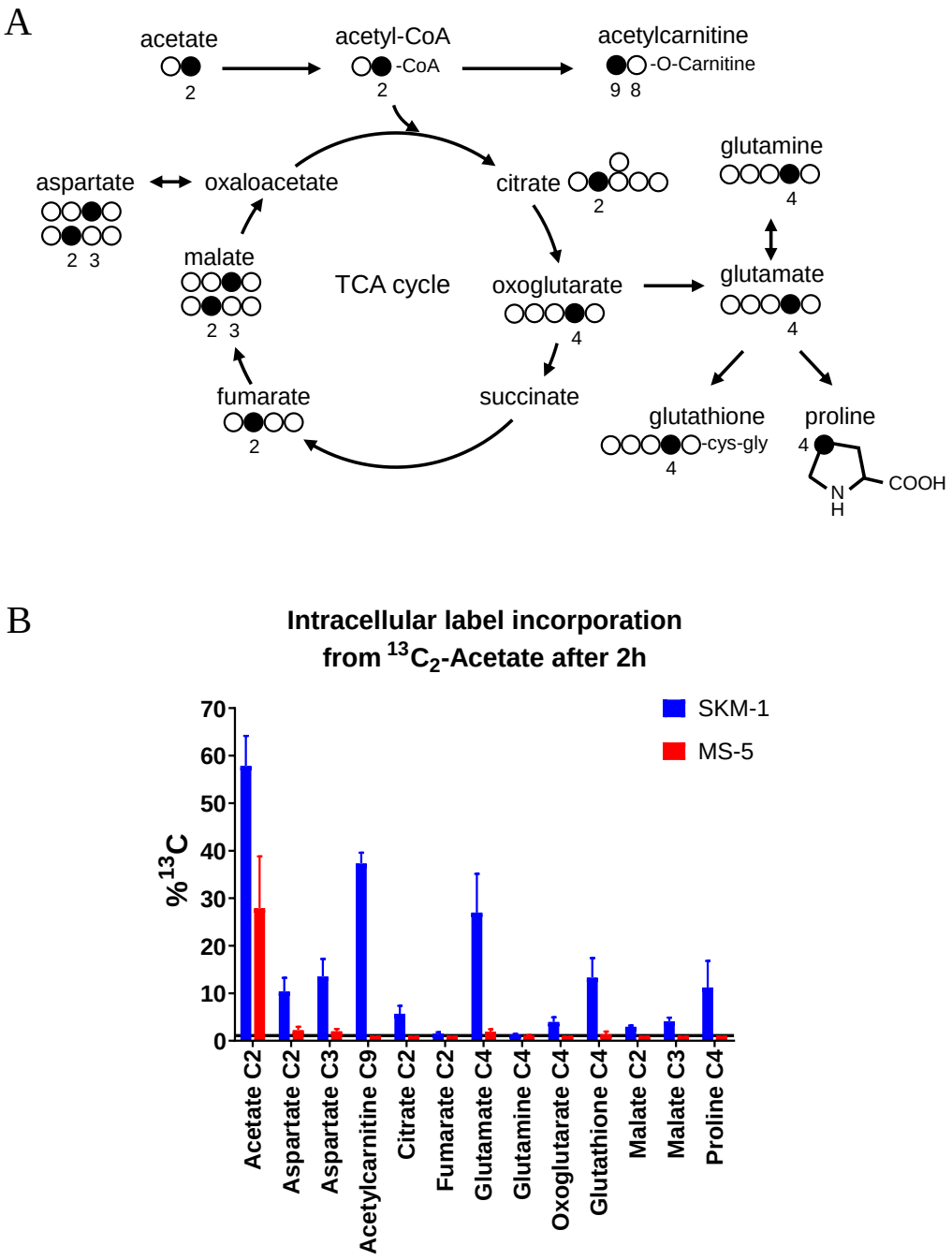

Figure 5.3 [2-^{13}C] Acetate labelling in SKM-1 and MS-5 cells: labelling pattern scheme and label incorporation in intracellular metabolites.

A) Label distribution arising from [2-^{13}C] acetate in TCA cycle intermediates. Black circles correspond to expected labelled positions. B) ^{13}C percentages of label incorporation in polar metabolites from labelled acetate in SKM-1 and MS-5 cells. SKM-1 and MS-5 cells were cultured separately in 4 mM sodium 2-^{13}C-acetate medium or 4 mM unlabelled sodium acetate for 2 hours before intracellular metabolite extraction. Polar samples were analysed by ^{1}H-^{13}C-HSQC NMR spectroscopy. ^{13}C percentages were calculated as a ratio of the labelled and unlabelled sample and multiplied by the natural abundance of ^{13}C (1.1%). Bars represent the mean of the ^{13}C percentage and error bars represent the standard deviation for n=3 independent experiments. ^{13}C natural abundance is represented as a black bar at ^{13}C% = 1.1.

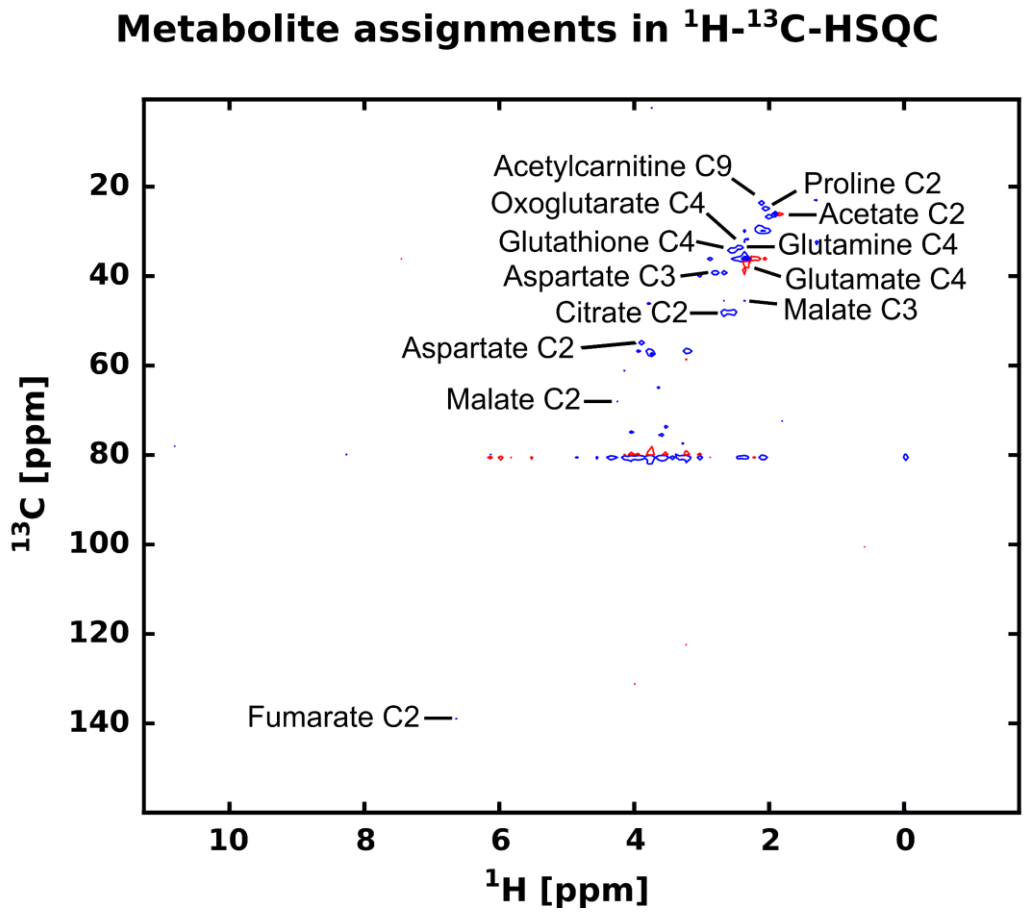

Figure 5.4 Metabolites assigned in ^{1}H-^{13}C-HSQC spectra from polar extracts incubated with [2-^{13}C] acetate. Example of a ^{1}H-^{13}C-HSQC spectrum from a polar extract from SKM-1 cells cultured with [2-^{13}C] acetate for 2 hours. ^{13}C percentages were calculated in 13 carbons from 11 different metabolites. The exact chemical shifts for each carbon are: acetate C2, 1.91 ppm (^{1}H) – 26.1 ppm (^{13}C); aspartate C2, 3.89 ppm (^{1}H) – 55.0 ppm (^{13}C); aspartate C3, 2.82 ppm (^{1}H) – 39.4 ppm (^{13}C); acetylcarnitine C9, 2.15 ppm (^{1}H) – 23.4 ppm (^{13}C); citrate C2, 2.52 ppm (^{1}H) – 48.2 ppm (^{13}C); fumarate C2, 6.51 ppm (^{1}H) – 138.2 ppm (^{13}C); glutamate C4, 2.34 ppm (^{1}H) – 36.1 ppm (^{13}C); glutamine C4, 2.44 ppm (^{1}H) –33.7 ppm (^{13}C); oxoglutarate C4, 2.43 ppm (^{1}H) – 33.4 ppm (^{13}C); glutathione C4, 2.55 ppm (^{1}H) – 34.2 ppm (^{13}C); malate C2, 4.28 ppm (^{1}H) – 73.2 ppm (^{13}C); malate C3, 2.68 ppm (^{1}H) – 45.4 ppm (^{13}C); and proline C4, 2 ppm (^{1}H) – 26.6 ppm (^{13}C).

5.2.2. Are SKM-1 cells consuming and using acetate in co-culture?

Next, it was crucial to investigate whether SKM-1 cells would consume and use acetate in co-culture in a similar way as they do when cultured alone. I first decided to determine whether changing the ratio of SKM-1 to MS-5 cells in co-culture would result in differences in acetate levels related to SKM-1 cells consuming acetate.

SKM-1 and MS-5 cells were cultured with increasing ratios of SKM-1 to MS-5 (1:1, 4:1 and 8:1) and MS-5 cells cultured alone were also analysed as comparison. Samples of medium were collected at 0, 20 and 24 hours and analysed by ^{1}H-NMR spectroscopy to determine the levels of extracellular acetate in each condition.

As shown in Figure 5.5, acetate levels did not significantly change by increasing the ratio of SKM-1 to MS-5 cells. Moreover, there was a tendency to higher levels of acetate with increasing number of SKM-1 cells. As a control, co-culture samples presented, in all cases, significantly higher levels of acetate than MS-5 cells cultured alone. These results suggest that the increase in number of SKM-1 cells does not induce changes in the extracellular acetate levels. The fact that acetate levels remain similar with an increase of the ratio of SKM-1 to MS-5 cells could be explained by: (i) SKM-1 cells induce more acetate secretion by MS-5 cells but the increase in production is similar to the increase in consumption by SKM-1 cells; or (ii) the induction of acetate secretion is contact dependent and is limited by the available contact surface of the layer of MS-5 cells.

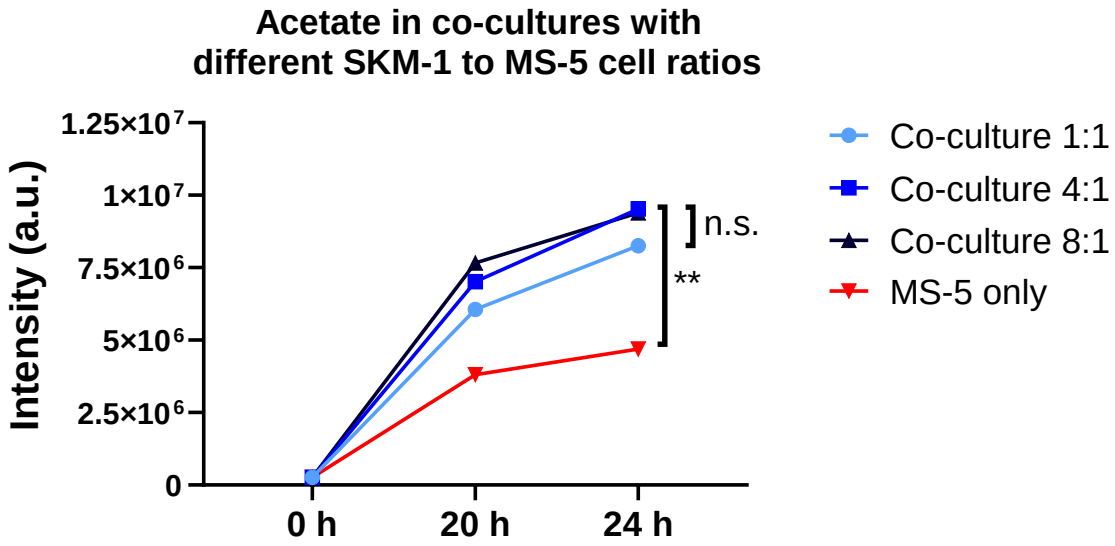

Figure 5.5 Extracellular acetate levels in co-cultures with different ratios of SKM-1 to MS-5 cells.

SKM-1 and MS-5 cells were cultured together in 1:1, 4:1 and 8:1 ratio and MS-5 cells were also cultured alone for 24 hours. Samples of medium were collected at 0, 20 and 24 hours and acetate levels were determined by ^{1}H-NMR spectroscopy. Each point represents the mean of n=3 independent experiments and error bars represent standard deviation. An unpaired t-student test was applied for the levels at 24 hours and p-values were represented as n.s. for not significant, * for p-value<0.05, ** for p-value<0.01 and *** for p-value<0.001.

As the previous experiment did not clarify whether SKM-1 cells consume acetate in co-culture, I decided to use labelled acetate to trace the consumption of acetate by SKM-1 and MS-5 cells in co-culture.

SKM-1 and MS-5 cells were co-cultured for 24 hours before adding extra sodium [2-^{13}C] acetate or unlabelled sodium acetate to the medium to a 4 mM final concentration. Co-cultured cells were incubated for 8 hours more before separation and polar metabolite extraction (Figure 5.6A). Polar metabolites were analysed by ^{1}H-^{13}C-HSQC NMR spectroscopy. Percentages of ^{13}C were calculated, as previously described, dividing the intensities found in the labelled samples by the corresponding unlabelled sample and multiplied by the natural abundance of ^{13}C (1.1%).

As can be seen in Figure 5.6B, only SKM-1 cells imported acetate in co-culture, presenting approximately 30% of labelled acetate intracellularly whilst MS-5 cells presented a ^{13}C percentage equal to the natural abundance of ^{13}C. Several metabolites, such as acetylcarnitine, glutamate and glutathione, showed label incorporation in SKM-1 cells. This result indicates that only SKM-1 cells consumed and metabolised acetate in co-culture whilst MS-5 cells did not import or use acetate in co-culture.

The metabolites that presented label incorporation from acetate in SKM-1 cells resemble the ones detected in SKM-1 cells cultured alone with labelled acetate (Figure 5.3B vs Figure 5.6B). The ^{13}C percentages were lower in this experiment probably because the incubation time with acetate was 4 times longer (from 2 to 8 hours) and the label was used up with time. The fact that label incorporations were similar in SKM-1 cells cultured alone and in co-culture suggests that SKM-1 cells do not use acetate differently in co-culture.

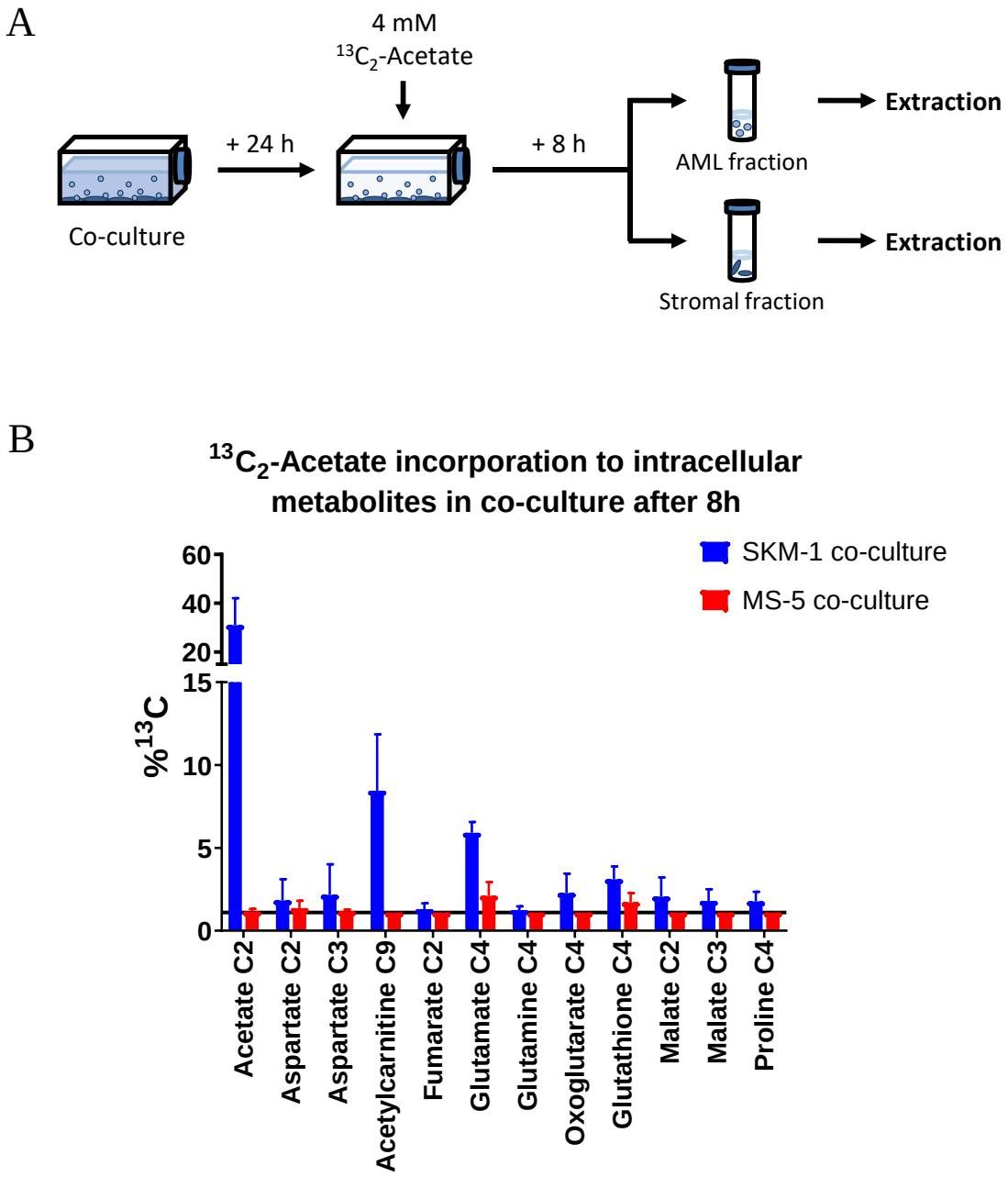

Figure 5.6 Acetate label incorporation in SKM-1 and MS-5 cells in co-culture.

A) Experimental scheme for acetate labelling in co-culture. In brief, SKM-1 and MS-5 cells were co-cultured for 24 hours before the addition of extra 4 mM sodium [2-^{13}C] acetate or extra 4 mM unlabelled sodium acetate. After 8 hours of the addition of acetate, cells were separated, and polar metabolites were extracted. Polar samples were analysed by ^{1}H-^{13}C-HSQC NMR spectroscopy. B) ^{13}C percentages on polar metabolites in SKM-1 and MS-5 cells in co-culture with labelled or unlabelled acetate medium. ^{13}C percentages were calculated as a ratio between the labelled and unlabelled sample and multiplied by the natural abundance of ^{13}C (1.1%). Bars represent the mean of the ^{13}C percentage and error bars represent the standard deviation of n=3 independent experiments. ^{13}C natural abundance is represented as a black bar at ^{13}C% = 1.1.

5.2.3. Does hypoxia increase the consumption of acetate by SKM-1 cells?

In previous sections, it was found that SKM-1 cells consume acetate both when cultured alone as well as in co-culture. The rate of acetate consumption was determined to be low compared to other metabolites, which could potentially cause the accumulation of acetate detected when culturing AML and MS-5 cells. It has been reported that cancer cells increase the usage of acetate under hypoxia [215]. Therefore, I decided to test whether hypoxia would increase the consumption of acetate by SKM-1 cells and, thus, alter the level of extracellular acetate in co-culture.

MS-5 cells were cultured alone and co-cultured with SKM-1 cells under normal oxygen conditions (20%) and under hypoxia (5%) for 48 hours. Samples of medium were collected at 0, 24 and 48 hours and analysed by ^{1}H-NMR spectroscopy. Acetate and glucose levels are shown in Figure 5.7A.

In MS-5 cells cultured alone, the levels of acetate remained unaltered in hypoxia compared to normoxia (Figure 5.7A, left, red scale). In co-culture, levels of extracellular acetate were significantly lower under hypoxic conditions compared to normal oxygen conditions (normoxia) (Figure 5.7A, left, green scale). As MS-5 cells cultured alone did not present lower acetate levels in hypoxia, these results could suggest that SKM-1 cells consumed more acetate under hypoxia. However, glucose, which was shown to be the precursor of acetate in the previous chapter, was consumed completely after 24 hours in co-culture under hypoxia but not in co-culture under normoxia (Figure 5.7A, right, green scale) suggesting that the lower levels of acetate detected in co-culture under hypoxia are more likely to be caused by the exhaustion of glucose than by SKM-1 cells increasing acetate consumption.

To characterise whether SKM-1 increase acetate consumption under hypoxia, SKM-1 cells were cultured with 3 mM acetate for 48 hours under normoxic and under hypoxic conditions. Samples of medium were collected at 0 and 48 hours and analysed by ^{1}H-NMR spectroscopy. Acetate levels at 0 and 48 hours were converted into relative change over 48 hours.

The relative acetate consumption in SKM-1 cells cultured under hypoxia compared to normoxia did not change significantly (Figure 5.7B). This result indicates that SKM-1 cells did not alter the rate of acetate consumption under hypoxia, suggesting that hypoxia could not be an important factor for acetate consumption.

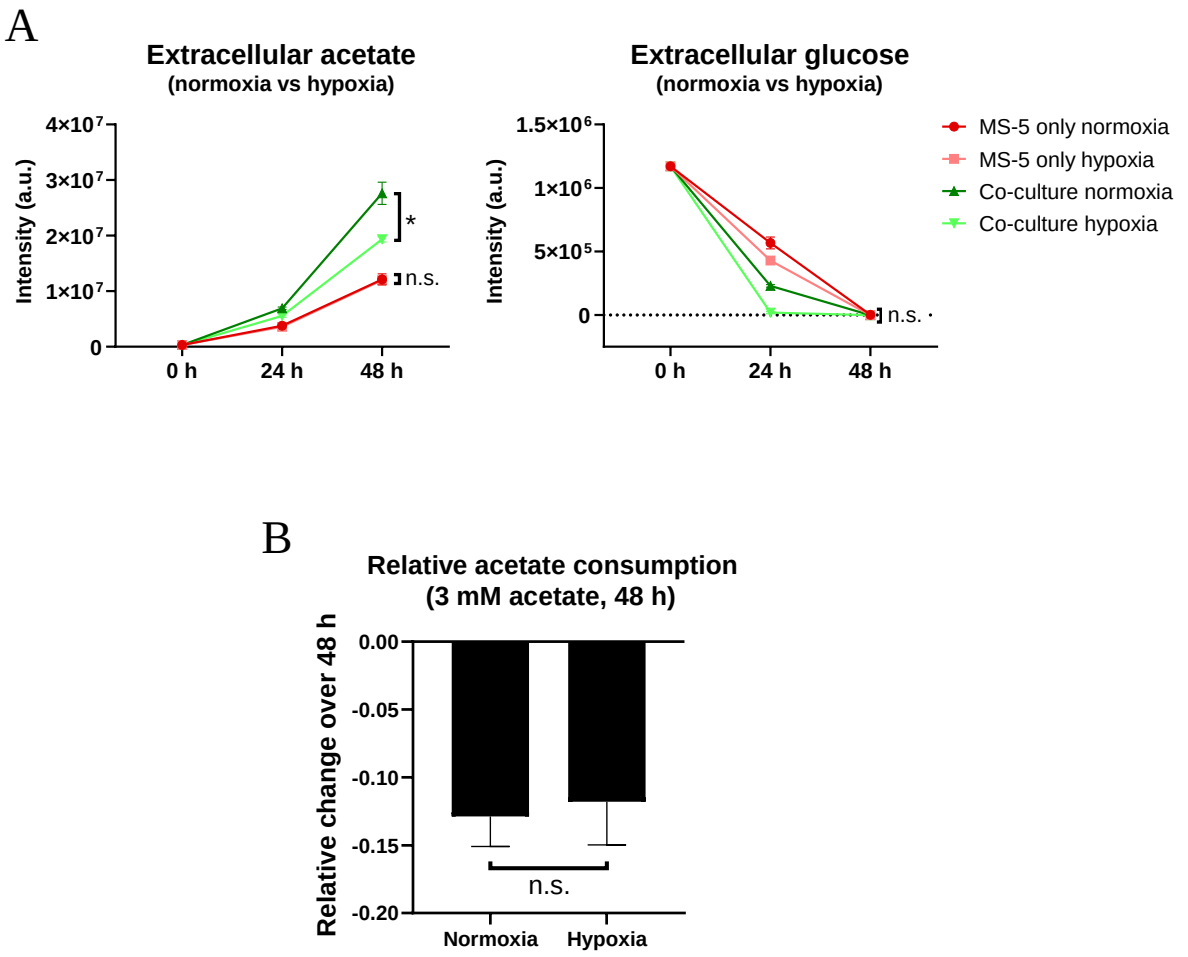

Figure 5.7 Effect of hypoxia on co-cultures and acetate consumption.

A) Acetate and glucose levels in MS-5 cells cultured alone and in co-culture under normal or hypoxic conditions of oxygen concentration. MS-5 cells were cultured alone and in co-culture with SKM-1 cells for 48 hours under normal oxygen conditions (20%) and under hypoxia (5%). Samples of medium were collected at 0, 24 and 48 hours and analysed by ^{1}H-NMR spectroscopy. Each point represents the mean of n=3 independent experiments and error bars represent standard deviation. B) Extracellular relative acetate consumption of SKM-1 cells cultured for 48 hours under normal oxygen conditions vs under hypoxia. Metabolite levels for acetate were converted to relative change over time where negative values represent consumption of a certain metabolite. Bars represent the mean of n=3 independent experiments and error bars represent standard deviation. For both A) and B) an unpaired t-student test was applied for the levels/rates at 48 hours and p-values were represented as n.s. for not significant, * for p-value<0.05, ** for p-value<0.01 and *** for p-value<0.001.

5.2.4. Is it possible to inhibit acetate usage by SKM-1 cells in co-culture?

After characterising that SKM-1 cells consume acetate in co-culture and that acetate consumption is not altered under hypoxia, I decided to inhibit acetate usage and study the effect in SKM-1 cells in co-culture. As previously described, ACSS1 and ACSS2 are the main enzymes involved in the conversion of acetate to acetyl-CoA. An inhibitor was identified for ACSS2, N-(2,3-di-2-thienyl-6-quinoxalinyl)-N´-(2-methoxyethyl)urea, capable of impeding lipid and histone incorporation of acetate in mouse embryonic fibroblasts [213]. Thus, I decided to use this ACSS2 inhibitor with SKM-1 and MS-5 cells in co-culture.

SKM-1 and MS-5 cells were co-cultured for 24 hours with and without the ACSS2 inhibitor at a final concentration of 20 μM, similar to other studies using the same inhibitor [182, 183]. Samples of medium were collected at 0, 4, 8 and 24 hours and acetate levels were characterised by ^{1}H-NMR spectroscopy.

The overall extracellular acetate level after 24 hours was significantly lower in the co-cultures treated with the ACSS2 inhibitor than in the non-treated control (Figure 5.8A).This result was unexpected as inhibiting the usage of acetate was expected to increase the levels of extracellular acetate or maintain them unaltered, but not to decrease them. One of the possible explanations for this result could be that the inhibitor was also inhibiting ACSS2 in MS-5 cells and, in turn, this was decreasing the production of acetate by MS-5 cells in co-culture.

In order to test whether MS-5 cells could be affected by ACSS2 inhibition, MS-5 cells were cultured alone for 24 hours with and without the ACSS2 inhibitor following the same protocol as in the previous experiment with cells in co-culture.

The levels of extracellular acetate secreted by MS-5 cells when treated with the ACSS2 inhibitor decreased in a similar manner as observed in co-culture (Figure 5.8B). This result

indicates that the ACSS2 inhibitor is reducing acetate secretion by MS-5 cells, probably by inhibiting acetate synthesis from acetyl-CoA, as previously reported [245]. Therefore, this inhibitor cannot be used to selectively prevent acetate conversion to acetyl-CoA in AML cells in co-culture.

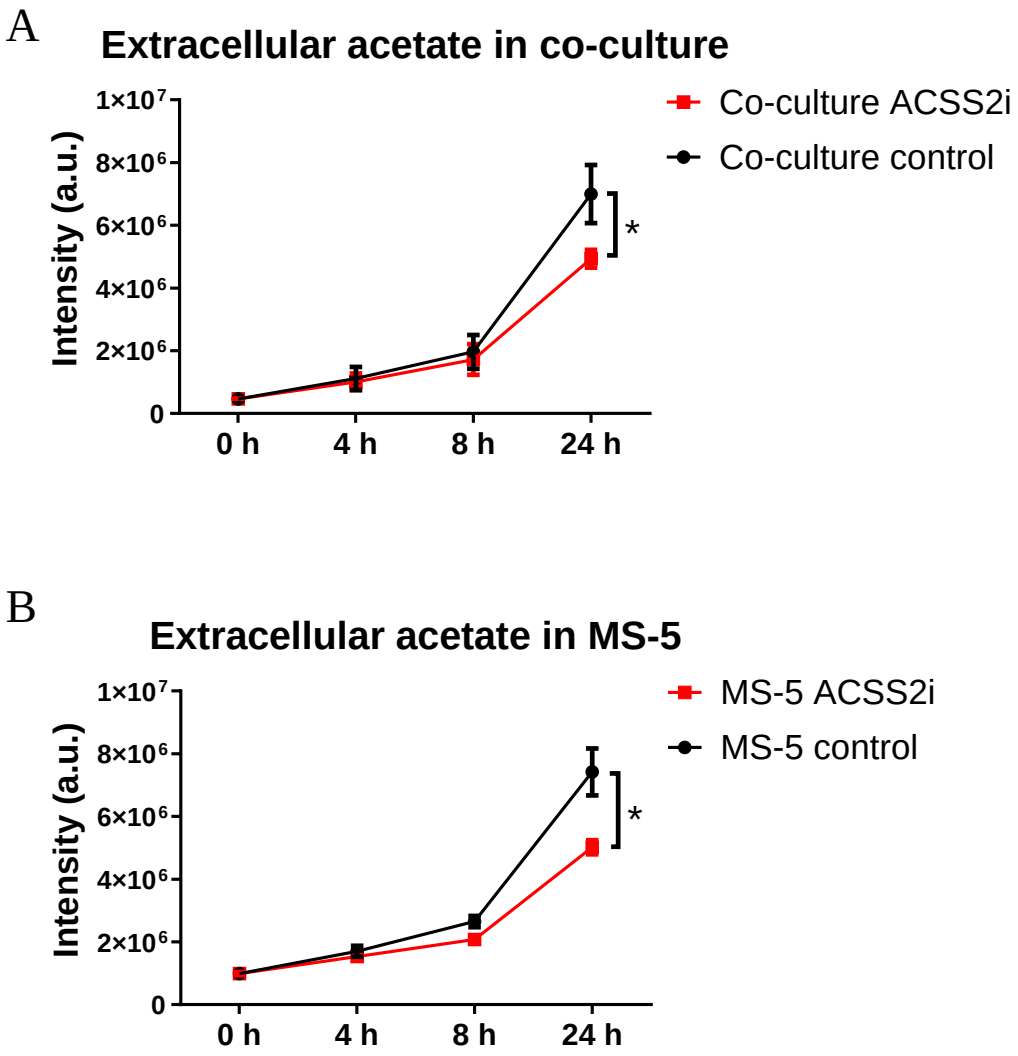

Figure 5.8 Extracellular acetate levels in co-culture and MS-5 cells when treated with ACSS2 inhibitor.

A) SKM-1 and MS-5 were co-cultured in medium with 20 µM ACSS2 inhibitor (in DMSO) or with a control medium with the equivalent volume of DMSO for 24 hours. B) MS-5 cells were cultured alone in medium with 20 µM ACSS2 inhibitor (in DMSO) or with a control medium with the equivalent volume of DMSO for 24 hours. For both A) and B) samples of medium were collected at 0, 4, 8 and 24 hours and analysed by ^{1}H-NMR spectroscopy. Each point represents the mean of n=3 independent experiments and error bars represent standard deviation. An unpaired t-student test was applied for the levels at 24 hours and p-values were represented as * for p-value<0.05, ** for p-value<0.01 and *** for p-value<0.001.

5.2.5. What is the effect of preventing acetate usage in AML cells?

In the previous section, it was established that the ACSS2 inhibitor was not selective in co-culture, as it inhibited acetate synthesis from acetyl-CoA in MS-5 cells, yielding lower extracellular acetate levels in both MS-5 cells alone and in co-culture with SKM-1 cells. To selectively block acetate usage in AML cells, it was necessary to generate cell lines lacking the acetyl-CoA synthetase activity by knocking-out ACSS1 and ACSS2.

An HL-60 cell line containing a Cas9 region was used to generate ACSS1, ACSS2 and ACSS1+ACSS2 knock-out cell lines. Two types of single guide RNAs (sgRNAs) for each gene were cloned into two different lentiviral vectors with reporter genes. ACSS1 sgRNAs were cloned into an EGFP lentiviral vector and ACCS2 sgRNAs were cloned into an E2Crimson lentiviral vector. Additionally, a non-targeted control (NTC) was also used and cloned into the EGFP lentiviral vector. Vectors were transduced into the Cas9 HL-60 cell line and cells were sorted according to the reporter gene expressed (Figure 5.9A). The Cas9 HL-60 cell line and the ACSS1/ACSS2 KO cell lines were generated in the Goethe University (Frankfurt) by Dr Frank Schnütgen, as part of a collaboration within the HaemMetabolome-ITN.

Protein extracts from the sorted Cas9 transduced cell lines were collected and analysed for ACSS1 and ACSS2 expression by Western blotting (Figure 5.9B). The analysis of expression revealed that all the cell lines analysed presented detectable expression of both ACSS1 and ACSS2 proteins indicating that none of the cell lines present a complete deletion of the gene. This result could be explained because transduced cells were pooled after sorting and not grown as single clones, therefore, generating mixed populations of KO and normal protein expression cells.

None of the ACSS1-targetting cell lines presented a decrease in the expression of ACSS1 (Figure 5.9B, 11, 12, 1121, 1221, 1122 and 1222). Some of the ACSS1-targetting cell lines seemed to have a higher expression of ACSS1 than the non-targeted control. This result could indicate that knocking-out ACSS1 leads to a great growth disadvantage and clones with the ACSS1 KO were overgrown by clones with normal or higher expression of ACSS1.

A considerable decrease of the expression of ACSS2 was found in two of the cell lines (Figure 5.9B, 21 and 1222). The ACSS2 sgRNA#1 (21) cell line was selected to be used in further studies as a partial ACSS2 knock-out cell line.

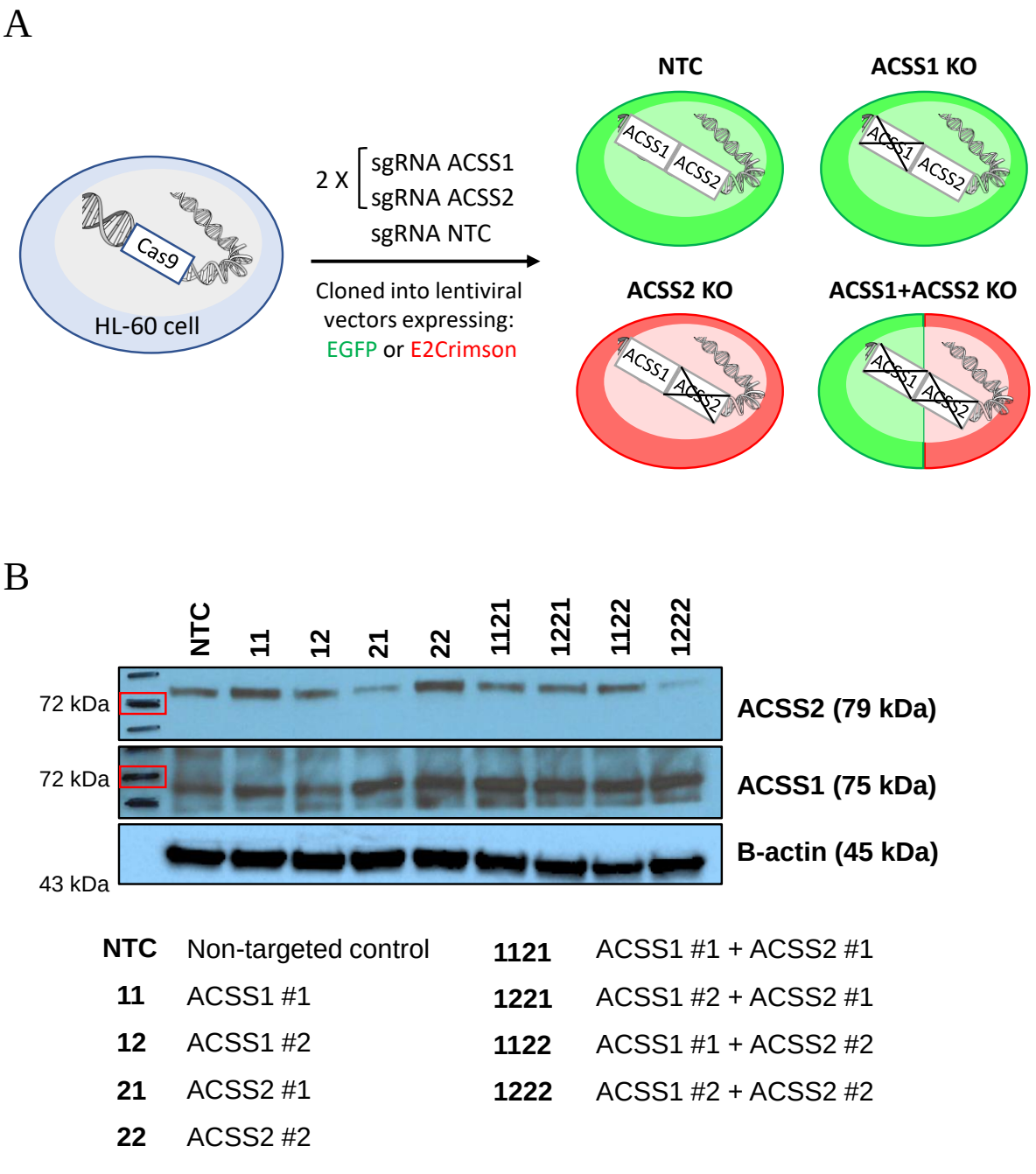

Figure 5.9 Generating ACSS1/ACSS2 KO cell lines from a Cas9 HL-60 cell line.

A) Scheme of ACSS1/ACSS2 KO cell lines generation. In brief, a Cas9 coding HL-60 cell line was transduced with 2 types of lentiviral vectors with sgRNAs targeting ACSS1 and/or ACSS2. A non-targeting lentiviral vector was also transduced as a control (NTC). Finally, cells were sorted according to the reporter gene (green for ACSS1 and red for ACSS2). B) Analysis of ACSS1 and ACSS2 protein expression by Western Blot of the different transduced cell lines. B-actin was used as a loading control. The first lane includes the coloured size marker used and the red square indicates the size marker corresponding to 72 kDa.

In order to assess the effect of the partial ACSS2 KO on acetate consumption and usage, I decided to use [2-^{13}C] acetate and trace its import and usage and compare the effect of the ACSS2 inhibitor to the partial ACSS2 KO on HL-60 cells.

HL-60 non-targeted control cells, HL-60 non-targeted control cells in 20 μM ACSS2 inhibitor medium and HL-60 with partial ACSS2 KO cells were cultured in 4 mM sodium [2-^{13}C] acetate and in 4 mM unlabelled sodium acetate for 24 hours before polar metabolite extraction. Polar extracts were analysed by ^{1}H-^{13}C-HSQC NMR spectroscopy. Only acetate, N-acetylaspartate, glutamate and glutathione could be unequivocally assigned in ^{1}H-^{13}C-HSQC spectra of these samples. Percentages of ^{13}C were calculated, as previously described, dividing the intensities found in the labelled samples by the corresponding unlabelled sample and multiplied by the natural abundance of ^{13}C (1.1%).

As can be seen in Figure 5.10, label incorporation in intracellular acetate did not decrease in either the ACSS2 inhibitor treated cells or the partial KO cells. This result indicates that inhibiting or preventing the usage of acetate does not seem to be affecting the import of acetate into cells. Moreover, the partial KO cells presented higher levels of intracellular acetate than the control cells suggesting that acetate could be accumulating in the partial KO cells.

The only other metabolite that presented label incorporation was N-acetylaspartate (Figure 5.10). There was a clear decrease in the label incorporation in N-acetylaspartate upon ACSS2 inhibition or partial KO indicating that the partial KO of ACSS2 has a similar effect to the ACSS2 inhibitor in preventing the usage of acetate in cells.

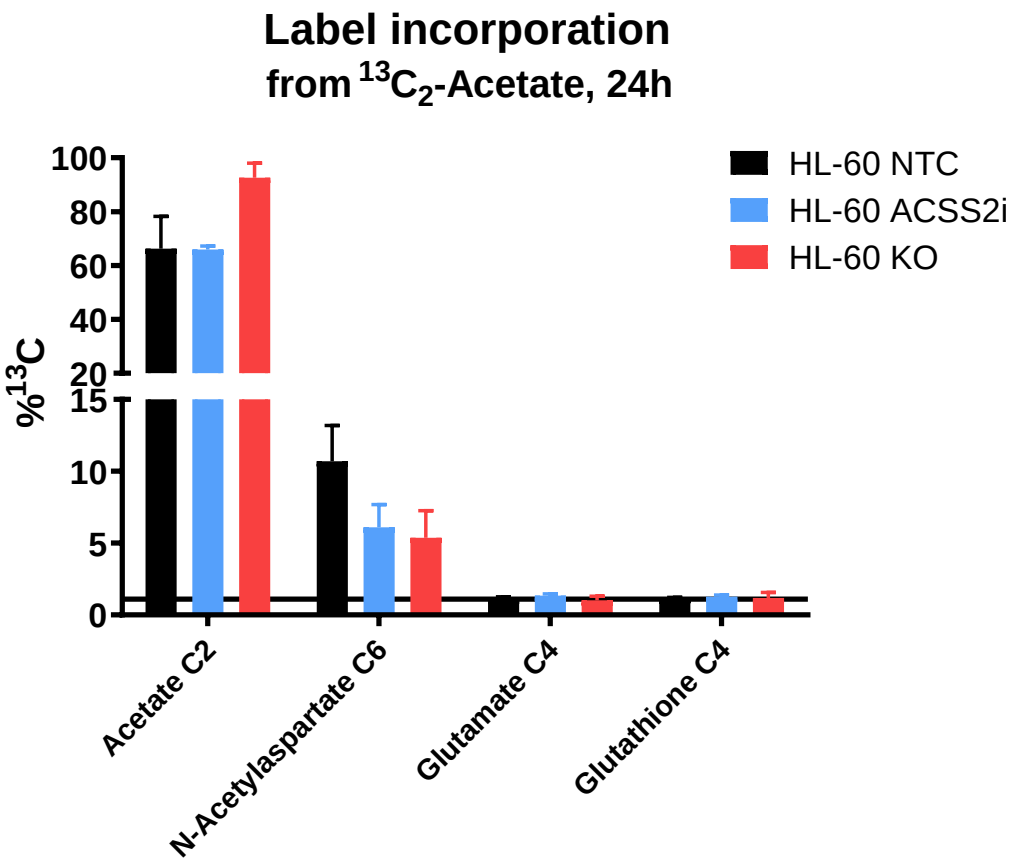

Figure 5.10 Acetate labelling incorporation in HL-60 cells: ACSS2 KO vs ACSS2 inhibitor.

^{13}C percentages on polar metabolites in non-targeted control (NTC) HL-60 cells vs ACSS2 inhibitor NTC HL-60 cells vs partial ACSS2 KO HL-60 cells. NTC HL-60 cells, NTC HL-60 cells treated with 20 µM ACSS2 inhibitor and HL-60 partial ACSS2 KO cells were cultured in 4 mM sodium [2-^{13}C] acetate or extra 4 mM unlabelled sodium acetate medium. After 24 hours, polar metabolites were extracted and analysed by ^{1}H-^{13}C-NMR spectroscopy. ^{13}C percentages were calculated as a ratio between the labelled and unlabelled sample and multiplied by the natural abundance of ^{13}C (1.1%). Bars represent the mean of the ^{13}C percentage and error bars represent the standard deviation of n=2 independent experiments. ^{13}C natural abundance is represented as a black bar at $^{13}C\%$ = 1.1. The exact chemical shift for N-acetylaspartate is acetate C2, 1.91 ppm (^{1}H) – 26.1 ppm (^{13}C).

Once established that the partial ACSS2 KO cell presented some impairment metabolising acetate, I decided to perform co-cultures to test whether impeding acetate usage would lead to acetate accumulation in the extracellular medium.

Non-targeted HL-60 control cells, ACSS2 partial KO HL-60 cells and MS-5 cells were co-cultured and cultured separately for 24 hours. Samples of medium were collected at 0, 20 and 24 hours and analysed by ^{1}H-NMR spectroscopy.

Extracellular acetate levels in both the control and the KO co-cultures were significantly higher than in MS-5 cells cultured alone (Figure 5.11A). Acetate levels in the partial KO cells in co-culture were slightly higher than in the control co-culture, although the increase was not statistically significant. This result suggests that acetate could be accumulating in co-culture when ACSS2 is partially knocked-out in HL-60 cells. Moreover, glucose consumption in both the control and partial KO co-cultures was not different (Figure 5.11B) suggesting that the amount of acetate generated in both co-cultures was similar and, therefore, supporting the hypothesis that acetate was accumulated in the KO co-culture.

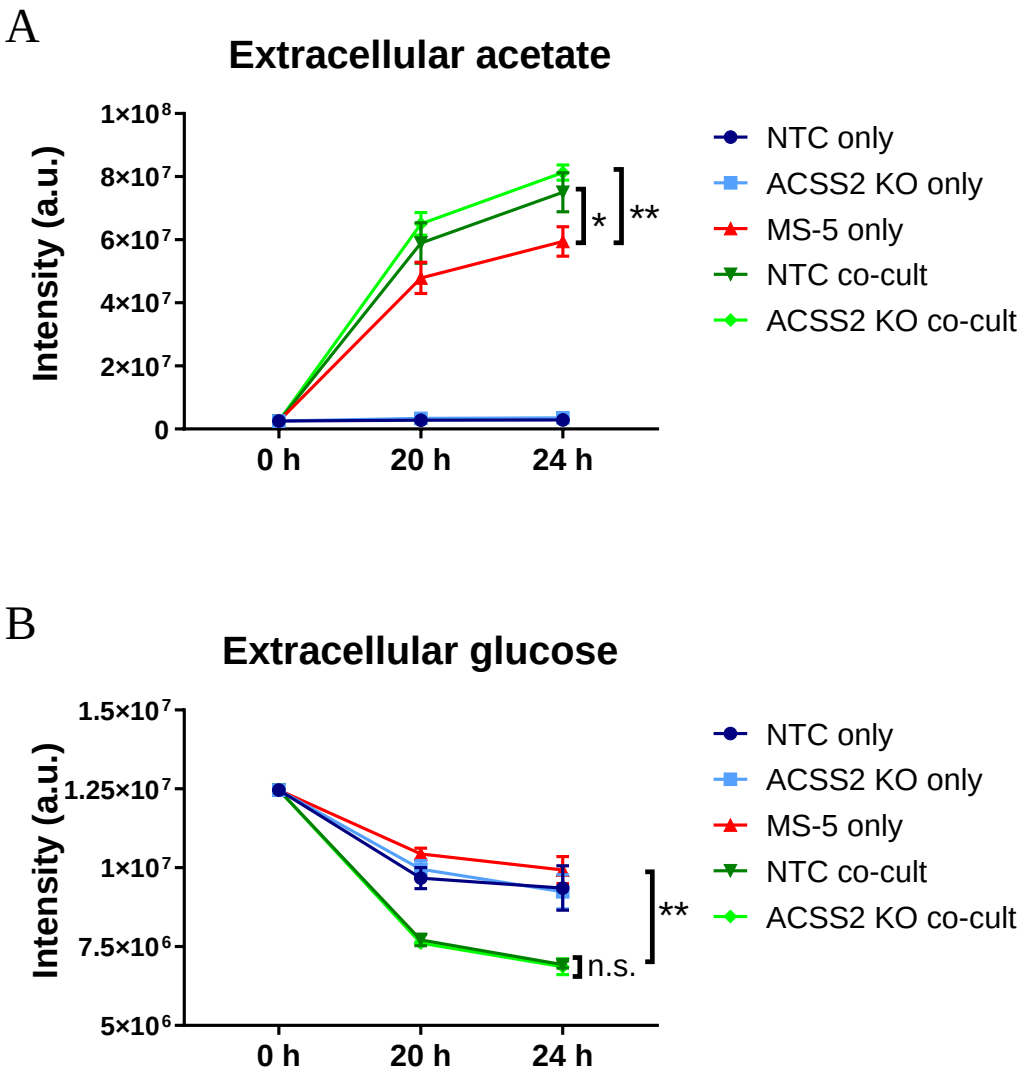

Figure 5.11 Acetate and glucose levels in co-culture with partial ACSS2 KO HL-60 cells vs NTC HL-60 cells.

NTC HL-60 cells and partial ACSS2 KO HL-60 cells were cultured alone and were co-cultured with MS-5 cells for 24 hours. Samples of medium were collected at 0, 20 and 24 hours and extracellular levels of A) acetate and B) glucose were analysed by ^{1}H-NMR spectroscopy. Each point represents the mean of n=3 independent experiments and error bars represent standard deviation. An unpaired t-student test was applied for each metabolite level at 24 hours and p-values were represented as * for p-value<0.05, ** for p-value<0.01 and *** for p-value<0.001.

5.3. Discussion

5.3.1. SKM-1 cells consume and use acetate in a similar manner in co-culture than when cultured alone

The aim of this chapter was to investigate whether AML cells could benefit from the secreted acetate in co-culture. In the previous chapter, transcriptomic analysis in SKM-1 cells in co-culture compared to cultured alone revealed that acetate metabolism-related genes were not altered in co-culture and, thus, that SKM-1 cells were not adapted to efficiently use acetate in co-culture. However, whether SKM-1 or other AML cells can import and use acetate was not answered. To characterise whether SKM-1 cells consume and use acetate in co-culture, several experiments were performed, including acetate consumption and tracer-based studies culturing cells with [2-^{13}C] acetate.

Acetate consumption studies revealed that SKM-1 cells can consume acetate both in co-culture concentration (3 mM) and physiological concentration (0.25 mM) (Figure 5.2A). This result agrees with early findings on leukaemic leukocytes being able to import acetate [256] and, in general, with cancer cells using acetate as an alternative acetyl-CoA source [213].

The rate of consumption of acetate in SKM-1 cells was significantly lower than the rates of consumption of glucose and glutamine (Figure 5.2B). This result suggests that SKM-1 can consume acetate but not to a great extent, which agrees with data from other cancers, such as hepatocellular carcinoma, showing that acetate consumption can be more than 10-fold lower than glucose consumption [210]. In addition, the fact that SKM-1 cells do not present a high rate of acetate consumption is also consistent with acetate being accumulated in the extracellular medium when cells are co-cultured.

Tracer based studies using [2-^{13}C] acetate in SKM-1 and MS-5 cells revealed that both cell lines can import acetate but only SKM-1 cells can metabolise it (Figure 5.3B). SKM-1 cells presented label incorporations from acetate in several TCA cycle-related metabolites suggesting that acetate metabolism could be in part directed towards feeding the TCA cycle in SKM-1 cells. Acetate flux into the TCA cycle had been previously reported by our group in the Kasumi cell line [173]; and by others in breast cancer, where label incorporation was found in citrate [215], and in brain tumours, where 50% of the total carbon in TCA cycle intermediates derived from acetate [257]. Further experiments aiming at characterising acetate incorporation into lipids and histone acetylation, for example using ^{14}C-acetate [213], could provide a complete picture on acetate metabolism in AML cells.

Co-cultures increasing the ratio of SKM-1 cells to MS-5 cells led to similar overall extracellular acetate concentrations (Figure 5.5). This result did not clarify whether SKM-1 cells consume acetate to a greater extent in co-culture, as it could be interpreted in both ways: (i) the increase in ratio of SKM-1 cells induces more acetate secretion by MS-5 cells and, simultaneously, results in more consumption by SKM-1 cells leaving similar overall acetate levels; or (ii) the increase in ratio of SKM-1 cells does not lead to higher secretion of acetate because acetate secretion is contact dependent and the available surface on the MS-5 layer is not altered by the increase in SKM-1 cells.

Co-cultures of SKM-1 and MS-5 cells in the presence of labelled [2-^{13}C] acetate revealed that only SKM-1 cells consume acetate in co-culture (Figure 5.6). The pattern of label incorporation in intracellular metabolites from acetate in SKM-1 cells in co-culture was very similar to SKM-1 cells cultured alone (Figure 5.3B), indicating that SKM-1 cells consume acetate in co-culture but do not present a distinct metabolism of acetate in co-culture than when cultured alone, which

is consistent with the transcriptomic data obtained in the previous chapter. Overall, these results suggest that a crosstalk between SKM-1 and MS-5 cells could be taking place in co-culture, initiated by a signal sent by SKM-1 cells that triggers acetate to be secreted by MS-5 cells and to be later consumed by SKM-1 cells.

5.3.2. Hypoxia does not alter acetate consumption in SKM-1 cells

There are extensive reports about the role of hypoxia in the metabolism of cancer cells, as reviewed in [221]. It had also been reported that cancer cells increase acetate uptake and metabolism under hypoxic conditions [204, 214, 258, 259]. The mechanisms described for this increase in acetate consumption included upregulation of ACSS2 [258], ACSS2-HIF2 signalling [259] and acetate functioning as an epigenetic metabolite upregulating lipid synthesis [214].

Co-culturing SKM-1 and MS-5 cells under hypoxia led to lower overall levels of extracellular acetate compared to co-cultures under normal conditions of oxygen (Figure 5.7A). This result seemed to suggest, at first, that SKM-1 cells could increase acetate consumption under hypoxia and, thus, the overall extracellular levels of acetate would be lower than in normal conditions of oxygen. However, the lower levels of acetate seemed to be caused by a faster exhaustion of glucose under hypoxic conditions (Figure 5.7A). Rapid consumption of glucose under hypoxic conditions had been reported in several types of cells and in blood levels [260-262]. An additional experiment that could clarify whether SKM-1 cells consume more acetate in co-culture under hypoxia would involve adding [2-^{13}C] acetate to SKM-1 and MS-5 cells in co-culture and analysing the label incorporation to intracellular metabolites on each cell type.

Acetate consumption experiments comparing hypoxic and normal oxygen conditions in SKM-1 cells cultured alone indicated that acetate consumption is not altered in hypoxia (Figure 5.7B). This finding is contradictory to data from other cancers presenting an increased acetate uptake under hypoxia [204, 214, 258, 259]. As none of these studies have been carried out in haematological cancers, one of the possible explanations for this result could be that is increased acetate uptake in hypoxia is cell specific. Another possible explanation could be related to the

methodology used to culture cells under hypoxic conditions. First, cells were not previously exposed to hypoxia and the experiment lasted 48 hours, therefore, cells were only exposed to acute hypoxia [263]. Secondly, an oxygen-controlled incubator was used, and cells were exposed to normal oxygen levels when sampling the medium. Finally, oxygen levels were lowered until a 5% concentration which is higher than concentration of oxygen used in most of the aforementioned hypoxic studies (1%) [204, 214, 258, 259]. Further experiments using a hypoxia chamber, lower oxygen levels and inducing acute and chronic hypoxia could give insight and clarify whether acetate consumption in SKM-1 is unaltered in hypoxia.

5.3.3. Preventing acetate usage by partially knocking-out ACSS2 leads to slight acetate accumulation in co-culture

One of the aims of this chapter was to block acetate consumption by AML cells to prove that AML cells consume the acetate secreted in co-culture and to study how it affects the crosstalk established between AML and MS-5 cells in co-culture. In order to prevent the usage of acetate once imported into cells, ACSS1 and ACSS2 enzymes were targeted in AML cells.

Inhibition of ACSS2 in co-culture yielded lower extracellular acetate levels compared to the control co-culture (Figure 5.8A). This was not the expected result, as inhibiting ACSS2 in SKM-1 cells should have led to higher acetate available, due to cells not being able to use it, or similar levels, if cells import acetate and it accumulates intracellularly or if the inhibitor had no effect. However, it was also possible that the inhibitor was acting on MS-5 cells and was inhibiting the reverse reaction, the synthesis of acetate from acetyl-CoA [245], yielding lower levels of acetate. Testing the inhibitor on MS-5 cells confirmed that acetate secretion was lowered in treated MS-5 cells in a similar manner as observed in the treated co-culture (Figure 5.8B). These results indicate that the ACSS2 inhibitor cannot be used in co-culture as it is affecting both cell types and, thus, altering the overall extracellular acetate concentration.

The generation of ACSS1 and ACSS2 KO cell lines did not result in a complete KO for any of the two isoforms (Figure 5.9B), only a partial ACSS2 KO was found in two cell lines. The main explanation for not achieving a complete KO could be that, after sorting the transfected cells, cells were not cultured as single clones leading to a mixed population cell line where selective growth of certain clones could occur. Single clone selection was not performed due to time limitations and a slow recovery after transfection and sorting. Repeating the experiment and

performing a single clone selection after sorting could increase the chances of obtaining complete KO cell lines.

The fact that not even a partial KO was achieved with ACSS1 was not expected. A study blocking ACSS1 and ACSS2 in hepatocellular carcinoma using small interfering RNAs revealed that the survival of cells was lowered to 60% and 10% in ACSS1 and ACSS2 [264], respectively. Moreover, another study where ACSS1 and ACSS2 were knocked-down revealed that ACSS2 had a stronger effect in decreasing the incorporation of acetate into lipids and histone proteins than ACSS1 [213]. These findings seem to indicate that ACSS2 KO should have a larger effect and be more detrimental to cells. However, ACSS2 KOs have been reported in fibroblasts [230], mice [265] and glioma [266] and no ACSS1 KOs have been reported yet. Overall, why the ACSS1 KO was not achieved could be related to not performing a single clone selection and/or to ACSS1 being essential for cell survival. More experiments including siRNAs targeting ACSS1 and ACSS2 could bring clarification by allowing to study the effect of silencing both genes at early time points.

Labelling with [2-^{13}C] acetate in the partial ACSS2 KO cell line compared to the NTC and NTC treated with ACSS2 inhibitor cell lines resulted in a similar decrease in label incorporation into N-acetylaspartate in the partial ACSS2 KO and the ACSS2 inhibitor treated NTC cell lines (Figure 5.10). This result indicates that knocking-out ACSS2 had a similar effect than using the ACSS2 inhibitor. Acetate import did not decrease in the KO or inhibited cells indicating that the decrease in label incorporation into N-acetylaspartate was caused by the lack or inhibition of ACSS2 and not by a lower availability of acetate. These results are in line with several studies showing a decrease in acetate incorporation to intracellular metabolites when ACSS2 is down-regulated or knocked-out [213, 214, 258, 264].

Another observation derived from [2-^{13}C] acetate labelling in all the HL-60 cell lines (partial ACSS2 KO, treated with ACSS2 inhibitor and control) was that acetate metabolism was only reflected in N-acetylaspartate. This result seems to indicate that HL-60 cells did not use acetate to generate flux into TCA cycle metabolites and, thus, how they used acetate could not be easily characterised by NMR spectroscopy. It would be interesting to study how a KO or knock-down in ACSS1 and ACSS2 would affect the metabolism of SKM-1 cells in co-culture, as most of the experiments generated in thesis were performed in SKM-1 cells.

Finally, the extracellular levels of acetate in the partial ACSS2 KO cell line in co-culture with MS-5 cells were slightly higher than in the NTC cell line in co-culture after 24 hours (Figure 5.11A). This result suggests that HL-60 cells with the partial ACSS2 KO were less able to use the acetate secreted by MS-5 cells and, therefore, acetate was accumulated to a higher extent in the extracellular medium. Glucose levels in both the partial ACSS2 KO and NTC co-cultures were very similar (Figure 5.11B) indicating that a similar amount of acetate must have been generated in co-culture by MS-5 cells. This result supports the hypothesis that HL-60 cells with the partial ACSS2 KO use less acetate in co-culture and it accumulates in the extracellular medium. Overall, these results support the hypothesis that a crosstalk between AML and MS-5 cells mediated by acetate is taking place. Further experiments, such as acetate consumption or the addition of extra labelled acetate to the co-cultures, could confirm this hypothesis.

In this chapter, the mechanisms behind acetate utilisation by AML cells have been studied. Acetate consumption in AML cells was characterised revealing that acetate can be incorporated into the TCA cycle metabolites. Labelling experiments with acetate revealed that SKM-1 cells consume and use acetate in co-culture. Additionally, blocking acetate usage in HL-60 cells led to the accumulation of acetate in co-culture. Overall, the results presented in this chapter

evidence that the acetate secreted by MS-5 cells in co-culture is imported and used by AML cells, indicating that an acetate-mediated crosstalk is occurring in co-culture.

6. Final discussion

6.1. Summary of main findings

AML cells are known to interact and remodel niche cells through various mechanisms, including the secretion of soluble factors, cytokines or metabolites, resulting in a better support of AML cells at the expense of normal haematopoiesis [49, 60, 65]. Stromal cells can establish multiple interactions with AML cells, enhancing AML proliferation and chemotherapy resistance [120, 121, 125]. However, whether AML and stromal cells can communicate through a metabolic crosstalk is not yet clear. Therefore, the aim of this thesis was to characterise metabolic interactions between AML and stromal cells that could be beneficial for AML cells.

The strategy followed here to identify potential crosstalk targets was to compare the metabolism in AML and stromal cells in co-culture to the metabolism of AML and stromal cells cultured alone under the same conditions of media, vessel, cell number and density. Additional experiments, including tracer-based NMR spectroscopy, flow-cytometry, transcriptome profiling, metabolite consumption and knock-out assays, were performed to characterise the mechanism behind the metabolic crosstalk between AML and stromal cells.

The major metabolic variation found by comparing AML-stromal co-cultures to cells cultured alone was an increased acetate secretion to the extracellular medium. Acetate secretion was found to be related to a complete reprogramming of stromal metabolism which included an increase in glycolysis and a ROS-mediated conversion of pyruvate to acetate. Moreover, the acetate secreted by stromal cells was found to be consumed and metabolised by AML cells. Furthermore, several mechanisms were proposed on how AML cells could be secreting signals and modulating stromal cells into secreting acetate. The complete proposed mechanism is depicted in Figure 6.1, and the data supporting this model is explained below.

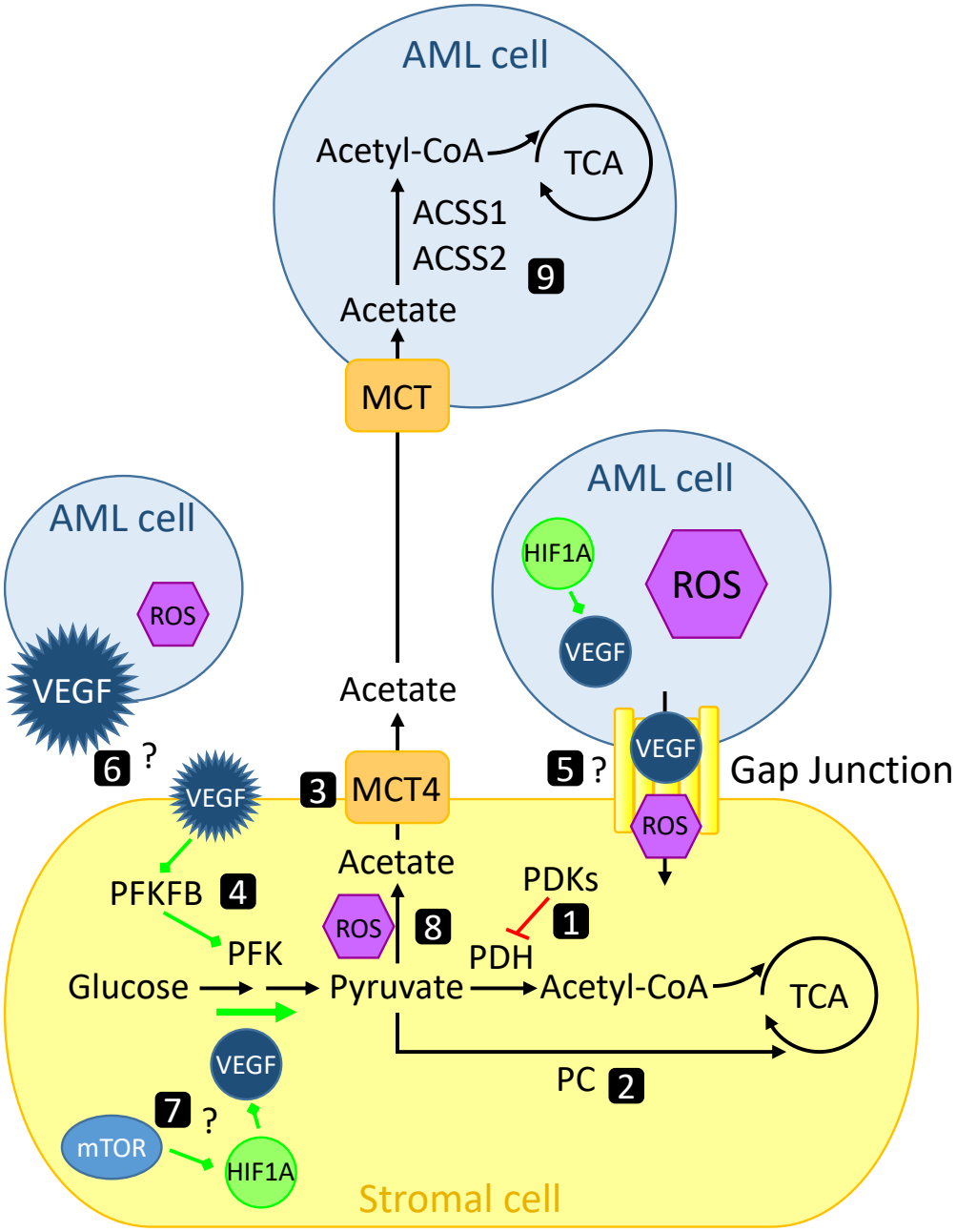

Figure 6.1 Proposed model for metabolic crosstalk between AML and stromal cells. Schematic representation of the proposed model of interaction between AML and stromal cells.

Briefly, co-culturing AML and stromal cells results in an increase in glycolysis in stromal cells. The increase in glycolysis was related to an increase of VEGF expression in MS-5 cells, which caused PFKFB and subsequent PFK activation (4). Moreover, the increase in VEGF expression was proposed to occur through three possible mechanisms: (i) direct transfer from AML to MS-5 cells possibly mediated by gap junction (5); (ii) exosome transfer (6); and mTOR activation leading to HIF signalling and VEGF (7). The increase in glycolysis was presented along with a downregulation of PDH and increase in PDKs (1) leading to pyruvate accumulation, which was corroborated by the usage of PC (2) as an alternative entry to the TCA cycle. Pyruvate accumulation was related to acetate production mediated by ROS (8) and MCT4 was suggested to be involved in the export of acetate (3). AML cells were also proposed to transfer ROS through gap junctions (5). Additionally, AML cells consumed and activated acetate by converting it to acetyl-CoA, through the acetyl-CoA synthetases ACSS1 and ACSS2, and use it as a carbon source to feed the TCA (9).

First, co-culturing AML cell lines with MS-5 cells resulted in an almost 2-fold increase in acetate secretion. Co-cultures using primary AML patient samples led to the same result in three out of four metabolically active samples. Moreover, co-cultures of MS-5 cells and healthy donor samples did not result in higher levels of acetate, suggesting that only AML cells can yield this effect.

Furthermore, several evidences revealed that MS-5 cells were responsible for acetate secretion: (i) MS-5 cells cultured alone did secrete acetate, at a lower level than in co-culture, whilst AML cells did not, with the exception of a considerably small secretion by one of the AML cell lines (HL-60); (ii) MS-5 cells cultured separately after being in co-culture continued to secrete acetate at a similar rate as in co-culture whilst AML cells cultured separately presented similar or lower levels of acetate as in co-culture; and (iii) ^{13}C-glucose labelling showed that the acetate found in co-culture derives from glucose and MS-5 cells cultured alone were the only cells with the ability of secreting acetate derived from glucose.

The mechanism behind acetate secretion by MS-5 cells was found to involve an increase in glycolysis, which was characterised by the upregulation of most of the genes involved in the breakdown of glucose to pyruvate. Moreover, a block in the entry to the TCA cycle through pyruvate dehydrogenase leading to an accumulation of pyruvate was found and was attributed to a downregulation of the expression of PDH and an upregulation of the PDH inhibitors (PDKs) (Figure 6.1, square 1). This pyruvate accumulation was further evidenced using [1,2-^{13}C] glucose which revealed a preferential usage of the alternative entry to the TCA cycle through pyruvate carboxylase in co-culture (Figure 6.1, square 2), where PC-derived glutamate was only detected in MS-5 cells in co-culture. Additionally, acetate was proposed to be secreted to the extracellular medium by MS-5 cells through a monocarboxylate transporter (MCT4)

(Figure 6.1, square 3), as the expression of *MCT4* in MS-5 cells in co-culture was found to be strongly upregulated according to RNA sequencing.

The increase in glycolysis and pyruvate accumulation in MS-5 cells was proposed to be, at least partially, a result of an increase in VEGF in MS-5 cells, as the expression of VEGF in MS-5 was found to be upregulated in co-culture. Moreover, upregulation of glycolysis by VEGF was reported to be caused by an upregulation of PFKFB [237] (Figure 6.1, square 4), which was also found to be upregulated in MS-5 cells. The increase in VEGF was proposed to be caused by either direct or exosome transfer from AML cells (Figure 6.1, squares 5 and 6, respectively) or by an upregulation by HIF-1α linked to mTOR activation (Figure 6.1, square 7). One of the limitations of this study is that VEGF was not blocked to prove its role in the enhancement of glycolysis and the mechanism behind the upregulation of VEGF was not elucidated.

As PDH was found to be downregulated and blocked by the PDKs, the preferential mechanism of acetate production in MS-5 cells was hypothesised to involve the non-enzymatical decarboxylation of pyruvate into acetate mediated by reactive oxygen species (Figure 6.1, square 8). In support of this hypothesis, transcriptomic data revealed that the ROS signalling pathway was part of the top upregulated pathways in MS-5 cells in co-culture compared to cultured alone. The role of ROS in acetate secretion was corroborated by a detected increase in ROS levels in MS-5 cells in co-culture compared to MS-5 cells cultured alone. Moreover, increasing the levels of ROS, by the addition of H_2O_2, led to an increase in acetate secretion; and decreasing ROS levels by using a ROS scavenger (NAC) decreased the level of acetate secretion in co-culture, recovering the level of acetate secretion of MS-5 cells cultured alone.

The proposed mechanism for the increase in ROS in MS-5 cells involved ROS transfer from AML to stromal cells via gap junction (Figure 6.1, square 5), as the expression of several gap

junction genes was found to be upregulated in both SKM-1 and MS-5 cells. Moreover, acetate secretion was found to be contact dependent, which tallies with the need to establish a gap junction connexion for ROS transfer. However, another limitation of this study is that experiments disrupting the possible gap junctions were not performed.

Furthermore, transcriptomic data of SKM-1 cells in co-culture revealed that SKM-1 cells did not present an altered metabolism to optimally use acetate as: (i) the import of acetate through the monocarboxylate transporters was not found to be majorly upregulated; (ii) the activation of acetate by the conversion to acetyl-CoA, catalysed by ACSS1 and ACSS2, remained unaltered; and (iii) no further pathways related to the metabolism of acetate and acetyl-CoA, such as the TCA, fatty acid synthesis and histone acetylation, were found to be upregulated.

Nonetheless, SKM-1 cells cultured alone were found to consume acetate at both physiological and co-culture acetate concentrations. Moreover, labelling studies using [2-^{13}C] acetate revealed that SKM-1 consumed acetate and used it to flux the TCA cycle (Figure 6.1, square 9). In contrast, MS-5 cells did not metabolise acetate, although they were capable to import it. However, the addition of [2-^{13}C] acetate to co-cultures of SKM-1 and MS-5 cells revealed that only SKM-1 were importing and metabolising acetate in co-culture.

Additionally, to block acetate usage in AML cells a partial ACSS2 knock-out cell line was generated. Tracer studies using [2-^{13}C] acetate in cells with the partial ACSS2 KO resulted in lower label incorporations in by-products of acetate metabolism whilst acetate import remained unaltered. Moreover, co-culturing the partial ACSS2 KO cells with MS-5 cells resulted in slightly higher levels of extracellular acetate compared to co-culturing control cells. This result indicated that partial KO cells used less acetate in co-culture, supporting the previous findings

showing that AML cells import and use the acetate secreted by MS-5 cells in co-culture and highlighting that acetate is part of a metabolic crosstalk between AML and stromal cells.

6.2. Implications of research findings

In this thesis, a metabolic crosstalk between AML and stromal cells has been characterised in cell lines and primary AML patient samples. These findings will undoubtedly contribute to a better understanding on how AML cells remodel other cell types present in their microenvironment. It is important to remark that, even though increased acetate secretion could be specific for MS-5 cells, the signalling that AML cells establish with MS-5 cells, such as ROS or VEGF transfer, could also occur similarly with other stromal cell types yielding different metabolic results. The specific metabolic changes that AML cells promote in the surrounding cells could thus potentially serve as the basis for the development of new therapies. For instance, by disrupting gap junctions, using of ROS scavengers, blocking VEGF transfer or impeding acetate activation.

Another interesting point is that increased acetate secretion was found in all the cell lines tested and most of the primary AML samples used, indicating that the AML signals that reprogram the metabolism of stromal cells could occur independently of the AML subtype. Hence, therapies aiming at targeting any of the mechanisms that lead to acetate secretion could potentially be used to treat many different types of AML patients, which would mean that the treatment would not be as personalised as other treatments that target specific genetic vulnerabilities, and would also be much more cost-effective.

6.3. Further questions and future perspectives

Although the mechanism behind the metabolic interaction between AML and stromal cells has been almost completely elucidated and most of the aims of this project have been accomplished, several questions remain unanswered.

First, some of the proposed mechanisms behind the metabolic reprogramming of MS-5 cells by AML cells could be further investigated. For instance, ROS transfer mediated by gap junction could be corroborated by characterising the ROS levels of AML cells before and after co-culture. Moreover, inhibiting ROS transfer by using a gap junction disruptor could further confirm the whole mechanism and show therapeutic potential. Similarly, VEGF transfer could be inhibited using an anti-VEGF monoclonal antibody to determine its contribution to the glycolytic rate increase.

It could be also interesting to investigate whether the metabolic interactions between AML and stromal cells characterised in this thesis could play a role in chemo resistance. For instance, by inhibiting contact or ROS transfer and/or adding acetate whilst using a chemotherapeutic agent in AML cells cultured alone or in co-culture. These experiments could clarify whether ROS transfer or acetate consumption are crucial for AML survival.

Furthermore, an expansion of this work into using more patient-derived material could bring more insight on how this mechanism translates to *ex vivo* models. For instance, more primary AML cells including different types of AML (e.g. M0 to M7 in the FAB classification) could clarify whether AML status, cytogenetics or specific mutations play a role in the AML-stromal acetate interaction. Additionally, using primary MSCs to perform co-cultures could also answer whether primary stromal cells can be reprogrammed in a similar manner as MS-5 cells in co-culture.

Another possible diversion of this study would be to characterise whether aspartate could be another type of metabolic interaction between AML and stromal cells. As presented in chapter 3, stromal cells were found to secrete aspartate whilst AML cells were consuming it and, thus, a potential crosstalk through aspartate was hypothesised. Although transcriptomic data did not reveal any alterations in pathways related to aspartate or asparagine metabolism in neither stromal nor AML cells, other types of experiments could be performed to further investigate this potential interaction, such as aspartate/asparagine depletions or blocking key enzymes in aspartate metabolism e.g. asparagine synthetase or asparaginase.

Finally, it would also be interesting to extend this work by performing co-cultures adding other niche cell types and define whether metabolism is reprogrammed in these other cell types and if so, whether the metabolic changes that are occurring between AML and these other niche cells affect similar pathways or new ones. The culmination of these studies would be the characterisation of these metabolic changes using 3D co-cultures to spatially mimic the bone marrow microenvironment.

6.4. Conclusion

Overall, this thesis provides evidence of a novel type of communication between AML and stromal cells. The main findings include the complete reprogramming of the metabolism of stromal cells into secreting acetate and the consumption of the secreted acetate by AML cells. Moreover, several mechanisms on how this metabolic rewiring occurs in stromal cells are proposed. This study highlights the importance of understanding how AML cells can modulate and alter niche cells to their own advantage. The mechanisms behind the different types of crosstalk between AML and niche cells are starting to be exploited for the development of new therapies. Therefore, I believe this data not only provides a better understanding on how AML cells communicate with stromal cells but could also serve as a basis to develop novel treatments for AML.

7. References

1. Till, J.E. and C.E. Mc, *A direct measurement of the radiation sensitivity of normal mouse bone marrow cells.* Radiat Res, 1961. **14**: p. 213-22.

2. Morrison, S.J. and I.L. Weissman, *The long-term repopulating subset of hematopoietic stem cells is deterministic and isolatable by phenotype.* Immunity, 1994. **1**(8): p. 661-73.

3. Yang, L., et al., *Identification of Lin(-)Sca1(+)kit(+)CD34(+)Flt3- short-term hematopoietic stem cells capable of rapidly reconstituting and rescuing myeloablated transplant recipients.* Blood, 2005. **105**(7): p. 2717-23.

4. Akashi, K., et al., *A clonogenic common myeloid progenitor that gives rise to all myeloid lineages.* Nature, 2000. **404**(6774): p. 193-7.

5. Kondo, M., I.L. Weissman, and K. Akashi, *Identification of clonogenic common lymphoid progenitors in mouse bone marrow.* Cell, 1997. **91**(5): p. 661-72.

6. Zhu, J. and S.G. Emerson, *Hematopoietic cytokines, transcription factors and lineage commitment.* Oncogene, 2002. **21**(21): p. 3295-313.

7. Laurenti, E. and B. Gottgens, *From haematopoietic stem cells to complex differentiation landscapes.* Nature, 2018. **553**(7689): p. 418-426.

8. Cheng, H., Z. Zheng, and T. Cheng, *New paradigms on hematopoietic stem cell differentiation.* Protein Cell, 2020. **11**(1): p. 34-44.

9. Yamamoto, R., et al., *Clonal analysis unveils self-renewing lineage-restricted progenitors generated directly from hematopoietic stem cells.* Cell, 2013. **154**(5): p. 1112-1126.

10. Cheshier, S.H., et al., *In vivo proliferation and cell cycle kinetics of long-term self-renewing hematopoietic stem cells.* Proc Natl Acad Sci U S A, 1999. **96**(6): p. 3120-5.

11. Boulais, P.E. and P.S. Frenette, *Making sense of hematopoietic stem cell niches.* Blood, 2015. **125**(17): p. 2621-9.

12. Kumar, S. and H. Geiger, *HSC Niche Biology and HSC Expansion Ex Vivo.* Trends Mol Med, 2017. **23**(9): p. 799-819.

13. Estey, E. and H. Dohner, *Acute myeloid leukaemia.* Lancet, 2006. **368**(9550): p. 1894-907.

14. Lindsley, R.C., et al., *Acute myeloid leukemia ontogeny is defined by distinct somatic mutations.* Blood, 2015. **125**(9): p. 1367-76.

15. Bennett, J.M., et al., *Proposals for the classification of the acute leukaemias. French-American-British (FAB) co-operative group.* Br J Haematol, 1976. **33**(4): p. 451-8.

16. Arber, D.A., et al., *The 2016 revision to the World Health Organization classification of myeloid neoplasms and acute leukemia.* Blood, 2016. **127**(20): p. 2391-405.

17. Kelly, L.M. and D.G. Gilliland, *Genetics of myeloid leukemias.* Annu Rev Genomics Hum Genet, 2002. **3**: p. 179-98.

18. Byrd, J.C., et al., *Pretreatment cytogenetic abnormalities are predictive of induction success, cumulative incidence of relapse, and overall survival in adult patients with de novo acute myeloid leukemia: results from Cancer and Leukemia Group B (CALGB 8461).* Blood, 2002. **100**(13): p. 4325-36.

19. Kumar, C.C., *Genetic abnormalities and challenges in the treatment of acute myeloid leukemia.* Genes Cancer, 2011. **2**(2): p. 95-107.

20. Saultz, J.N. and R. Garzon, *Acute Myeloid Leukemia: A Concise Review.* J Clin Med, 2016. **5**(3).

21. Dohner, H., D.J. Weisdorf, and C.D. Bloomfield, *Acute Myeloid Leukemia.* N Engl J Med, 2015. **373**(12): p. 1136-52.

22. Naeim, F., *Atlas of hematopathology : morphology, immunophenotype, cytogenetics, and molecular approaches.* 2018.

23. Grove, C.S. and G.S. Vassiliou, *Acute myeloid leukaemia: a paradigm for the clonal evolution of cancer?* Dis Model Mech, 2014. **7**(8): p. 941-51.

24. Lapidot, T., et al., *A cell initiating human acute myeloid leukaemia after transplantation into SCID mice.* Nature, 1994. **367**(6464): p. 645-8.

25. Bonnet, D. and J.E. Dick, *Human acute myeloid leukemia is organized as a hierarchy that originates from a primitive hematopoietic cell.* Nat Med, 1997. **3**(7): p. 730-7.

26. Dick, J.E., *Acute myeloid leukemia stem cells.* Ann N Y Acad Sci, 2005. **1044**: p. 1-5.

27. Jordan, C.T., *The leukemic stem cell.* Best practice & research. Clinical haematology, 2007. **20**(1): p. 13-18.

28. Vu, L.P. and M.G. Kharas, *Targeting the Residual Leukemia Cells after Chemotherapy.* Cancer Cell, 2018. **34**(3): p. 353-355.

29. Lichtman, M.A., *A historical perspective on the development of the cytarabine (7days) and daunorubicin (3days) treatment regimen for acute myelogenous leukemia: 2013 the 40th anniversary of 7+3.* Blood Cells Mol Dis, 2013. **50**(2): p. 119-30.

30. Graf, N., P. Riesinger, and H. Reinhard, *Retinoids in the treatment of acute promyelocytic leukemia. Review of the literature.* Klin Padiatr, 1995. **207**(2): p. 43-7.

31. Bross, P.F., et al., *Approval summary: gemtuzumab ozogamicin in relapsed acute myeloid leukemia.* Clin Cancer Res, 2001. **7**(6): p. 1490-6.

32. Jen, E.Y., et al., *FDA Approval: Gemtuzumab Ozogamicin for the Treatment of Adults with Newly Diagnosed CD33-Positive Acute Myeloid Leukemia.* Clin Cancer Res, 2018. **24**(14): p. 3242-3246.

33. Lai, C., K. Doucette, and K. Norsworthy, *Recent drug approvals for acute myeloid leukemia.* J Hematol Oncol, 2019. **12**(1): p. 100.

34. DeBerardinis, R.J. and N.S. Chandel, *Fundamentals of cancer metabolism.* Sci Adv, 2016. **2**(5): p. e1600200.

35. Farber, S. and L.K. Diamond, *Temporary remissions in acute leukemia in children produced by folic acid antagonist, 4-aminopteroyl-glutamic acid.* N Engl J Med, 1948. **238**(23): p. 787-93.

36. Warburg, O., F. Wind, and E. Negelein, *THE METABOLISM OF TUMORS IN THE BODY.* J Gen Physiol, 1927. **8**(6): p. 519-30.

37. Vander Heiden, M.G., L.C. Cantley, and C.B. Thompson, *Understanding the Warburg effect: the metabolic requirements of cell proliferation.* Science, 2009. **324**(5930): p. 1029-33.

38. Herst, P.M., et al., *The level of glycolytic metabolism in acute myeloid leukemia blasts at diagnosis is prognostic for clinical outcome.* J Leukoc Biol, 2011. **89**(1): p. 51-5.

39. Chen, W.L., et al., *A distinct glucose metabolism signature of acute myeloid leukemia with prognostic value.* Blood, 2014. **124**(10): p. 1645-54.

40. Wang, Y.H., et al., *Cell-state-specific metabolic dependency in hematopoiesis and leukemogenesis.* Cell, 2014. **158**(6): p. 1309-1323.

41. Ju, H.Q., et al., *ITD mutation in FLT3 tyrosine kinase promotes Warburg effect and renders therapeutic sensitivity to glycolytic inhibition.* Leukemia, 2017. **31**(10): p. 2143-2150.

42. Poulain, L., et al., *High mTORC1 activity drives glycolysis addiction and sensitivity to G6PD inhibition in acute myeloid leukemia cells.* Leukemia, 2017. **31**(11): p. 2326-2335.

43. Chen, W.L., et al., *Enhanced Fructose Utilization Mediated by SLC2A5 Is a Unique Metabolic Feature of Acute Myeloid Leukemia with Therapeutic Potential.* Cancer Cell, 2016. **30**(5): p. 779-791.

44. DeBerardinis, R.J., et al., *Beyond aerobic glycolysis: Transformed cells can engage in glutamine metabolism that exceeds the requirement for protein and nucleotide synthesis.* 2007. **104**(49): p. 19345-19350.

45. Willems, L., et al., *Inhibiting glutamine uptake represents an attractive new strategy for treating acute myeloid leukemia.* Blood, 2013. **122**(20): p. 3521-32.

46. Gallipoli, P., et al., *Glutaminolysis is a metabolic dependency in FLT3(ITD) acute myeloid leukemia unmasked by FLT3 tyrosine kinase inhibition.* Blood, 2018. **131**(15): p. 1639-1653.

47. Jacque, N., et al., *Targeting glutaminolysis has antileukemic activity in acute myeloid leukemia and synergizes with BCL-2 inhibition.* Blood, 2015. **126**(11): p. 1346-56.

48. Samudio, I., et al., *Pharmacologic inhibition of fatty acid oxidation sensitizes human leukemia cells to apoptosis induction.* J Clin Invest, 2010. **120**(1): p. 142-56.

49. Tabe, Y., et al., *Bone Marrow Adipocytes Facilitate Fatty Acid Oxidation Activating AMPK and a Transcriptional Network Supporting Survival of Acute Monocytic Leukemia Cells.* Cancer Res, 2017. **77**(6): p. 1453-1464.

50. Farge, T., et al., *Chemotherapy-Resistant Human Acute Myeloid Leukemia Cells Are Not Enriched for Leukemic Stem Cells but Require Oxidative Metabolism.* Cancer Discov, 2017. **7**(7): p. 716-735.

51. Pizer, E.S., et al., *Fatty acid synthase (FAS): a target for cytotoxic antimetabolites in HL60 promyelocytic leukemia cells.* Cancer Res, 1996. **56**(4): p. 745-51.

52. Southam, A.D., et al., *Drug Redeployment to Kill Leukemia and Lymphoma Cells by Disrupting SCD1-Mediated Synthesis of Monounsaturated Fatty Acids.* 2015. **75**(12): p. 2530-2540.

53. Baccelli, I., et al., *Mubritinib Targets the Electron Transport Chain Complex I and Reveals the Landscape of OXPHOS Dependency in Acute Myeloid Leukemia.* Cancer Cell, 2019. **36**(1): p. 84-99.e8.

54. Yucel, B. and M. Sonmez, *Repression of oxidative phosphorylation sensitizes leukemia cell lines to cytarabine.* Hematology, 2018. **23**(6): p. 330-336.

55. Pollyea, D.A., et al., *Venetoclax with azacitidine disrupts energy metabolism and targets leukemia stem cells in patients with acute myeloid leukemia.* Nat Med, 2018. **24**(12): p. 1859-1866.

56. Mussai, F., et al., *Arginine dependence of acute myeloid leukemia blast proliferation: a novel therapeutic target.* Blood, 2015. **125**(15): p. 2386-96.

57. Miraki-Moud, F., et al., *Arginine deprivation using pegylated arginine deiminase has activity against primary acute myeloid leukemia cells in vivo.* Blood, 2015. **125**(26): p. 4060-8.

58. Raffel, S., et al., *BCAT1 restricts αKG levels in AML stem cells leading to IDHmut-like DNA hypermethylation.* Nature, 2017. **551**(7680): p. 384-388.

59. Keenan, M.M. and J.T. Chi, *Alternative fuels for cancer cells.* Cancer J, 2015. **21**(2): p. 49-55.

60. Shafat, M.S., et al., *Leukemic blasts program bone marrow adipocytes to generate a protumoral microenvironment.* Blood, 2017. **129**(10): p. 1320-1332.

61. Marlein, C.R., et al., *NADPH oxidase-2 derived superoxide drives mitochondrial transfer from bone marrow stromal cells to leukemic blasts.* Blood, 2017. **130**(14): p. 1649-1660.

62. Moschoi, R., et al., *Protective mitochondrial transfer from bone marrow stromal cells to acute myeloid leukemic cells during chemotherapy.* Blood, 2016. **128**(2): p. 253-64.

63. Stuani, L., M. Sabatier, and J.E. Sarry, *Exploiting metabolic vulnerabilities for personalized therapy in acute myeloid leukemia.* BMC Biol, 2019. **17**(1): p. 57.

64. Pinho, S. and P.S. Frenette, *Haematopoietic stem cell activity and interactions with the niche.* Nat Rev Mol Cell Biol, 2019. **20**(5): p. 303-320.

65. Mendez-Ferrer, S., et al., *Bone marrow niches in haematological malignancies.* Nat Rev Cancer, 2020. **20**(5): p. 285-298.

66. Schofield, R., *The relationship between the spleen colony-forming cell and the haemopoietic stem cell.* Blood Cells, 1978. **4**(1-2): p. 7-25.

67. Kiel, M.J., et al., *SLAM family receptors distinguish hematopoietic stem and progenitor cells and reveal endothelial niches for stem cells.* Cell, 2005. **121**(7): p. 1109-21.

68. Calvi, L.M., et al., *Osteoblastic cells regulate the haematopoietic stem cell niche.* Nature, 2003. **425**(6960): p. 841-6.

69. Acar, M., et al., *Deep imaging of bone marrow shows non-dividing stem cells are mainly perisinusoidal.* Nature, 2015. **526**(7571): p. 126-30.

70. Kusumbe, A.P., S.K. Ramasamy, and R.H. Adams, *Coupling of angiogenesis and osteogenesis by a specific vessel subtype in bone.* Nature, 2014. **507**(7492): p. 323-328.

71. Zhao, M., et al., *N-Cadherin-Expressing Bone and Marrow Stromal Progenitor Cells Maintain Reserve Hematopoietic Stem Cells.* Cell Rep, 2019. **26**(3): p. 652-669 e6.

72. Mendez-Ferrer, S., et al., *Haematopoietic stem cell release is regulated by circadian oscillations.* Nature, 2008. **452**(7186): p. 442-7.

73. Sugiyama, T., et al., *Maintenance of the hematopoietic stem cell pool by CXCL12-CXCR4 chemokine signaling in bone marrow stromal cell niches.* Immunity, 2006. **25**(6): p. 977-88.

74. Taichman, R.S. and S.G. Emerson, *Human osteoblasts support hematopoiesis through the production of granulocyte colony-stimulating factor.* J Exp Med, 1994. **179**(5): p. 1677-82.

75. Nakamura-Ishizu, A., et al., *Megakaryocytes are essential for HSC quiescence through the production of thrombopoietin.* Biochem Biophys Res Commun, 2014. **454**(2): p. 353-7.

76. Bruns, I., et al., *Megakaryocytes regulate hematopoietic stem cell quiescence through CXCL4 secretion.* Nat Med, 2014. **20**(11): p. 1315-20.

77. Ho, Y.H., et al., *Remodeling of Bone Marrow Hematopoietic Stem Cell Niches Promotes Myeloid Cell Expansion during Premature or Physiological Aging.* Cell Stem Cell, 2019. **25**(3): p. 407-418 e6.

78. Ogawa, M., et al., *Expression and function of c-kit in hemopoietic progenitor cells.* J Exp Med, 1991. **174**(1): p. 63-71.

79. Ding, L., et al., *Endothelial and perivascular cells maintain haematopoietic stem cells.* Nature, 2012. **481**(7382): p. 457-62.

80. Nilsson, S.K., et al., *Osteopontin, a key component of the hematopoietic stem cell niche and regulator of primitive hematopoietic progenitor cells.* Blood, 2005. **106**(4): p. 1232-9.

81. Yoshihara, H., et al., *Thrombopoietin/MPL signaling regulates hematopoietic stem cell quiescence and interaction with the osteoblastic niche.* Cell Stem Cell, 2007. **1**(6): p. 685-97.

82. Arai, F., et al., *Tie2/angiopoietin-1 signaling regulates hematopoietic stem cell quiescence in the bone marrow niche.* Cell, 2004. **118**(2): p. 149-61.

83. Zhou, B.O., L. Ding, and S.J. Morrison, *Hematopoietic stem and progenitor cells regulate the regeneration of their niche by secreting Angiopoietin-1.* Elife, 2015. **4**: p. e05521.

84. Mendez-Ferrer, S., et al., *Mesenchymal and haematopoietic stem cells form a unique bone marrow niche.* Nature, 2010. **466**(7308): p. 829-34.

85. Mendez-Ferrer, S. and P.S. Frenette, *Hematopoietic stem cell trafficking: regulated adhesion and attraction to bone marrow microenvironment.* Ann N Y Acad Sci, 2007. **1116**: p. 392-413.

86. Yokota, T., et al., *Adiponectin, a new member of the family of soluble defense collagens, negatively regulates the growth of myelomonocytic progenitors and the functions of macrophages.* Blood, 2000. **96**(5): p. 1723-32.

87. Naveiras, O., et al., *Bone-marrow adipocytes as negative regulators of the haematopoietic microenvironment.* Nature, 2009. **460**(7252): p. 259-63.

88. Zhu, R.J., et al., *Hematopoietic recovery following chemotherapy is improved by BADGE-induced inhibition of adipogenesis.* Int J Hematol, 2013. **97**(1): p. 58-72.

89. Greenbaum, A., et al., *CXCL12 in early mesenchymal progenitors is required for haematopoietic stem-cell maintenance.* Nature, 2013. **495**(7440): p. 227-30.

90. Butler, J.M., et al., *Endothelial cells are essential for the self-renewal and repopulation of Notch-dependent hematopoietic stem cells.* Cell Stem Cell, 2010. **6**(3): p. 251-64.

91. Himburg, H.A., et al., *Distinct Bone Marrow Sources of Pleiotrophin Control Hematopoietic Stem Cell Maintenance and Regeneration.* Cell Stem Cell, 2018. **23**(3): p. 370-381 e5.

92. Winkler, I.G., et al., *Vascular niche E-selectin regulates hematopoietic stem cell dormancy, self renewal and chemoresistance.* Nat Med, 2012. **18**(11): p. 1651-7.

93. Méndez-Ferrer, S., et al., *Haematopoietic stem cell release is regulated by circadian oscillations.* Nature, 2008. **452**(7186): p. 442-7.

94. Katayama, Y., et al., *Signals from the sympathetic nervous system regulate hematopoietic stem cell egress from bone marrow.* Cell, 2006. **124**(2): p. 407-21.

95. Lucas, D., et al., *Chemotherapy-induced bone marrow nerve injury impairs hematopoietic regeneration.* Nat Med, 2013. **19**(6): p. 695-703.

96. Yamazaki, S., et al., *Nonmyelinating Schwann cells maintain hematopoietic stem cell hibernation in the bone marrow niche.* Cell, 2011. **147**(5): p. 1146-58.

97. Winkler, I.G., et al., *Bone marrow macrophages maintain hematopoietic stem cell (HSC) niches and their depletion mobilizes HSCs.* Blood, 2010. **116**(23): p. 4815-28.

98. Hirata, Y., et al., *CD150(high) Bone Marrow Tregs Maintain Hematopoietic Stem Cell Quiescence and Immune Privilege via Adenosine.* Cell Stem Cell, 2018. **22**(3): p. 445-453 e5.

99. Decker, M., et al., *Hepatic thrombopoietin is required for bone marrow hematopoietic stem cell maintenance.* Science, 2018. **360**(6384): p. 106-110.

100. Rupec, R.A., et al., *Stroma-mediated dysregulation of myelopoiesis in mice lacking I kappa B alpha.* Immunity, 2005. **22**(4): p. 479-91.

101. Raaijmakers, M.H., et al., *Bone progenitor dysfunction induces myelodysplasia and secondary leukaemia*. Nature, 2010. **464**(7290): p. 852-7.

102. Kode, A., et al., *Leukaemogenesis induced by an activating beta-catenin mutation in osteoblasts.* Nature, 2014. **506**(7487): p. 240-4.

103. Sala-Torra, O., et al., *Evidence of donor-derived hematologic malignancies after hematopoietic stem cell transplantation.* Biol Blood Marrow Transplant, 2006. **12**(5): p. 511-7.

104. Schepers, K., T.B. Campbell, and E. Passegue, *Normal and leukemic stem cell niches: insights and therapeutic opportunities.* Cell Stem Cell, 2015. **16**(3): p. 254-67.

105. Wang, B., et al., *Exosomes derived from acute myeloid leukemia cells promote chemoresistance by enhancing glycolysis-mediated vascular remodeling.* J Cell Physiol, 2019. **234**(7): p. 10602-10614.

106. Ramadan, S.M., et al., *Acute myeloid leukemia developing in patients with autoimmune diseases.* Haematologica, 2012. **97**(6): p. 805-17.

107. Kristinsson, S.Y., et al., *Chronic immune stimulation might act as a trigger for the development of acute myeloid leukemia or myelodysplastic syndromes.* J Clin Oncol, 2011. **29**(21): p. 2897-903.

108. Flores-Figueroa, E., et al., *Functional analysis of myelodysplastic syndromes-derived mesenchymal stem cells.* Leuk Res, 2008. **32**(9): p. 1407-16.

109. Flores-Figueroa, E., et al., *In vitro characterization of hematopoietic microenvironment cells from patients with myelodysplastic syndrome.* Leuk Res, 2002. **26**(7): p. 677-86.

110. Welner, R.S., et al., *Treatment of chronic myelogenous leukemia by blocking cytokine alterations found in normal stem and progenitor cells.* Cancer Cell, 2015. **27**(5): p. 671-81.

111. Reynaud, D., et al., *IL-6 controls leukemic multipotent progenitor cell fate and contributes to chronic myelogenous leukemia development.* Cancer Cell, 2011. **20**(5): p. 661-73.

112. Arranz, L., et al., *Neuropathy of haematopoietic stem cell niche is essential for myeloproliferative neoplasms.* Nature, 2014. **512**(7512): p. 78-81.

113. Carmeliet, P. and R.K. Jain, *Molecular mechanisms and clinical applications of angiogenesis.* Nature, 2011. **473**(7347): p. 298-307.

114. Dias, S., et al., *Inhibition of both paracrine and autocrine VEGF/ VEGFR-2 signaling pathways is essential to induce long-term remission of xenotransplanted human leukemias.* Proc Natl Acad Sci U S A, 2001. **98**(19): p. 10857-62.

115. Hussong, J.W., G.M. Rodgers, and P.J. Shami, *Evidence of increased angiogenesis in patients with acute myeloid leukemia.* Blood, 2000. **95**(1): p. 309-13.

116. Weidenaar, A.C., et al., *High acute myeloid leukemia derived VEGFA levels are associated with a specific vascular morphology in the leukemic bone marrow.* Cell Oncol (Dordr), 2011. **34**(4): p. 289-96.

117. Schmidt, T., et al., *Loss or inhibition of stromal-derived PlGF prolongs survival of mice with imatinib-resistant Bcr-Abl1(+) leukemia.* Cancer Cell, 2011. **19**(6): p. 740-53.

118. Passaro, D., et al., *Increased Vascular Permeability in the Bone Marrow Microenvironment Contributes to Disease Progression and Drug Response in Acute Myeloid Leukemia.* Cancer Cell, 2017. **32**(3): p. 324-341 e6.

119. Duarte, D., et al., *Inhibition of Endosteal Vascular Niche Remodeling Rescues Hematopoietic Stem Cell Loss in AML.* Cell Stem Cell, 2018. **22**(1): p. 64-77 e6.

120. Xia, B., et al., *c-Myc plays part in drug resistance mediated by bone marrow stromal cells in acute myeloid leukemia.* Leuk Res, 2015. **39**(1): p. 92-9.

121. Garrido, S.M., et al., *Acute myeloid leukemia cells are protected from spontaneous and drug-induced apoptosis by direct contact with a human bone marrow stromal cell line (HS-5).* Exp Hematol, 2001. **29**(4): p. 448-57.

122. Schelker, R.C., et al., *TGF-β1 and CXCL12 modulate proliferation and chemotherapy sensitivity of acute myeloid leukemia cells co-cultured with multipotent mesenchymal stromal cells.* Hematology, 2018. **23**(6): p. 337-345.

123. Kouzi, F., et al., *Disruption of gap junctions attenuates acute myeloid leukemia chemoresistance induced by bone marrow mesenchymal stromal cells.* Oncogene, 2020. **39**(6): p. 1198-1212.

124. Azadniv, M., et al., *Bone marrow mesenchymal stromal cells from acute myelogenous leukemia patients demonstrate adipogenic differentiation propensity with implications for leukemia cell support.* Leukemia, 2020. **34**(2): p. 391-403.

125. Geyh, S., et al., *Functional inhibition of mesenchymal stromal cells in acute myeloid leukemia.* Leukemia, 2016. **30**(3): p. 683-91.

126. Zeng, Z., et al., *Targeting the leukemia microenvironment by CXCR4 inhibition overcomes resistance to kinase inhibitors and chemotherapy in AML.* Blood, 2009. **113**(24): p. 6215-24.

127. Zeng, Z., et al., *Inhibition of CXCR4 with the novel RCP168 peptide overcomes stroma-mediated chemoresistance in chronic and acute leukemias.* Mol Cancer Ther, 2006. **5**(12): p. 3113-21.

128. Krevvata, M., et al., *Inhibition of leukemia cell engraftment and disease progression in mice by osteoblasts.* Blood, 2014. **124**(18): p. 2834-46.

129. Baryawno, N., et al., *A Cellular Taxonomy of the Bone Marrow Stroma in Homeostasis and Leukemia.* Cell, 2019. **177**(7): p. 1915-1932 e16.

130. Hawkins, E.D., et al., *T-cell acute leukaemia exhibits dynamic interactions with bone marrow microenvironments.* Nature, 2016. **538**(7626): p. 518-522.

131. Kumar, B., et al., *Acute myeloid leukemia transforms the bone marrow niche into a leukemia-permissive microenvironment through exosome secretion.* Leukemia, 2018. **32**(3): p. 575-587.

132. Hanoun, M., et al., *Acute myelogenous leukemia-induced sympathetic neuropathy promotes malignancy in an altered hematopoietic stem cell niche.* Cell Stem Cell, 2014. **15**(3): p. 365-375.

133. Isidori, A., et al., *The role of the immunosuppressive microenvironment in acute myeloid leukemia development and treatment.* Expert Rev Hematol, 2014. **7**(6): p. 807-18.

134. Zhang, L., T.F. Gajewski, and J. Kline, *PD-1/PD-L1 interactions inhibit antitumor immune responses in a murine acute myeloid leukemia model.* Blood, 2009. **114**(8): p. 1545-52.

135. Calcinotto, A., et al., *Modulation of microenvironment acidity reverses anergy in human and murine tumor-infiltrating T lymphocytes.* Cancer Res, 2012. **72**(11): p. 2746-56.

136. Mougiakakos, D., *The Induction of a Permissive Environment to Promote T Cell Immune Evasion in Acute Myeloid Leukemia: The Metabolic Perspective.* Front Oncol, 2019. **9**: p. 1166.

137. Lyssiotis, C.A. and A.C. Kimmelman, *Metabolic Interactions in the Tumor Microenvironment.* Trends Cell Biol, 2017. **27**(11): p. 863-875.

138. Sousa, C.M., et al., *Pancreatic stellate cells support tumour metabolism through autophagic alanine secretion.* Nature, 2016. **536**(7617): p. 479-83.

139. Ye, H., et al., *Leukemic Stem Cells Evade Chemotherapy by Metabolic Adaptation to an Adipose Tissue Niche.* Cell Stem Cell, 2016. **19**(1): p. 23-37.

140. Zhang, W., et al., *Stromal control of cystine metabolism promotes cancer cell survival in chronic lymphocytic leukaemia.* Nat Cell Biol, 2012. **14**(3): p. 276-86.

141. Boutter, J., et al., *Image-based RNA interference screening reveals an individual dependence of acute lymphoblastic leukemia on stromal cysteine support.* Oncotarget, 2014. **5**(22): p. 11501-12.

142. Saito, Y., et al., *Induction of cell cycle entry eliminates human leukemia stem cells in a mouse model of AML.* Nat Biotechnol, 2010. **28**(3): p. 275-80.

143. Uy, G.L., et al., *A phase 1/2 study of chemosensitization with the CXCR4 antagonist plerixafor in relapsed or refractory acute myeloid leukemia.* Blood, 2012. **119**(17): p. 3917-24.

144. Ghobrial, I.M., et al., *Phase I/II trial of the CXCR4 inhibitor plerixafor in combination with bortezomib as a chemosensitization strategy in relapsed/refractory multiple myeloma.* Am J Hematol, 2019. **94**(11): p. 1244-1253.

145. Abraham, M., et al., *The CXCR4 inhibitor BL-8040 induces the apoptosis of AML blasts by downregulating ERK, BCL-2, MCL-1 and cyclin-D1 via altered miR-15a/16-1 expression.* Leukemia, 2017. **31**(11): p. 2336-2346.

146. Dimitroff, C.J., et al., *CD44 is a major E-selectin ligand on human hematopoietic progenitor cells.* J Cell Biol, 2001. **153**(6): p. 1277-86.

147. Natoni, A., et al., *E-selectin ligands recognised by HECA452 induce drug resistance in myeloma, which is overcome by the E-selectin antagonist, GMI-1271.* Leukemia, 2017. **31**(12): p. 2642-2651.

148. Godavarthy, P.S., et al., *The vascular bone marrow niche influences outcome in chronic myeloid leukemia via the E-selectin - SCL/TAL1 - CD44 axis.* Haematologica, 2020. **105**(1): p. 136-147.

149. Jin, L., et al., *Targeting of CD44 eradicates human acute myeloid leukemic stem cells.* Nat Med, 2006. **12**(10): p. 1167-74.

150. Garcia, J., et al., *Bevacizumab (Avastin(R)) in cancer treatment: A review of 15 years of clinical experience and future outlook.* Cancer Treat Rev, 2020. **86**: p. 102017.

151. Karp, J.E., et al., *Targeting vascular endothelial growth factor for relapsed and refractory adult acute myelogenous leukemias: therapy with sequential 1-beta-d-arabinofuranosylcytosine, mitoxantrone, and bevacizumab.* Clin Cancer Res, 2004. **10**(11): p. 3577-85.

152. Zahiragic, L., et al., *Bevacizumab reduces VEGF expression in patients with relapsed and refractory acute myeloid leukemia without clinical antileukemic activity.* Leukemia, 2007. **21**(6): p. 1310-2.

153. Ossenkoppele, G.J., et al., *Addition of bevacizumab to chemotherapy in acute myeloid leukemia at older age: a randomized phase 2 trial of the Dutch-Belgian Cooperative Trial Group for Hemato-Oncology (HOVON) and the Swiss Group for Clinical Cancer Research (SAKK).* Blood, 2012. **120**(24): p. 4706-11.

154. Benito, J., et al., *Hypoxia-Activated Prodrug TH-302 Targets Hypoxic Bone Marrow Niches in Preclinical Leukemia Models.* Clin Cancer Res, 2016. **22**(7): p. 1687-98.

155. Konopleva, M., et al., *Phase I/II study of the hypoxia-activated prodrug PR104 in refractory/relapsed acute myeloid leukemia and acute lymphoblastic leukemia.* Haematologica, 2015. **100**(7): p. 927-34.

156. Badar, T., et al., *Phase I study of evofosfamide, an investigational hypoxia-activated prodrug, in patients with advanced leukemia.* 2016. **91**(8): p. 800-805.

157. Javidi-Sharifi, N., et al., *FGF2-FGFR1 signaling regulates release of Leukemia-Protective exosomes from bone marrow stromal cells.* Elife, 2019. **8**.

158. Saha, S., et al., *Effect of Ranolazine in Patients with Chest Pain and Normal Coronaries- A Hospital Based Study.* J Clin Diagn Res, 2017. **11**(4): p. Oc14-oc16.

159. Jang, C., L. Chen, and J.D. Rabinowitz, *Metabolomics and Isotope Tracing.* Cell, 2018. **173**(4): p. 822-837.

160. Marshall, D.D. and R. Powers, *Beyond the paradigm: Combining mass spectrometry and nuclear magnetic resonance for metabolomics.* Prog Nucl Magn Reson Spectrosc, 2017. **100**: p. 1-16.

161. Emwas, A.H., *The strengths and weaknesses of NMR spectroscopy and mass spectrometry with particular focus on metabolomics research.* Methods Mol Biol, 2015. **1277**: p. 161-93.

162. Graaf, R.A.d., *In vivo NMR spectroscopy : principles and techniques*. 2019.

163. Levitt, M.H., *Spin dynamics : basics of nuclear magnetic resonance*. 2005, Chichester: John Wiley & Sons.

164. Keeler, J., *Understanding NMR Spectroscopy.* 2013.

165. *Organic Structure Determination Using 2-D NMR Spectroscopy*. 2012: Elsevier.

166. Bruice, P.Y., *Organic chemistry*. 2017.

167. Kostidis, S., et al., *Quantitative NMR analysis of intra- and extracellular metabolism of mammalian cells: A tutorial.* Anal Chim Acta, 2017. **980**: p. 1-24.

168. Beckonert, O., et al., *Metabolic profiling, metabolomic and metabonomic procedures for NMR spectroscopy of urine, plasma, serum and tissue extracts.* Nat Protoc, 2007. **2**(11): p. 2692-703.

169. Haasnoot, C.A. and C.W. Hilbers, *Effective water resonance suppression in 1D- and 2D-FT-1H-NMR spectroscopy of biopolymers in aqueous solution.* Biopolymers, 1983. **22**(5): p. 1259-66.

170. Van, Q.N., et al., *Comparison of 1D and 2D NMR spectroscopy for metabolic profiling.* J Proteome Res, 2008. **7**(2): p. 630-9.

171. Kruk, J., et al., *NMR Techniques in Metabolomic Studies: A Quick Overview on Examples of Utilization.* Appl Magn Reson, 2017. **48**(1): p. 1-21.

172. Chong, M., et al., *Combined Analysis of NMR and MS Spectra (CANMS).* Angew Chem Int Ed Engl, 2017. **56**(15): p. 4140-4144.

173. Saborano, R., et al., *A framework for tracer-based metabolism in mammalian cells by NMR.* Sci Rep, 2019. **9**(1): p. 2520.

174. Smith, T.B., et al., *High-Speed Tracer Analysis of Metabolism (HS-TrAM).* Wellcome Open Res, 2018. **3**: p. 5.

175. Reed, M.A.C., et al., *Quantitative Isotopomer Rates in Real-Time Metabolism of Cells Determined by NMR Methods.* Chembiochem, 2019. **20**(17): p. 2207-2211.

176. Heikkinen, S. and I. Kilpelainen, *Gradient BIRDR: a method to select uncoupled magnetization.* J Magn Reson, 1999. **137**(1): p. 93-9.

177. Maher, E.A., et al., *Metabolism of [U-13 C]glucose in human brain tumors in vivo.* NMR Biomed, 2012. **25**(11): p. 1234-44.

178. Lane, A.N., et al., *Stable isotope-resolved metabolomics (SIRM) in cancer research with clinical application to nonsmall cell lung cancer.* OMICS, 2011. **15**(3): p. 173-82.

179. Lee, J.H., Y. Okuno, and S. Cavagnero, *Sensitivity enhancement in solution NMR: emerging ideas and new frontiers.* J Magn Reson, 2014. **241**: p. 18-31.

180. Dixon, W.T., *The relation of signal/noise to magnetic field strength and sample size in magic-angle-spinning solid experiments.* J Magn Reson, 1984. **57**(2): p. 289-293.

181. Topgaard, D., et al., *"Shim pulses" for NMR spectroscopy and imaging.* Proc Natl Acad Sci U S A, 2004. **101**(51): p. 17576-81.

182. Wen, H., et al., *Glucose-derived acetate and ACSS2 as key players in cisplatin resistance in bladder cancer.* Biochim Biophys Acta Mol Cell Biol Lipids, 2019. **1864**(3): p. 413-421.

183. Mews, P., et al., *Acetyl-CoA synthetase regulates histone acetylation and hippocampal memory.* Nature, 2017. **546**(7658): p. 381-386.

184. Ludwig, C. and U.L. Gunther, *MetaboLab--advanced NMR data processing and analysis for metabolomics.* BMC Bioinformatics, 2011. **12**: p. 366.

185. Hyberts, S.G., et al., *Application of iterative soft thresholding for fast reconstruction of NMR data non-uniformly sampled with multidimensional Poisson Gap scheduling.* J Biomol NMR, 2012. **52**(4): p. 315-27.

186. Livak, K.J. and T.D. Schmittgen, *Analysis of relative gene expression data using real-time quantitative PCR and the 2(-Delta Delta C(T)) Method.* Methods, 2001. **25**(4): p. 402-8.

187. Kumar, R., P.S. Godavarthy, and D.S. Krause, *The bone marrow microenvironment in health and disease at a glance.* J Cell Sci, 2018. **131**(4).

188. Morrison, S.J. and D.T. Scadden, *The bone marrow niche for haematopoietic stem cells.* Nature, 2014. **505**(7483): p. 327-34.

189. Shafat, M.S., et al., *The bone marrow microenvironment - Home of the leukemic blasts.* Blood Rev, 2017. **31**(5): p. 277-286.

190. Ishikawa, F., et al., *Chemotherapy-resistant human AML stem cells home to and engraft within the bone-marrow endosteal region.* Nat Biotechnol, 2007. **25**(11): p. 1315-21.

191. Kohli, L. and E. Passegue, *Surviving change: the metabolic journey of hematopoietic stem cells.* Trends Cell Biol, 2014. **24**(8): p. 479-87.

192. Ito, K. and K. Ito, *Hematopoietic stem cell fate through metabolic control.* Exp Hematol, 2018. **64**: p. 1-11.

193. Kreitz, J., et al., *Metabolic Plasticity of Acute Myeloid Leukemia.* Cells, 2019. **8**(8).

194. Griessinger, E., et al., *A niche-like culture system allowing the maintenance of primary human acute myeloid leukemia-initiating cells: a new tool to decipher their chemoresistance and self-renewal mechanisms.* Stem Cells Transl Med, 2014. **3**(4): p. 520-9.

195. van Gosliga, D., et al., *Establishing long-term cultures with self-renewing acute myeloid leukemia stem/progenitor cells.* Exp Hematol, 2007. **35**(10): p. 1538-49.

196. Zhu, J. and C.B. Thompson, *Metabolic regulation of cell growth and proliferation.* Nat Rev Mol Cell Biol, 2019. **20**(7): p. 436-450.

197. Gruszka, A.M., et al., *Adhesion Deregulation in Acute Myeloid Leukaemia.* Cells, 2019. **8**(1).

198. Kapoore, R.V., et al., *Influence of washing and quenching in profiling the metabolome of adherent mammalian cells: a case study with the metastatic breast cancer cell line MDA-MB-231.* Analyst, 2017. **142**(11): p. 2038-2049.

199. Bendall, L.J., K. Kortlepel, and D.J. Gottlieb, *Human acute myeloid leukemia cells bind to bone marrow stroma via a combination of beta-1 and beta-2 integrin mechanisms.* Blood, 1993. **82**(10): p. 3125-32.

200. Samudio, I., et al., *The warburg effect in leukemia-stroma cocultures is mediated by mitochondrial uncoupling associated with uncoupling protein 2 activation.* Cancer Res, 2008. **68**(13): p. 5198-205.

201. Krall, A.S., et al., *Asparagine promotes cancer cell proliferation through use as an amino acid exchange factor.* Nat Commun, 2016. **7**: p. 11457.

202. Bertero, T., et al., *Tumor-Stroma Mechanics Coordinate Amino Acid Availability to Sustain Tumor Growth and Malignancy.* Cell Metab, 2019. **29**(1): p. 124-140 e10.

203. Berg, J.M., J.L. Tymoczko, and L. Stryer, *Biochemistry*. 2012, Basingstoke: W.H. Freeman.

204. Kamphorst, J.J., et al., *Quantitative analysis of acetyl-CoA production in hypoxic cancer cells reveals substantial contribution from acetate.* Cancer Metab, 2014. **2**: p. 23.

205. Long, X., et al., *Stromal CYR61 Confers Resistance to Mitoxantrone via Spleen Tyrosine Kinase Activation in Human Acute Myeloid Leukaemia.* Br J Haematol, 2015. **170**(5): p. 704-18.

206. Roecklein, B.A. and B. Torok-Storb, *Functionally distinct human marrow stromal cell lines immortalized by transduction with the human papilloma virus E6/E7 genes.* Blood, 1995. **85**(4): p. 997-1005.

207. Pessina, A., et al., *Establishment and characterization of a new murine cell line (SR-4987) derived from marrow stromal cells.* Cytotechnology, 1992. **8**(2): p. 93-102.

208. Whitaker-Menezes, D., et al., *Evidence for a stromal-epithelial "lactate shuttle" in human tumors: MCT4 is a marker of oxidative stress in cancer-associated fibroblasts.* Cell Cycle, 2011. **10**(11): p. 1772-83.

209. Sonveaux, P., et al., *Targeting lactate-fueled respiration selectively kills hypoxic tumor cells in mice.* J Clin Invest, 2008. **118**(12): p. 3930-42.

210. Jeon, J.Y., et al., *Regulation of Acetate Utilization by Monocarboxylate Transporter 1 (MCT1) in Hepatocellular Carcinoma (HCC).* Oncol Res, 2018. **26**(1): p. 71-81.

211. Ferro, S., et al., *Characterization of acetate transport in colorectal cancer cells and potential therapeutic implications.* Oncotarget, 2016. **7**(43): p. 70639-70653.

212. Lyssiotis, C.A. and L.C. Cantley, *Acetate fuels the cancer engine.* Cell, 2014. **159**(7): p. 1492-4.

213. Comerford, S.A., et al., *Acetate dependence of tumors.* Cell, 2014. **159**(7): p. 1591-602.

214. Gao, X., et al., *Acetate functions as an epigenetic metabolite to promote lipid synthesis under hypoxia.* Nat Commun, 2016. **7**: p. 11960.

215. Schug, Z.T., et al., *Acetyl-CoA synthetase 2 promotes acetate utilization and maintains cancer cell growth under metabolic stress.* Cancer Cell, 2015. **27**(1): p. 57-71.

216. Bose, S., V. Ramesh, and J.W. Locasale, *Acetate Metabolism in Physiology, Cancer, and Beyond.* Trends Cell Biol, 2019. **29**(9): p. 695-703.

217. Subramanian, A., et al., *Gene set enrichment analysis: a knowledge-based approach for interpreting genome-wide expression profiles.* Proc Natl Acad Sci U S A, 2005. **102**(43): p. 15545-50.

218. Ros, S. and A. Schulze, *Balancing glycolytic flux: the role of 6-phosphofructo-2-kinase/fructose 2,6-bisphosphatases in cancer metabolism.* Cancer & Metabolism, 2013. **1**(1): p. 8.

219. Yi, M., et al., *6-Phosphofructo-2-kinase/fructose-2,6-biphosphatase 3 and 4: A pair of valves for fine-tuning of glucose metabolism in human cancer.* Mol Metab, 2019. **20**: p. 1-13.

220. Halestrap, A.P., *The SLC16 gene family - structure, role and regulation in health and disease.* Mol Aspects Med, 2013. **34**(2-3): p. 337-49.

221. Al Tameemi, W., et al., *Hypoxia-Modified Cancer Cell Metabolism.* Front Cell Dev Biol, 2019. **7**: p. 4.

222. Schug, Z.T., J. Vande Voorde, and E. Gottlieb, *The metabolic fate of acetate in cancer.* Nat Rev Cancer, 2016. **16**(11): p. 708-717.

223. De Graaf, R.A., *In vivo NMR spectroscopy : principles and techniques*. 2nd ed. ed. 2007, Hoboken, N.J.: Wiley ; Chichester : John Wiley [distributor].

224. Liu, X., et al., *Acetate Production from Glucose and Coupling to Mitochondrial Metabolism in Mammals.* Cell, 2018. **175**(2): p. 502-513 e13.

225. Tiziani, S., et al., *Metabolomic profiling of drug responses in acute myeloid leukaemia cell lines.* PLoS One, 2009. **4**(1): p. e4251.

226. Figueroa, D., M. Asaduzzaman, and F. Young, *Real time monitoring and quantification of reactive oxygen species in breast cancer cell line MCF-7 by 2',7'-dichlorofluorescin diacetate (DCFDA) assay.* J Pharmacol Toxicol Methods, 2018. **94**(Pt 1): p. 26-33.

227. Gomes, A., E. Fernandes, and J.L. Lima, *Fluorescence probes used for detection of reactive oxygen species.* J Biochem Biophys Methods, 2005. **65**(2-3): p. 45-80.

228. Liu, X., et al., *N-acetylcysteine alleviates H2O2-induced damage via regulating the redox status of intracellular antioxidants in H9c2 cells.* Int J Mol Med, 2019. **43**(1): p. 199-208.

229. Aruoma, O.I., et al., *The antioxidant action of N-acetylcysteine: its reaction with hydrogen peroxide, hydroxyl radical, superoxide, and hypochlorous acid.* Free Radic Biol Med, 1989. **6**(6): p. 593-7.

230. Vysochan, A., et al., *ACSS2-mediated acetyl-CoA synthesis from acetate is necessary for human cytomegalovirus infection.* Proc Natl Acad Sci U S A, 2017. **114**(8): p. E1528-E1535.

231. Shan, T., et al., *Cancer-associated fibroblasts enhance pancreatic cancer cell invasion by remodeling the metabolic conversion mechanism.* Oncol Rep, 2017. **37**(4): p. 1971-1979.

232. Migneco, G., et al., *Glycolytic cancer associated fibroblasts promote breast cancer tumor growth, without a measurable increase in angiogenesis: evidence for stromal-epithelial metabolic coupling.* Cell Cycle, 2010. **9**(12): p. 2412-22.

233. Cruz-Bermudez, A., et al., *Cancer-associated fibroblasts modify lung cancer metabolism involving ROS and TGF-beta signaling.* Free Radic Biol Med, 2019. **130**: p. 163-173.

234. Haouas, H., *Angiogenesis and acute myeloid leukemia.* Hematology, 2014. **19**(6): p. 311-23.

235. Fiedler, W., et al., *Vascular endothelial growth factor, a possible paracrine growth factor in human acute myeloid leukemia.* Blood, 1997. **89**(6): p. 1870-5.

236. Mourah, S., et al., *Quantification of VEGF isoforms and VEGFR transcripts by qRT-PCR and their significance in acute myeloid leukemia.* Int J Biol Markers, 2009. **24**(1): p. 22-31.

237. De Bock, K., et al., *Role of PFKFB3-driven glycolysis in vessel sprouting.* Cell, 2013. **154**(3): p. 651-63.

238. Skinner, H.D., et al., *Vascular endothelial growth factor transcriptional activation is mediated by hypoxia-inducible factor 1alpha, HDM2, and p70S6K1 in response to phosphatidylinositol 3-kinase/AKT signaling.* J Biol Chem, 2004. **279**(44): p. 45643-51.

239. Nilsson, I., M. Shibuya, and S. Wennström, *Differential activation of vascular genes by hypoxia in primary endothelial cells.* Exp Cell Res, 2004. **299**(2): p. 476-85.

240. Agani, F. and B.H. Jiang, *Oxygen-independent regulation of HIF-1: novel involvement of PI3K/AKT/mTOR pathway in cancer.* Curr Cancer Drug Targets, 2013. **13**(3): p. 245-51.

241. Dodd, K.M., et al., *mTORC1 drives HIF-1α and VEGF-A signalling via multiple mechanisms involving 4E-BP1, S6K1 and STAT3.* Oncogene, 2015. **34**(17): p. 2239-50.

242. Reed, M.A.C., et al., *Malonate as a ROS product is associated with pyruvate carboxylase activity in acute myeloid leukaemia cells.* Cancer Metab, 2016. **4**: p. 15.

243. Bartnik, B.L., D.A. Hovda, and P.W. Lee, *Glucose metabolism after traumatic brain injury: estimation of pyruvate carboxylase and pyruvate dehydrogenase flux by mass isotopomer analysis.* J Neurotrauma, 2007. **24**(1): p. 181-94.

244. Jitrapakdee, S., et al., *Structure, mechanism and regulation of pyruvate carboxylase.* Biochem J, 2008. **413**(3): p. 369-87.

245. Yoshii, Y., et al., *Cytosolic acetyl-CoA synthetase affected tumor cell survival under hypoxia: the possible function in tumor acetyl-CoA/acetate metabolism.* Cancer Sci, 2009. **100**(5): p. 821-7.

246. Taniguchi Ishikawa, E., et al., *Connexin-43 prevents hematopoietic stem cell senescence through transfer of reactive oxygen species to bone marrow stromal cells.* Proc Natl Acad Sci U S A, 2012. **109**(23): p. 9071-6.

247. Rozental, R., M. Srinivas, and D.C. Spray, *How to close a gap junction channel. Efficacies and potencies of uncoupling agents.* Methods Mol Biol, 2001. **154**: p. 447-76.

248. Moschen, I., et al., *Significance of short chain fatty acid transport by members of the monocarboxylate transporter family (MCT).* Neurochem Res, 2012. **37**(11): p. 2562-8.

249. Ullah, M.S., A.J. Davies, and A.P. Halestrap, *The plasma membrane lactate transporter MCT4, but not MCT1, is up-regulated by hypoxia through a HIF-1alpha-dependent mechanism.* J Biol Chem, 2006. **281**(14): p. 9030-7.

250. Yoshimura, Y., et al., *Molecular cloning of rat acss3 and characterization of mammalian propionyl-CoA synthetase in the liver mitochondrial matrix.* J Biochem, 2017. **161**(3): p. 279-289.

251. Fujino, T., et al., *Acetyl-CoA synthetase 2, a mitochondrial matrix enzyme involved in the oxidation of acetate.* J Biol Chem, 2001. **276**(14): p. 11420-6.

252. Luong, A., et al., *Molecular characterization of human acetyl-CoA synthetase, an enzyme regulated by sterol regulatory element-binding proteins.* J Biol Chem, 2000. **275**(34): p. 26458-66.

253. Wolin, M.J. and T.L. Miller, *Interactions of microbial populations in cellulose fermentation.* Fed Proc, 1983. **42**(1): p. 109-13.

254. Stephens, F.B., D. Constantin-Teodosiu, and P.L. Greenhaff, *New insights concerning the role of carnitine in the regulation of fuel metabolism in skeletal muscle.* J Physiol, 2007. **581**(Pt 2): p. 431-44.

255. Childress, C.C., B. Sacktor, and D.R. Traynor, *Function of carnitine in the fatty acid oxidase-deficient insect flight muscle.* J Biol Chem, 1967. **242**(4): p. 754-60.

256. Miras, C., G. Lewis, and J. Mantzos, *In vitro incorporation of sodium acetate-1-C14 into leukocyte lipids of normal and leukaemic subjects as a function of incubation time.* Nucl Med (Stuttg), 1961. **2**: p. 165-72.

257. Mashimo, T., et al., *Acetate is a bioenergetic substrate for human glioblastoma and brain metastases.* Cell, 2014. **159**(7): p. 1603-14.

258. Bulusu, V., et al., *Acetate Recapturing by Nuclear Acetyl-CoA Synthetase 2 Prevents Loss of Histone Acetylation during Oxygen and Serum Limitation.* Cell Rep, 2017. **18**(3): p. 647-658.

259. Chen, R., et al., *The acetate/ACSS2 switch regulates HIF-2 stress signaling in the tumor cell microenvironment.* PLoS One, 2015. **10**(2): p. e0116515.

260. Loike, J.D., et al., *Hypoxia induces glucose transporter expression in endothelial cells.* Am J Physiol, 1992. **263**(2 Pt 1): p. C326-33.

261. Park, H.S., et al., *Hypoxia induces glucose uptake and metabolism of adiposederived stem cells.* Mol Med Rep, 2016. **14**(5): p. 4706-4714.

262. Abu Eid, S., et al., *Life Under Hypoxia Lowers Blood Glucose Independently of Effects on Appetite and Body Weight in Mice.* Front Endocrinol (Lausanne), 2018. **9**: p. 490.

263. Saxena, K. and M.K. Jolly, *Acute vs. Chronic vs. Cyclic Hypoxia: Their Differential Dynamics, Molecular Mechanisms, and Effects on Tumor Progression.* Biomolecules, 2019. **9**(8).

264. Yun, M., et al., *The importance of acetyl coenzyme A synthetase for 11C-acetate uptake and cell survival in hepatocellular carcinoma.* J Nucl Med, 2009. **50**(8): p. 1222-8.

265. Huang, Z., et al., *ACSS2 promotes systemic fat storage and utilization through selective regulation of genes involved in lipid metabolism.* Proc Natl Acad Sci U S A, 2018. **115**(40): p. E9499-E9506.

266. Li, X., et al., *Nucleus-Translocated ACSS2 Promotes Gene Transcription for Lysosomal Biogenesis and Autophagy.* Mol Cell, 2017. **66**(5): p. 684-697 e9.

8. Appendix

8.1. NMRPipe script

```
#!/bin/csh -f
bruk2pipe -in ser -bad 0.0 -aswap -DMX -decim 2560 -dspfvs 20 -grpdly
67.9842376708984  \
•     xN              2048  -yN              4096  \
•     xT              1024  -yT              2048  \
•     xMODE            DQD  -yMODE        States-TPPI  \
•     xSW         7812.500  -ySW        24390.244  \
•     xOBS         600.173  -yOBS         150.925  \
•     xCAR           4.773  -yCAR          82.733  \
•     xLAB              1H  -yLAB             13C  \
•     ndim               2  -aq2D          States  \
| nmrPipe -fn SOL -fl 64 \
| nmrPipe -fn SP -off 0.48 -end 0.95 -pow 2 -c 0.5 \
| nmrPipe -fn ZF -auto \
| nmrPipe -fn FT -auto \
| nmrPipe -fn PS -hdr \
| nmrPipe -fn PS -p0 174.8 -p1 127 -di                        \
| nmrPipe -fn EXT -sw \
| nmrPipe -fn TP \
| istHMS -xN 8192 -vlist nuslist  -itr 400  \
#| istHMS -xN 8192 -vlist nuslist -i_mult 0.70 -e_mult 0.70 -itr 25  \
| nmrPipe -fn SP -off 0.5 -end 0.98 -c 0.5   \
| nmrPipe -fn ZF -auto \
| nmrPipe -fn FT -auto \
| nmrPipe -fn PS -p0 -8.6 -p1 4 -di -verb \
| nmrPipe -fn POLY -auto \
| nmrPipe -fn TP \
| nmrPipe -fn POLY -auto \
•     ov -out data2.ft2
```

The two optional istHMS lines use the IST algorithm by Sven Hyberts and Gerhard Wagner [185] with two different parameter sets, as suggested by Hyberts.

8.2. ^{1}H-^{13}C-HSQC pulse program

```
;hsqcphprsp.ug4
;avance-version (12/01/11)
;HSQC
;2D H-1/X correlation via double inept transfer
;phase sensitive
;with decoupling during acquisition
;with 15N decoupling during incrementation
;
;G. Bodenhausen & D.J. Ruben, Chem. Phys. Lett. 69, 185 (1980)
;
;$CLASS=HighRes
;$DIM=2D
;$TYPE=
;$SUBTYPE=
;$COMMENT=

; with 13C 180deg soft pulses and gradients

#include <Avance.incl>
#include <Delay.incl>
#include <Grad.incl>


"p2=p1*2"
"p4=p3*2"
"d4=1s/(cnst2*4)"
"p22=p21*2"
"d11=30m"
"d12=20u"
"d13=4u"


"d0=3u"
"in0=inf1/2"

;"DELTA=d0*2+p2"
"DELTA1=d4-larger(p2,p14)/2-p19-d16-4u"

1 ze
d11 pl12:f2 pl3:f3
2 d11 do:f2

# ifdef FLAG_BLK
  4u BLKGRAD
#   else
  4u
```

```
#   endif /*FLAG_BLK*/

  d12 pl9:f1
  d1 cw:f1 ph29
  d13 do:f1
  d12 pl1:f1
  p1 ph1
  ;d4 pl2:f2
  4u UNBLKGRAD
  p19:gp4
  d16
  DELTA1 pl0:f2
   (center (p2 ph1) (p14:sp3 ph9):f2 )
  4u
  p19:gp4
d16
DELTA1 pl2:f2
 (p1 ph3)
4u
p16:gp1
d16
(p3 ph6):f2
d0
(p2 ph8)
d0
  (p4 ph7):f2
DELTA
  (p3 ph7):f2
4u
p16:gp2
d16
(p1 ph4)
4u
p19:gp3
d16
DELTA1 pl0:f2
 (center (p2 ph1) (p14:sp3 ph5):f2 )
4u
DELTA1
p19:gp3
d16 pl12:f2

#   ifdef FLAG_BLK
  4u
#   else
  4u BLKGRAD
#   endif /*FLAG_BLK*/

  go=2 ph31 cpd2:f2
```

```
  d11 do:f2 mc #0 to 2 F1PH(calph(ph6, +90) & calph(ph9, +90) & calph(ph29,
+90), caldel(d0, +in0))
exit

ph0=0
ph1=0
ph2=0
ph3=1
ph4=1
ph5=0 0 0 0 0 0 0 0 2 2 2 2 2 2 2 2
ph6=0 2
ph7=0 0 0 0 2 2 2 2
ph8=0 0 2 2
ph9=0 0 0 0 0 0 0 0 2 2 2 2 2 2 2 2
ph29=0
ph31=0 2 0 2 2 0 2 0


;pl1 : f1 channel - power level for pulse (default)
;pl2 : f2 channel - power level for pulse (default)
;pl9 : f1 channel - power level for presaturation
;pl12: f2 channel - power level for CPD/BB decoupling
;p1 : f1 channel -  90 degree high power pulse
;p2 : f1 channel - 180 degree high power pulse
;p3 : f2 channel -  90 degree high power pulse
;p4 : f2 channel - 180 degree high power pulse
;d0 : incremented delay (2D)                          [3 usec]
;d1 : relaxation delay; 1-5 * T1
;d4 : 1/(4J)XH
;d11: delay for disk I/O                              [30 msec]
;d12: delay for power switching                       [20 usec]
;d13: short delay                                     [4 usec]
;cnst2: = J(XH)
;inf1: 1/SW(X) = 2 * DW(X)
;in0: 1/(2 * SW(X)) = DW(X)
;nd0: 2
;ns: 4 * n
;ds: 16
;td1: number of experiments
;FnMODE: States-TPPI, TPPI, States or QSEQ
;cpd2: decoupling according to sequence defined by cpdprg2
;pcpd2: f2 channel - 90 degree pulse for decoupling sequence

;for z-only gradients:
;gpz1: 60%
;gpz2: 55%
;gpz3: 11%
;gpz4: 6%
```

```
;use gradient files:
;gpnam1: SMSQ10.100
;gpnam2: SMSQ10.100
;gpnam3: SMSQ10.100
;gpnam4: SMSQ10.100

;preprocessor-flags-start
;LABEL_CN: for C-13 and N-15 labeled samples start experiment with
;             option -DLABEL_CN (eda: ZGOPTNS)
;preprocessor-flags-end

;preprocessor-flags-start
;FLAG_BLK: for BLKGRAD before d1 rather than go
;             option -DFLAG_BLK: (eda: ZGOPTNS)
;preprocessor-flags-end
```

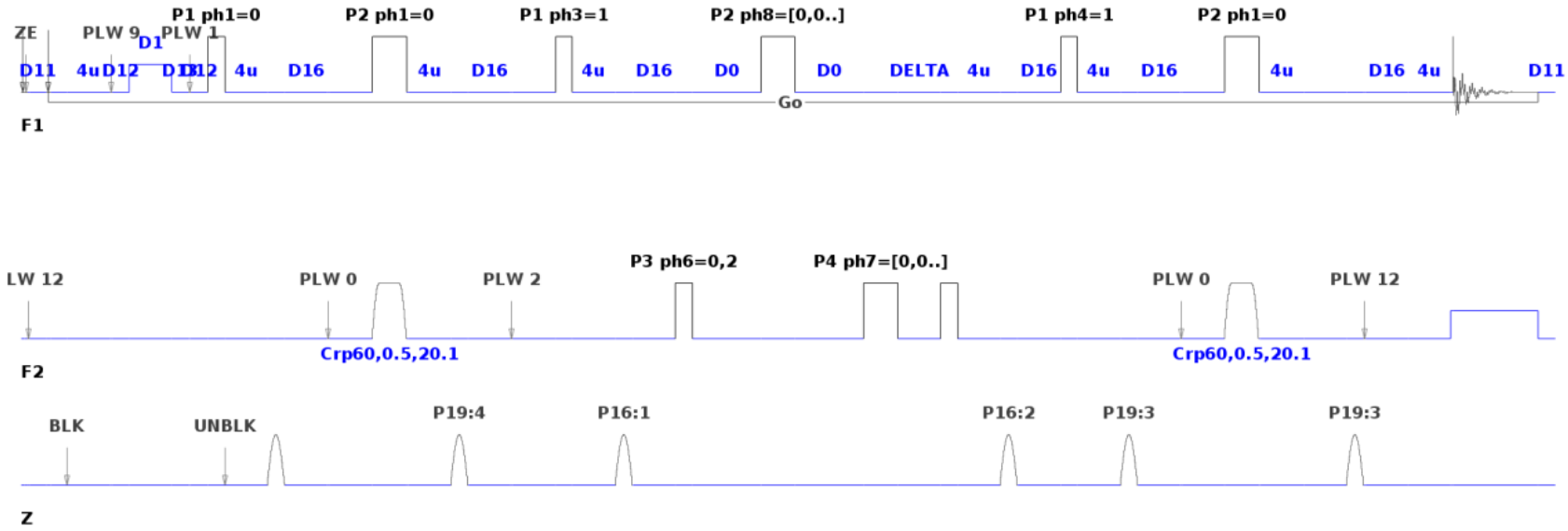
P1 ph1=0
P2 ph1=0
P1 ph3=1
P2 ph8=[0,0..]
P1 ph4=1
P2 ph1=0
ZE
PLW 9
D1
PLW 1
D11 4u D12 D11 D12 4u D16 4u D16 4u D16 D0 D0 DELTA 4u D16 4u D16 4u D16 4u D11
Go
F1
LW 12
PLW 0
PLW 2
P3 ph6=0,2
P4 ph7=[0,0..]
PLW 0
PLW 12
Crp60,0.5,20.1
Crp60,0.5,20.1
F2
BLK
UNBLK
P19:4
P16:1
P16:2
P19:3
P19:3
Z